



Meteorologisk
institutt

No. 2/2026

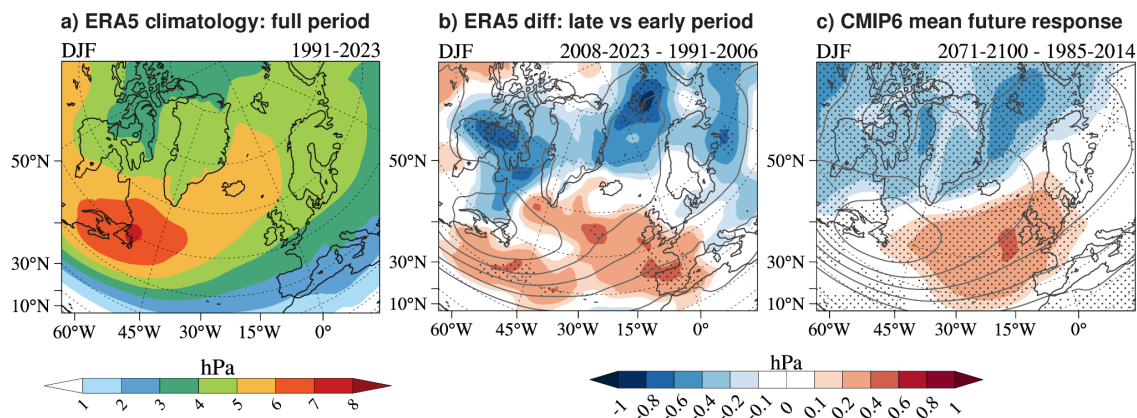
ISSN 2387-4201

Climate

METreport

The Impact of Climate Change on Aviation Weather during Winter in Northern Norway

Morten Køltzow, Tor Ivar Mathisen, Jostein Mamen, Lise Seland Graff



Storm track activity and changes in storm track activity during December, January and February for a historical period and a future scenario. See Figure 5.1 for details.

[Classification: open]

Title The Impact of Climate Change on Aviation Weather during Winter in Northern Norway	Date [date]
Section Climate	Report no. No. 2/2026
Author(s) Morten Køltzow, Tor Ivar Mathisen, Jostein Mamen, Lise Seland Graff	Classification • Free <input type="radio"/> Restricted
Client(s) The Norwegian Safety Investigation Authority	Client's reference
<p>Abstract</p> <p>This report has investigated severe aviation weather conditions during wintertime in Northern Norway and Svalbard. The aim has been to provide an overview of when conditions favouring icing, low-level turbulence, strong wind, precipitation, convection and lightning occur. Furthermore, the report analyses the frequency and intensity of such conditions and estimates their historical changes (1991-2023) and anticipated future change. A wide range of data, such as in-situ observations and metar-data from individual airports, lightning observations, AIREPs (pilot reports), regional and global reanalysis and global climate simulations has been utilized in the analysis.</p> <p>The main conclusion is that severe wintertime aviation weather conditions in Northern Norway and at Svalbard often are steered by the location and intensity of the large-scale low pressure systems entering the Norwegian and Barents Sea region. There is in general no historical trend towards a worsening of the aviation weather conditions during the recent 3 decades, but a significant interannual variability in the frequency and severity of the weather conditions is seen. However, some modest local (e.g. on airport level) changes and trends are seen, some to improve and some to worsen the local aviation weather conditions. There is further no indication of a general trend towards a worsening in the wintertime aviation weather conditions in the future, but some anticipated differences for specific weather elements and between airports and regions are expected.</p>	
<p>Keywords Aviation weather, climate change, winter, Northern Norway</p>	

Content

Acronym List	8
1. Introduction	10
2. Data used in this Report	12
2.1 AIREP/pilot reports and Incident reports from SHK	12
2.2 METAR observations	12
2.3 Lightning observations	13
2.4 Reanalysis - ERA5 & CARRA	13
2.5 Climate projections and observations from the Norwegian Centre for Climate Services (Norsk Klimaservicesenter)	14
2.6 Coupled Model IntercomParison sixth phase (CMIP6)	14
3. Today's Climatological Conditions in Northern Norway	19
3.1 Introduction	19
3.2 Mean Seasonal Mean Sea Level Pressure (MSLP) and Wind Conditions for Northern Norway	20
3.3 Mean Seasonal Temperature for Northern Norway	22
3.4 Mean Seasonal Precipitation for Northern Norway	23
3.5 Climatology in Nordland, Troms, Finnmark and at Svalbard	25
3.5.1 Weather and Climate in Nordland	25
3.5.2 Weather and Climate in Troms	25
3.5.3 Weather and Climate in Finnmark	26
3.5.4 Weather and Climate at Svalbard	27
3.6 Synoptic Low Pressure Systems vs Polar Lows	28
3.7 Cold Air Outbreak (CAO)	29
4. Case Study of the 12. February 2023 Incident at Langnes	31
4.1 Introduction	31
4.2 Weather Situation	31
4.3 Meteorological parameters	35
4.3.1 Wind and Turbulence	35
4.3.2 Icing	37
4.3.3 Lightning and CB-activity	40

4.4 Similar Historical Events	42
4.5 Summary of the 12. February 2023 case	44
5. Low Pressure Systems and Storm Tracks	45
6. Meteorological Aerodrome Observations and Trends	52
6.1 Introduction	52
6.2 Bodø airport	54
6.2.1 Main findings	54
6.2.2 Location	54
6.2.3 Wind conditions	55
6.2.3.1 Mean wind speed	55
6.2.3.2 Wind roses	56
6.2.3.3 Differences in wind in a mild and a cold winter month	57
6.2.3.4 Wind gusts	58
6.2.3.5 Crosswinds	60
6.2.3.6 Trends for crosswind	61
6.2.3.7 Crosswind of long duration	63
6.2.3.8 Extreme wind	64
6.2.4 Freezing precipitation	65
6.2.5 Freeze/thaw events	66
6.3 Tromsø airport	68
6.3.1 Main findings	68
6.3.2 Location	68
6.3.3 Wind conditions	69
6.3.3.1 Mean wind speed	69
6.3.3.2 Wind roses	70
6.3.3.3 Differences in wind in a mild and a cold winter month	71
6.3.3.4 Wind gusts	72
6.3.3.5 Crosswind	74
6.3.3.6 Trends for crosswind	75
6.3.3.7 Crosswind of long duration	77
6.3.3.8 Extreme winds	78
6.3.4 Freezing precipitation	80
6.3.5 Freeze-thaw events	81
6.4 Kirkenes Lufthavn	82
6.4.1 Main findings	82
6.4.2 Location	82
6.4.3 Wind conditions	83
6.4.3.1 Mean wind speed	83

6.4.3.2 Wind roses	83
6.4.3.3 Differences in wind in a mild and a cold winter month	84
6.4.3.4 Wind gusts	85
6.4.3.5 Crosswind	87
6.4.3.6 Trends for crosswind components	88
6.4.3.7 Crosswind of long duration	90
6.4.3.8 Trends for extreme wind	91
6.4.4 Freezing precipitation at ground level	92
6.4.5 Freeze/thaw events	92
6.5 Svalbard Lufthavn	93
6.5.1 Main findings	93
6.5.2 Location	94
6.5.3 Wind conditions	94
6.5.3.1 Mean wind speed	94
6.5.3.2 Wind roses	95
6.5.3.3 Differences in wind in a mild and a cold winter month	96
6.5.3.4 Wind gusts	97
6.5.3.5 Crosswind	99
6.5.3.6 Trends for crosswind components	100
6.5.3.7 Crosswind of long duration	102
6.5.3.8 Trends for extreme wind	103
6.5.4 Freezing precipitation at ground level	104
6.5.5 Freeze/thaw events	104
6.6 Evenes airport	106
6.6.1 Main findings	106
6.6.2 Location	106
6.6.3 Wind conditions	107
6.6.3.1 Mean wind speed	107
6.6.3.2 Wind roses	109
6.6.3.3 Differences in wind in a mild and a cold winter month	110
6.6.3.4 Wind gusts	111
6.6.3.5 Crosswinds	113
6.6.3.6 Trends for crosswind	114
6.6.3.7 Crosswind of long duration	116
6.6.3.8 Extreme wind	117
6.6.4 Freezing precipitation	118
6.6.5 Freeze/thaw events	119
6.7 Andøya airport	120

6.7.1 Main findings	120
6.7.2 Location	120
6.7.3 Wind conditions	121
6.7.3.1 Mean wind speed	121
6.7.3.2 Wind roses	123
6.7.3.3 Differences in wind in a mild and a cold winter month	123
6.7.3.4 Wind gusts	125
6.7.3.5 Crosswind	127
6.7.3.6 Trends for crosswind	128
6.7.3.7 Crosswind of long duration	130
6.7.3.8 Extreme wind	131
6.7.4 Freezing precipitation	132
6.7.5 Freeze/thaw events	133
6.8 Bardufoss airport	134
6.8.1 Main findings	134
6.8.2 Location	134
6.8.3 Wind conditions	135
6.8.3.1 Mean wind speed	135
6.8.3.2 Wind roses	136
6.8.3.3 Differences in wind in a mild and a cold winter month	137
6.8.3.4 Wind gusts	138
6.8.3.5 Crosswind	140
6.8.3.6 Trends for crosswind	141
6.8.3.7 Crosswind of long duration	142
6.8.3.8 Extreme wind	142
6.8.4 Freezing precipitation	143
6.8.5 Freeze/thaw events	144
6.9 Alta airport	145
6.9.1 Main findings	145
6.9.2 Location	145
6.9.3 Wind conditions	146
6.9.3.1 Mean wind speed	146
6.9.3.2 Wind roses	147
6.9.3.3 Differences in wind in a mild and a cold winter month	149
6.9.3.4 Wind gusts	150
6.9.3.5 Crosswind	153
6.9.3.6 Trends for crosswind	153
6.9.3.7 Crosswind of long duration	155

6.9.3.8 Extreme wind	155
6.9.4 Freezing precipitation	156
6.9.5 Freeze/thaw events	157
6.10 Banak airport	158
6.10.1 Main findings	158
6.10.2 Location	158
6.10.3 Wind conditions	159
6.10.3.1 Mean wind speed	159
6.10.3.2 Wind roses	160
6.10.3.3 Differences in wind in a mild and a cold winter month	162
6.10.3.4 Wind gusts	163
6.10.3.5 Crosswind	166
6.10.3.6 Trends for crosswind	166
6.10.3.7 Crosswind of long duration	168
6.10.3.8 Extreme wind	169
6.10.4 Freezing precipitation	170
6.10.5 Freeze/thaw events	171
7. Meteorological Analysis of Reported Weather Related Events & Historical and Future Trends in Large-scale Aviation Weather	172
7.1 Wind and Turbulence	172
7.2 Icing	183
7.3 Convective activity	190
7.4 Lightning	198
7.5 Other Aviation Weather Related Parameters	209
7.5.1 2-m Air Temperature (T2m)	210
7.5.2 Precipitation	217
7.5.3 Relative Humidity (RH2m)	223
8. Takeaways for the Meteorological Operational Community	226
9. Summary and Conclusion	229
References	235

Acronym List

Acronym	Definition/Explanation
AIREP	Aircraft Report
AIRMET	Airmen's Meteorological Information
AMSL	Above Mean Sea Level
AR6	Intergovernmental Panel of Climate Change 6th Assessment Report
CAO	Cold Air Outbreak
CARRA	Copernicus Arctic Regional Reanalysis
CAT	Clear Air Turbulence
CB	Cumulonimbus Cloud
CMIP	Coupled Model InterComparison
DJF	December, January and February
ECMWF	European Centre for Medium-Range Weather Forecasts
ERA5	ECMWF Reanalysis v.5
FL	Flight Level
IPCC	Intergovernmental Panel of Climate Change
JJA	June, July and August
LWC	Liquid Water Content
MAM	March, April and May
METAR	Meteorological Aerodrome Report.
MET Norway	Norwegian Meteorological Institute
MSLP	Mean Sea Level Pressure
MTW	Mountain Waves

NH	Northern Hemisphere
NWP	Numerical Weather Prediction
ONDJFMA	October - April
RH2m	2-m Relative Humidity
SCLWC	Supercooled Specific Cloud Liquid Water Content
SHK	Statens Havarikommisjon
SIGMET	Significant Meteorological Information
SON	September, October and November
SST	Sea Surface Temperature
SYNOP	Surface Synoptic Observation
T2m	2-m air temperature
TAF	Terminal Area Forecast
TCSLW	Total Column of Supercooled Liquid Water
TCU	Towering Cumulus Cloud
TKE	Turbulent Kinetic Energy
WMO	World Meteorological Organization
WS	Wind Shear / Wind Shear Warning

1. Introduction

The primary goal of this report is to provide meteorological insights for the Norwegian Safety Investigation Authority's project, "Thematic Research on How Climate Change Affects Aviation in Northern Norway" (<https://havarikommisjonen.no/Luftfart/Undersokelser/23-359>). This report analyses aviation winter weather conditions and climate change in Northern Norway over the past 30 years. Additionally, the report includes a discussion of the anticipated future aviation weather conditions in Northern Norway towards the end of the century.

The investigation was triggered by a severe weather event on Sunday, 12. February 2023, causing multiple incidents at Tromsø Airport, Langnes, affecting several flights. SAS, Widerøe, and Norwegian all faced challenges due to intense showers and strong winds. Two Widerøe aircraft were struck by lightning and experienced severe icing conditions. One Norwegian aircraft was also hit by lightning and received a warning about strong wind shear just before landing. SAS encountered wind shear during its approach, leading to an aborted landing, and one of its engines experienced strong vibrations. The aircraft declared a mayday to secure a priority landing, as snow ploughing was scheduled on the runway. These incidents, along with other events during the winter of 2022/2023, led to the initiation of this project.

The Norwegian Meteorological Institute (Met Norway) was tasked with several objectives: 1) to conduct a meteorological analysis of the 12. February 2023 event; 2) to describe large-scale low pressure systems, polar lows, and convection in Northern Norway and their impact on aviation weather; 3) to analyse the frequency and intensity of these systems, and estimate their historical changes and their anticipated future changes; 4) to provide climatological data on conditions that promote icing, turbulence, precipitation, convection and lightning; and 5) to analyse observed wind conditions (both direction and strength) at airports in Northern Norway. The main focus period is wintertime (defined as October to April) from 1991 to 2023, although some analyses have shorter time frames due to limited observation data.

As the research has progressed, numerous opportunities for further investigation into aviation-related topics have emerged. While some of these avenues have been explored, many still hold the potential for deeper study. This is particularly true for understanding the variability and specifics of historical weather events that lead to severe aviation conditions. Additionally, some topics have only been briefly addressed and not examined in depth. For instance, findings on Clear Air Turbulence are only

based on existing literature, and there has been no analysis on how changes in permafrost affect airports. Moreover, discussions about future scenarios tend to be somewhat oversimplified and lack detailed quantifications as they rely on analysed scenarios for storm track activity and the established relationship between aviation-related weather and storms, along with a review of existing literature. It's important to note that this report focuses primarily on winter conditions (October-April) in Northern Norway, and the results should not be generalised to other regions or seasons.

A number of recent scientific studies have reviewed how climate change impacts the aviation industry (e.g. Burbridge et al., 2024, Paraschi, 2023, Voskaki et al., 2023, Ryley et al., 2020). These studies summarise key findings from existing studies and are detailing many of the impacts on operations, safety and infrastructure. A number of weather conditions are discussed in the context of adaptation; extreme temperatures, severe storms, heavy rainfall and flooding, wind shear, icing conditions, turbulence, lightning strikes, low visibility, drought and permafrost thawing. Some of these topics are less relevant for Northern Norway and are not included in our study, while others are relevant, but not further elaborated in our study (e.g. low visibility and permafrost thawing). A common feature of existing studies is often the lack of focus on wintertime conditions and our area of interest. Hence, this study is to a large degree complementary to the existing body of knowledge regarding how climate change impacts aviation.

This report is structured as follows: Starting with a description of the data set applied (section 2), followed by a general introduction to the climatology of the region (section 3). Section 4 analyses the meteorological conditions of the trigger case from the 12. February 2023. The next three sections focus on historical climatology and trends. Section 5 discusses low pressure systems and storm track activity. Section 6 presents a detailed investigation of individual airports based on observational data. Section 7 offers a regional overview of aviation-related weather parameters, including icing, turbulence, convective activity, lightning, temperature, and precipitation conditions based on reanalysis data. This section also includes an analysis of reported weather incidents and their relationship to low pressure systems, along with a discussion connecting the findings from section 5 and existing literature to potential future scenarios. Finally, section 8 summarises key takeaways for the operational aviation forecasting community, and section 9 presents the main summary and conclusions of the report.

2. Data used in this Report

This section describes data used in this report with the exception of in-situ observations from airports. These are described with their local details when they are applied in section 6. The other data sets are described briefly with references to more in depth descriptions. In addition, since all data sets do have strengths and weaknesses, some of these are briefly mentioned in the following.

2.1 AIREP/pilot reports and Incident reports from SHK

Aircraft pilots that experience conditions, e.g. related to icing, turbulence or wind shear can issue a report about location, altitude, time and severity. In Norway, these reports will be received by aviation forecasters on duty and disseminated to all other pilots in an AIREP. These reports therefore provide valuable information on aviation related weather conditions. At MET Norway, an archive of AIREP reports exists from 2015. Unfortunately, a number of problems are associated with these observations; only cases with some sort of difficult weather conditions are reported, pilots often do not report if the conditions already are forecasted or reported on, the severity is subjectively judged and can also be influenced by e.g. applied de-icing measures and how experienced the pilots are. Despite weaknesses they provide a valuable source of information as they do identify challenging situations, and they are widely used in science related to aviation forecasting (e.g. Engdahl et al., 2022). For the work in this report, we had available 1757 AIREPs for the period of 2015-2023. In addition to AIREPs a set of incident reports collected by AVINOR and SHK was made available. This data set includes a total of 147 reports. However, some of these reports duplicate what is already found by the AIREPs. It has not been possible to utilise all reports for different reasons, lack of exact positioning or timing are among the most common reasons.

The main strength with the data set is that it is possible to identify situations with challenging aviation weather conditions. However, the observations do not provide certain information that challenging weather conditions did not occur and can not be used directly to investigate trends or spatial patterns.

2.2 METAR observations

METAR are routine weather reports for aviation providing weather information at airports. The reports are used by pilots for flight planning and for traffic management of airport departures and arrivals. The content of a METAR is a mix of automatic measurements and manual observations of present weather conditions. In this study we use in particular observations that can be related to convective activity, e.g. reports on CB, TCU, lightning, precipitation in the form of hail or graupel and showers in

general. All these observation types are taken manually (we exclude all automatic METARS for quality reasons), and are therefore dependent on the observer, the view of the surroundings, on daylight conditions and on the opening hours of the airport.

The main strength with an historical data set of manual observations from METARs is that it is able to identify situations where convection most likely has occurred. However, that convection is not observed at a given time is not always necessarily enough to say that it didn't happen. Comparing trends and spatial differences in the observations should be done with a lot of care or even avoided as the observation practises can vary between airports and over time.

2.3 Lightning observations

The Norwegian sensor network for detecting lightning was initially built up from the 1980s in cooperation between Statnett, Sintef and MET Norway. Since 2017, MET Norway has had the responsibility for operating the network and archiving lightning activity in the Norwegian economic zone. An introduction of new sensors and processing units since the first set up have improved the accuracy and detection efficiency of the system. Today, MET Norway exchanges sensor data with neighbouring countries to further improve the observational coverage and accuracy. The system is documented in some detail in Køltzow et al. (2018).

The main strength of the data is the identification of lightning events. The main weaknesses of the data set is the lack of spatial and temporal consistency due to changes in the system over time. The data can therefore not be used for trend analysis. Furthermore, far away from sensors, i.e. offshore, the detection efficiency and accuracy is reduced.

2.4 Reanalysis - ERA5 & CARRA

Reanalysis is the most complete historical description of the climate system and provides 3-dimensional “maps without gaps” backwards in time. They are constructed by an optimal combination of numerical models of the climate system and a wide range of observations (see <https://climate.copernicus.eu/climate-reanalysis> for a brief introduction).

In this study we apply the fifth generation ECMWF reanalysis, ERA5 (Hersbach et al., 2020) and the Copernicus Arctic Regional Reanalysis, CARRA (Yang et al., 2020) data sets. Both data sets are available from the Copernicus Climate Change Services Climate Data Store (<https://cds.climate.copernicus.eu/>). ERA5 is one of the most used climate data sets on earth and provides global information about a large set of atmospheric parameters near the surface, as integrals of the atmospheric column and at a selection of vertical levels. The data is available on a horizontal resolution of

approximately 30 x 30 km (one value represents an area of 30x30 km) and for the period of 1940 and until today with a few days delay. Compared to this, CARRA is a regional reanalysis covering most of the European Arctic including both (near) surface and upper air parameters. Data is available on a horizontal resolution of 2.5 x 2.5 km for the period of 1991 and until today with a few months delay.

The main difference between the two reanalyses are in particular the horizontal resolution where CARRA provides much more details and a better description of extremes and rare events. CARRA also applies more local observations and provides a more targeted description of cold processes in the climate system. However, ERA5 provides global coverage, longer time series and some additional parameters to what CARRA can provide. Both reanalyses describe better parameters that are constrained by the observations assimilated into the system (e.g. pressure, near-surface temperature) than other non-observed parameters (e.g. details on cloud water and ice).

The main strengths of reanalysis are the provision of 3 dimensional consistent maps without gaps for historical weather conditions for a wide range of atmospheric parameters. However, the accuracy of the parameters not strongly constrained by the utilised observations depend on the underlying numerical weather model. For such parameters the use of multiple reanalysis data sets can be useful to estimate the uncertainty. In addition, some aviation related parameters are not available and need to be estimated from other parameters.

2.5 Climate projections and observations from the Norwegian Centre for Climate Services (Norsk Klimaservicesenter)

In the report we use a number of figures from the Norwegian Centre for Climate Services (Norsk Klimaservicesenter: <https://klimaservicesenter.no/>). They include both long term observational data records, but also future climate scenarios. The climate projections are then based on assumptions about future emissions of greenhouse gases and global and regional climate models. The results from the global climate models (typically from CMIP, see section 2.6) are not detailed enough to be used in local adaptation and planning, hence different methods of downscaling are used to increase the degree of detail from the global climate models.

2.6 Coupled Model IntercomParison sixth phase (CMIP6)

The climate model data directly used in this report is taken from the sixth phase of the Coupled Model Intercomparison Project (CMIP6; Eyring et al., 2016; <https://www.wcrp-climate.org/wgcm-cmip>). CMIP is an initiative under the World Climate Research Programme (WCRP) and provides a comprehensive collection of coordinated climate model experiments that can be used to understand climate change

of the past, present and future. Based on detailed common modelling protocols, modelling centres across the globe carry out the same model experiments, but using different models. The result is a comprehensive multi-model ensemble. Here, we use data from two different modelling experiments, the CMIP6 historical experiment (protocol described in Eyring et al. 2016) and SSP5-8.5 (protocol described in O'Neill et al. 2016), for 29 different world-class climate models (Table 2.6.1). The future climate projections provided by CMIP6, including SSP5-8.5, are also used by the Intergovernmental Panel of Climate Change (IPCC) in their 6th assessment report (AR6). Data from CMIP6 is freely available to anyone through the Earth System Grid Federation (ESGF), using one of the ESGF nodes (<https://esgf.github.io/nodes.html>).

The main strength of the CMIP6 data for our purposes is the ability to compare state-of-the-art end-of-the-century climate scenarios with experiments for the historical period for studying projected future changes in large-scale patterns. In addition, CMIP6 provides a wide range of climate models making it possible to sample the model uncertainty. A weakness is the relatively coarse resolution of the models, implying that not all relevant processes are appropriately described. Also the choice of future scenario impacts the results. Here, we focus on the high-end emission scenario within the CMIP6 ScenarioMIP, however, more low-end or middle-of-the-road scenarios could have been considered in addition to shed more light on the projected range of future responses.

Table 2.6.1: Overview of CMIP6 models used in this study (column 1), the institute(s) that carried out the model experiments (column 2), and digital object identifiers (DOI's)/links for each experiment (column 3).

Model	Institute	DOI's
ACCESS-CM2	CSIRO-ARCCSS: Commonwealth Scientific and Industrial Research Organisation and Australian Research Council Centre of Excellence for Climate System Science, Australia	10.22033/ESGF/CMIP6.4271 10.22033/ESGF/CMIP6.4332
ACCESS-ESM1-5	CSIRO: Commonwealth Scientific and Industrial Research Organisation, Australia	10.22033/ESGF/CMIP6.4272 10.22033/ESGF/CMIP6.4333
BCC-CSM2-MR	BBC: Beijing Climate Center, China	10.22033/ESGF/CMIP6.2948 10.22033/ESGF/CMIP6.3050
CESM2	NCAR: National Center for Atmospheric Research, USA	10.22033/ESGF/CMIP6.7627 10.22033/ESGF/CMIP6.10115

CESM2-WACCM	NCAR	10.22033/ESGF/CMIP6.10071 10.22033/ESGF/CMIP6.10115
CMCC-CM2-SR5	CMCC: Fondazione Centro Euro-Mediterraneo sui Cambiamenti Climatici, Italy	10.22033/ESGF/CMIP6.3825 10.22033/ESGF/CMIP6.3896
CNRM-CM6-1	CNRM-CERFACS: Centre National de Recherches Meteorologiques and Centre Europeen de Recherche et de Formation Avancee en Calcul Scientifique, France	10.22033/ESGF/CMIP6.4066 10.22033/ESGF/CMIP6.4224
CNRM-ESM2-1	CNRM-CERFACS	10.22033/ESGF/CMIP6.4068 10.22033/ESGF/CMIP6.4226
CanESM5	CCCma: Canadian Centre for Climate Modelling and Analysis, Environment and Climate Change Canada, Canada	10.22033/ESGF/CMIP6.3610 10.22033/ESGF/CMIP6.3696
EC-Earth3	EC-Earth-Consortium: AEMET, Spain; BSC, Spain; CNR-ISAC, Italy; DMI, Denmark; ENEA, Italy; FMI, Finland; Geomar, Germany; ICHEC, Ireland; ICTP, Italy; IDL, Portugal; IMAU, The Netherlands; IPMA, Portugal; KIT, Karlsruhe, Germany; KNMI, The Netherlands; Lund University, Sweden; Met Eireann, Ireland; NLeSC, The Netherlands; NTNU, Norway; Oxford University, UK; surfSARA, The Netherlands; SMHI, Sweden; Stockholm University, Sweden; Unite ASTR, Belgium; University College Dublin, Ireland; University of Bergen, Norway; University of Copenhagen, Denmark; University of Helsinki, Finland; University of Santiago de Compostela, Spain; Uppsala University, Sweden; Utrecht University, The Netherlands; Vrije Universiteit Amsterdam, the Netherlands; Wageningen University, The Netherlands.	10.22033/ESGF/CMIP6.4700 10.22033/ESGF/CMIP6.4912

EC-Earth3-Veg	EC-Earth-Consortium	10.22033/ESGF/CMIP6.4706 10.22033/ESGF/CMIP6.4914
FGOALS-g3	CAS: Chinese Academy of Sciences, China	10.22033/ESGF/CMIP6.3356 10.22033/ESGF/CMIP6.3503
GFDL-CM4	NOAA-GFDL: National Oceanic and Atmospheric Administration, Geophysical Fluid Dynamics Laboratory, USA	10.22033/ESGF/CMIP6.8594 10.22033/ESGF/CMIP6.9268
GFDL-ESM4	NOAA-GFDL	10.22033/ESGF/CMIP6.8597 10.22033/ESGF/CMIP6.8706
HadGEM3-GC31-LL	MOHC: Met Office Hadley Centre, UK	10.22033/ESGF/CMIP6.6109 10.22033/ESGF/CMIP6.10901
HadGEM3-GC31-MM	MOHC	10.22033/ESGF/CMIP6.6112 10.22033/ESGF/CMIP6.10902
INM-CM4-8	INM: Institute for Numerical Mathematics, Russian Academy of Science, Russia	10.22033/ESGF/CMIP6.5069 10.22033/ESGF/CMIP6.12337
IPSL-CM6A-LR	IPSL: Institut Pierre Simon Laplace, France	10.22033/ESGF/CMIP6.5195 10.22033/ESGF/CMIP6.5271
KACE-1-0-G	NIMS-KMA: National Institute of Meteorological Sciences/Korea Meteorological Administration, Climate Research Division, Republic of Korea	10.22033/ESGF/CMIP6.8378 10.22033/ESGF/CMIP6.8456
KIOST-ESM	KIOST: Korea Institute of Ocean Science and Technology, Republic of Korea	10.22033/ESGF/CMIP6.5296 10.22033/ESGF/CMIP6.11249
MIROC-ES2L	MIROC: Japan Agency for Marine-Earth Science and Technology (JAMSTEC), Atmosphere and Ocean Research Institute (AORI), The University of Tokyo, National Institute for Environmental Studies (NIES), and RIKEN Center for Computational Science (R-CCS), Japan	10.22033/ESGF/CMIP6.5602 10.22033/ESGF/CMIP6.5770

MIROC6	MIROC	10.22033/ESGF/CMIP6.5603 10.22033/ESGF/CMIP6.5771
MPI-ESM1-2-HR	MPI-M (historical): Max Planck Institute for Meteorology, Germany DKRZ (ssp585): Deutsches Klimarechenzentrum, Germany	10.22033/ESGF/CMIP6.6594 10.22033/ESGF/CMIP6.4403
MPI-ESM1-2-LR	MPI-M	10.22033/ESGF/CMIP6.6595 10.22033/ESGF/CMIP6.6705
MRI-ESM2-0	MRI: Meteorological Research Institute, Japan	10.22033/ESGF/CMIP6.6842 10.22033/ESGF/CMIP6.6929
NESM3	NUIST: Nanjing University of Information Science and Technology, China	10.22033/ESGF/CMIP6.8769 10.22033/ESGF/CMIP6.8790
NorESM2-LM	NCC: NorESM Climate modeling Consortium consisting of Center for International Climate and Environmental Research (CICERO), Norwegian Meteorological Institute (MET Norway), Nansen Environmental and Remote Sensing Center (NERSC), Norwegian Institute for Air Research (NILU), University of Bergen (UiB), University of Oslo (UiO), and Uni Research (UNI), Norway	10.22033/ESGF/CMIP6.8036 10.22033/ESGF/CMIP6.13781
NorESM2-MM	NCC	10.22033/ESGF/CMIP6.8040 10.22033/ESGF/CMIP6.8321
UKESM1-0-LL	MOHC	10.22033/ESGF/CMIP6.6113 10.22033/ESGF/CMIP6.6405

3. Today's Climatological Conditions in Northern Norway

3.1 Introduction

Parts of the climatological input in this section is written by Met Norway and published in Store Norske Leksikon (snl.no) and adapted to the purpose of this report.

Norway's climate is characterised by major differences due to its geographical and topographical conditions. Deep fjords and valleys surrounded by high mountain terrain are factors contributing to these differences. An impact of the shielding effect of the mountains is that large parts of the country, in particular Eastern Norway and Finnmarksvidda, have a more continental climate than the distance from the coast would suggest. The mountains also significantly influence the distribution of clouds and precipitation in the different regions. In Northern Norway, some winters are dominated by westerly winds, resulting in a relatively mild and wet weather, while other winters may be dominated by cold continental air masses from the east.

3.2 Mean Seasonal Mean Sea Level Pressure (MSLP) and Wind Conditions for Northern Norway

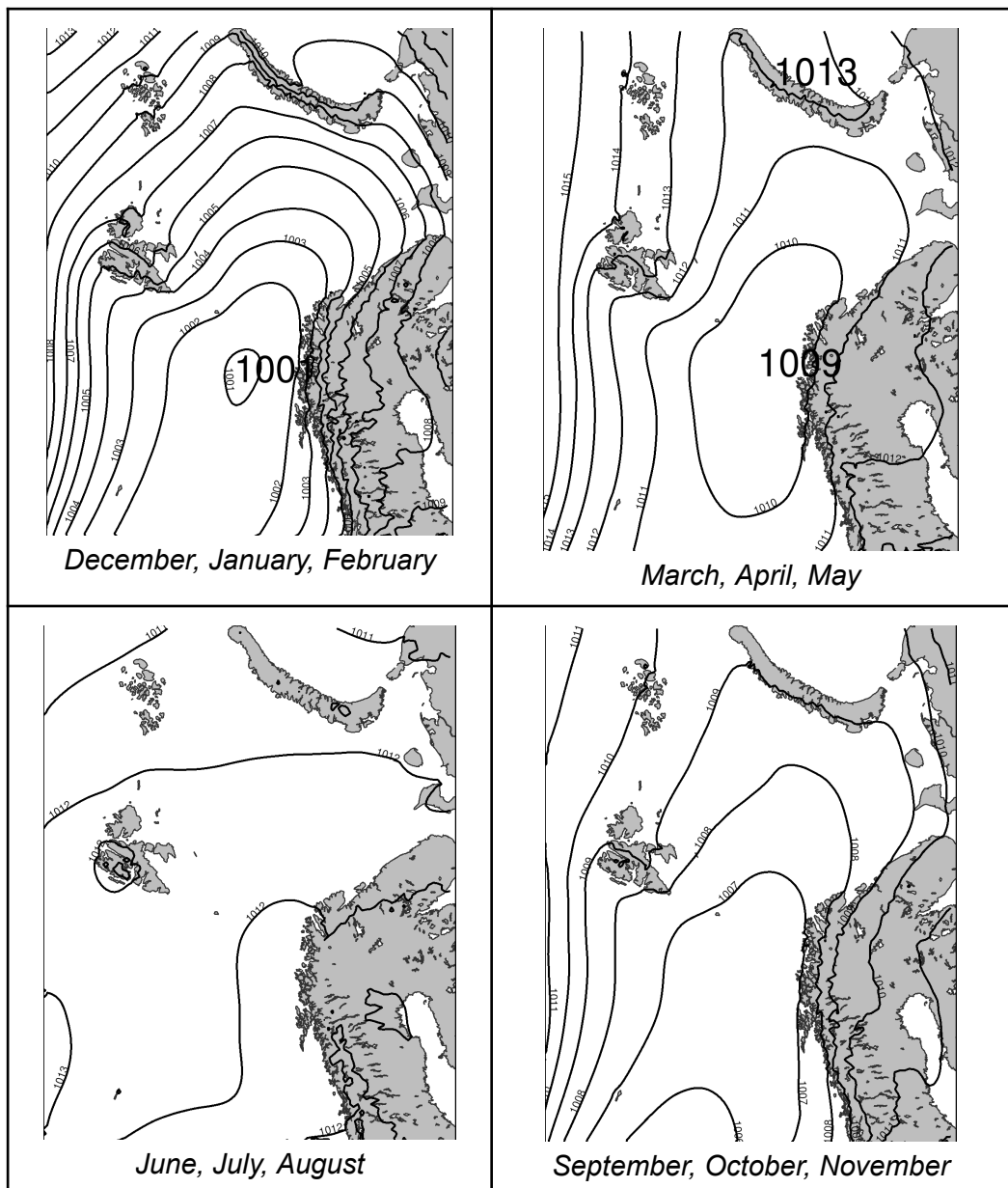


Figure 3.2.1: Mean Mean Sea Level Pressure per season (1991-2023). DJF (December-February), MAM (March-May), JJA (June-August), SON (September-November). Data: CARRA.

In Figure 3.2.1, the seasonal average of Mean Sea Level Pressure (MSLP) is shown. During winter (DJF) and spring (MAM), the lowest average MSLP is in the Norwegian Sea just west of Troms, but deeper and more spatial gradients occur during DJF. In autumn (SON) there is a southwestward shift in the location of the lowest MSLP. During summer (JJA), the MSLP pattern is not that strong, due to weaker pressure systems and a weaker temperature gradient between the North Pole and Equator.

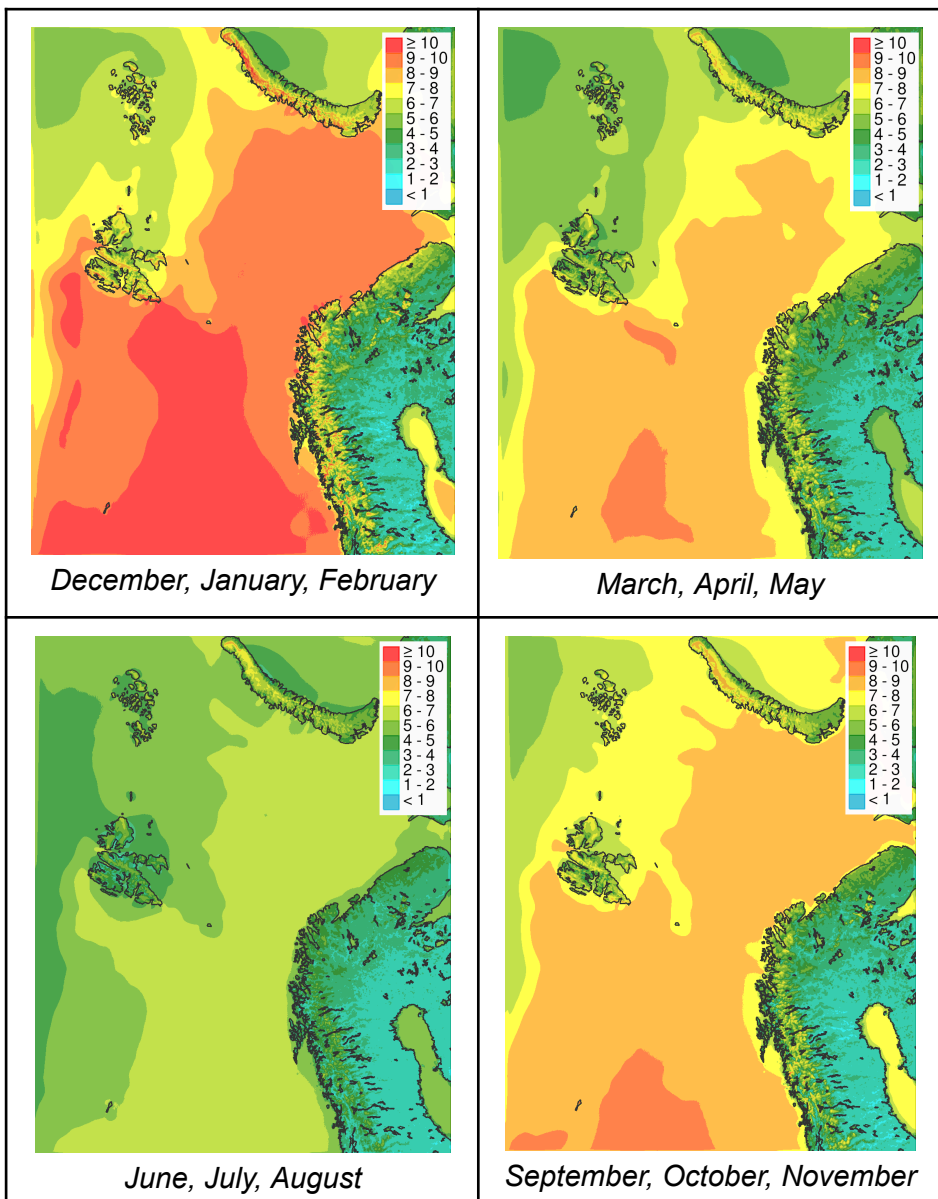


Figure 3.2.2: Same as Figure 3.2.1, but for Mean 10m Wind Speed (m/s).

Since the low pressure systems are more intense during winter, the average wind speed is at its strongest during DJF (Figure 3.2.2). In general, we find the strongest wind speeds in the Norwegian Sea, along the coast and in the mountain area. On average, the weakest wind speeds are during summer.

3.3 Mean Seasonal Temperature for Northern Norway

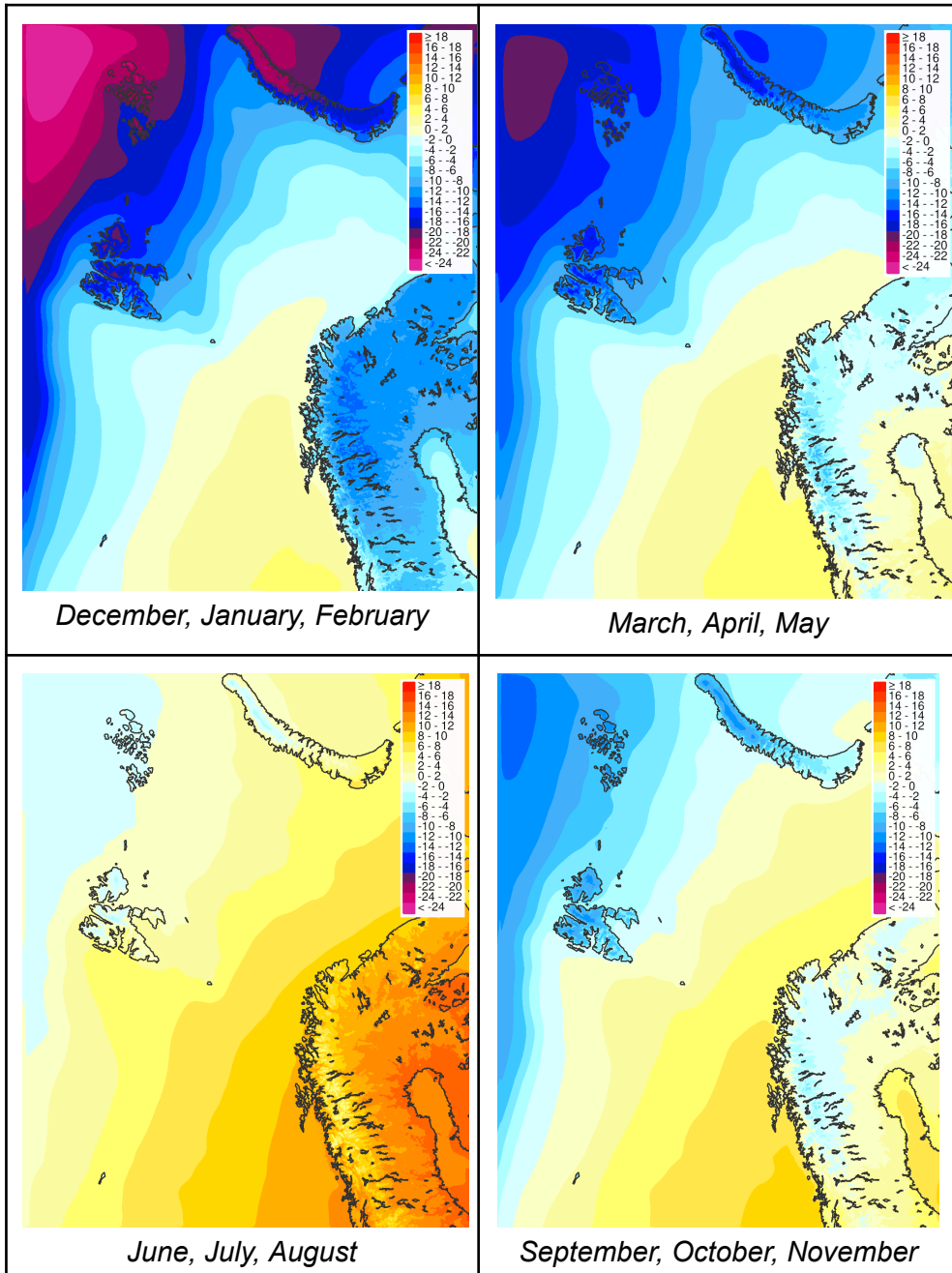
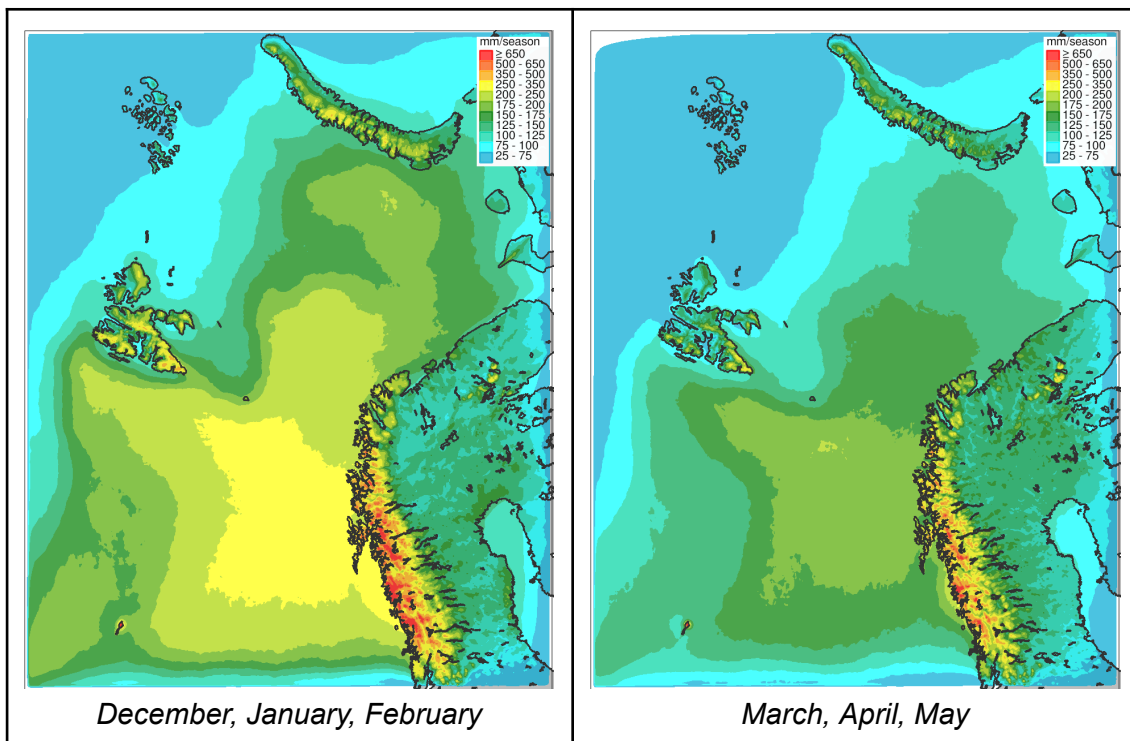


Figure 3.3.1: Same as Figure 3.2.1, but for Mean 2-m Air Temperature (°C)

In Figure 3.3.1, the mean seasonal 2-m air temperature for Northern Norway and Svalbard is shown. The temperature distribution is characterised by relatively small zonal (north-south) contrasts, but large land-ocean contrasts. Average coastal winter temperatures are above freezing as far north as Røst (Lofoten). The annual average temperature rises to approximately 8 °C along the west coast, while in the central mountain areas the annual average temperature is below 0 °C at levels higher than 750–1000 metres above mean sea level (AMSL). In Finnmark, the seasonal averages are as low as -1 to -2 °C even at lowland observation stations. The difference between the lowest (cold) and highest (warm) seasonal average is between 25 and 30 °C inland, and between 10 and 15 °C along the Norwegian west coast. The coldest period of the year inland is mid January and February along the coast and in the mountain area, and March in the Arctic region. The warmest annual period is mid-July and in the beginning of August along the coast and in the mountain area. For the sea surface temperature, the warmest and coldest months are approximately offset by one month later than the warmest and coldest month for the air temperature.

3.4 Mean Seasonal Precipitation for Northern Norway



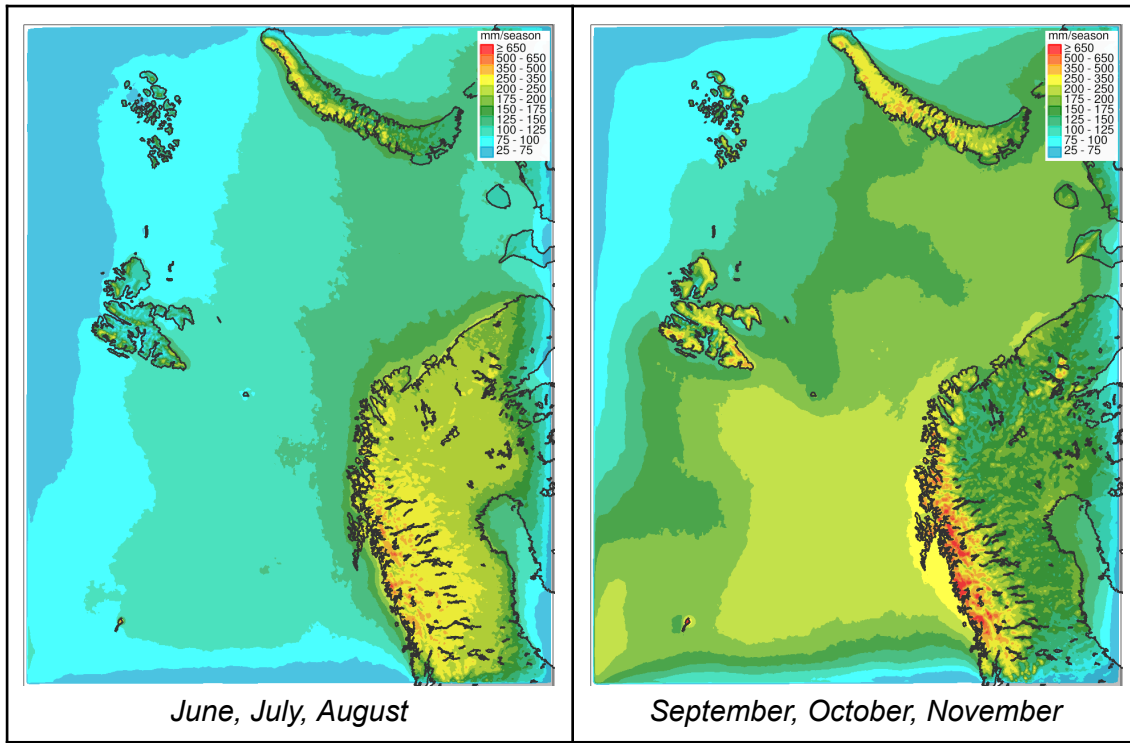


Figure 3.4.1, same as Figure 3.2.1, but for seasonal precipitation amounts (mm).

A spatial climatology of seasonal precipitation is available from the CARRA data set, but as with all precipitation data sets there are uncertainties associated with the estimate. Details of the presented climatology should therefore be interpreted with care. As shown in Figure 3.4.1, the annual rainfall varies significantly with the geographical and topographical location, from 600–1000 mm along the coast to more than 1200-2000 mm in the coastal mountain area in Nordland and Troms, while only 300-600 mm in the sheltered valley areas. The coastal areas receive most of the precipitation during autumn and winter, often as showers. On an annual average, Finnmark is the driest county in Norway. Annual rainfall amounts are 600–1000 mm in a narrow zone along the coast in the west, while the rest of the county receives between 300 and 500 mm. The inland region (e.g. Finnmarksvidda) receives most of the rainfall during summer and much less during late winter and spring.

At Svalbard, the precipitation in general comes from clouds at low altitude. Its distribution is therefore strongly influenced by the terrain. The annual precipitation amounts are estimated to be between 200 and 500 mm, with a maximum in late summer and autumn.

3.5 Climatology in Nordland, Troms, Finnmark and at Svalbard

3.5.1 Weather and Climate in Nordland

Despite Nordland's large north-south extension, the coastal climate is fairly uniform north to Lofoten–Vesterålen where a natural climate barrier is located. The county is particularly exposed to low pressure systems intensifying in the Iceland–Jan Mayen area, moving east- and northeastwards.

The most dominant wind direction is the southwesterlies (southwesterly winds), however with significant variability. Cold winds from east and southeast are common during winter, often reaching gale force when a strong low pressure system is approaching from the west, locally generating turbulent conditions. During calm summer situations, the wind usually blows from north or northwest along the coast. The frequency of near gale force (13.9-17.1 m/s) or more is approximately 10%.

Due to the influence of the cold sea, February is on average the coldest month. The average temperature is approximately 0°C along the coast and the archipelagos. However, no other global location at the same latitude has such a mild winter climate as Lofoten. Shielded inland areas near the Swedish border have January averages of -5 to -10°C. The average temperature for July varies between 11-15 °C within the county.

The annual rainfall varies significantly with the geographical and topographical location, from 600–700 mm on the outermost islands to more than 2000 mm in the coastal mountain area. In the Lofoten–Vesterålen area, there are significant differences in the precipitation amounts over short distances, largely due to the fact that even moderate heights can trigger and intensify the precipitation pattern. In the eastmost valleys, the annual rainfall is approximately 500–750 mm. Most of the precipitation in these easternmost areas are coming during summer, while the maximum precipitation along the coast is coming during autumn.

3.5.2 Weather and Climate in Troms

The climate in Troms is characterised by its complex topography with a significant difference between the coastal and inland areas.

During the summer season, the wind direction is typically north–northeast along the coast, while in the fjords and valleys it blows towards the warmer inland areas. During the winter season, cold winds from east and southeast are common, potentially

generating turbulent conditions, while the wind direction along the coast usually is between southeast and southwest.

The coldest month is usually February, with an average temperature in the coastal areas of approximately -2 °C, and between -6 to -9 °C further inland with low minimum temperatures near -30 to -40 °C. The average temperature in July is 11–12 °C in the coastal area and approximately 14 °C further inland with maximum temperatures occasionally as high as 30 °C.

Precipitation varies significantly within the region. The annual rainfall is around 750 mm near the coast, 1000–1500 mm as a maximum zone over the coastal mountains, while only 300–600 mm in the sheltered valley areas. During the winter time in the coastal mountain area, unstable maritime air from northwest may lead to events with heavy snowfall and Cold Air Outbreaks which might cause challenges for aviation.

The coastal areas may have some fog in the summer season, otherwise fog occurs quite rarely.

3.5.3 Weather and Climate in Finnmark

A large geographical area, complicated coastline and deep fjords make significant differences in the climate within Finnmark. The inland climate is quite continental. During the winter season offshore winds (southeast - southwest) inland are common, caused by a heavy cooling over land and blowing outwards through the valleys and fjords, typically from a southwesterly to southeasterly direction, locally generating severe turbulent conditions. In connection with low pressure activity, storm force during the winter season is common. In January the wind speed is at near gale force or more in 30-40% of the time along the coast.

February is the coldest month in the coastal area, with an average temperature ranging from -2 °C to -7 °C. The inland area has a consistently average temperature of -10 °C to -15 °C in January and February. At Finnmarksvidda the temperatures are particularly low during the winter months with minimum temperatures ranging from -40 °C to -45 °C. The lowest temperature ever recorded in Norway was measured in Karasjok on 1 January 1886, -51.4 °C.

Midsummer, onshore wind between north and east along the coast is common. The sea breeze moves into the fjords and valleys and decreases the summer heat. The average temperature in July is 10–12 °C in the coastal area, and approximately 14 °C in the inland area. The highest temperature occurs with air masses from the southeast. During the midnight sun period, maximum temperatures can reach more than 30 °C in the inland areas.

On average, Finnmark is the driest county in Norway. Annual rainfall amounts are 600–1000 mm in a narrow zone along the coast in the west, 600–800 mm near the northern coast, while the rest of the county receives between 300 and 500 mm. The coastal areas receive most of the precipitation during autumn and early winter, often as snow showers due to north or northwesterly winds and associated Cold Air Outbreaks. The inland region receives most of the rainfall during summer and much less during late winter and spring.

Occasionally there is some fog during the summer season in the coastal area, with a frequency of 2–5% in July. In the fjords, especially in the Varangerfjord, arctic sea smoke may occur during low temperature events.

3.5.4 Weather and Climate at Svalbard

The climate on Svalbard is classified as a tundra climate, since the highest average monthly temperatures are between 0 and 10 °C. It is heavily influenced by the surrounding ocean climate with a lot of fog and clouds due to its location between an area of almost permanent sea ice cover in the northeast and open sea south and west of Spitsbergen. A small shift in the low pressure tracks could have a significant impact on the weather at Svalbard, in particular during the winter season. The Norwegian Atlantic Current flowing along the west coast of Spitsbergen and further east along the northern coast is of significant importance to the weather and climate at Spitsbergen. Even during midwinter, the sea is usually open in this region. At the same time, the east coast can be blocked by sea ice.

In general, the archipelago is influenced by the polar easterlies (easterly wind). The prevailing wind direction is between northeast and southeast. During the short summer season, westerlies (westerly winds) sometimes can be more dominant than the easterlies on the west coast and fjords.

The average temperature during the coldest month, usually February or March, varies from approximately -7 °C on Bjørnøya to -15 °C or slightly lower in the inner fjord areas of Spitsbergen and approximately around -20 °C in the northeastern most areas. The low minimum temperature record at Svalbard Airport is -46 °C. The average temperature during the summer season is between 3 to 6 °C, slightly warmer in the valley areas on Spitsbergen, slightly colder further east. The maximum temperatures are above 15 °C. At Bjørnøya and Svalbard Airport more than 20 °C have been measured.

In general, the precipitation comes from clouds at low altitude. Its distribution is therefore strongly influenced by the terrain. The annual precipitation amounts are

estimated to be between 200 and 500 mm, with a maximum in late summer and autumn. Certain sheltered areas in the north of Spitsbergen are considered to have less than 100 mm of annual precipitation, while in a maximum zone in the southeast the amounts are probably 10 times bigger.

Svalbard is dominated by cloudy weather, often in high pressure situations as well. The frequency of fog is higher than at any lowland station on the mainland, approximately 8–10% over the sea and along the southern coast, but less than 1% in the inner fjord and valley areas. There is a clear summer maximum, but fog can occur during all seasons.

3.6 Synoptic Low Pressure Systems vs Polar Lows

The satellite image in Figure 3.6.1 shows the different characteristics of a 'normal' low pressure system (large-scale synoptic low, extratropical cyclone, polar front low pressure) and a polar low pressure system.

A synoptic low pressure system in our region generally occurs in the middle latitudes in the North Atlantic (between 30° and 60° latitude), often moving and developing north-eastwards. The typical horizontal scale of a synoptic low pressure system is 1000-2500 km.

A polar low, on the other hand, is a mesoscale, short-lived but fairly intense atmospheric low pressure system that is found over the ocean areas poleward of the main polar front. The horizontal scale of the polar low is approximately 150-600 km. An example is shown in Figure 3.6.1, with a polar low north of the synoptic low pressure system. Polar lows are most common in the Norwegian and Barents Sea, mainly east of the 0°-meridian and between 65 and 76 °N. Polar lows are uniquely associated by Cold Air Outbreaks from the polar sea ice areas (next chapter).

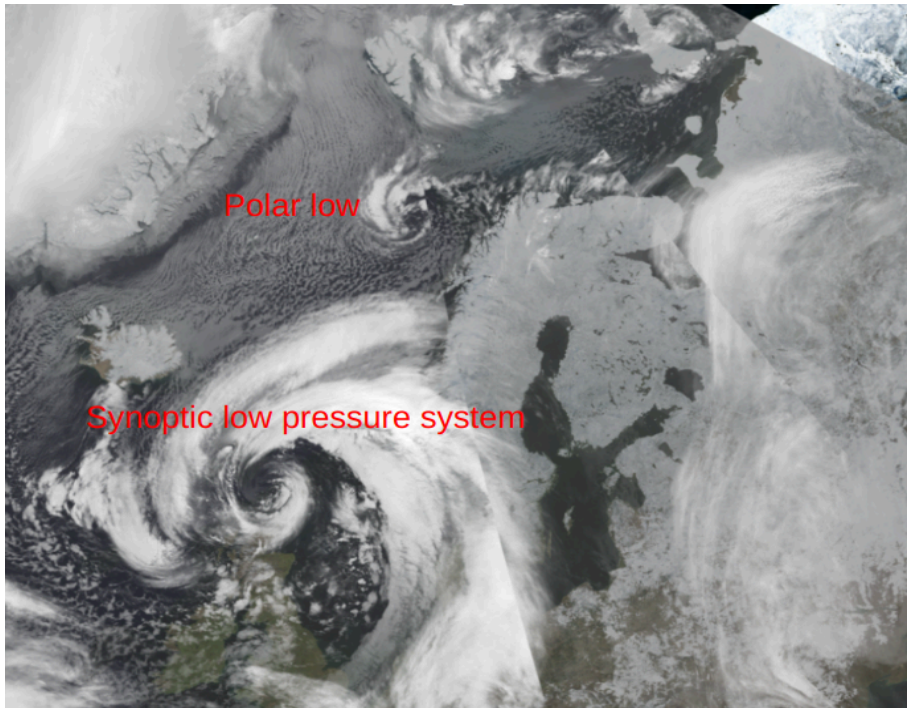


Figure 3.6.1: Storm “Tuva” on 31. January 2008. Two main features: Typical size and scale of a synoptic storm low pressure system versus a polar low. Source: EUMETNET/METEOSAT

3.7 Cold Air Outbreak (CAO)

Figure 3.7.1 depicts a well developed Cold Air Outbreak (CAO) in the Norwegian Sea. CAOs are characterised by extreme air-sea energy exchanges and low-level convective clouds over large areas in the high-latitude oceans. CAOs occur when cold, dry air usually from the Arctic sea ice is transported over the relatively warm ocean, where the ocean surface can then release large amounts of heat and moisture into the air, developing convective clouds such as towering cumulus (TCUs) and cumulonimbus (CBs), during wintertime often resulting in intense showers of sleet, snow or hail.

In the satellite image (Figure 3.7.1), the CAO and the associated convective cells (TCUs and CBs) are organised along lines (NW-SE), developing and intensifying in the Norwegian Sea as they move south- and southeastwards and approaching the coast of Norway. Occasionally well developed and more intense CB-systems might occur during a CAO event (so called troughs), in the satellite image seen as white clouds (CBs) stretching from Lofoten to Trøndelag. When the conditions are right, also polar lows might develop during a CAO event.

CAO events are common during the winter season in Northern Norway and might be challenging for aviation in general and for aerodrome operations.

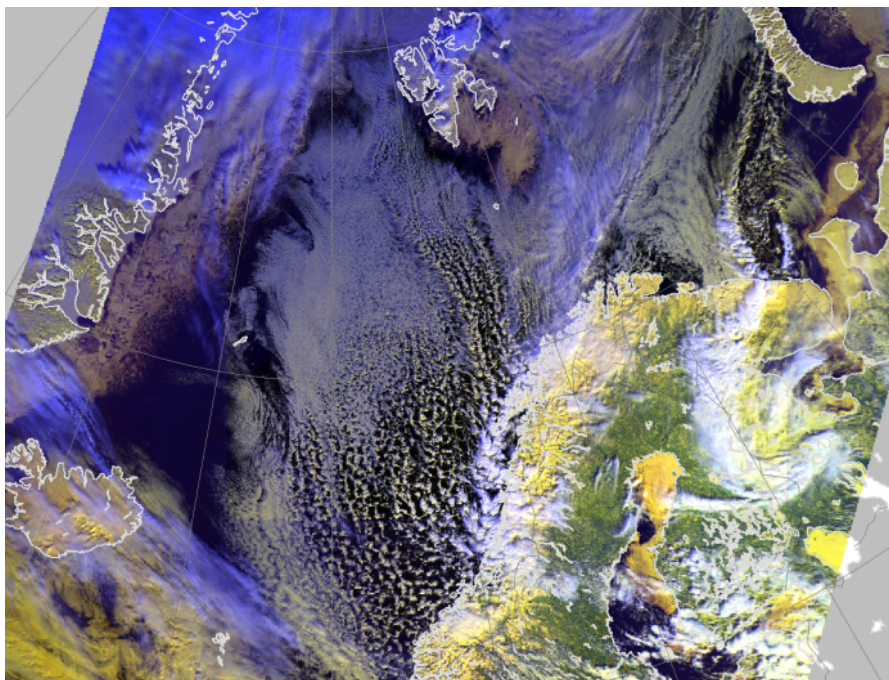


Figure 3.7.1: A characteristic and well developed Cold Air Outbreak (CAO) in the Norwegian Sea. Source: NOAA.

4. Case Study of the 12. February 2023 Incident at Langnes

4.1 Introduction

On Sunday the 12. February 2023, there were several weather related incidents near or at Tromsø Airport, Langnes, causing challenges for several aircraft.

SAS, Widerøe and Norwegian all experienced incidents related to intense rain showers (CBs) and strong winds. Two aircraft from Widerøe were struck by lightning and reported severe icing. One aircraft from Norwegian was struck by lightning and was warned of a strong windshear just before landing. SAS had an incident during approach with a strong wind shear and aborted the approach and experiencing strong vibrations in one of the engines, declaring a mayday in order to get priority landing since snow ploughing was planned on the runway.

In this section this weather related weather event is studied and described in more detail.

4.2 Weather Situation

On the 11. February a synoptic low pressure system was developing between Greenland and Iceland, moving east-northeastwards and intensifying on 12. February (Figure 4.2.1). A stationary high pressure system located over northwestern Europe forced the wide low pressure system to pass north of the high pressure system, resulting in a strong and long westerly fetch towards Nordland and Troms. A 'direct' westerly wind flow at the coast in this area is quite rare - usually the wind is shifted towards southwest or northwest along the coast in these situations. The westerly flow resulted in difficult crosswind and turbulence conditions at Langnes as well as forced topographic lifting of humid air masses from the sea with icing conditions and later a strong convective activity (CBs) as a result.

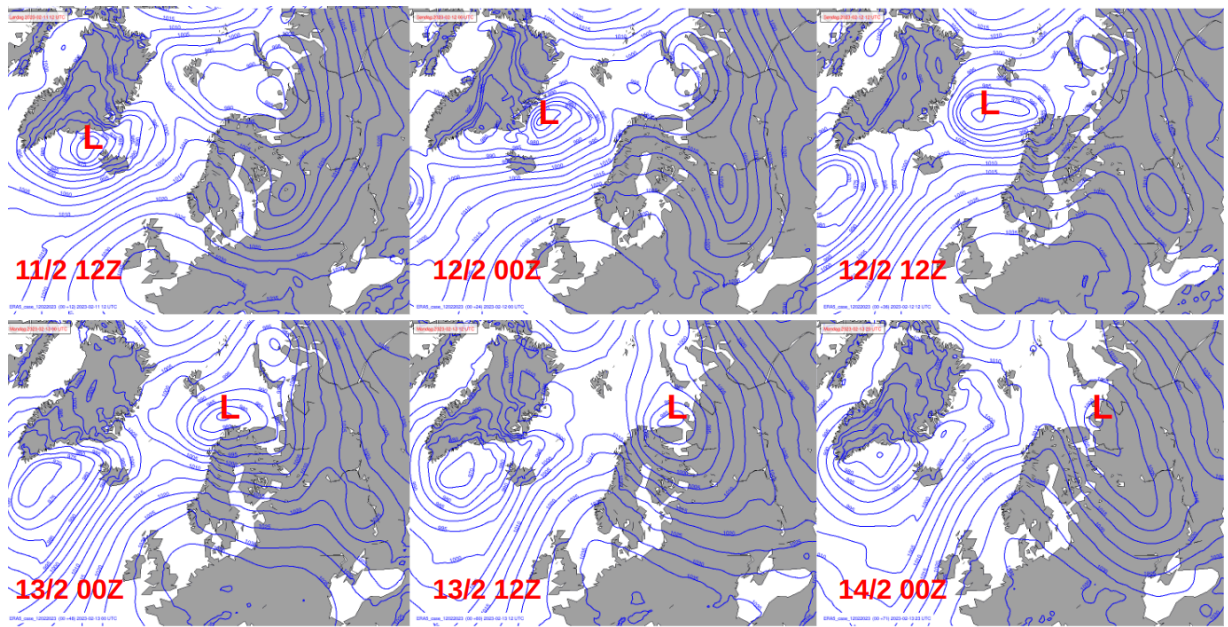


Figure 4.2.1: Mean Sea Level Pressure development of the 12.02.2023 low pressure system every 12 hours from 11.02 at 12 UTC until 14.02 at 00 UTC. Data from ERA5.

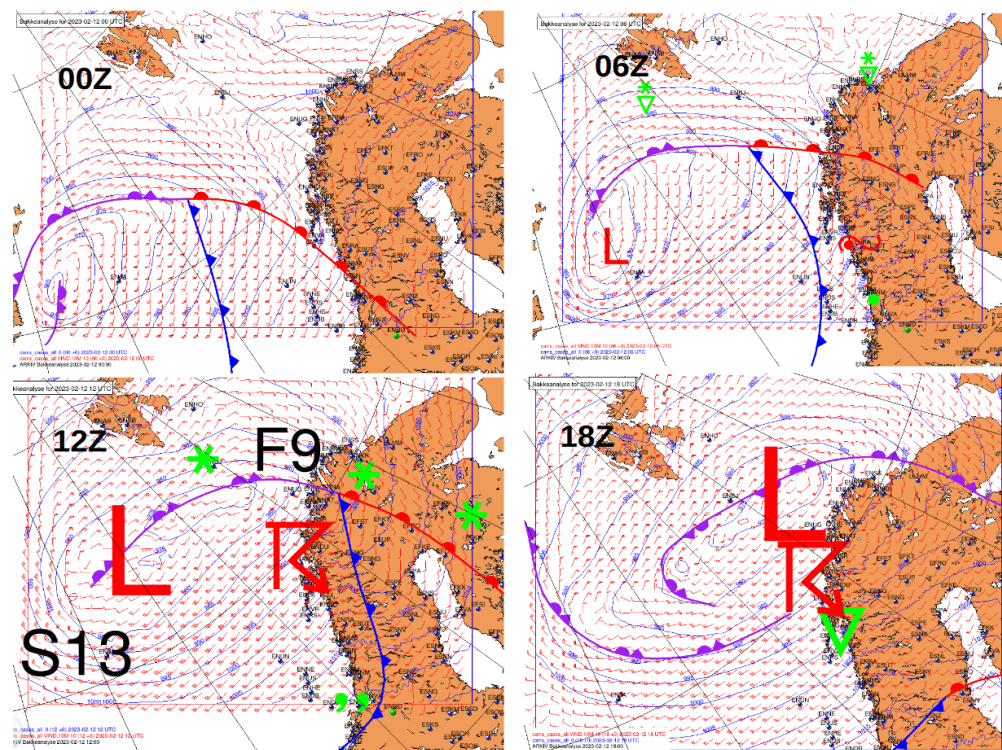


Figure 4.2.2: Surface analysis at 00, 06, 12 and 18 UTC on 12. February 2023. Source: MET Norway.

Accompanied by the low pressure system north in the Norwegian sea, a warm front was passing Nordland, Troms and Finnmark between 00 UTC and 06 UTC on 12. February (Figure 4.2.2) causing gale force winds along the coast and wind directions between southeast and southwest and frontal precipitation. During the forenoon (around 09 UTC), the cold front was passing the region and the wind was veering to a strong westerly flow with showers (CB's) and lightning strikes (marked as green squares in Figure 4.2.3). The strong westerly flow continued for several hours (15-20 hours), and peaked at Langnes late afternoon and early evening on the 12. February. In Figure 4.2.4, a satellite image of the frontal clouds and the accompanied convective activity and clouds (CBs) behind the cold front (west of the frontal clouds) is shown.

The observation data (METAR) from Langnes show a maximum average wind speed of 36 kt and gusting 53 kt from 260 degrees (W). At Kjølen (2600ft) the wind speed was at a maximum 58 kt and gusting 81 kt from 260 degrees (W). The weather observations from the METAR data indicate CB activity and a mix of showers - rain, sleet and hail (SHRA, SHSNRA, SHSNGS). The Terminal Area Forecast (TAF) for Langnes forecasted a maximum of 28035G50KT, heavy CB activity with showers (SHSNRAGS) and risk of thunderstorms (TS). A SIGMET on severe mountain waves (SEV MTW) in the area was issued (Bodø to Varanger) from the surface (SFC) up to FL200.

In Figure 4.2.5 significant weather charts (Met Norway) at 12Z (12. Feb) and 00Z (13. feb) are shown. In the area of interest, MOD/SEV mountain waves (MTW) is expected as well as strong surface winds, CB-activity, and lightning activity.

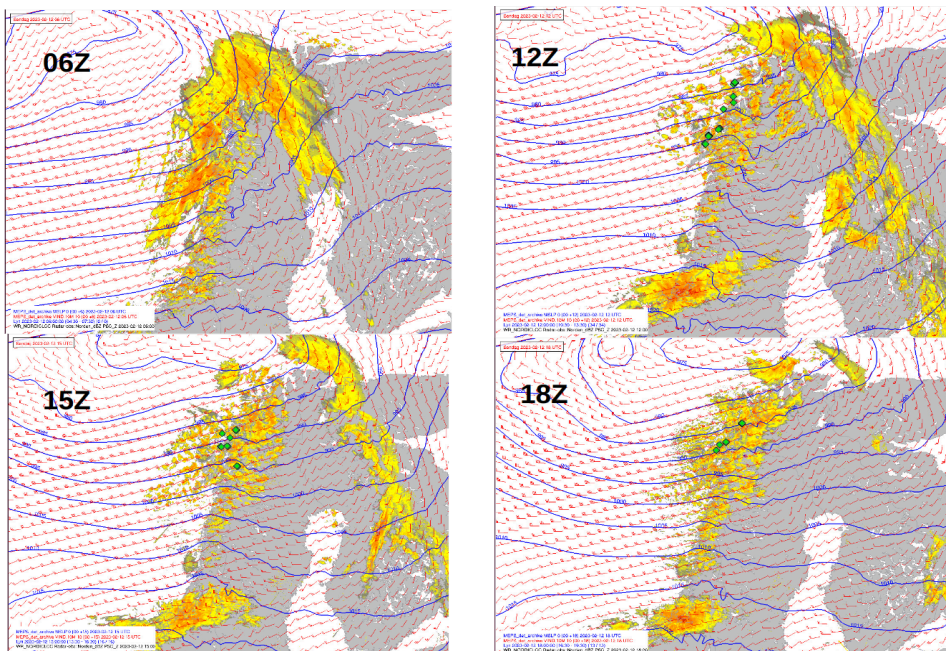


Figure 4.2.3: Radar echo and lightning observations (green points) at 06, 12, 15 and 18 UTC on the 12. February 2023. Source: MET Norway.

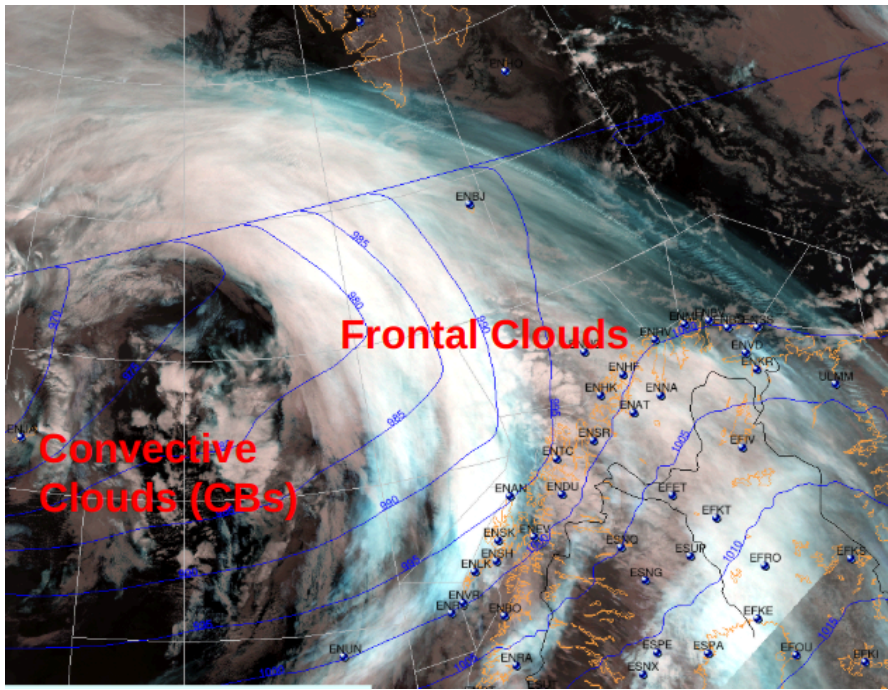


Figure 4.2.4: Satellite image at 04 UTC (12. Feb). Source: MET Norway/NOAA.

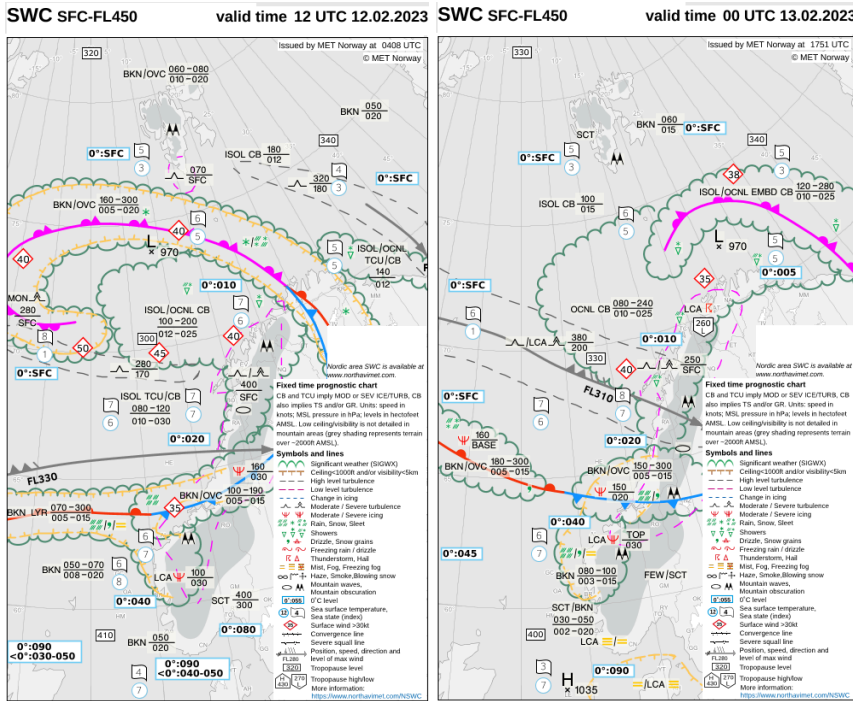


Figure 4.2.5: Significant Weather Charts at 12 UTC (12. Feb) and 00 UTC (13. Feb). Source: Met Norway

4.3 Meteorological parameters

4.3.1 Wind and Turbulence

The main cause for the wind challenges at Langnes during the event, was the strong, westerly flow, continuing for several hours and peaking at Langnes early evening on the 12. February. At Langnes, it was measured a maximum mean wind speed (10 min average) of 36 kt and gusting 53 kt from 260 degrees (W). At Kjølen (2600ft) the wind speed was at a maximum 58 kt and gusting 81 kt from 260 degrees (W).

As mentioned above, several aircraft experienced incidents related to strong winds and wind shear conditions at approach.

A strong westerly wind flow along the coast and into Langnes is rare. Usually the wind is shifted towards the southwest or northwest along the coast during a westerly flow situation. In Table 4.3.1.1 the frequency of wind from a westerly direction and an average wind of more than 17,2 m/s (33.4 kt) is between 0 and 0.1%, hence demonstrating the rareness of such events. The strong westerly flow resulted in challenging crosswind and turbulent conditions in the surrounding areas of Langnes.

Table 4.3.1.1: Frequency distribution of wind measurements (average wind and direction) at Langnes (ENTC) for the winter season (October - March 1993-2023).

Middelvind (m/s) ↑	N	NNØ	NØ	ØNØ	Ø	ØSØ	SØ	SSØ	S	SSV	SV	VSV	V	VNV	NV	NNV	SUM
0,0-0,2																	2,5
0,3-1,5	0,6	1	1,7	2,2	2,7	2,1	2,2	2,1	1,6	0,7	0,5	0,3	0,2	0,1	0,1	0,2	18,5
1,6-3,3	0,6	1,2	1,7	1,6	1	0,6	0,8	1,5	3	1,7	1,8	1,5	0,7	0,2	0,1	0,2	18,1
3,4-5,4	0,7	0,9	0,8	0,4	0,1	0,1	0,1	0,7	6	3,4	2,9	1,4	0,8	0,3	0,2	0,2	19,1
5,5-7,9	0,8	0,4	0,6	0,2	0,1	0	0	0,5	9,4	5,6	1,9	0,5	0,7	0,4	0,3	0,3	21,6
8,0-10,7	0,3	0,1	0,2	0	0	0	0	0,2	5,6	4	1,2	0,3	0,5	0,3	0,2	0,1	13,2
10,8-13,8	0,1	0	0	0	0	0	0	0	1,6	1,3	0,9	0,2	0,3	0,1	0,1	0,1	4,8
13,9-17,1	0	0	0	0	0	0	0	0	0,2	0,2	0,3	0,1	0,1	0	0	0	1
17,2-20,7	0	0	0	0	0	0	0	0	0	0	0	0	0	0	0	0	0,1
20,8-24,4	0	0	0	0	0	0	0	0	0	0	0	0	0	0	0	0	0
24,5-28,4	0	0	0	0	0	0	0	0	0	0	0	0	0	0	0	0	0
28,5-32,6	0	0	0	0	0	0	0	0	0	0	0	0	0	0	0	0	0
>32,6	0	0	0	0	0	0	0	0	0	0	0	0	0	0	0	0	0
SUM	3,1	3,7	4,9	4,4	3,9	2,9	3	5	27,4	17	9,5	4,3	3,4	1,5	1,1	1,1	100

 [Last ned tabell](#)  [Del](#) Rader per side: 25 ▾ 1-14 of 14 < >

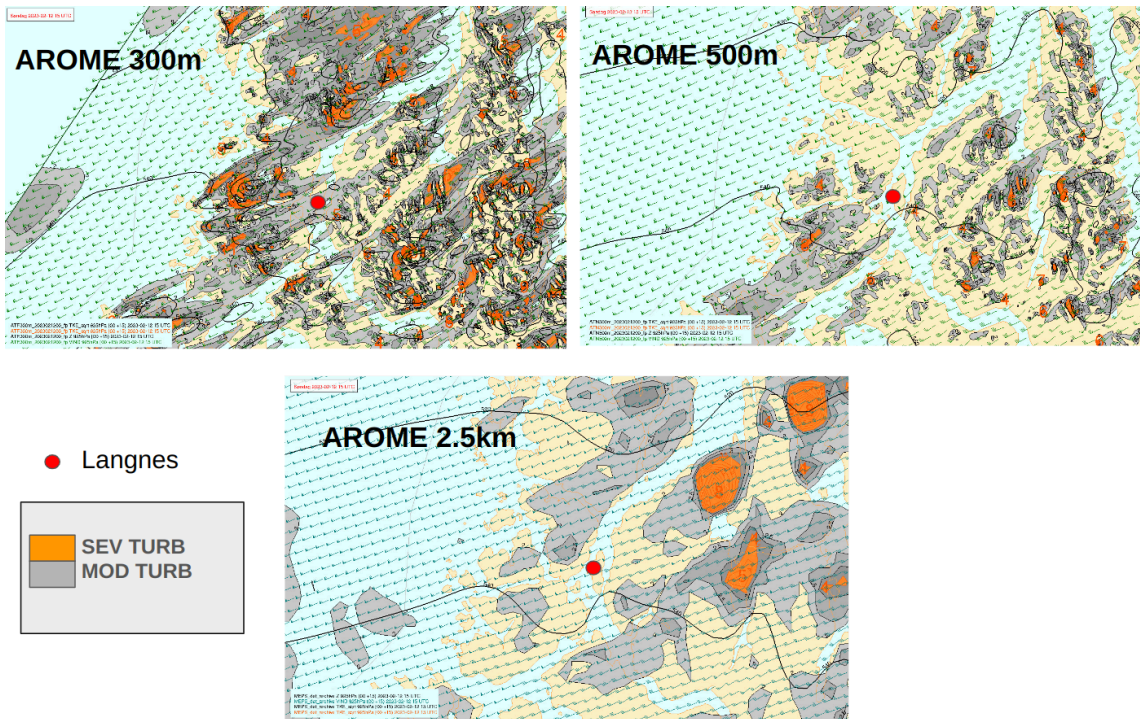


Figure 4.3.1.1: Areas with simulated turbulence ($\text{SQRT}(TKE)$) from the Harmonie-Arome model system with 300m, 500m and 2.5km between each grid point at 15 UTC on the 12. February. Grey areas (MOD TURB), orange areas (SEV TURB).

As a part of this case study, high resolution models alongside the operational model were run for the Troms area in order to analyse if the high resolution models better captured the local turbulence and wind shear conditions in the Langnes area on 12. February. The model configuration is the same in all three cases, except for the model resolution (300m, 500m and 2.5km). The 300m and 500m models are not run on a regular basis due to the needed computing resources, but are used for research purposes and re-runs only. The operational run is in the resolution and many model configuration aspects similar to the CARRA data set applied in this study. All three models show areas with moderate (MOD) and severe (SEV) turbulence (Figure 4.3.1.1). However, the high resolution models, and in particular AROME 300 m, are providing more local details in the turbulence. While all three resolutions do forecast areas with severe and moderate turbulence they do differ in the extent and location of these areas. Without more detailed observations of turbulence it is difficult to evaluate the three forecasts, but the high resolution model runs produce detailed areas of turbulence in a realistic way from what is expected due to the complex terrain in the area.

A SIGMET on severe mountain waves and turbulence (SEV MTW) in the area was issued (Bodø to Varanger) from the surface and up to FL200 on 12. February. One of the main sources used by the operational forecaster to determine whether to issue a SIGMET on turbulence or not is the output from the operational 2.5 km weather forecast model.

4.3.2 Icing

Due to the westerly flow, a forced topographic lifting of moist air masses from the sea, locally resulted in moderate and severe icing conditions, followed by a strong convective activity (CBs) behind the cold front passage.

A moderate icing incident was reported by a DH8 aircraft southwest of Bodø at 19:00 UTC between FL080 and FL100. The model output of LWC (Liquid Water Content) from the operational forecast model indicates moderate and severe icing along a vertical cross section (along the red solid line in Figure 4.3.2.1) in the area. The purple colour shows areas with severe icing conditions, while the orange colour shows areas with moderate icing conditions. At 18 UTC the highest values of LWC (MOD and SEV ICE) seem to be between FL050 and FL 100 over the coastal mountains in Nordland with temperatures around -16 to -6 °C.

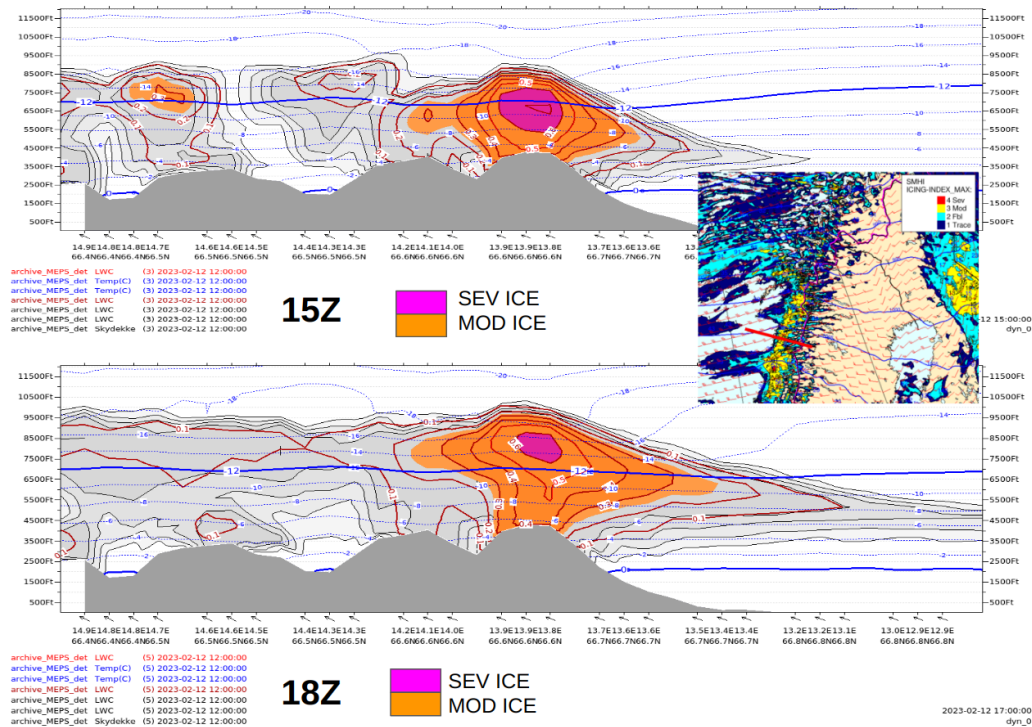


Figure 4.3.2.1: A East-West (E-W) Cross Section (along the red solid line) of the Liquid Water Content (LWC) close to Bodø at 15 and 18Z on the 12. February from the operational model system with 2.5 km horizontal resolution. The purple area indicates SEV ICE conditions, orange area indicates MOD ICE conditions.

As for turbulence, high resolution models alongside the operational model (2.5 km) were analysed for Nordland and Troms for the 12. February case in order to see if the model output from these models described the icing conditions associated with the CBs in the Langnes area in more detail. Figure 4.3.2.2 shows the Icing conditions (LWC and Icing Index) in the Langnes area and a cross section (left hand side in the figures) at 20 UTC from the operational forecasting model AROME 2.5km (top), AROME 500m (middle) and AROME 300m (bottom).

An Airbus 320 aircraft reported (AIREP SPECIAL) SEV ICE at 20:00 UTC 10 NM north of ENTC at 5500 ft. The AROME 300m and 500m models provide a more detailed picture of the icing conditions associated with the CBs than the operational 2.5 km model, in AROME 300m even some patches of SEV ICE (orange/red) are seen. Since CBs are “operating” on a mesoscale, the high resolution models seem to in a better way be able to capturing the icing and LWC pattern within the domain at this resolution.

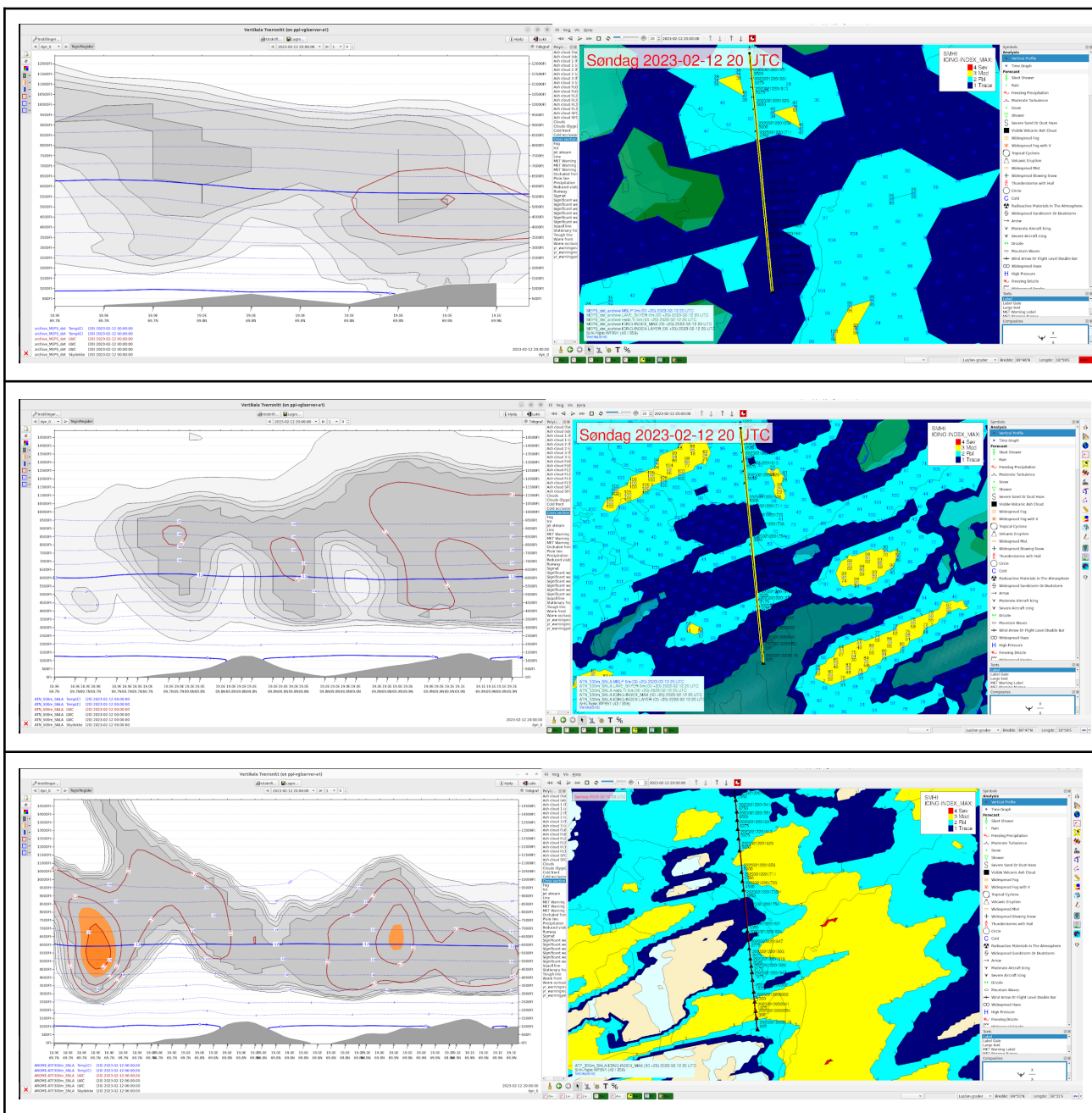


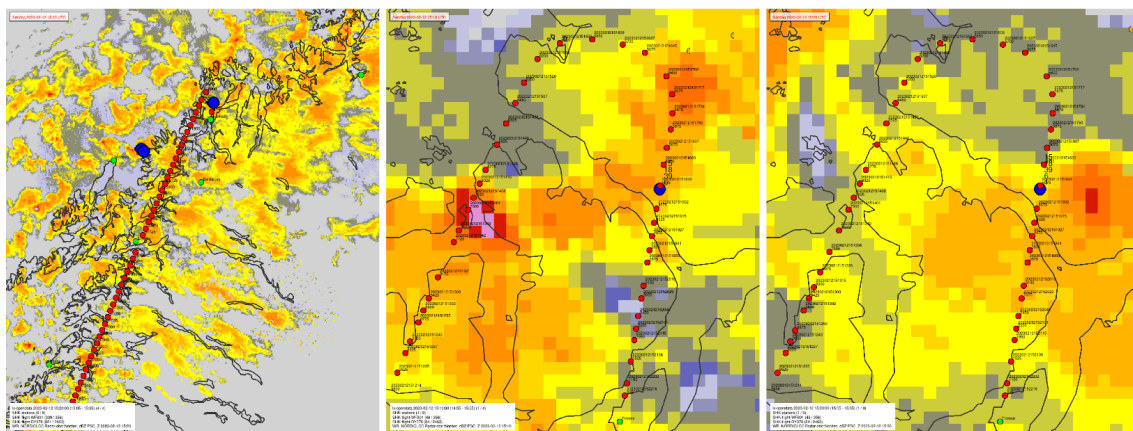
Figure 4.3.2.2: Icing conditions (LWC and Icing Index) from the operational forecast model AROME 2.5km (top), AROME 500m (middle), AROME 300m (bottom) in the Langnes domain and along a Cross Section (ENTC approach) at 20 UTC on the 12. February 2023.

4.3.3 Lightning and CB-activity

During the afternoon on 12. February 2023, two aircraft from Widerøe were struck by lightning and reported severe icing associated with CB clouds. One aircraft from Norwegian was struck by lightning and was warned of a strong windshear just before landing.

Due to the strong westerly flow and the long fetch over the sea, the CB activity was intense in the area during the afternoon and evening. In Figure 4.3.3.1 the approach towards Langnes of a Norwegian aircraft (DY378) is tracked in the map, including the radar image (precipitation intensity) and observed lightning (blue dots). The aircraft reported to be hit by lightning at ~15:20 UTC at the final approach at 4000-5000 ft. An intense CB cell from the radar image at that time (red/purple colour) was moving rapidly eastwards, and the aircraft was most likely struck by lightning from this cell when passing the southernmost part of Ringvassøya, where the track of the flight coincides with an observed lightning.

DY378 12.02.2023 ~1520 UTC



Flight track: red circles
 Observed lightning +- an hour in blue (left) and as lightning symbols in zoom

Observed lightning at day 12, 15.18.39 UTC
 strength 6kA, "cloud-to-cloud" (1), flight level ~ 5000 FT

Figure 4.3.3.1: Track of a Norwegian aircraft (DY378) approaching Langnes (red dots), including the radar image showing the precipitation intensity and observed lightning (blue dots). Airports shown as green circles. Overview plot of Troms/Nordland (left) with radar images valid at 15.10 UTC and zoomed in over the approach to Langnes at 15.10 UTC (mid) and 15.20 UTC (right).

About 30 minutes later, a Widerøe aircraft (WF852) was struck by lightning associated with another intense CB cell almost in the same area (in the fjord between Kvaløya and Ringvassøya) in 4400 FT (Figure 4.3.3.2). Again we find, within the uncertainty of exact location of the observed lightning, a coincidence of the flight track and observed lightning.

WF852 12.02.2023 ~1550 UTC

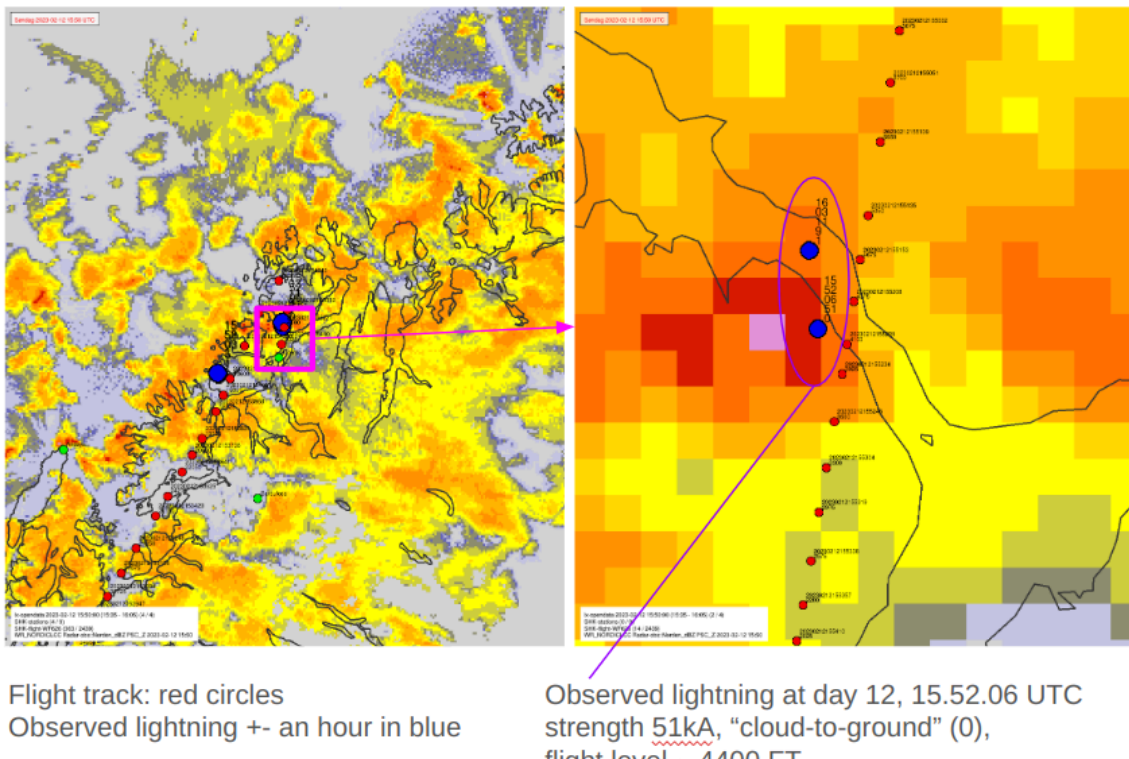


Figure 4.3.3.2: Similar plot as Figure 4.3.3.1, but track of a Widerøe aircraft (WF852) approaching Langnes with radar image valid at 15.50 UTC.

4.4 Similar Historical Events

In order to understand the frequency of events with long lasting and strong westerlies (westerly wind flow) and how rare these events are at Langnes, 'only' eight 'similar' situations since 2006 are found (Table 4.4.1). Note that in this Table only events where the westerly wind (250-290 degrees) is the predominant wind direction are included and with a mean wind speed of more than 35 knots. The two events associated with the strongest westerlies seem to be from November 2010 and December 2013 with wind gusts at Langnes up to 62 knots and with a total duration of 9-12 hours. On 12. February 2023, the maximum wind gust was 53 knots and with a duration of approximately 7 hours.

Table 4.4.1: Summary of eight long-lasting strong westerly events at Langnes between 2007 and 2023 (time period with hourly measurements)

Start	End	Duration	Strongest Average Wind (FF) in knots	Strongest Wind Gust (FG) in knots
19.12.2007 09	19.12.2007 18	9	36	56
01.11.2010 22	02.11.2010 07	9	43	62
03.12.2013 12	03.12.2013 24	12	44	61
09.02.2015 15	10.02.2015 10	4, 5 and 5	38	51
12.02.2017 18	13.02.2017 17	4 and 6	37	51
06.11.2020 14	06.11.2020 21	7	38	53
23.03.2021 13	23.03.2021 19	6	37	49
12.02.2023 14	12.02.2023 21	7	38	53

The low pressure tracks of the eight events are shown in Figure 4.4.1. The position of the low pressure centre is shown as red squares every 6. hours, starting at -36h, ending at +36h. The red 'L' represents the low pressure centre at 0h - at the time of the peak of the event. In most of the cases, the low pressure systems are developing and intensifying between Iceland and Greenland (Denmark Strait), moving

east-northeastwards, passing close to Jan Mayen and peaking between Vest-Finnmark and Svalbard at time 0h. These events are often accompanied by a stationary high pressure area over the European Continent, forcing the low pressure systems to strengthen and move north- and northeastwards of the high pressure area. The event from 12. February 2023 is following this pattern. The low pressure system is developing and intensifying in the Denmark Strait at -36h, moving east-northeastwards, setting up a strong and long lasting westerly fetch towards Northern Norway.

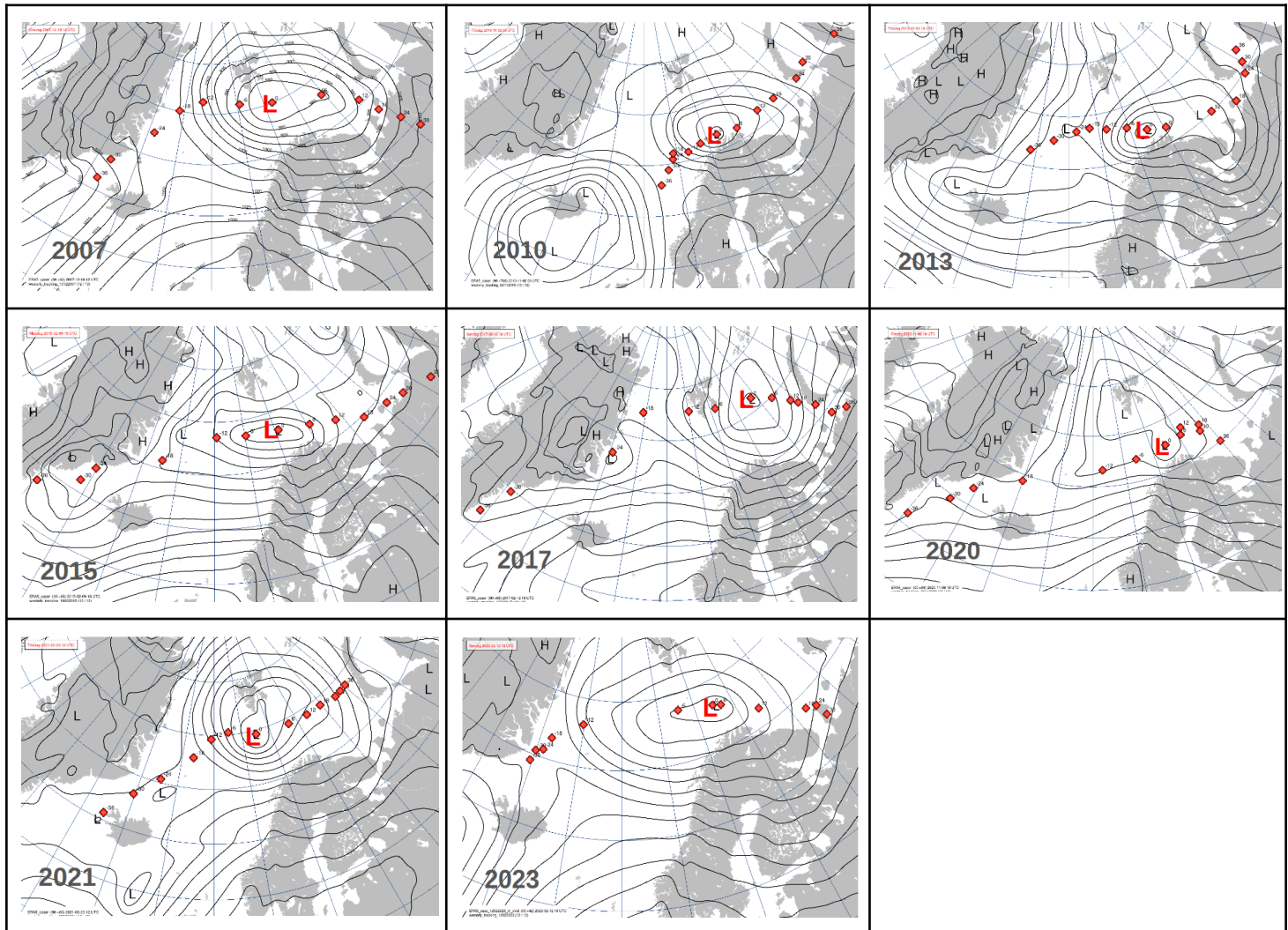


Figure 4.4.1: Low Pressure System Tracking of similar situations with strong westerlies at Langnes, from 2007, 2010, 2013, 2015, 2017, 2020, 2021 and 2023. Red square represents the low pressure centre location every 6. hours (-36h, 30h,...0h, +6h,...+36h). Red 'L' represents the Low Pressure Centre at 0h.

As shown later in the detailed weather analysis at Tromsø/Langnes (section 6.3), the frequency of a strong westerly cross-wind component at Langnes shows a large interannual variability of between 0.2% to 1.8% per year, and with no clear trend.

4.5 Summary of the 12. February 2023 case

On the 12. February, an intense low pressure system located west and northwest of Troms and a zonal, stationary high pressure system in the northwestern parts of the Continent set up a strong and long westerly fetch (wind flow) over the ocean towards Nordland and Troms. This westerly flow was accompanied by challenging crosswind and turbulent conditions at Langnes, as well as forced topographic lifting of humid air masses from the sea with strong convective activity (CBs) as a result, including icing and lightning strikes on aircraft near Langnes. A 'direct' westerly wind flow at the coast in this area is quite rare, and only 8 similar long-lasting situations during the last 16 years are found in the observational record.

5. Low Pressure Systems and Storm Tracks

Summary; *It is likely that Northern Norway and Svalbard will experience slightly less large-scale low pressure system activity, in particular in winter, in the future than during present day conditions, but the uncertainties about future scenarios are high. For recent historical periods, less storm-track activity was found during DJF for 2008-2023 when compared to 1991-2006. This can be attributed to inherent variability within the climate system and/or ongoing climate change. The results presented in this report are in agreement with other studies on historical and future changes in storm tracks.*

Why are synoptic low pressure systems and storm track activity important for aviation weather? The location and intensity of low pressure systems impacts aviation weather in Northern Norway during winter. In general, intense low pressure systems are often accompanied by strong winds and heavy precipitation, making the runway conditions and operations challenging. An onshore large-scale flow of humid air lifted towards the mountainous Norwegian coast has also the potential to produce large amounts of supercooled liquid water, resulting in aircraft icing conditions. Strong flow over the complex topography, again set-up by a low pressure system, can also create conditions favourable for turbulence. Challenging weather conditions are also experienced during intense convective showers, typically in the north- and northwesterly flow behind low pressure systems. These convective showers may also generate lightning, which also is associated with intense winter low pressure systems.

All these severe aviation weather conditions are analysed and discussed in more detail in section 7. However, a key to explaining historical changes and to providing estimates of future changes, is knowledge about changes in the storm tracks. Storm tracks can be generally defined as regions where the frequency of low-pressure systems, or baroclinic¹ waves are high relative to the surrounding regions. Such regions are found at mid- and high latitudes in both hemispheres, over the North Atlantic, North Pacific, and Southern Ocean. Here, we focus on the North Atlantic storm track, which stretches from the east coast of North America and north-eastward up to the Barents Sea.

Storm track activity climatology, recent changes and future potential changes. Here, we examine the storm tracks in terms of storm-track activity, a metric that combines changes in the intensity and frequency of baroclinic waves (see method below). Present-day climatology of storm track activity from ERA5 (Hersbach et al.

¹ Atmospheric baroclinicity refers to the situation where there is a strong temperature difference across a horizontal region of the atmosphere. This temperature contrast causes variations in air pressure and density, which in turn create wind and drive weather systems. Essentially, baroclinic conditions occur when warm and cold air masses meet, leading to the development of storms, cyclones, and other dynamic weather patterns.

2022), present-day changes for the last 30 years in ERA5, and projected future changes towards the end of the century under the Shared Socioeconomic Pathway corresponding to an increased radiative forcing of 8.5 W/m² by the end of the 21st Century (SSP5-8.5; O’Niell et al. 2016) scenario compared with the CMIP6 historical run (Eyring et al. 2016) are shown in Figure 5.1 to 5.4 for winter (DJF), spring (MAM), summer (JJA) and autumn (SON), respectively.

The highest activity during DJF is found on the east coast of North America where a majority of the low pressure systems are typically initially developing, further moving north eastwards and intensifying towards Iceland and the Barents sea region, indicated by larger storm track activity (Figure 5.1a). The main differences between the second and first half of the 1991-2023 period (Figure 5.1b) is the reduced activity north of 70°N in the European Arctic with the largest reduction centred around Svalbard. At the same time increased activity is seen south of 60°N over the North Atlantic and over south-west Europe. These changes are not significant for all regions, but they are significant around Svalbard and for the region around Spain. The mean future response in CMIP6 simulations (Figure 5.1c) shows a similar pattern for the difference between the end of the century (2071-2100) and the historical period of 1985-2014. These projected future changes are supported by the majority of the CMIP6 models (black dots marks where more than 60% of the models agree on the sign of the changes). Hence, a tendency of less storm track activity in Northern Norway, but an increase in storm track activity further south, is seen both in recent historical changes and in the future climate model scenarios.

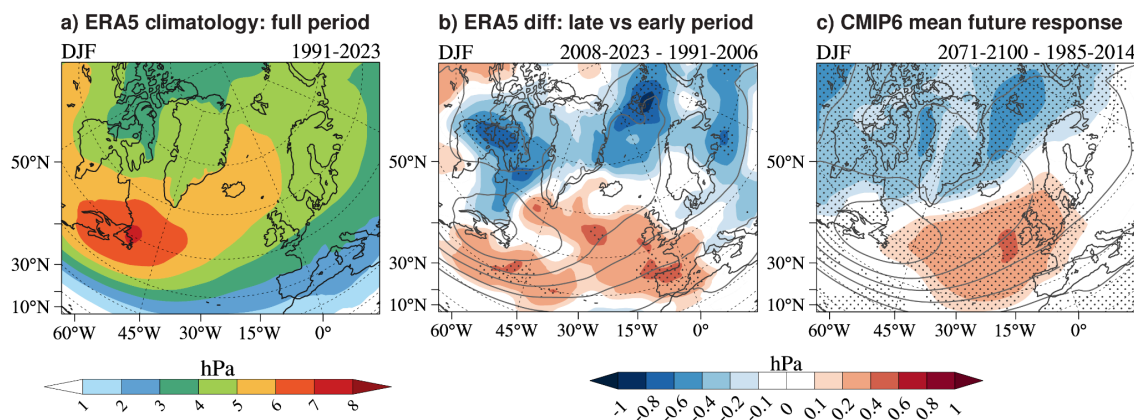


Figure 5.1 Storm track activity and changes in storm track activity during December, January and February (DJF). a) Climatology of storm track activity 1991-2023 (ERA5). Higher values indicate more storm track activity. b) Changes in storm track activity between the two historical periods 1991-2006 to 2008-2023 (ERA5). Significant changes (90% confidence interval) are marked with black dots. Red colours indicate increased storm activity in the last period, blue colours indicate less storm activity. c) Changes in storm track activity between a historical period, 1985-2014, and end of the

century, 2071-2100 for the multi-model mean of 29 CMIP6 models under scenario SSP5-8.5. Regions where more than 60% of the CMIP6 climate models agree on the sign of the change are marked with black dots. Red colours indicate increased storm activity in the last period, blue colours indicate less storm activity.

The spatial pattern of the climatology in MAM is similar to during DJF, but the storm track activity is weaker (Figure 5.2a). The changes over 1991-2023 indicate an increase in storm track activity over Norway (except for in the south east), however opposite to DJF these differences are not significant (Figure 5.2b). In general, changes in MAM are only significant over a few small areas on the east coast of North America. The projected future changes (Figure 5.2c) suggest a similar pattern as DJF with a decrease in the storm track activity in the Barents Sea and Svalbard region, but with smaller changes than DJF. This projected future reduction of storm track activity in MAM is supported by the majority of the CMIP6 models (Figure 5.2c).

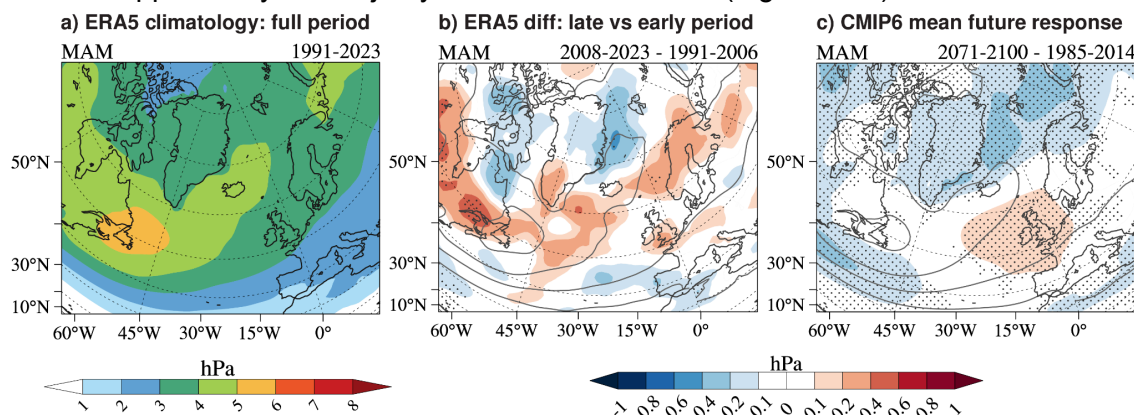


Figure 5.2 Same as Figure 5.1, but for March, April and May (MAM).

During summer (JJA) the storm track activity is further reduced in amplitude with a more zonal, that is, more west-east, orientation (Figure 5.3a). Only small changes are seen for the 1991-2023 period in our area of interest, where the only significant change is a small increase in storm track activity in the northern part of the Barents Sea, east of Svalbard (Figure 5.3b). Projected future changes are characterised by a small reduction in the storm track activity (Figure 5.3c).

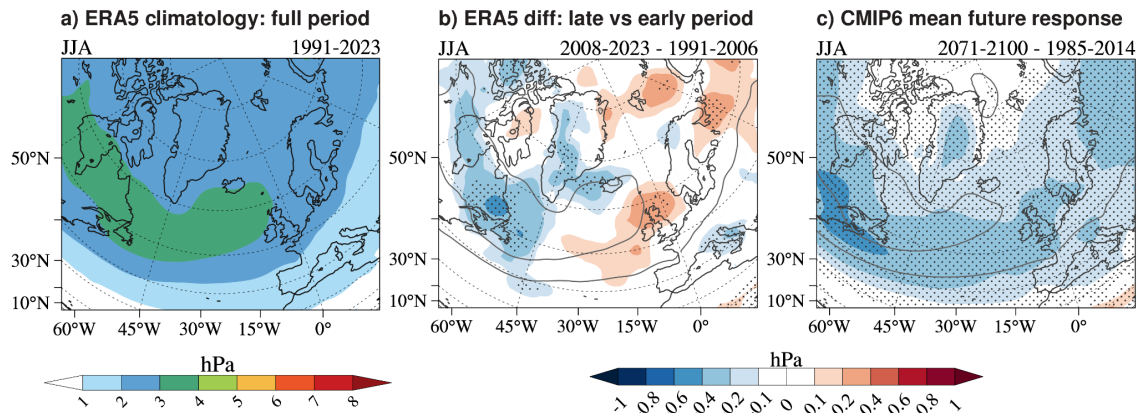


Figure 5.3 Same as Figure 5.1, but for June, July and August (JJA).

In autumn, the storm track activity increases again (Figure 5.4a), but changes are small, both during the 1991-2023 period (Figure 5.4b), and in the projected future mean response (Figure 5.4c). In the latter case, Norway and the surrounding ocean regions exhibit weak changes and poor model consensus, as indicated by the lack of black dots; this is caused by discrepancies between the projected future response for the individual models, with several models showing an increase and several showing a decrease. Hence, there is large uncertainty around the future changes in SON for this region.

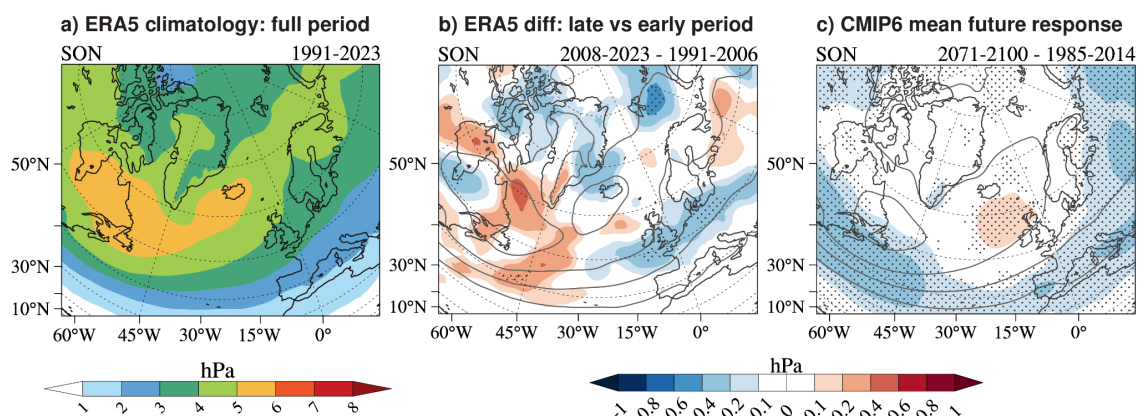


Figure 5.4 Same as Figure 5.1, but for September, October and November (SON).

What is the role of inter-annual and decadal variability? Feser et al. (2021) investigated changes in extratropical windstorms over the North Atlantic in observations, reanalysis datasets and a hindcast from a high-resolution atmospheric climate model. The general patterns are similar across the different data sets and show distinct decadal variability. For example, the yearly minimum pressure shows an increase until the mid 1960s, before a decrease is seen until reaching a minimum around 1990, before it again increases until around 2005 (their Figure 9a). Changes on

relatively short time scales, e.g. over the 1991–2023 period can therefore be impacted by the phase of these decadal variations. An example of this is that Wickström et al. (2019) found slightly different results (increased activity around Svalbard and reduced activity in the southeastern part of the Barents Sea) compared to our findings, mainly due to differences in the selection of periods (1979–2016). Schurer et al (2023) also noted that the observed multi-decadal variability is larger than what is simulated in the CMIP6 models. The role of decadal variability in the future scenarios are therefore somewhat uncertain.

To better our understanding of how results based on the two 15-year periods that were selected for studying recent historical changes in aviation weather conditions fit into the bigger picture, we examine the role of decadal and inter-annual variability for a region that exactly matches our particular area of interest. To this end, we expand upon the work of Feser et al. (2021), performing a similar analysis, but basing it only on ERA5, but including more recent data. The result is presented in Figure 5.5, which shows a time series for the lowest Mean Sea Level Pressure (MSLP) values (average of yearly 1%-tile of MSLP) for the area 0–25°E and 66–75°N during October to April. The 5-year running mean shows some of the same trends as Feser et al (2021) did for the North Atlantic with high MSLP around 1965, low MSLP values for 1980–2000 and then increasing values again. This is consistent with our findings based on computing differences between 1991–2006 and 2008–2023 (third and fourth horizontal dashed black lines from the left), the former period is clearly characterised by lower MSLP than the latter. At the same time, out of the four 15-year long periods that are highlighted in the Figure, 1991–2006 has the lowest MSLP on average (compare the four horizontal dashed black lines), that is, both the two earlier periods and the latest period are characterised by higher MSLP. The highest MSLP is seen for the earliest period, 1960–1975, meaning that even the most recent period has a 1%-tile MSLP which is lower. Hence, the time period shown in Figure 5.5 is characterised by pronounced decadal variability, and the changes we find when comparing 1990–2006 to 2008–2023 are likely to at least be partly explained by this variability. Even if we do see some slowly varying trend in the running means for different time periods, high interannual variability dominates over the more slowly varying underlying decadal trends, indicating any near-future projections for the next few years would be dominated by this variability.

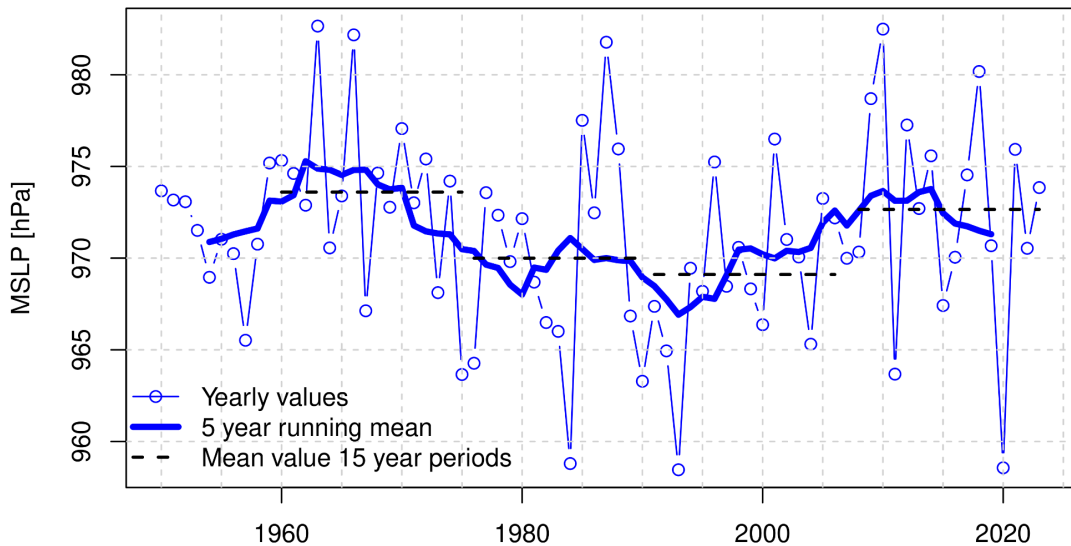


Figure 5.5 Time series of yearly 1%-tile MSLP (for ONDJFMA) averaged over 0–25°E and 66–75°N. Yearly values are shown in thin blue line and circles, and a 5 year running mean in thicker blue line. The thick dashed black horizontal lines show the mean values for four different 15-year periods: 1960–1975, 1976–1990, 1991–2006, and 2008–2023; note that the latter two periods are the periods we use for studying recent historical changes in aviation weather conditions. Data is from ERA5.

How do the presented results fit with the scientific literature? In the IPCC Sixth Assessment Report, The Physical Science Basis (IPCC, 2021) it is stated that there is low confidence in projected changes in the North Atlantic storm tracks. However, it is indicated that the density of winter storms is projected to decline with a few percent in future projections. Furthermore, the number of dynamical intense cyclones will also decrease in the Northern Hemisphere (NH) winter (but with geographical differences), while the number of storms with extreme precipitation will increase with global warming. Furthermore, Harvey et al (2020) evaluated the ability of several generations of climate models in representing NH storm tracks with a similar method as applied in our study. The latest generation of climate models (CMIP6) shows a much better representation of storm tracks than previous generations. However, the spatial pattern of future changes is similar across the different generations of CMIP, but larger changes are found for CMIP6. For our area of interest they found a possible future reduction in storm tracks in Northern Norway and an increase over southwest Europe during DJF, and a general mid-latitude decrease in JJA. These findings are very similar to what is presented for the mean future response in our Figure 5.1 and 5.3.

Priestly and Catto (2022) also investigated the response in CMIP6, but with a different approach. They separated between the changes in the storm track density, e.g. the number of low pressure systems, and the intensity of the low pressure systems. This was done under four different climate scenarios and for winter (DJF) and summer

(JJA). Also here a reduction of storm track density was found for our areas of interest and explained by a reduced lower tropospheric baroclinicity (reduced temperature difference between higher and lower latitudes) due to the polar amplification of global warming. However, they also investigated the change in intensity and found that the most extreme cyclones in the NH will have higher intensities in the future DJF (a small weakening during JJA), but did not distinguish this between different NH regions. The response was more pronounced for the high-end future scenarios (with stronger future warming). The general spatial patterns found in the results presented here (Figure 5.1-5.4), in AR6, in Harvey et al (2020) and by Priestly and Catto (2021) is further supported by Ye et al (2024) for a large ensemble of climate simulations for a climate change of 2C and substantial Arctic sea ice loss.

It should be noted that changes in future storm track activity is uncertain and that uncertainties are related to multiple aspects, e.g. in the exact geographical patterns, on change in intensity, related to the actual amount of future (limitations) in greenhouse gases and in the role of decadal variability which impact the dynamical response of the climate system. Future changes in the North-Atlantic storm track are moreover affected by the tug-of-war different changes that have opposing influence on the storm tracks, like Arctic warming, which reduces the low-level equator-to-pole temperature gradient and hence low-level baroclinicity, and tropical upper-level warming, which increases the high-level equator-to-pole temperature gradient and baroclinicity (e.g. Shaw et al. 2016). In addition, the transition seasons (autumn and spring) are less studied than winter and summer.

Method: Daily Sea level Pressure from reanalysis and climate models is (bandpass-)filtered in time, retraining fluctuations corresponding to frequencies of 2.5-6 days (e.g. Blackmon et al. 1977). Storm-track activity is then represented by the variability (standard deviation) of the bandpass-filtered field. Hence, both low and high pressure systems contribute to the activity, but it is dominated by low pressure systems. This is a similar method as applied by Harvey et al (2020). For the historical changes during the 1991–2023 period, significance is computed based on the seasonal storm-track activity values using a two-sided T-test. For the future changes, we examine results from a multi-model ensemble from CMIP6 (see section 2.6 on the CMIP6 data set). This allows us to assess the robustness of the results in terms of model consensus, that is, to what extent the models agree on the response. In Figures 5.1–5.4, we quantify the model consensus by counting the number of models with the same sign as the ensemble mean changes.

6. Meteorological Aerodrome Observations and Trends

6.1 Introduction

This analysis uses hourly (SYNOP) or half hourly (METAR) observations from the selected airports for the period 1 October to 30 April for the years 2006 to 2024. 2006 means the period 1 October 2005 to 30 April 2006.

The analysis covers what we can call the “winter months” from October to April. One might suspect that during this period there exists a relationship between average sea level air pressure and average mean wind speed, because high-pressure weather systems give calm weather, while frequent visits of low pressure systems will give higher wind speed.

Figure 6.1.1, which uses Tromsø - Langnes as example, shows that such a relationship actually exists: the regression line indicates that wind speed increases with falling air pressure.

CORRELATION BETWEEN MEAN SEA LEVEL PRESSURE AND MEAN WIND SPEED

Tromsø - Langnes October 2005 to April 2024

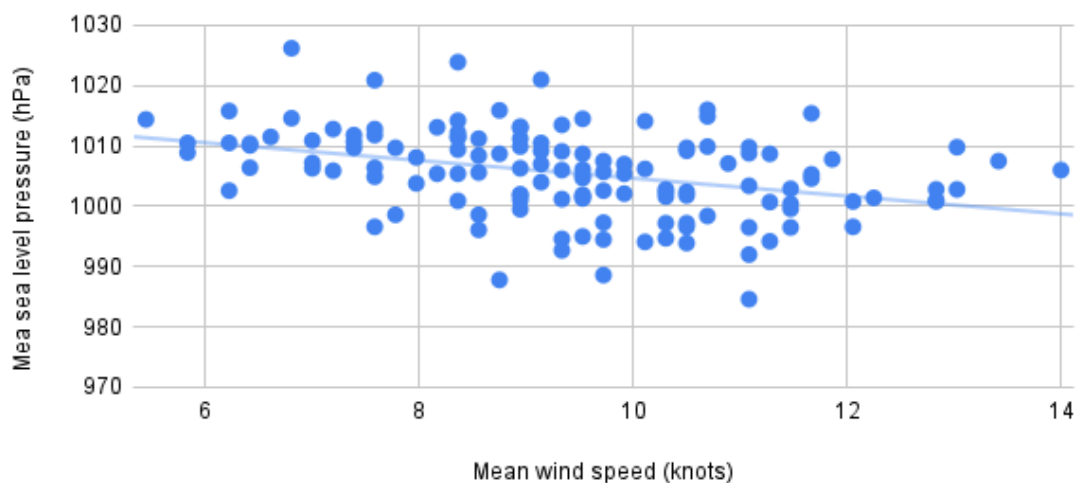


Figure 6.1.1. A plot showing monthly mean wind speed against mean sea level pressure.

Furthermore we can also expect that there is a relationship between air pressure and temperature, because high pressure gives fair weather which, in winter, also will give low temperatures.

6.2 Bodø airport

6.2.1 Main findings

The analysis of hourly wind speed observations from 2005 to 2024 for the seven month period October to April shows that the annual frequency of both southeasterly and northwesterly crosswind components of 20 knots or more varies from around 2 to 8 percent. Because the wind measurements were moved from the western to the eastern part of the airport in 2018, the trendlines are only computed for the years 2006 to 2018. The trendline for northwesterly wind shows a negative trend, while the trendline for southeasterly wind is almost flat. For southeasterly and northwesterly crosswind components of 35 knots or more the annual frequency is typically less than 1 percent, but southeasterly crosswind can sometimes occur for several hours, e.g. during the extreme weather event *Narve* in January 2006. The trend for the 99 percentile value, i.e. the value for the 1 percent highest wind gust each year, shows a *slightly decreasing* trend. Freezing precipitation occurs less than 0.5 % of the time, but the trend line shows a slightly increasing trend, probably because higher winter temperatures also will give more occurrences of freezing precipitation.

6.2.2 Location

Bodø airport is situated near the coast, north of Saltfjorden. See figure 6.2.2.1. The runway is oriented in the direction 07/25, i.e. 070/250 degrees. Consequently, winds from 160 and 340 degrees will result in crosswinds at the airport.



Figure 6.2.2.1. Bodø airport is located near the coast, north of Saltfjorden. Source: The Norwegian Mapping Authority

6.2.3 Wind conditions

6.2.3.1 Mean wind speed

Bodø airport began weather observations in 1954. Hourly measurements of mean wind speed, strongest mean wind in the last hour, and strongest 3-second wind gusts during the last hour started in September 2005. These wind measurements have been used in the analysis. In October 2018 the hourly wind observations were moved from the western to the eastern part of the airport, because of technical issues. The METAR observations were still taken at the western site, where the wind typically is 2-3 knots higher.

Figure 6.2.3.1.1 shows the average mean wind speed at Bodø airport over the seven-month period from October to April for the years 2005 to 2024. The year indications on the x-axis represent the end year of each period, so 2006 indicates the period from October 2005 to April 2006. The average mean wind speed varies around 15 knots. A trendline has been added, showing a slightly increasing trend.

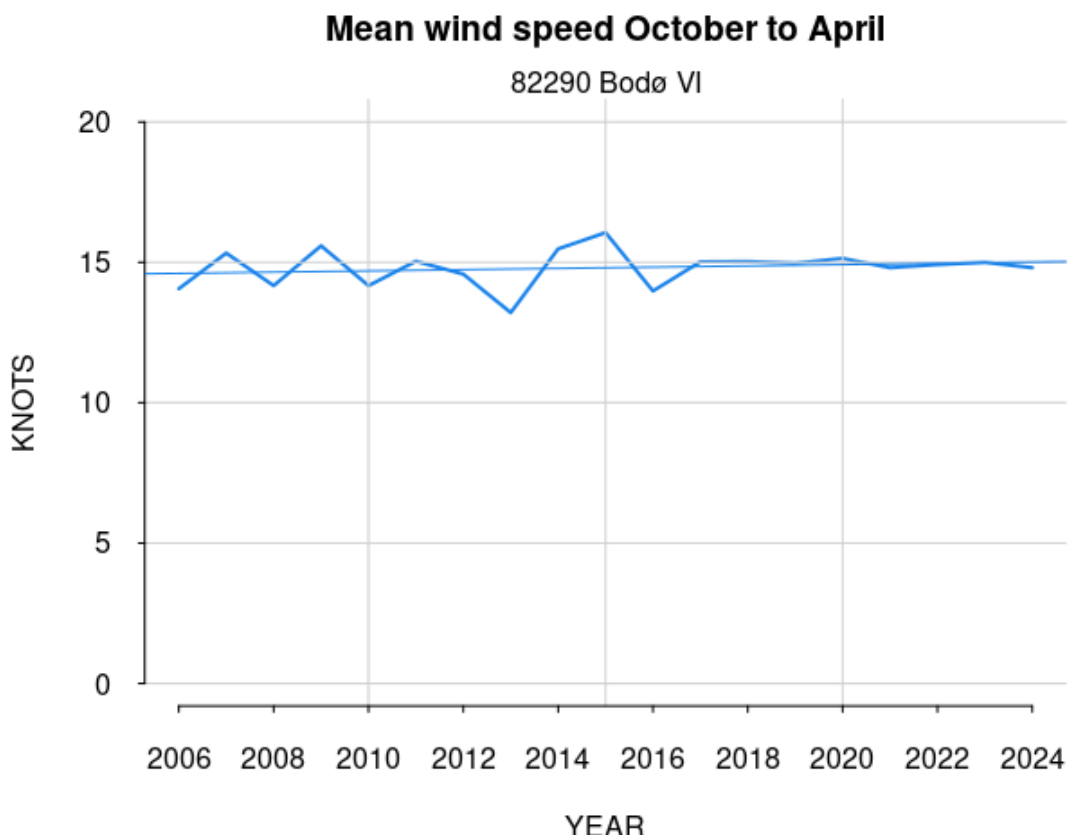
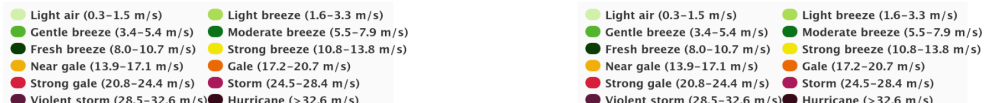
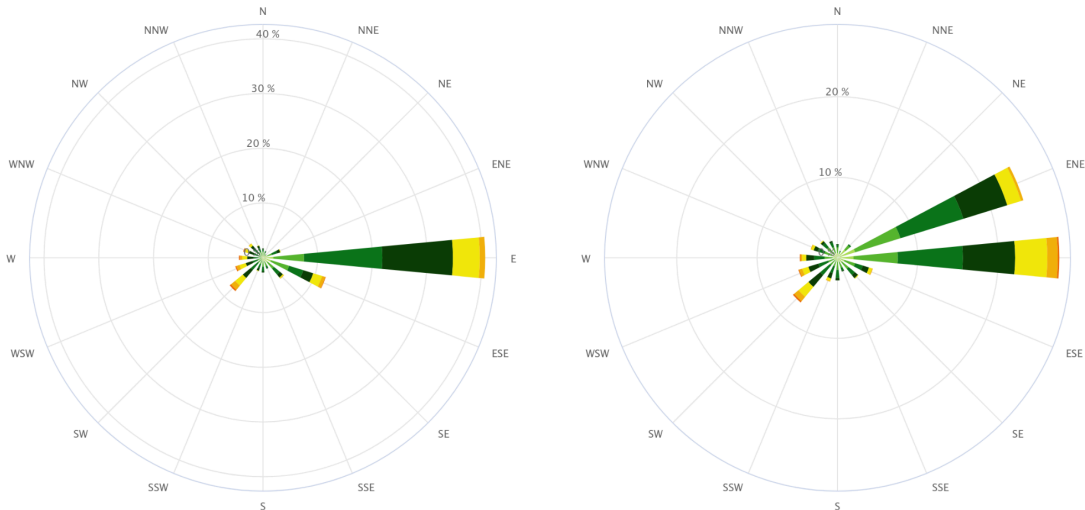


Figure 6.2.3.1.1. Average mean wind speed during the period from October to April.

6.2.3.2 Wind roses

Figure 6.2.3.2.1 shows wind roses for Bodø airport for the two periods October 2005 to April 2014 and October 2014 to April 2024. Comparing the two periods, we clearly see the dominance of easterly winds in Bodø. But in the first period wind from E and SE occurs 53 % of the time, while in the period 2005-2014 wind from E and NE have a frequency of 52 %. Wind from E has reduced the frequency between the two periods from 41 % to 28 % and wind from SE from 12 % to 5 %. Wind from NE has increased the frequency from 3 % to 24 %.



Highcharts.com

Highcharts.com

Figure 6.2.3.2.1 Wind roses for the period from October to April for the years 2005 to 2014 (left) and 2014 to 2024 (right). Wind speed in m/s.

6.2.3.3 Differences in wind in a mild and a cold winter month

As mentioned in the introduction to this chapter, there exists a relationship between a mild winter month and high wind speed, and a cold winter month and weaker winds. Therefore, it is interesting to compare the wind roses for Bodø in a mild and a cold winter month. February 2007 is one of the coldest winter months in Bodø in the period 2005–2024, while February 2014 is one of the mildest. Figure 6.2.3.3.1 shows the wind roses for these two months, with 2007 on the left and 2014 on the right. The average wind speed was 6 knots and 13 knots, respectively.

The easterly winds are dominating in both months, but in the cold February 2007 wind from ENE occurred more than 10 % of the time, while in the February 2014 mild winds from SW had a frequency of more than 5 %. Winds from SE and ESE occur more frequently in a mild than in a cold winter month. As the runway at Bodø is 070/250 degrees, a higher frequency of strong SW wind will not contribute to more occurrences of crosswind, while higher frequencies of strong ESE and SE winds will.

Wind Rose for Bodø VI (SN82290) in period; 2.2007–2.2007.
Calm (0.0–0.2 m/s) = 0 %

Wind Rose for Bodø VI (SN82290) in period; 2.2014–2.2014.
Calm (0.0–0.2 m/s) = 0.2 %

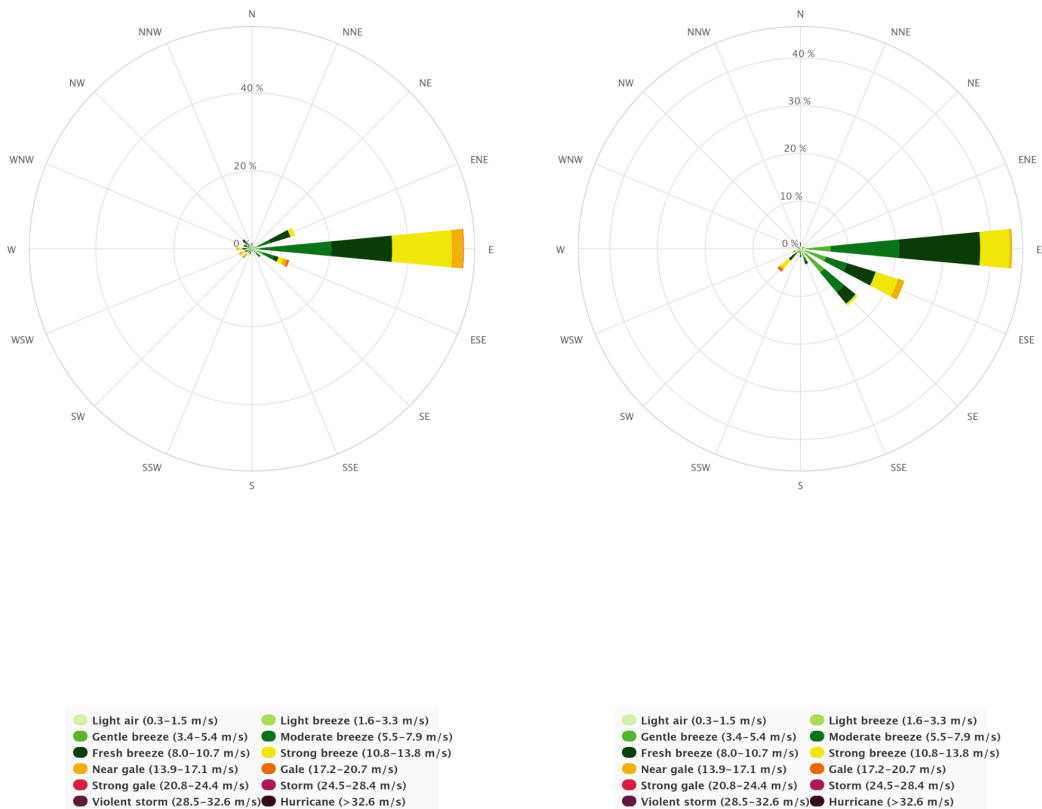


Figure 6.2.3.3.1 Wind roses in the cold February 2007 (left) and the mild February 2014 (right).

6.2.3.4 Wind gusts

The terrain near an airport influences the wind locally, creating wind conditions that will be typical for the various wind directions experienced at the airport.

One way to assess these local conditions is to observe how the gust factor changes with wind direction. The gust factor is defined as FG_1/FX_1 , where FG_1 is the strongest 3-second wind gust in the last hour and FX_1 is the strongest mean wind in the last hour. At weather stations with relatively flat and uniform terrain around the station, the gust factor typically lies around 1.2. In highly rugged terrain, wind gusts can be more than double the mean wind speed.

Figure 6.2.3.4.1 shows the average gust factor for each 10th degree, deca-degree, at Bodø for the months from October to April throughout the measurement period from 2005 to 2024. Wind from the north has the highest gust factor, around 1.5, while wind from the east has the lowest, around 1.25. Of particular interest is wind from the crosswind directions, 160 and 340 degrees, both between 1.4 and 1.5.

GUST FACTOR PER DECA-DEGREE 82290 BODØ VI 2005-2024

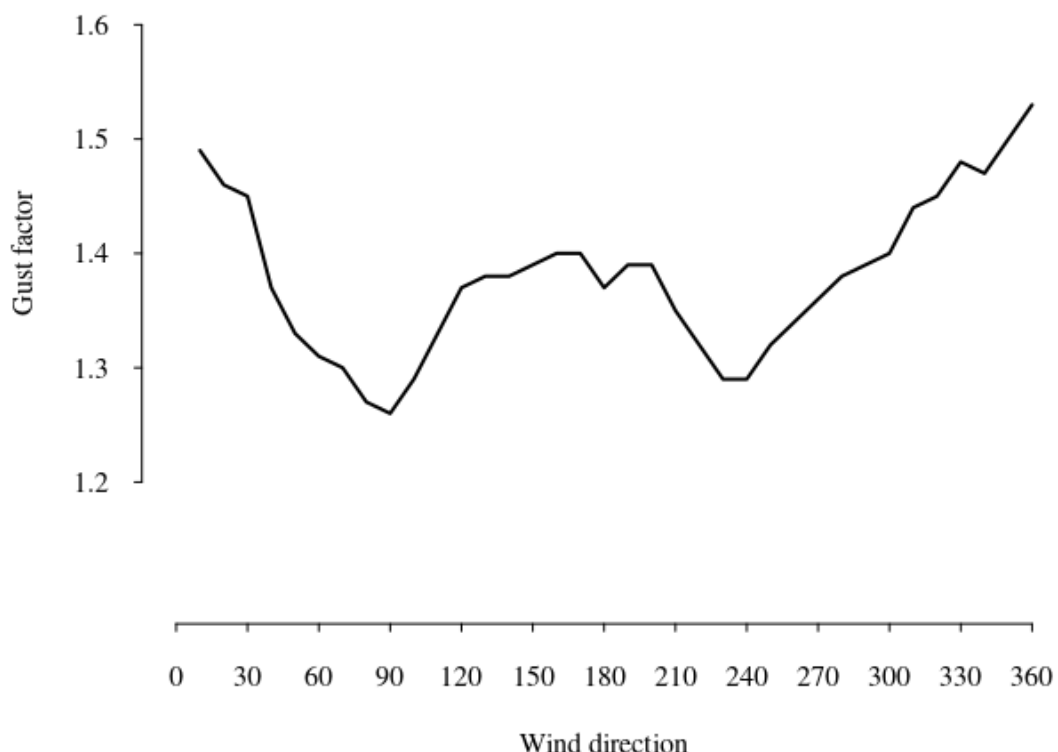


Figure 6.2.3.4.1. Gust factor per deca-degree at Bodø airport 2005-2024.

It is also interesting to examine the absolute strength of wind gusts that can occur with different wind directions. In Figure 6.2.3.4.2, both the average of the 25 strongest wind gusts and the single strongest wind gust recorded for each deca-degree are plotted. The strongest wind gust recorded at Bodø airport in the period 2005-2024 is 73 knots and was registered 26 March 2019 with wind from 260 degrees.

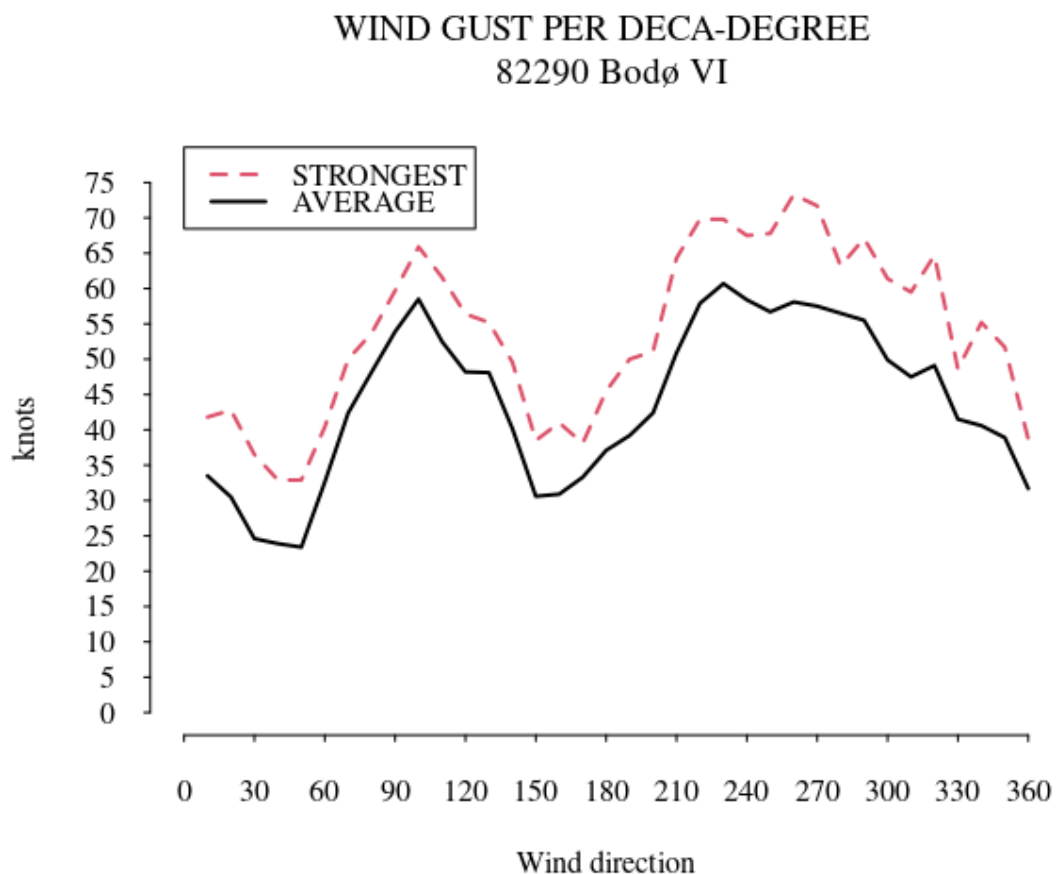


Figure 6.2.3.4.2. Strongest wind gusts and the average of the 25 strongest gusts per deca-degree at Bodø airport 2005-2024.

6.2.3.5 Crosswinds

Crosswinds at Bodø airport are, as mentioned earlier, from 160 and 340 degrees. Neither wind direction occurs often in Bodø. In figure 6.2.3.4.2 we see that wind from 340 degrees has a higher average and also a higher strongest recorded gust.

But strong wind from other directions can also give significant crosswind components. Table 6.2.3.5.1 shows the monthly frequencies of a crosswind component of more than 20 and 35 knots respectively. A 160 degrees wind gust of 30 knots, gives a

southeasterly component of 30 knots, while at 190 degrees wind gust of 30 knots, gives a southeasterly component of 26 knots, thus contributing to the total frequency. All strong winds from 70 and 250 degrees, will not contribute to a crosswind component at all.

Table 6.2.3.5.1 shows the monthly frequency of wind giving a crosswind component of 20 or 35 knots or more. In the period November to March, crosswinds from southeast are more frequent than northwesterly crosswinds, while in October and April crosswinds from northwest occur more often. Crosswinds above 35 occur usually well below 1 percent, but the high figure for southeasterly crosswinds in January, 0.7 %, is mainly due to the extreme weather event *Narve* in 2006. The synoptic situation was the same for several days giving strong southerly or southeasterly wind in Northern Norway.

Table 6.2.3.5.1. Monthly frequencies of crosswind components of 20 or 35 knots or more at Bodø airport

MONTH	NW >=20 knots	SE>=20 knots	NW>=35 knots	SE>=35 knots
OCTOBER	4.3 %	3.3 %	0.2 %	0.1 %
NOVEMBER	3.9 %	4.7 %	0.2 %	0.1 %
DECEMBER	4.5 %	6.5 %	0.4 %	0.1 %
JANUARY	3.6 %	8.7 %	0.3 %	0.7 %
FEBRUARY	3.9 %	5.8 %	0.4 %	0.1 %
MARCH	4.9 %	5.5 %	0.2 %	0.1 %
APRIL	3.0 %	2.1 %	0.2 %	0.0 %
TOTAL	4.0 %	5.2 %	0.3 %	0.2 %

6.2.3.6 Trends for crosswind

For all wind observations, crosswind components have been calculated with respect to the two directions 160 and 340 degrees. Then the frequency of values of more than 20 and 35 knots are calculated. These figures are shown in figure 6.2.3.6.1 and 6.2.3.6.2, respectively. Because the wind measurements were moved from the western part to the eastern part of the airport in October 2018, only the period 2006 to 2018 is included. The figure shows an almost flat trend for southeasterly crosswind of 20 knots or more, and a decreasing trend line for northwesterly crosswind of 20 knots or more.

For crosswinds above 35 knots, the trendlines for both northwesterly and southeasterly directions are decreasing.

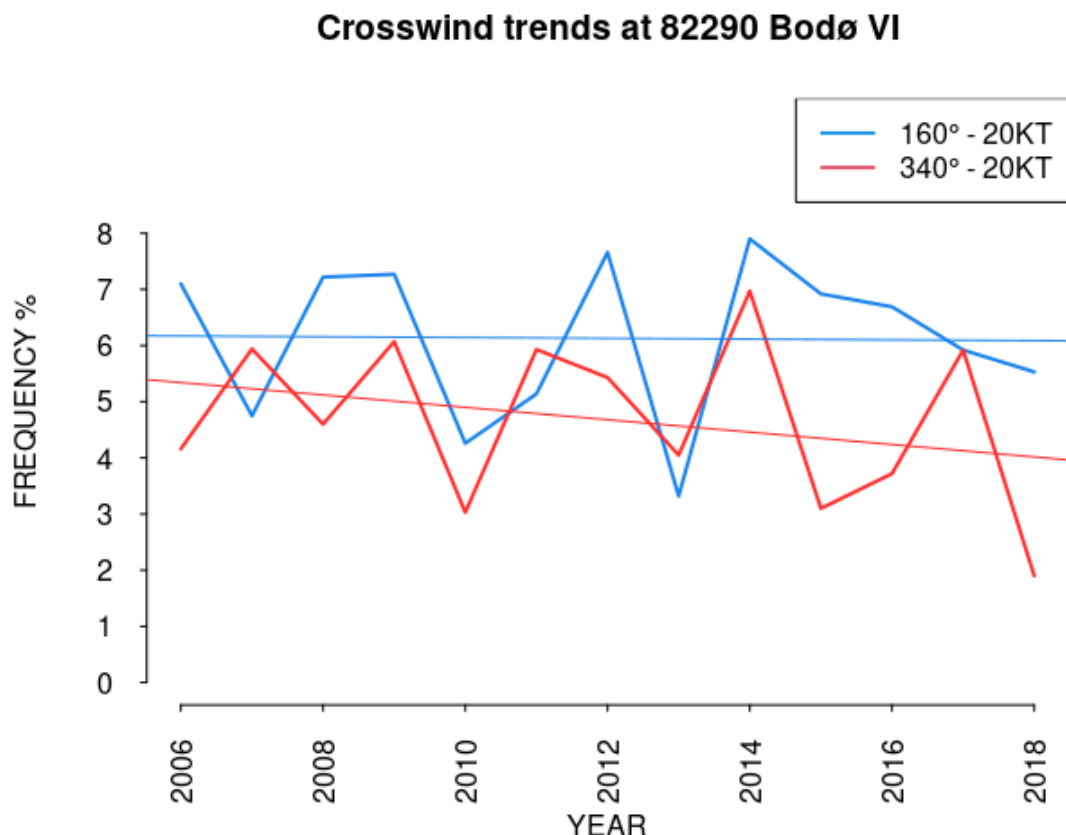


Figure 6.2.3.6.1. Annual frequency of crosswind components of 20 knots or more.

Crosswind trends at 82290 Bodø VI

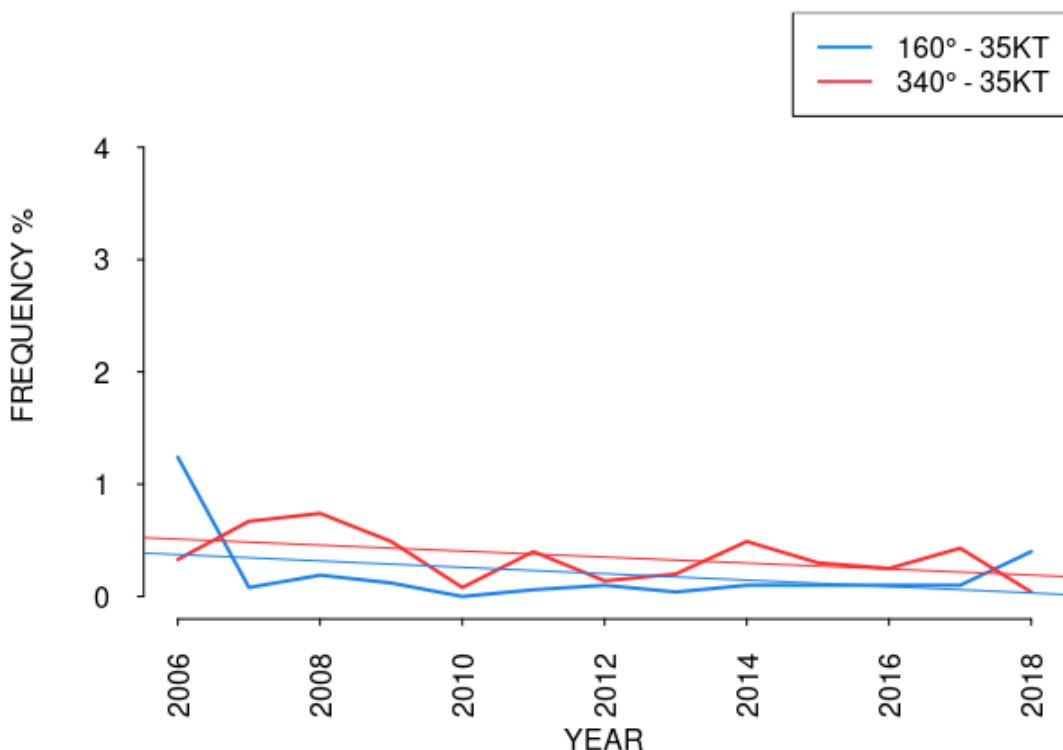


Figure 6.2.3.6.2. Annual frequency of crosswind components of 35 knots or more.

6.2.3.7 Crosswind of long duration

In figure 6.2.3.6.1 we see a crosswind component frequency of 35 knots or more from 160 degrees at 1.2 % in 2006. As mentioned earlier this is due to the extreme weather event *Narve* in January. The synoptic situation was the same for several days and a total of 49 hours of strong southeasterly crosswind was recorded.

Table 6.2.3.7.1 Events of prolonged and strong crosswind at Bodø airport

START	END	DURATION (HOURS)	DIRECTION AND STRONGEST MEAN WIND (knots)	STRONGEST CROSSWIND COMPONENT GUST (knots)
17.01.2006 00	21.01.2006 00	49 (not consecutive)	ESE 44 (severe gale)	46
25.01.2007 23	27.01.2007 05	19 (not consecutive)	NW 34 (gale)	48
13.02.2008 08	14.02.2008 11	25 (not consecutive)	NW 41 (severe gale)	44
07.02.2015 13	08.02.2015 00	11	WNW 50 (storm)	54
15.01.2018 13	16.01.2018 12	17 (not consecutive)	SE 40 (gale)	49

6.2.3.8 Extreme wind

For this analysis “extreme wind” is defined as wind gusts of 60 knots or more. In the period 1 October 2005 to 30 April 2024 this has occurred on 70 occasions, giving a frequency of 0.08 %. However, if we compute the crosswind components of these observations, only one of them is 60 knots or higher.

In many analyses the 99-percentile value is of special interest. The 99-percentile is the 1 % highest value of a dataset. For one year of hourly observations, which is 8760 hours in a normal year, this means the 88th highest ranked value. For the seven month period October to April, which is 5040 hours in a normal year, it means the 51st highest value.

Figure 6.2.3.8.1 shows the 99-percentile of wind gust speed for each year. The trendline shows a *slight decrease*.

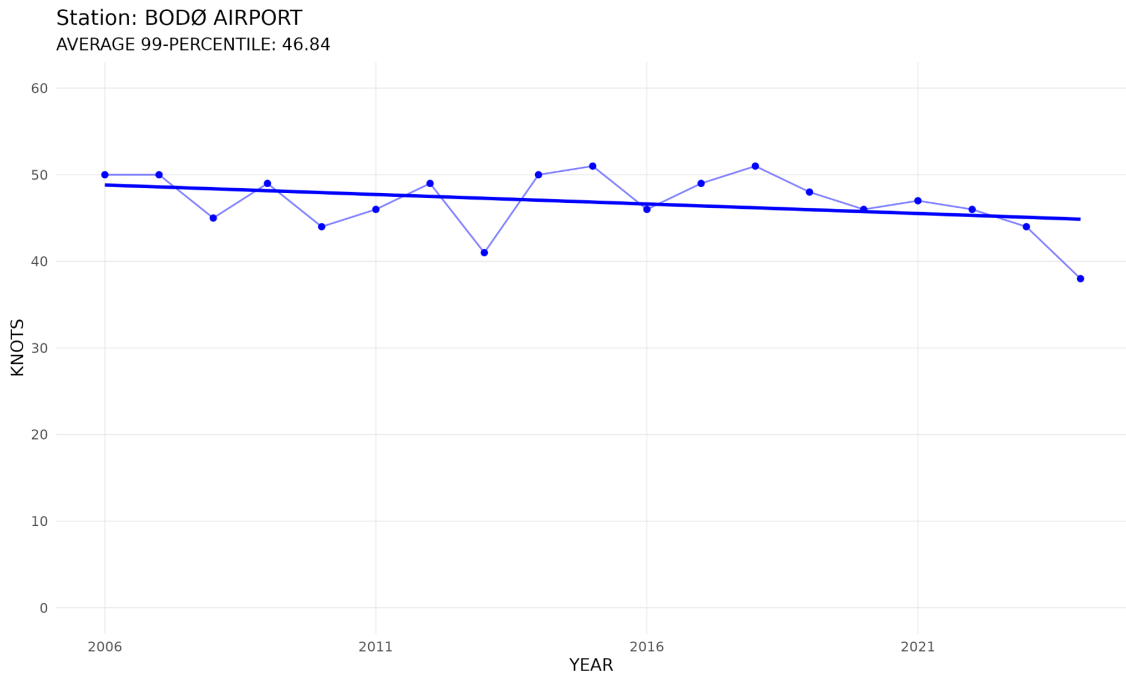


Figure 6.2.3.8.1 The annual value for the 99-percentile wind gust speed and the corresponding trend line.

6.2.4 Freezing precipitation

Freezing precipitation can be hazardous for aircraft operation. There are two main processes giving freezing precipitation: 1) Even if the temperature is less than 0 degrees Celsius, rain drops can exist as supercooled drops. They will momentarily freeze to ice when hitting the cold ground, buildings or vehicles. 2) Because cold air is heavier than warm air, it seeks to the lowest lying places. Rain drops, with a temperature above freezing, from warmer and lighter air aloft, will freeze when they are reaching the ground.

Figure 6.2.4.1 shows the annual frequency of both types of freezing precipitation at Bodø in the period October to April. The highest value is 0.35 % in 2022. The trend line shows an increasing trend. It is reasonable to expect that higher winter temperatures also will give more occurrences of freezing precipitation.

Frequency of freezing precipitation at 82290 Bodø VI

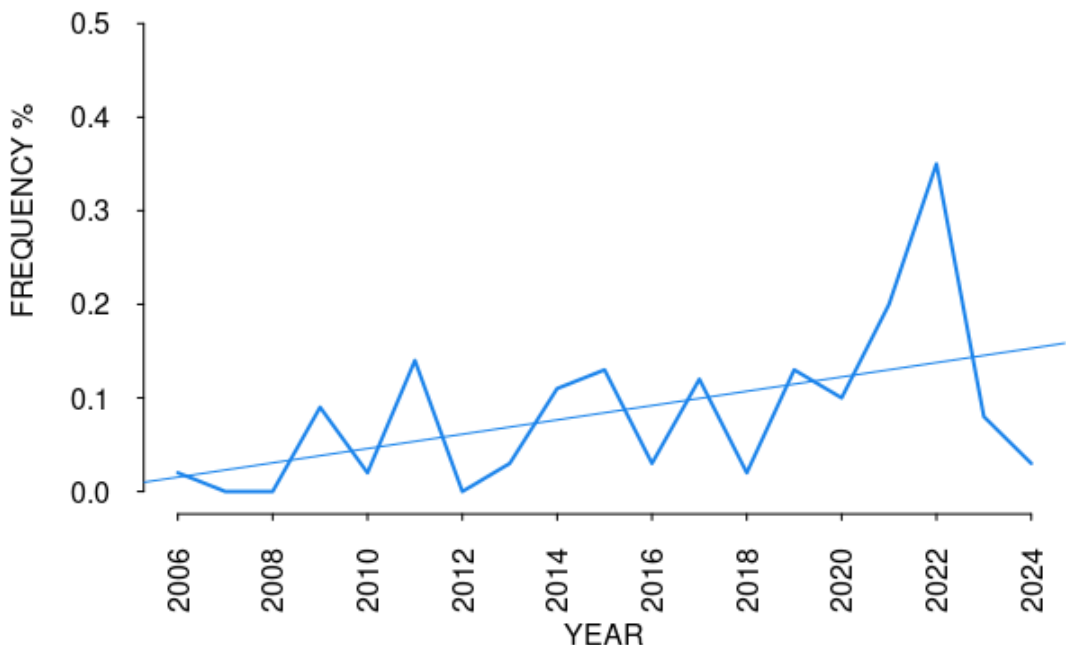


Figure 6.2.4.1 Frequency of freezing precipitation at Bodø airport

6.2.5 Freeze/thaw events

Since temperatures around 0°C often are challenging for airport operations, and in particular for the runway conditions, the number of freeze/thaw events are analysed.

Figure 6.2.5.1 shows the number of days when the temperature during a day both has been below and above 0 degrees at Bodø airport. This occurs typically on 50 to 80 days annually from 1 October to 30 April. The trend line is slightly decreasing.

Days with freeze/thaw events 82290 Bodø VI

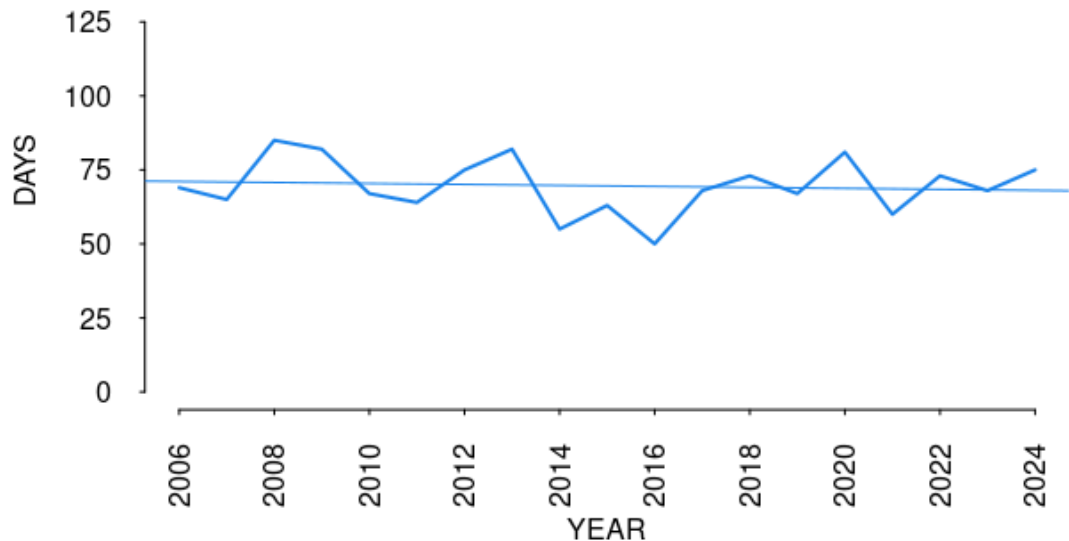


Figure 6.2.5.1 Annual number of days with temperature crossing 0 degrees Celsius

6.3 Tromsø airport

6.3.1 Main findings

The analysis of hourly wind speed observations from 2005 to 2024 for the seven month period October to April shows that the annual frequency of westerly crosswind components of 20 knots or more varies from 1.5 to 7.5 percent. The trendline shows a *decreasing* trend. For westerly crosswind components of 35 knots or more the annual frequency is less than 1 percent, and there is no significant trend. Easterly crosswind components of 20 knots or more have an annual frequency of up to 2 percent, and show a *slightly increased* trend. The trend for the value of the 99 percentile, i.e. the 1 percent highest wind gust each year, shows a *slightly increased* trend. Freezing precipitation occurs less than 0.5 % of the time, but the trend line shows a slightly increasing trend, probably because higher winter temperatures also will give more occurrences of freezing precipitation.

6.3.2 Location

Tromsø Airport - Langnes is situated on the west side of Tromsøya. The highest point on the island is 135 metres above sea level, while Kvaløya, to the west and north of the airport, has peaks reaching up to 765 metres above sea level. See figure 6.3.2.1. The runway is oriented in the direction 18/36, i.e. 180/360 degrees. Consequently, winds from 90 and 270 degrees will result in crosswind at the airport.



Figure 6.3.2.1. Langnes is located on the west side of Tromsøya, between Kvaløya to the west and north, and the mainland to the east. Source: The Norwegian Mapping Authority

6.3.3 Wind conditions

6.3.3.1 Mean wind speed

Langnes began weather observations in 1965. Hourly measurements of mean wind speed, strongest mean wind in the last hour, and strongest 3-second wind gusts in the last hour started in January 2005. These wind measurements have been used in the analysis. The wind measurements, both METAR and SYNOP, are taken from an anemometer standing west of the threshold of runway 36. Wind observations are also taken near the threshold of runway 18.

Figure 6.3.3.1.1 shows the average mean wind speed at Langnes over the seven-month period from October to April for the years 2005 to 2024. The year

indications on the x-axis represent the end year of each period, so 2006 indicates the period from October 2005 to April 2006. The average mean wind speed varies around 10 knots each year. A trendline has been added, showing a slightly negative trend.

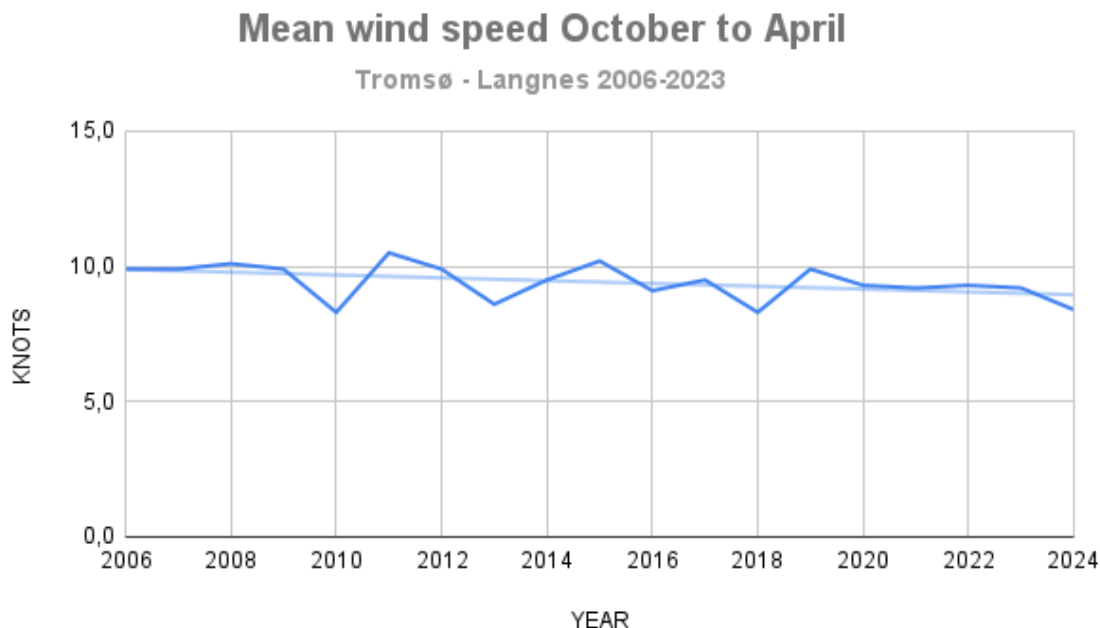


Figure 6.3.3.1.1. Average mean wind speed during the period from October to April.

6.3.3.2 Wind roses

Visually, the wind roses in Figure 6.3.3.2.1 appear to be very similar. The three most frequent wind directions, S, SSW, and SW, have a total frequency of 55 % and 52 % in the two periods, respectively.

Wind Rose for Tromsø – Langnes (SN90490) in period; 10.2005–4.2014. Months: 10,11,12,1,2,3,4
Calm (0.0–0.2 m/s) = 2.2 %

Vindrose for Tromsø – Langnes (SN90490) i perioden; 10.2014–4.2024. Mnd: 10,11,12,1,2,3,4
Stille (0.0–0.2 m/s) = 0.8 %

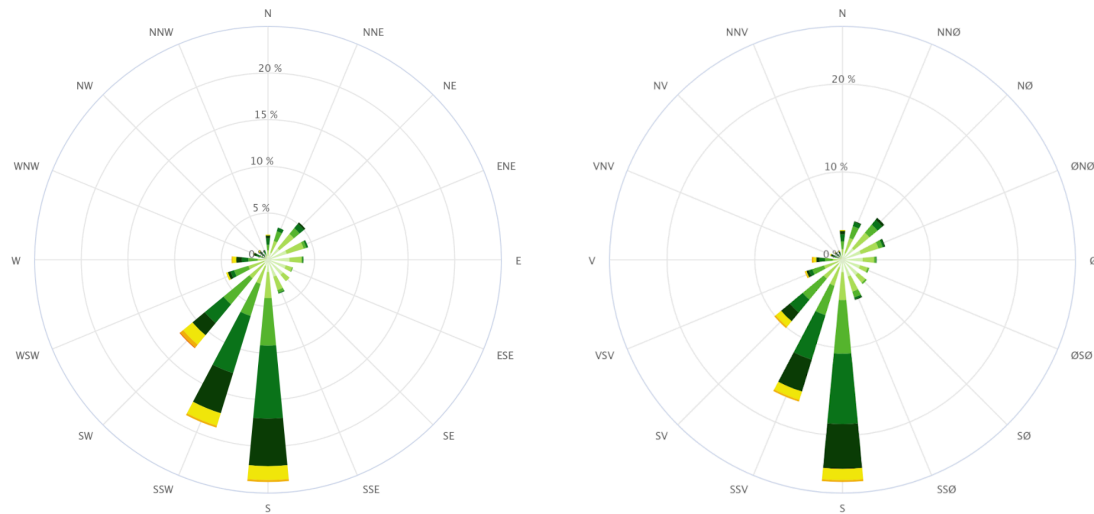


Figure 6.3.3.2.1. Wind roses for the period from October to April for the years 2005 to 2014 on the left and 2014 to 2023 on the right. Wind speed in m/s.

6.3.3.3 Differences in wind in a mild and a cold winter month

In the introduction to this chapter, a relationship between temperature and wind was suggested, where higher temperatures resulted in stronger winds. Therefore, it would be interesting to compare the wind conditions in a mild and a cold winter month.

January 2014 is the coldest winter month in Tromsø in the period from 2005 to 2023, while January 2017 is the mildest. Figure 6.3.3.3.1 shows the wind roses for these two months, with 2014 on the left and 2017 on the right. The average wind speed was 3.2 m/s (5.9 knots) and 6.6 m/s (12.2 knots), respectively. In January 2017, winds between

south (S) and west (W) occurred in 68 % of cases, while winds between north (N) and east (E) occurred in 16 % of cases. In January 2014, the corresponding figures were 48 % and 24 %. The proportion of wind from the crosswind direction of 270 degrees was 6 % and 1 %, respectively, indicating more occurrences of westerly crosswind in a mild than in a cold month.

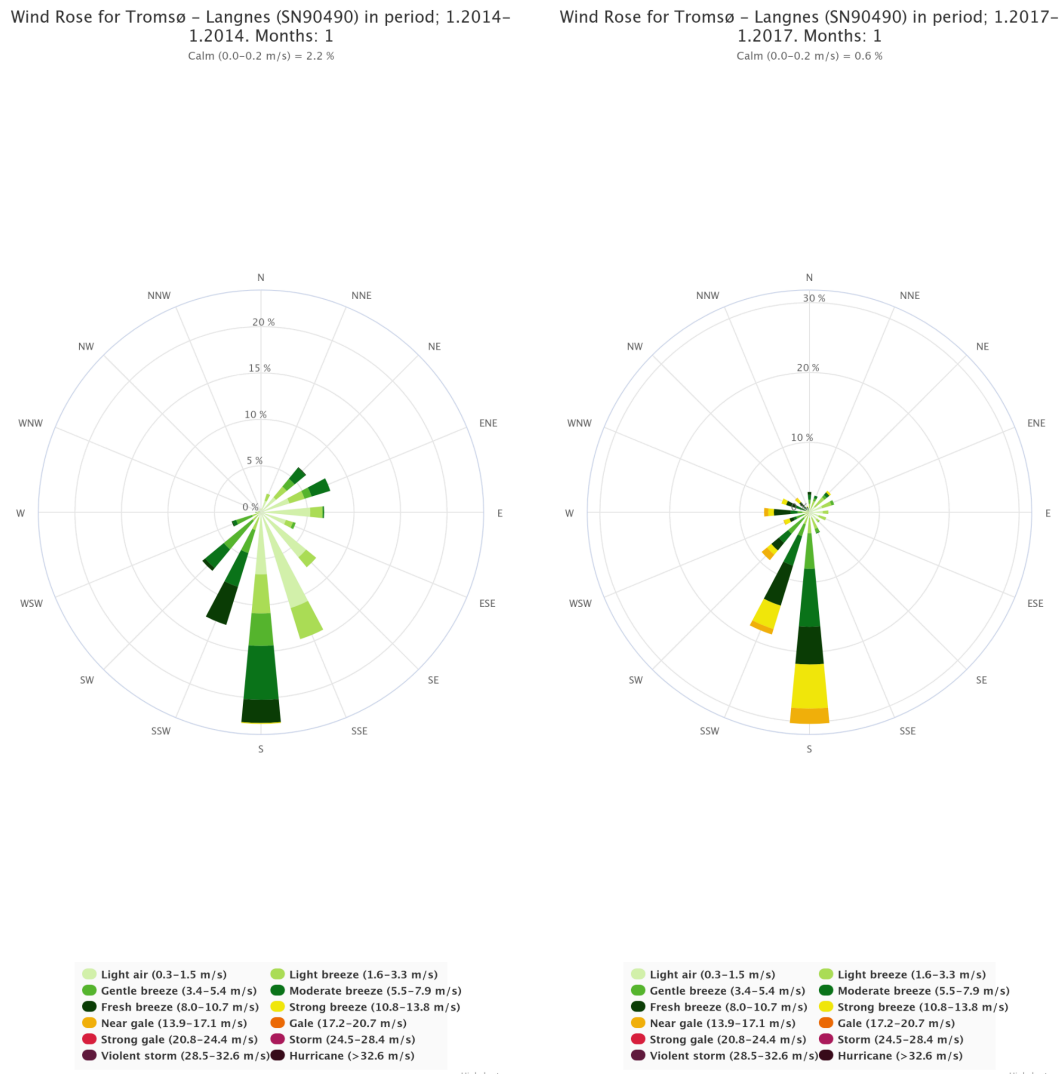


Figure 6.3.3.3.1 shows the wind roses for the cold January 2014 on the left and the mild January 2017 on the right. Wind speed in m/s.

6.3.3.4 Wind gusts

The terrain near an airport influences the wind locally, creating wind conditions that will be typical for the various wind directions experienced at the airport. One way to assess these local conditions is to observe how the gust factor changes with wind direction.

The gust factor is defined as FG_1/FX_1 , where FG_1 is the strongest 3-second wind gust in the last hour and FX_1 is the strongest mean wind in the last hour. At weather stations with relatively flat and uniform terrain around the station, the gust factor typically lies around 1.2. In highly rugged terrain, wind gusts can be more than double the mean wind speed.

Figure 6.3.3.4.1 shows the average gust factor for each 10th degree, deca-degree, at Langnes for the months from October to April throughout the measurement period from 2005 to 2024. Wind from the east has the highest gust factor, between 1.6 and 1.7, while wind from the southwest has the lowest, near 1.3. Of particular interest is wind from the crosswind direction west, where the gust factor is approximately 1.4.

GUST FACTOR PER DECA-DEGREE 90490 TROMSØ - LANGNES 2005-2024

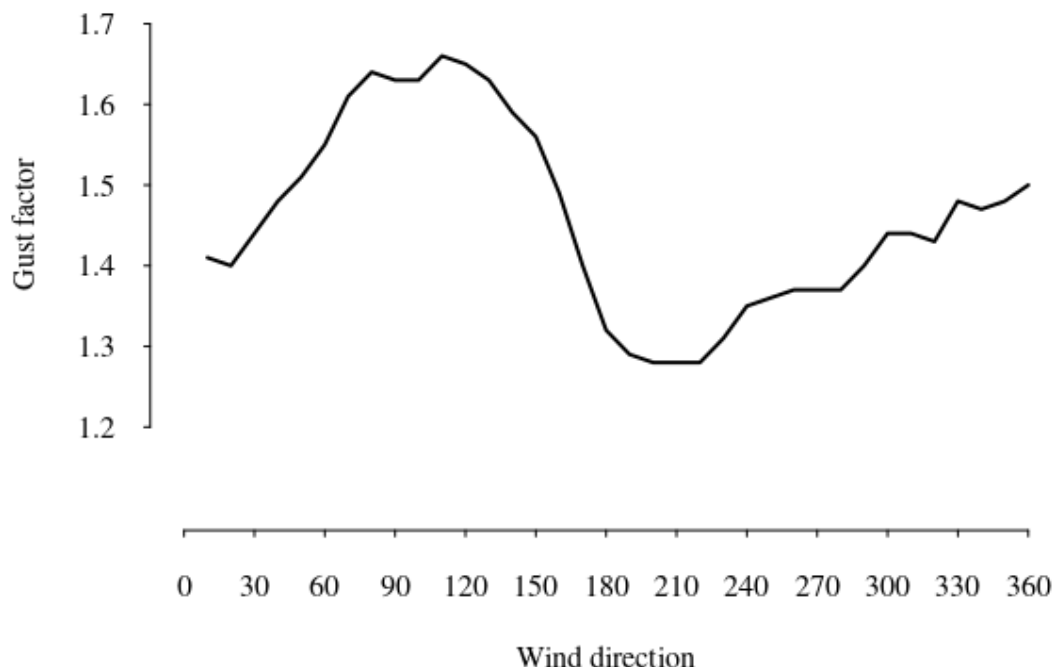


Figure 6.3.3.4.1. Gust factor per deca-degree at Tromsø - Langnes.

Although wind from the east has the highest gust factor, the wind roses in Figure 6.3.3.2.1 show that wind from this direction does not occur frequently, and only occasionally strong. Therefore, it is also interesting to examine the strength of wind

gusts that can occur with different wind directions. In Figure 6.3.3.4.2, both the average of the 25 strongest wind gusts and the single strongest wind gust recorded for each deca-degree are plotted.

The single strongest wind gust, 72 knots, was recorded at Langnes with wind from due north during the extreme weather event *Ole* in February 2015. Typically, this wind direction does not have the strongest wind gusts (see the curve for “Average” wind gusts in Figure 6.3.3.4.2), but in Figure 6.3.3.4.1, we observe that the gust factor is relatively high from this wind direction.

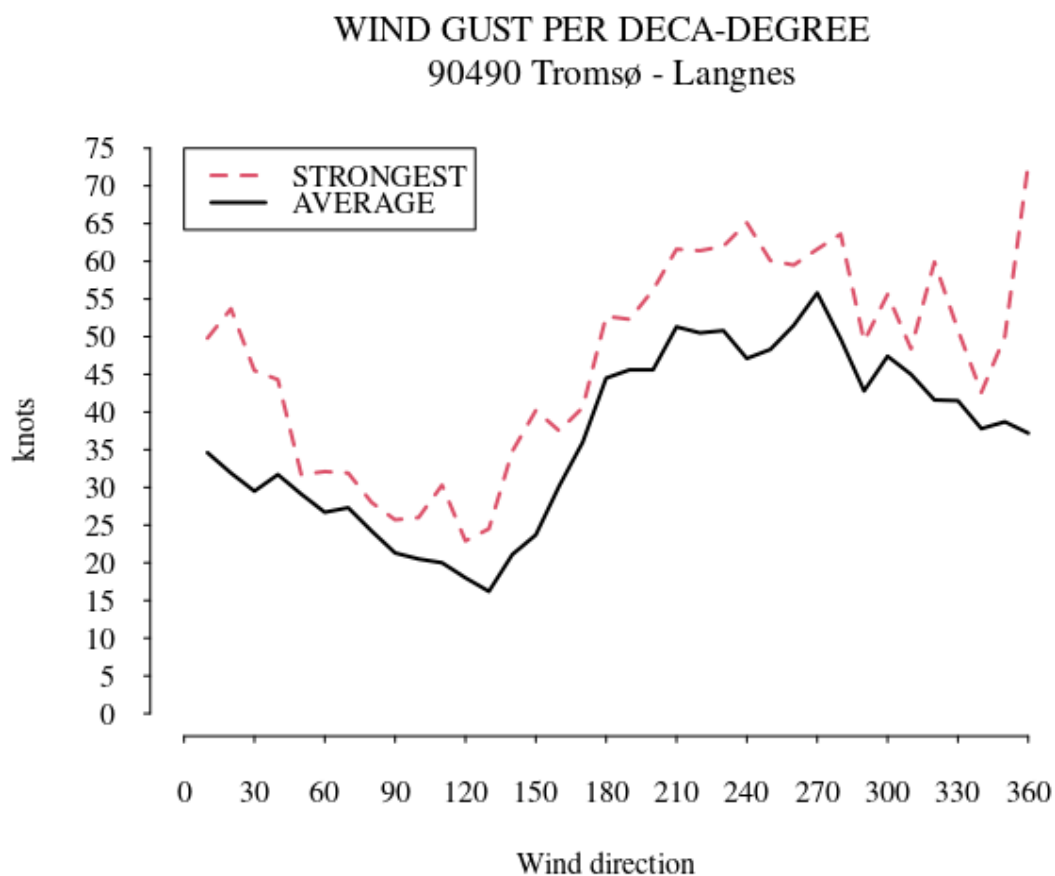


Figure 6.3.3.4.2. Strongest wind gusts and the average of the 25 strongest gusts per deca-degree at Tromsø - Langnes.

6.3.3.5 Crosswind

Crosswinds at Langnes, as previously mentioned, are at 90 and 270 degrees. Wind from 90 degrees occurs not often, and only occasionally generates strong wind gusts. However, wind from 270 degrees has the highest average, 56 knots, for the 25 strongest wind gusts from this direction.

But strong wind from other directions can also give significant crosswind components. Table 6.3.3.5.1 shows the monthly frequencies of a crosswind component of more than 20 and 35 knots respectively. A 270 degree wind gust of 30 knots, gives a westerly component of 30 knots, while a 240 degree wind gust at 30 knots, gives a westerly component of 26 knots, but still contributing to the total frequency. Strong winds from 180 and 360 degrees, will not contribute to a westerly crosswind component at all.

Westerly crosswinds above 20 knots occur most often in March. Easterly crosswinds above 20 knots occur usually well below 1 percent. Westerly crosswinds above 35 knots occur at around 1 percent at most in the period November to March.

Table 6.3.3.5.1. Frequency of crosswind component of 20 knots and 35 knots or more.

MONTH	Westerly >=20 knots	Easterly>=20 knots	Westerly>=35 knots
OCTOBER	3.9 %	0.2 %	0.3 %
NOVEMBER	4.2 %	0.1 %	0.8 %
DECEMBER	5.0 %	0.3 %	1.1 %
JANUARY	5.3 %	0.6 %	0.8 %
FEBRUARY	5.1 %	0.2 %	1.1 %
MARCH	7.1 %	0.1 %	1.0 %
APRIL	3.9 %	0.3 %	0.3 %
TOTAL	4.9 %	0.3 %	0.8 %

6.3.3.6 Trends for crosswind

Figure 6.3.3.6.1 and 6.3.3.6.2 show the frequency of all wind gust observations giving a 270 or 90 degrees wind component larger than 20 and 35 knots respectively.

The frequency for westerly crosswind components stronger than 20 knots varies from 1.5 percent to 7.5 percent annually. The trend lines show a *decreasing* trend. Easterly crosswind occurs up to around one percent in some years, but usually lies well below this figure. In both 2015 and 2022 strong easterly winds of long duration contributed to

the two pronounced tops in the red curve in figure 6.3.3.6.1. The curve has a *slightly increasing* trend line.

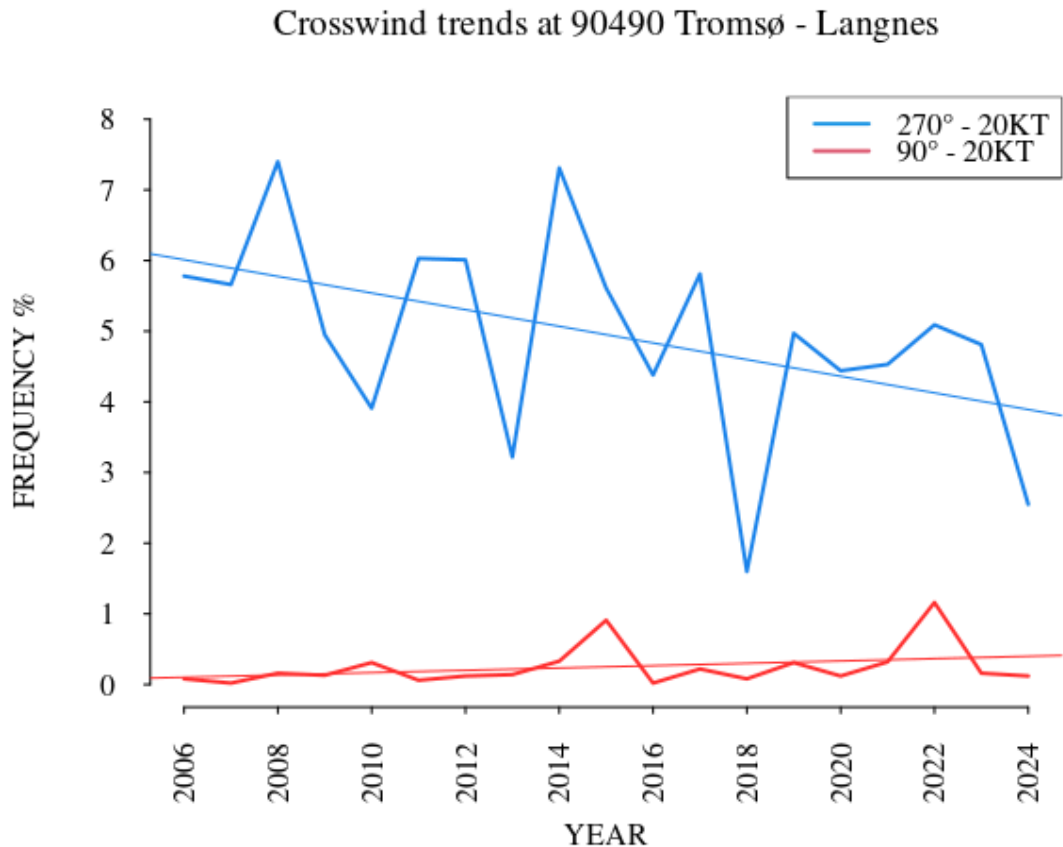


Figure 6.3.3.6.1. Frequency of crosswind \geq 20 knots

Figure 6.3.3.6.2 shows the frequency of a westerly crosswind component stronger than 35 knots. The frequency varies from a few tens of a percent to up to almost two percent. The corresponding trend line is almost flat. Easterly winds have never been strong enough to contribute to an easterly crosswind component of 35 knots or more.

Crosswind trends at 90490 Tromsø - Langnes

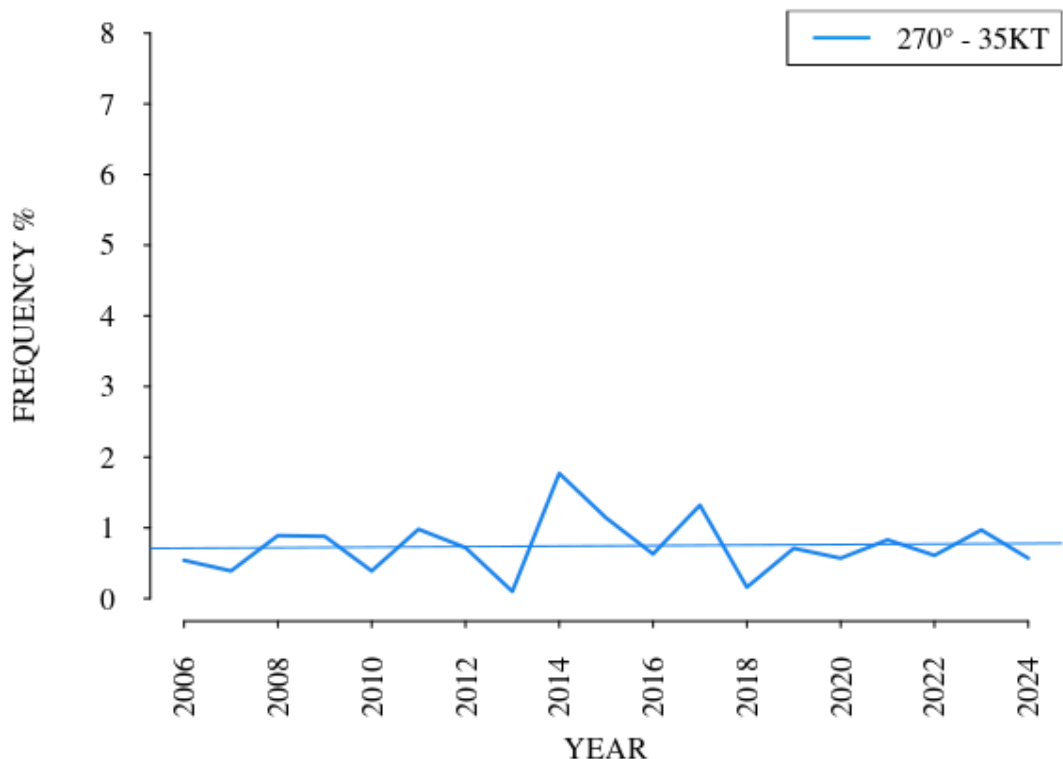


Figure 6.3.3.6.2. Frequency of a westerly crosswind component ≥ 35 knots

6.3.3.7 Crosswind of long duration

Events similar to the one in February 2023 occur occasionally. In the measurement series from 2005 to 2024, we did find 7 instances of prolonged strong wind from the west (Table 6.3.3.7.1). The criteria used were crosswind components having wind gusts of 35 knots or more and lasting for at least 12 hours, though allowing for shorter intervals with lesser wind.

Table 6.3.3.7.1. Events of prolonged and strong crosswind from at Tromsø - Langnes

START	END	DURATION (HOURS)	DIRECTION AND STRONGEST MEAN WIND (KNOTS)	STRONGEST CROSSWIND COMPONENT (KNOTS)
19.12.2007 07	19.12.2007 21	14	SW 36 (gale)	56
26.12.2008 00	27.12.2008 00	16 (not consecutive)	W 34 (near gale)	56
01.11.2010 18	02.11.2010 08	14	W 43 (severe gale)	62
03.12.2013 12	04.12.2013 03	19 (not consecutive)	W 44 (severe gale)	61
09.02.2015 14	11.02.2015 16	30 (not consecutive)	W 38 (gale)	60
12.02.2017 18	13.02.2017 17	16 (not consecutive)	W 37 (gale)	51
27.02.2022 13	28.02.2022 04	12 (not consecutive)	SW 46 (severe gale)	55
12.02.2023 12	13.02.2023 07	15 (not consecutive)	W 38 (gale)	52

6.3.3.8 Extreme winds

For this analysis “extreme wind” is defined as wind gusts of 60 knots or more. In the period 1 October 2005 to 30 April 2024 this has occurred on 15 occasions, a frequency of 0.02 %. However, if we compute the crosswind components of these observations, only four of them are higher than 60 knots. The number of occurrences are too few to compute a trend.

In many analyses the 99-percentile value is of special interest. The 99-percentile is the 1 % highest value of a dataset. For one year of hourly observations, which is 8760 hours in a normal year, this means the 88th highest ranked value. For the seven month period October to April, 5040 hours, it means the 51st highest value.

Figure 6.3.3.8.1 shows the 99-percentile wind gust speed for each year, i.e. the value for the 1 percent highest wind gust each year. The trendline shows a very *slight increase*.

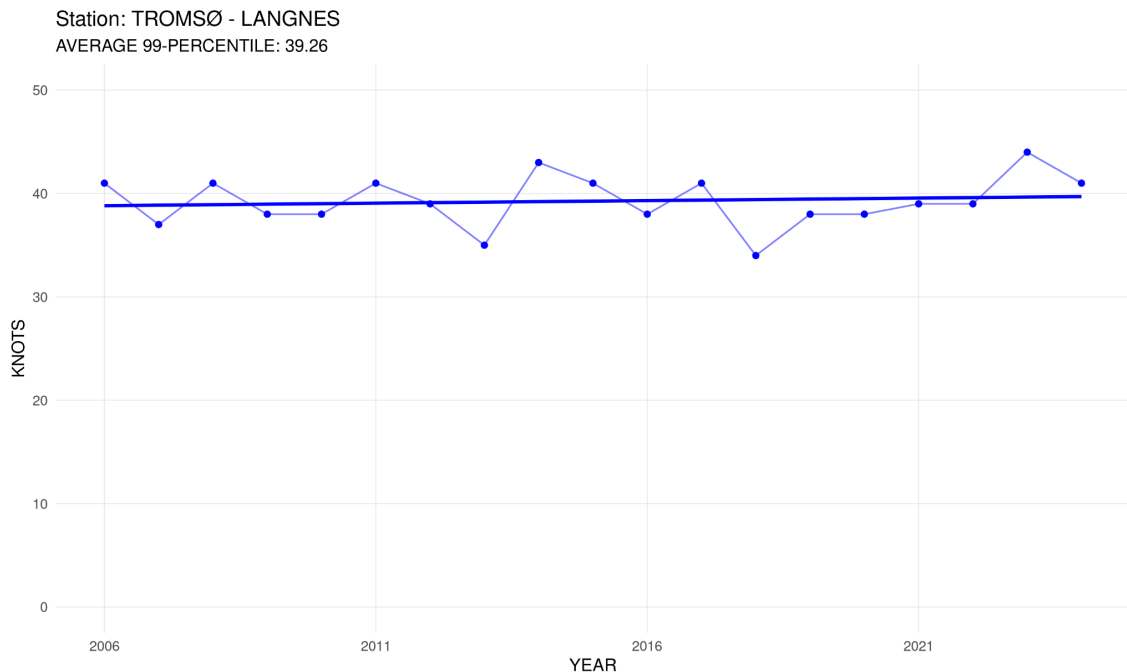


Figure 6.3.3.8.1. The annual value for the 99-percentile wind gust speed and the corresponding trend line.

6.3.4 Freezing precipitation

Freezing precipitation can be hazardous for aircraft operation. There are two main processes giving freezing precipitation: 1) Even if the temperature is less than 0 degrees Celsius, rain drops can exist as supercooled drops. They will momentarily freeze to ice when hitting the cold ground, buildings or vehicles. 2) Because cold air is heavier than warm air, it seeks to the lowest lying places. Rain drops, with a temperature above freezing, from warmer and lighter air aloft, will freeze when they are reaching the ground.

Figure 6.3.4.1 shows the annual frequency of freezing precipitation at Tromsø - Langnes. The highest value was 0.41 % in 2015. The trend line shows an increasing trend. It is reasonable to expect that increasing winter temperatures also will give more occurrences of freezing precipitation.

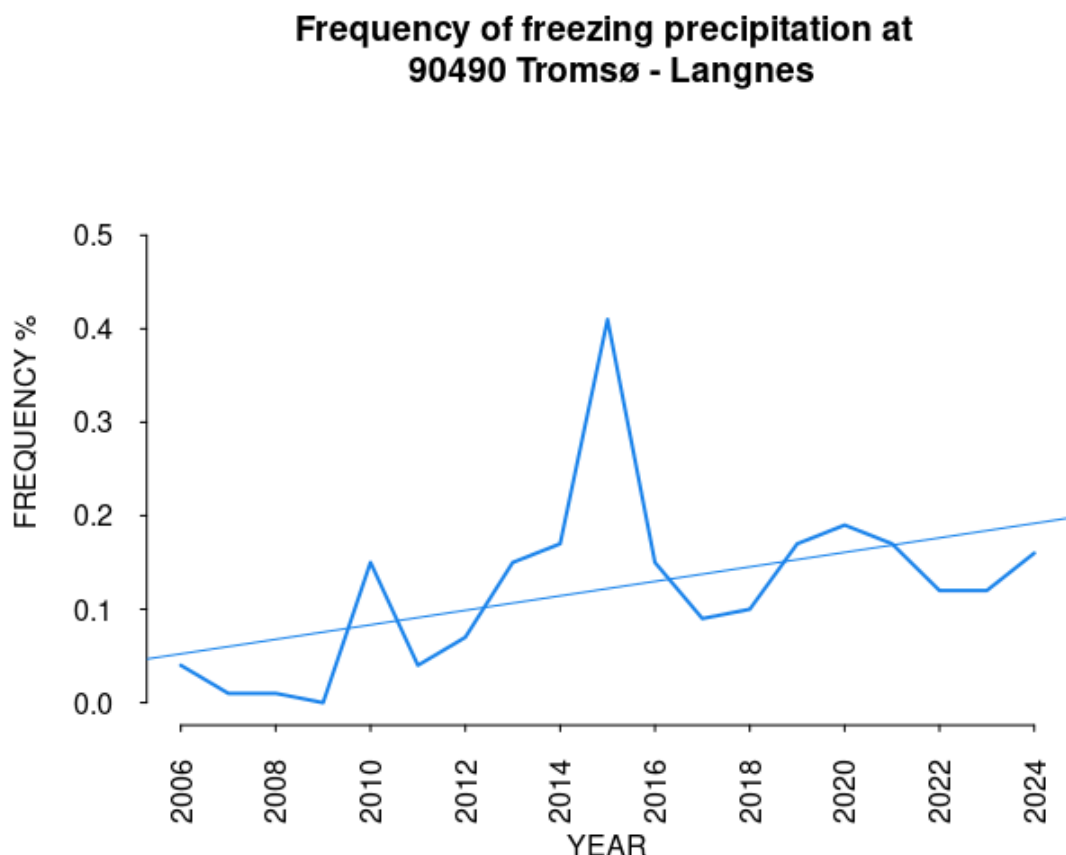


Figure 6.3.4.1. Frequency of freezing precipitation at 90490 Tromsø - Langnes.

6.3.5 Freeze-thaw events

Since temperatures around 0°C often are challenging for airport operations and in particular for the runway conditions, the number of freeze/thaw events are analysed.

Figure 6.3.5.1 shows the number of days when the temperature during a day both has been below and above 0 degrees at Tromsø - Langnes. We notice that this occurs on up to as much as almost half of the days in the 211/212 days long period from 1 October to 30 April. But there are large variations from year to year, and the trend line is almost flat.

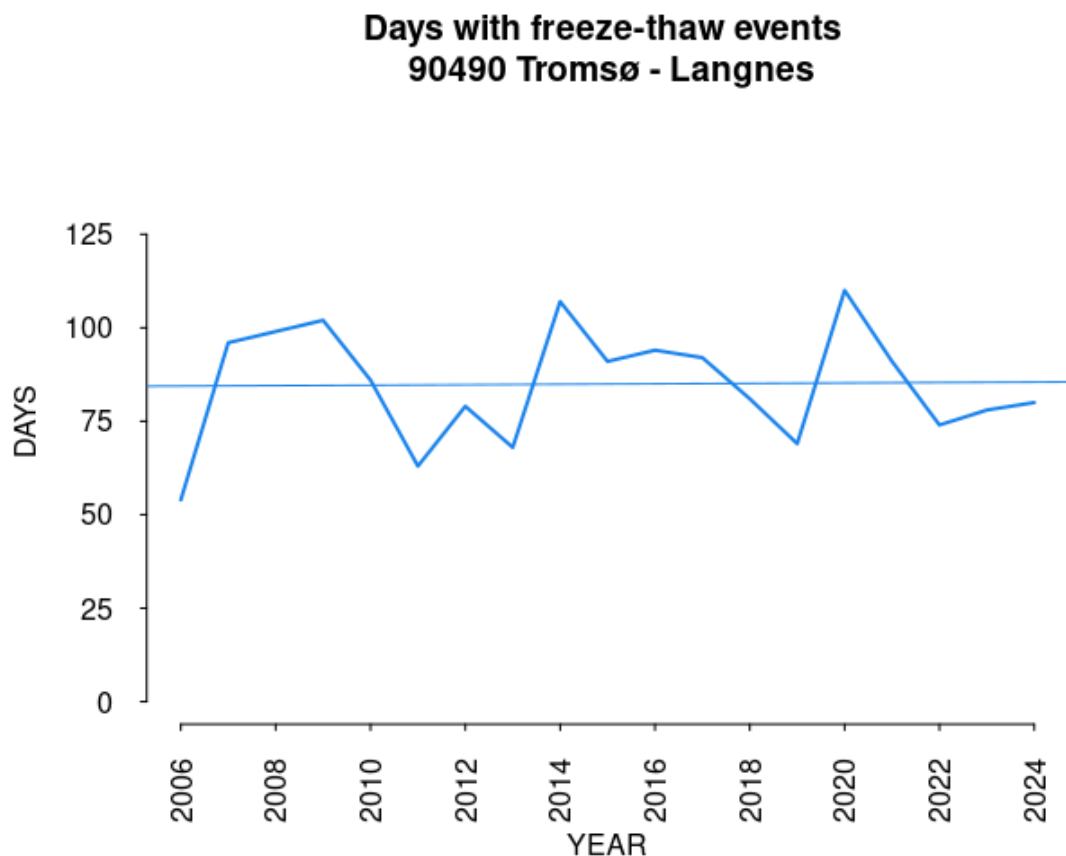


Figure 6.3.5.1. Annual number of days with temperature crossing 0 degrees Celsius

6.4 Kirkenes Lufthavn

6.4.1 Main findings

The analysis of hourly wind speed observations from 2005 to 2024 for the seven month period October to April, shows that the annual frequency of southeasterly crosswind components of 20 knots or more varies from 2 to 9 percent. The trendline shows an *increasing* trend. The trend for northwesterly crosswind components of 35 knots or more is *decreasing*. The frequency varies from a few tenths to 1 percent at most.

6.4.2 Location

Kirkenes Airport is situated at Høybuktmoen, 85 m above sea level, about 5 km southwest of Kirkenes. The nearest hills are between 200 and 250 m at most. See figure 6.4.2.1. The runway is oriented in the direction 05/23, i.e. 50/230 degrees. Consequently, winds from 140 and 320 degrees will result in crosswind at the airport.



Figure 6.4.2.1. Kirkenes airport is located in an undulating terrain about 5 km southwest of Kirkenes. Source: The Norwegian Mapping Authority

6.4.3 Wind conditions

6.4.3.1 Mean wind speed

Kirkenes airport began weather observations in 1957. Hourly measurements of mean wind speed, strongest mean wind in the last hour, and strongest 3-second wind gusts in the last hour started in January 2005. These wind measurements have been used in the analysis.

Figure 6.4.3.2 shows the average mean wind speed at Kirkenes airport over the seven month period from October to April for the years 2005 to 2024. The year indications on the x-axis represent the end year of each period, so 2006 indicates the period from October 2005 to April 2006. The average mean wind speed is typically around 10 knots each year. A trendline has been added, showing a slightly positive trend.

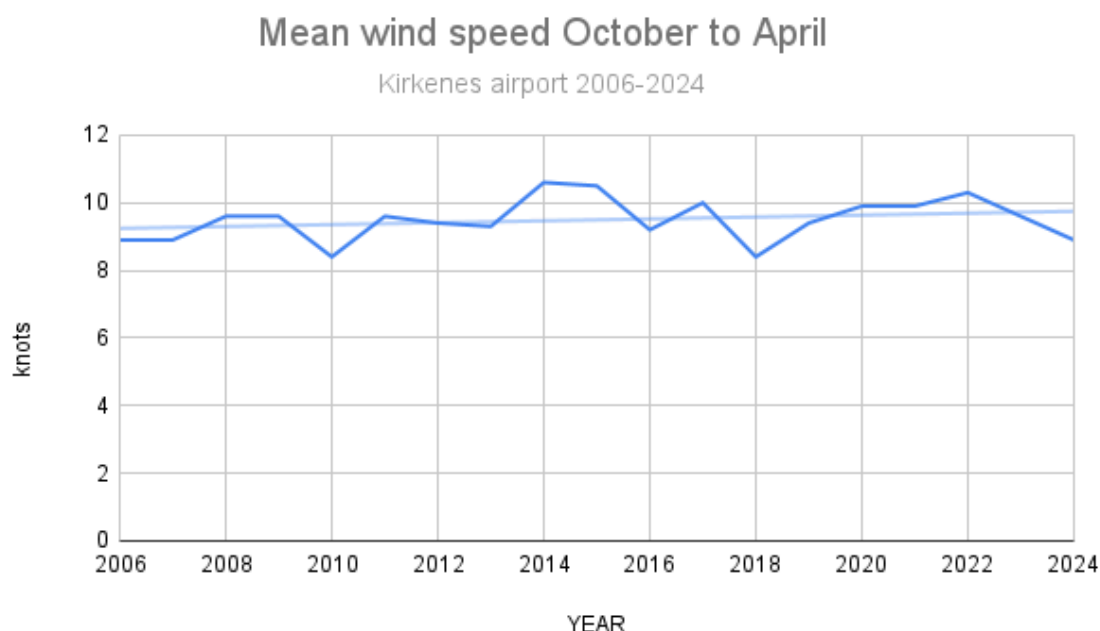
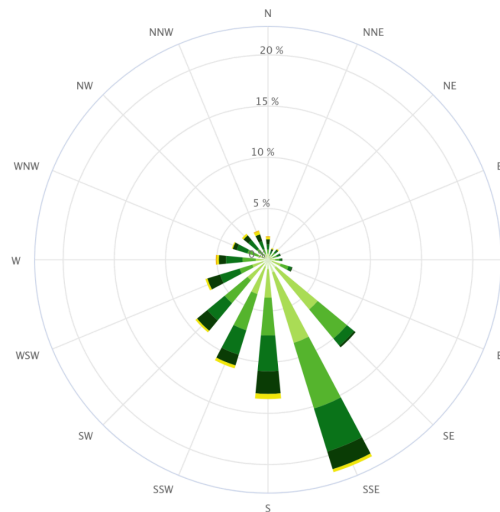


Figure 6.4.3.1.1. Average mean wind speed during the period from October to April.

6.4.3.2 Wind roses

Visually, the wind roses comparing the periods 2005-2014 and 2014-2024 in Figure 6.4.3.2.1 appear to be quite similar. The three most frequent wind directions, SE, SSE, and S, have total frequencies of 46 % and 43 % in the two periods, respectively.

Wind Rose for Kirkenes Lufthavn (SN99370) in period; 10.2005–4.2014. Months: 10,11,12,1,2,3,4
Calm (0.0–0.2 m/s) = 1.4 %



Wind Rose for Kirkenes Lufthavn (SN99370) in period; 10.2014–4.2024. Months: 10,11,12,1,2,3,4
Calm (0.0–0.2 m/s) = 2.4 %

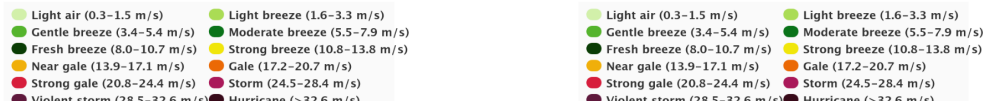
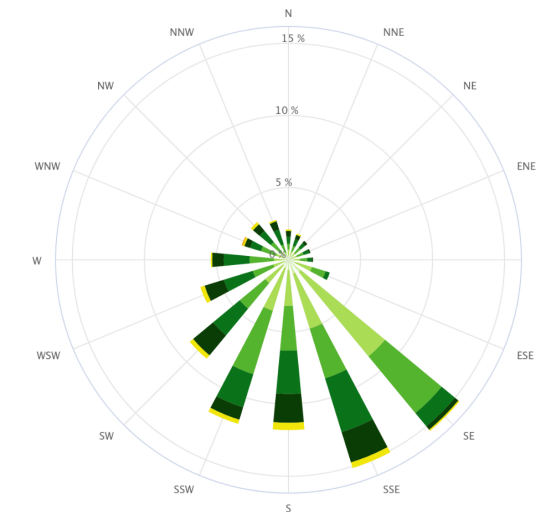


Figure 6.4.3.2.1 Wind roses for the period from October to April for the years 2005 to 2014 on the left and 2014 to 2024 on the right. Wind speed in m/s.

6.4.3.3 Differences in wind in a mild and a cold winter month

In the introduction to this chapter, a relationship between temperature and wind was suggested, where higher temperatures resulted in stronger winds. Therefore, it would be interesting to compare the wind conditions in a mild and a cold winter month.

February 2007 is the coldest winter month in Kirkenes in the period from 2005 to 2024, while February 2014 is the mildest. Figure 6.4.3.3.1 shows the wind roses for these two

months, with 2007 on the left and 2014 on the right. The average wind speed was 7.4 knots and 11.1 knots, respectively. In February 2007, winds from southsoutheast (SSE) occurred in more than 54 % of cases. In February 2014, the corresponding figure was 47 %. Southeasterly winds increased the frequency from 7 % to 20 %. Winds from SE give a higher crosswind component than winds from SSE.

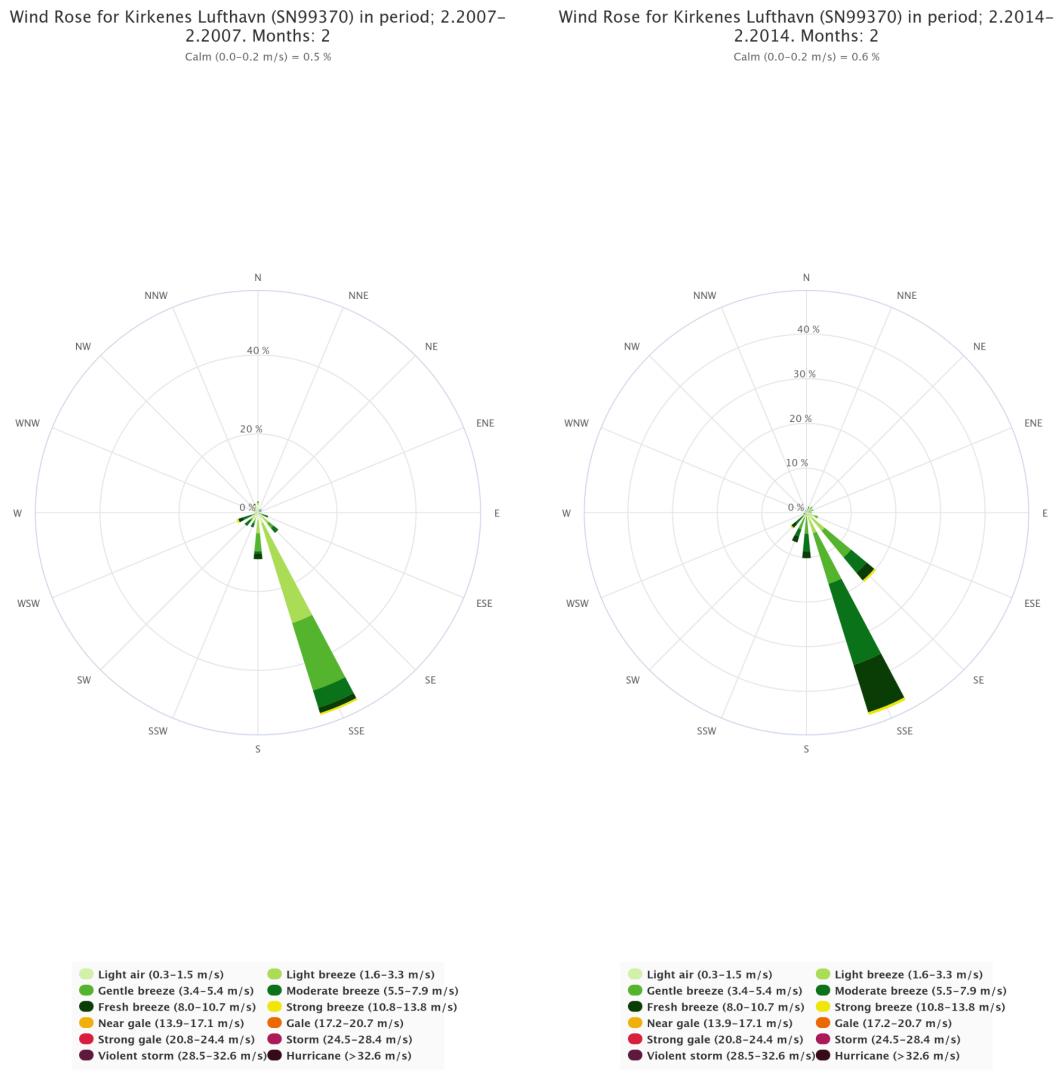


Figure 6.4.3.3.1 shows the wind roses for the cold February 2007 on the left and the mild February 2014 on the right. Wind speed in m/s.

6.4.3.4 Wind gusts

The terrain near an airport influences the wind locally, creating wind conditions that will be typical for the various wind directions experienced at the airport.

One way to assess these local conditions is to observe how the gust factor changes with wind direction. The gust factor is defined as FG_1/FX_1 , where FG_1 is the strongest 3-second wind gust in the last hour and FX_1 is the strongest mean wind in the last hour. At weather stations with relatively flat and uniform terrain around the station, the gust factor typically lies around 1.2. In highly rugged terrain, wind gusts can be more than double the mean wind speed.

Figure 6.4.3.4.1 shows the average gust factor for each 10th degree, deca-degree, at Kirkenes airport for the months from October to April throughout the measurement period from 2005 to 2024. Wind from the north and northeast has the highest gust factor, up to 1.4, while wind from the southeast has the lowest, around 1.25. This is also one of the crosswind directions.

GUST FACTOR PER DECA-DEGREE 99370 KIRKENES AIRPORT 2005-2024

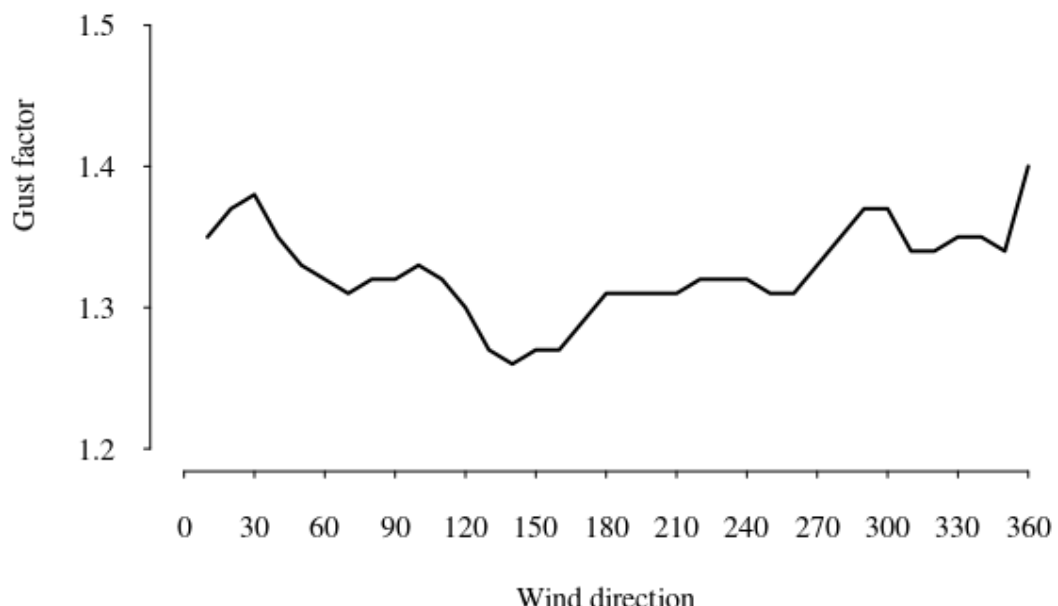


Figure 6.4.3.4.1. Gust factor per deca-degree at Kirkenes airport

It is also interesting to examine the strength of wind gusts that can occur with different wind directions. In Figure 6.4.3.4.2, both the average of the 25 strongest wind gusts and the single strongest wind gust recorded for each deca-degree are plotted.

The single strongest wind gust, 67 knots, was recorded at Kirkenes airport with wind from 300 degrees on 18 December 2007, during the extreme weather event *Rita*.

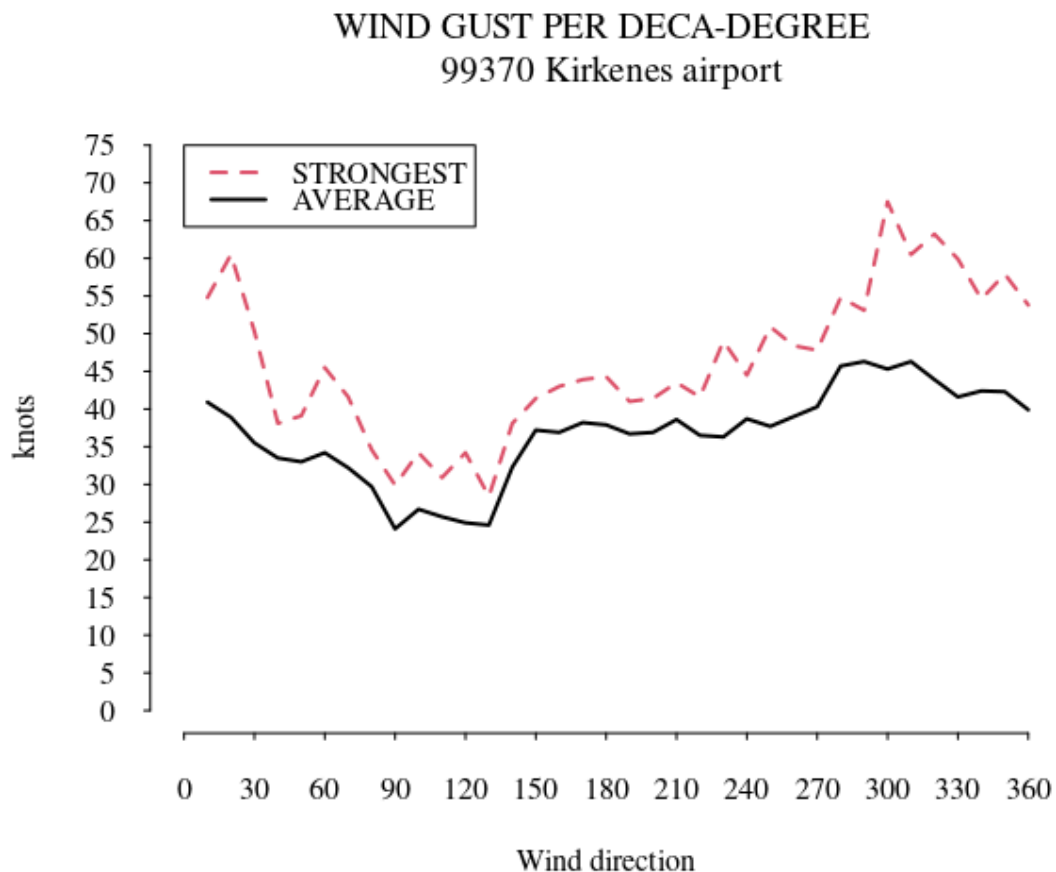


Figure 6.4.3.4.2. Strongest wind gusts and the average of the 25 strongest gusts per deca-degree at Tromsø - Langnes.

6.4.3.5 Crosswind

Crosswinds at Kirkenes airport, as previously mentioned, are at 140 and 320 degrees. But strong wind from other directions can also give significant crosswind components. Table 6.4.3.5.1 shows the monthly frequencies of crosswind components of more than 20 and 35 knots respectively. A 320 degree wind gust of 30 knots, gives a northwesterly component of 30 knots, while a 290 degree wind gust at 30 knots, gives a northwesterly component of 26 knots, still contributing to the total frequency. All

strong winds from 50 and 230 degrees, will not contribute to a crosswind component at all.

Southeasterly crosswinds of more than 20 knots have the highest frequency in November to February, while northwesterly crosswinds occur most often in October, March and April. The frequencies vary typically from 3 to up to 8 percent. For crosswind components of 35 knots or more, the annual frequencies lie below 0.5 percent for both crosswind directions, with crosswind from northwest occurring a little bit more often.

Table 6.4.3.5.1. Frequency of crosswind components of 20 knots and 35 knots or more

MONTH	Northwesterly >=20 knots	Southeasterly >=20 knots	Northwesterly >=35 knots	Southeasterly >=35 knots
OCTOBER	4,6 %	2,9 %	0,4 %	0,0 %
NOVEMBER	3,3 %	6,7 %	0,3 %	0,1 %
DECEMBER	2,9 %	7,5 %	0,3 %	0,2 %
JANUARY	4,0 %	7,5 %	0,3 %	0,1 %
FEBRUARY	3,6 %	7,6 %	0,4 %	0,1 %
MARCH	6,7 %	5,0 %	0,4 %	0,0 %
APRIL	5,3 %	2,5 %	0,3 %	0,0 %
TOTAL	4,3 %	5,7 %	0,4 %	0,1 %

6.4.3.6 Trends for crosswind components

Figure 6.4.3.6.1 and 6.4.3.6.2 show the frequency of all wind gust observations giving a 140 or 320 degrees wind component larger than 20 and 35 knots respectively.

The frequency for crosswinds stronger than 20KT varies from roughly from 2 percent to 9 percent annually. Southeasterly crosswinds have the highest frequencies. The trend lines show an *increasing* trend for southeasterly crosswind and an almost flat trend line for northwesterly crosswind.

Figure 6.4.3.6.2 shows the frequency of crosswind components stronger than 35 knots. Contrary to the 20KT crosswind components, northwesterly crosswind has the highest frequency, with up to 1 percent at most. The trend lines show a slightly decreasing trend for northwesterly crosswind and a slightly increasing trend line for southeasterly crosswind.

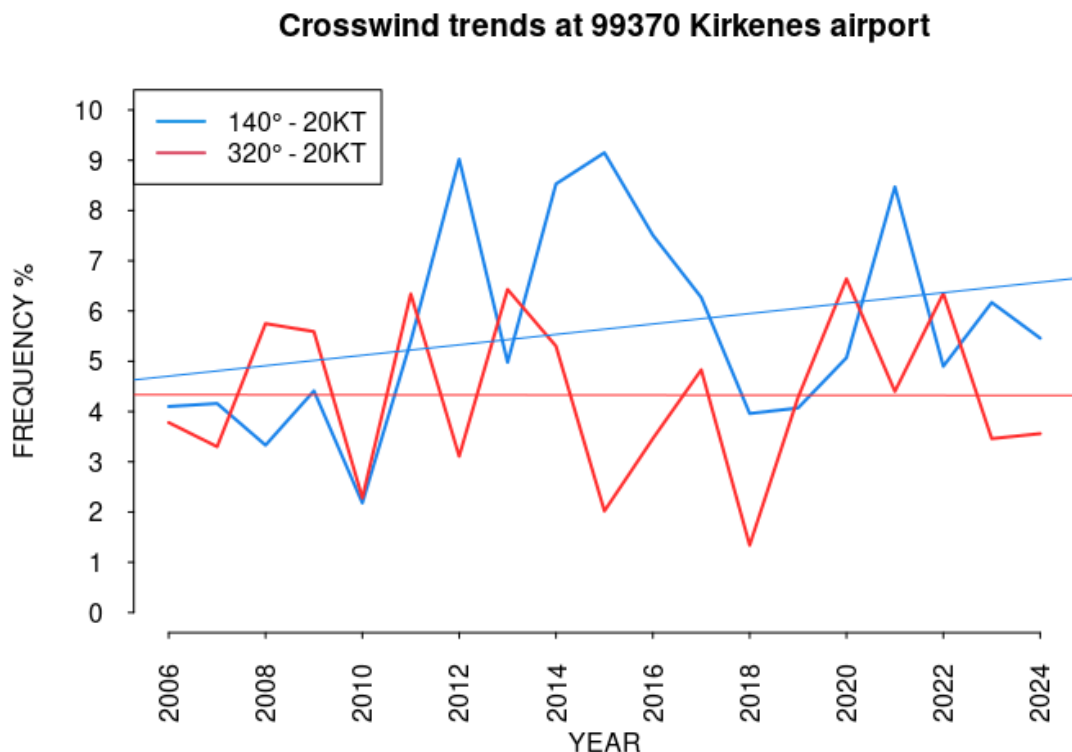


Figure 6.4.3.6.1. Frequency of crosswind components of more than 20 knots

Crosswind trends at 99370 Kirkenes airport

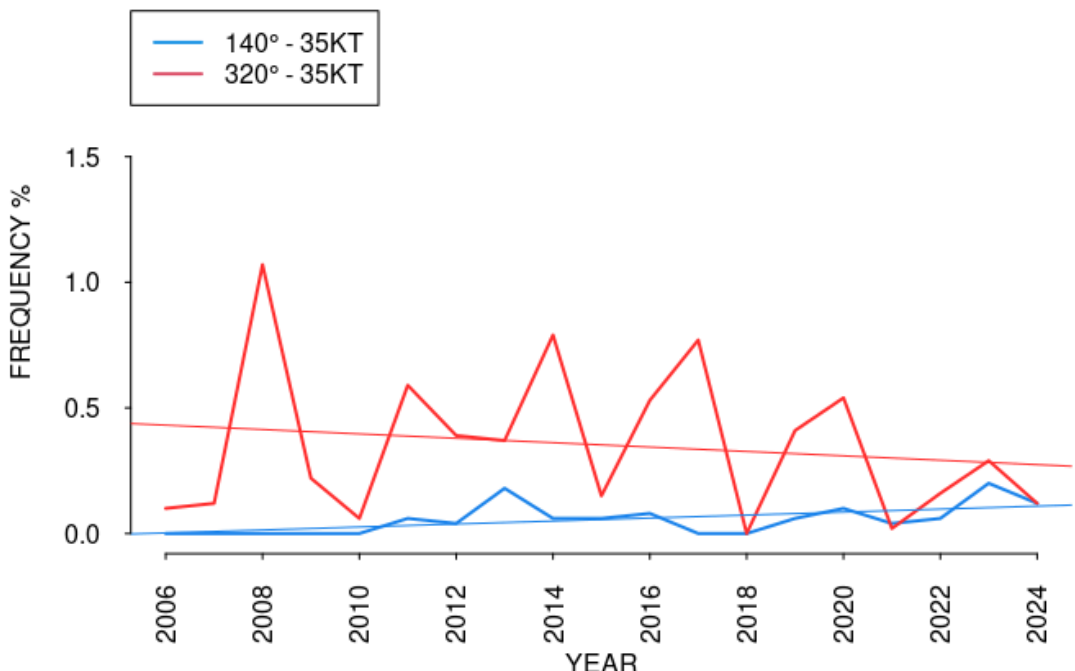


Figure 6.4.3.6.2. Frequency of crosswind components of more than 35 knots

6.4.3.7 Crosswind of long duration

It is interesting to find occasions of crosswinds of long duration. The criteria used were cross wind components of 35 knots or more for more than 10 hours, though not necessarily consecutive. The cases are listed in Table 6.4.3.7.1.

Table 6.4.3.7.1. Events of prolonged and strong wind from the crosswind directions at Kirkenes airport.

START	END	DURATION (HOURS)	STRONGEST MEAN WIND (KNOTS)	STRONGEST CROSS COMPONENT GUST (KNOTS)
13.11.2011 23	15.11.2011 02	18 (not consecutive)	NW 36 (gale)	49
13.10.2013 00	13.10.2013 12	11 (not consecutive)	NW 38 (gale)	51
15.03.2016 15	16.03.2016 08	17	WNW 42 (strong)	56

			gale)	
09.12.2016 02	10.12.2016 02	16 (not consecutive)	NW 46 (strong gale)	63

6.4.3.8 Trends for extreme wind

For this analysis “extreme wind” is defined as wind gusts of 60 knots or more. In the period 1 October 2005 to 30 April 2024 this has occurred 6 times, on all occasions with northwesterly wind. 3 of them gave a crosswind component of 60 knots or more.

In many analyses the 99-percentile value is of special interest. The 99-percentile is the 1 % highest value of a dataset. For one year of hourly observations, which is 8760 hours in a normal year, this means the 88th highest ranked value. For the seven month period October to April, 5040 hours, it means the 51st highest value. Figure 6.4.3.8.1 shows the 99-percentile wind gust speed for each year, i.e. the value for the 1 percent highest wind gust each year. The trendline is almost flat.

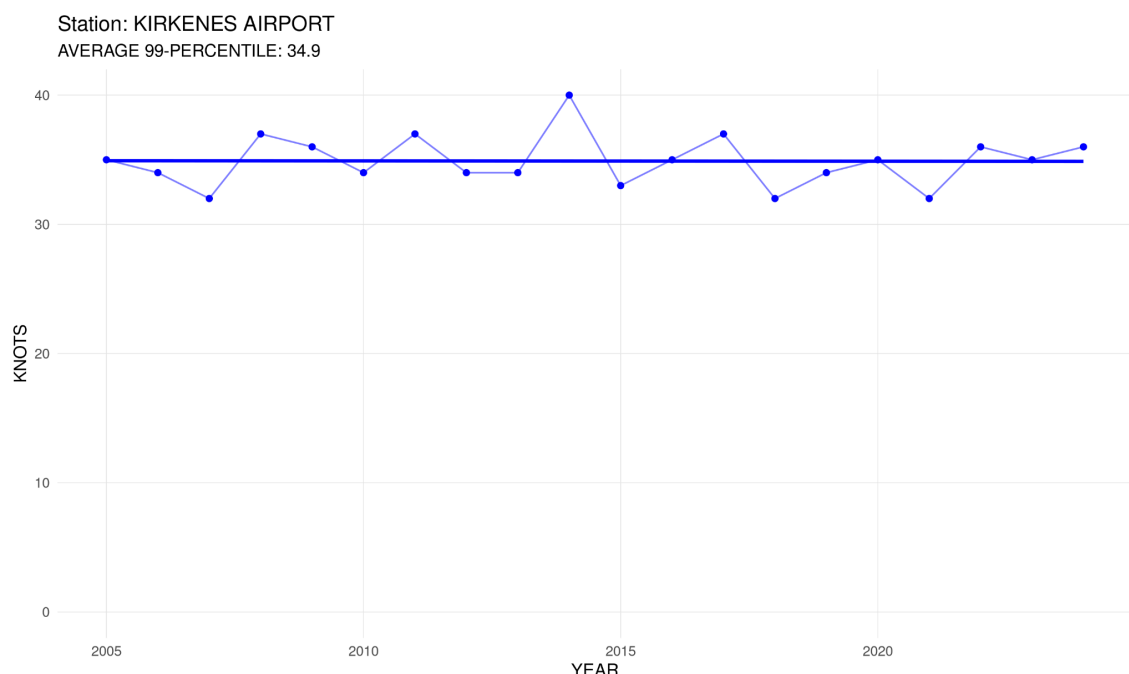


Figure 6.4.3.8.1. The annual value for the 99-percentile wind gust speed and the corresponding trend line.

6.4.4 Freezing precipitation at ground level

Freezing precipitation can be hazardous for aircraft operation. There are two main processes giving freezing precipitation: 1) Even if the temperature is less than 0 degrees Celsius, rain drops can exist as supercooled drops. They will momentarily freeze to ice when hitting the cold ground, buildings or vehicles. 2) Because cold air is heavier than warm air, it seeks to the lowest lying places. Rain drops, with a temperature above freezing, from warmer and lighter air aloft, will freeze when they are reaching the ground.

When the airport is closed for traffic, the weather observations are taken automatically. This is adequate for wind, temperature and humidity observations, but the instruments are not capable of detecting the type of precipitation. Inspecting the observation series for precipitation, it looks like the number of occurrences of freezing precipitation are overestimated by instruments compared to manual observations. Therefore the statistics for freezing precipitation at Kirkenes airport are omitted.

6.4.5 Freeze/thaw events

Since temperatures around 0°C often are challenging for airport operations, and in particular for the runway conditions, the number of freeze/thaw events are analysed.

Figure 6.4.5.1 shows the number of days when the temperature during a day both has been below and above 0 degrees at Kirkenes airport. This occurs typically on 30 to 75 days annually from 1 October to 30 April. The trend line is almost flat.

Days with freeze/thaw events 99370 Kirkenes airport

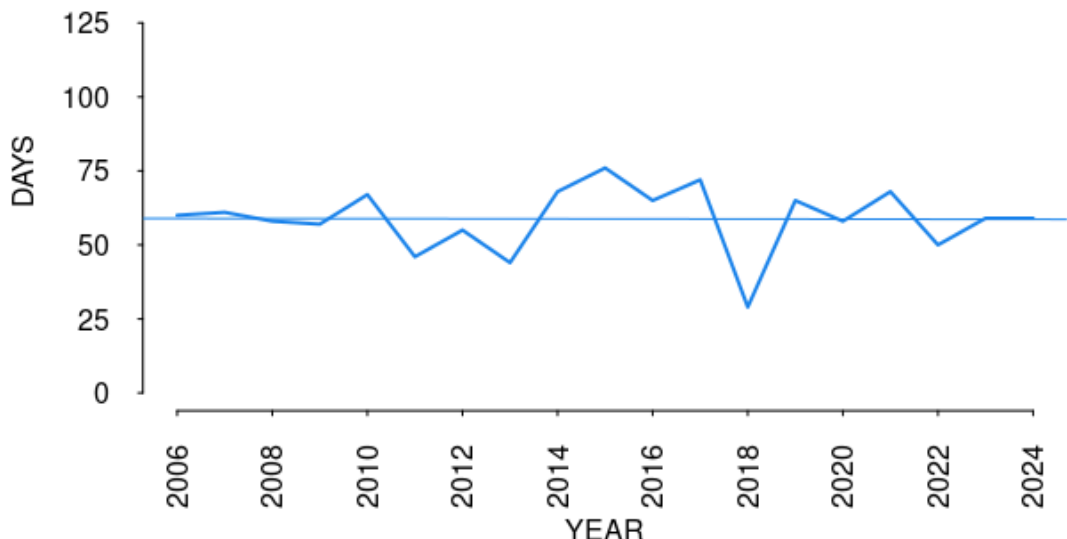


Figure 6.4.5.1. Annual number of days with temperature crossing 0 degrees Celsius

6.5 Svalbard Lufthavn

6.5.1 Main findings

The analysis of hourly wind speed observations from 2005 to 2024 for the seven month period October to April, shows that the annual frequency of southerly crosswind components of 20 knots or more varies from 3 to 8 percent. The trendline shows a *decreasing* trend. Southerly crosswind components of 35 knots or more have an annual frequency of less than 1 percent, and show a *slightly decreasing* trend. The trend for the 99-percentile value, i.e. the 1 percent highest wind gust each year, shows a *slightly decreasing* trend. Freezing precipitation at ground level varies between 0.1 and 1 percent. The trend line is *increasing*.

6.5.2 Location

Svalbard Airport is located at Hotellneset, facing Adventfjorden, and north of Platåberget, which has an elevation of 466 metres above sea level. The runway is oriented in the direction 09/27. Consequently, winds from 180 and 360 degrees will result in crosswinds at the airport. See Figure 6.5.2.1.



Figure 6.5.2.1. Svalbard Airport is located at Hotellneset, facing Adventfjorden, and north of Platåberget. Source: The Norwegian Mapping Authority

6.5.3 Wind conditions

6.5.3.1 Mean wind speed

Svalbard airport began weather observations in 1975. Hourly measurements of mean wind speed, strongest mean wind in the last hour, and strongest 3-second wind gusts in the last hour started in September 2004. These wind measurements have been used in the analysis.

The wind measurements are taken from an anemometer standing south of the threshold of runway 27.

Figure 6.5.3.1.1 shows the average mean wind speed at Svalbard airport over the seven-month period from October to April for the years 2005 to 2024. The year indications on the x-axis represent the end year of each period, so 2006 indicates the period from October 2005 to April 2006.

The average mean wind speed varies around 10-12 knots each year. A trendline has been added, showing an almost flat trend.

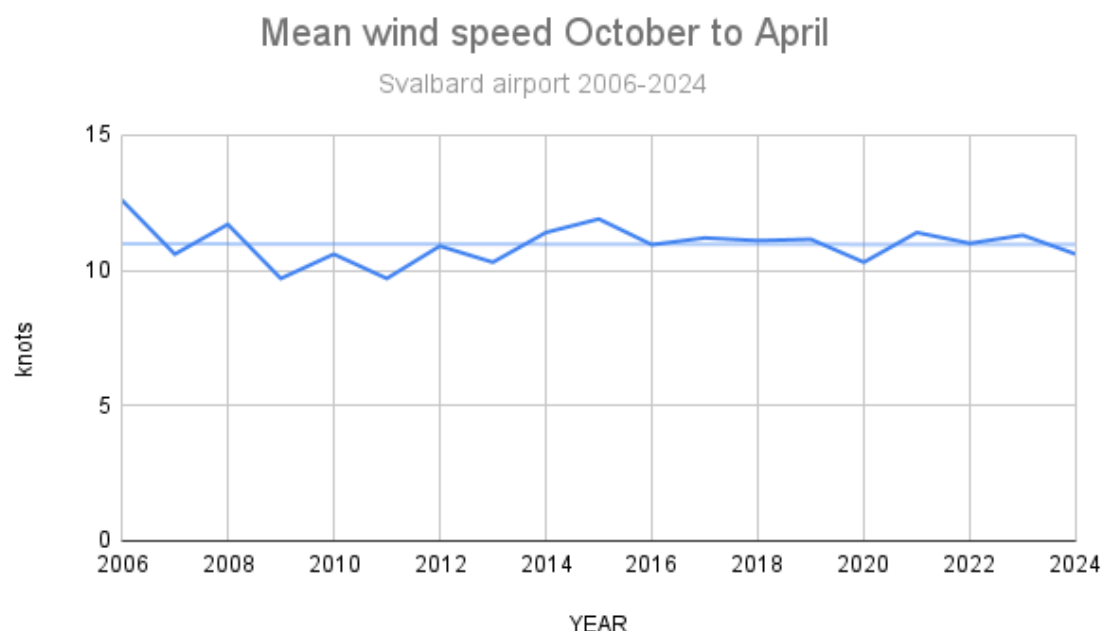
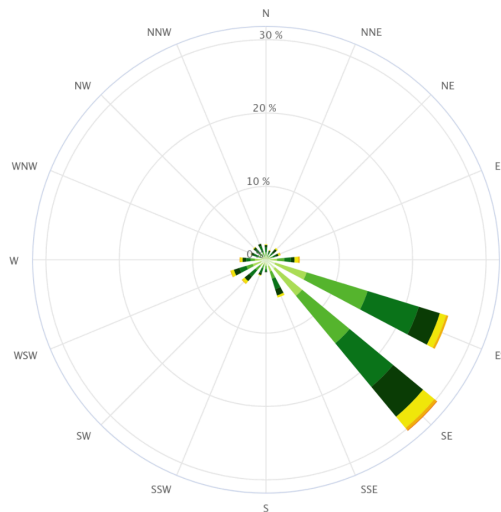


Figure 6.5.3.1.1. Average mean wind speed during the period from October to April.

6.5.3.2 Wind roses

If we compare the two wind roses (Figure 6.5.3.2.1), we see that winds between E and SSE account for 67 % of the observations in the first period, and 64 % in the second period, so the total is not so different. The main differences are that wind from SE has reduced its frequency from 30 % to 13 %, while ESE winds have increased its frequency from 26 % to 36 %.

Wind Rose for Svalbard Lufthavn (SN99840) in period; 10.2005–4.2014. Months: 10,11,12,1,2,3,4
Calm (0.0–0.2 m/s) = 1.7 %



Wind Rose for Svalbard Lufthavn (SN99840) in period; 10.2014–4.2024. Months: 10,11,12,1,2,3,4
Calm (0.0–0.2 m/s) = 0.4 %

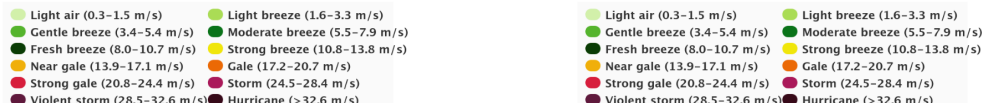
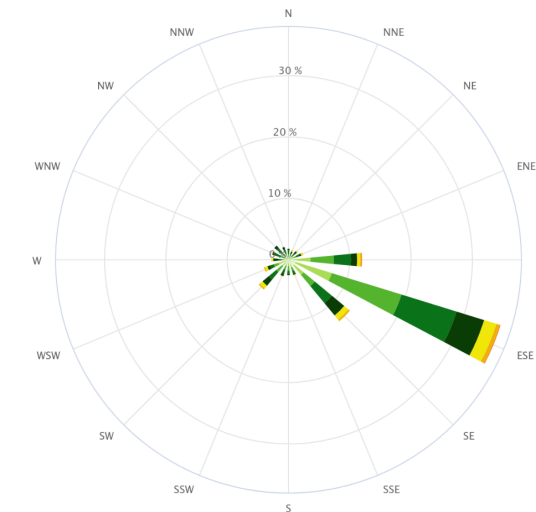


Figure 6.5.3.2.1. Wind roses for the period from October to April for the years 2005 to 2014 on the left and 2014 to 2024 on the right. Wind speed in m/s.

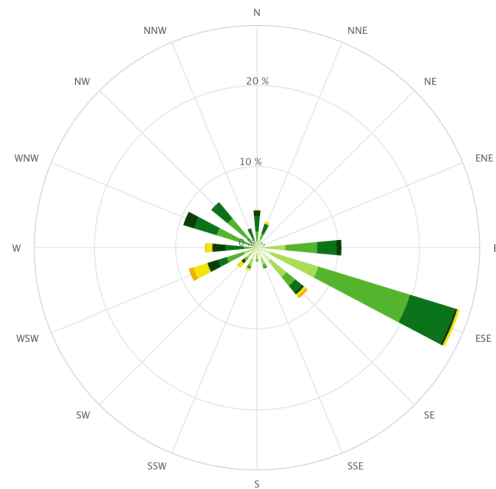
6.5.3.3 Differences in wind in a mild and a cold winter month

We could expect differences in wind conditions in a mild and cold winter month. In section 2.1, a relationship between temperature and wind was suggested, where higher temperatures resulted in stronger winds. Therefore, it would be interesting to compare the wind conditions in a mild and a cold winter month.

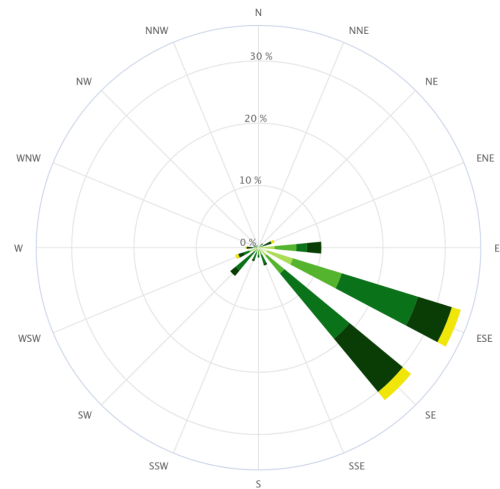
March 2020 is one of the coldest winter months in Svalbard in the period 2005 to 2024, while February 2014 is one of the mildest. Figure 6.5.3.3.1 shows the wind roses for these two months, with 2020 on the left and 2014 on the right. The average wind speed

was 4.9 m/s (9.5 knots) and 6.3 m/s (12.2 knots), respectively. In the mild February 2014, winds between east (E) and southeast (SE) occurred in 75 % of cases, while winds between westsouthwest (WSW) and northwest (NW) occurred in 7.5 % of cases. In March 2020, the corresponding figures were 44 % and 35 %.

Wind Rose for Svalbard Lufthavn (SN99840) in period; 3.2020–3.2020.
Calm (0.0–0.2 m/s) = 0.3 %



Wind Rose for Svalbard Lufthavn (SN99840) in period; 2.2014–2.2014.
Calm (0.0–0.2 m/s) = 0.5 %



Highcharts.com



Highcharts.com

Figure 6.5.3.3.1 shows the wind roses for the cold March 2020 on the left and the mild February 2014 on the right. Wind speed in m/s.

6.5.3.4 Wind gusts

The terrain near an airport influences the wind locally, creating wind conditions that will be typical for the various wind directions experienced at the airport.

One way to assess these local conditions is to observe how the gust factor changes with wind direction. The gust factor is defined as FG_1/FX_1 , where FG_1 is the strongest 3-second wind gust in the last hour and FX_1 is the strongest mean wind in the last hour. At weather stations with relatively flat and uniform terrain around the station, the gust factor typically lies around 1.2. In highly rugged terrain, wind gusts can be more than double the mean wind speed.

Figure 6.5.3.4.1 shows the average gust factor for each 10th degree, deca-degree, at Svalbard airport for the months from October to April throughout the measurement period from 2005 to 2024. Wind from the north has the highest gust factor, around 1.5. Note that this is one of the crosswind directions. Wind from the east has the lowest gust factor, near 1.2.

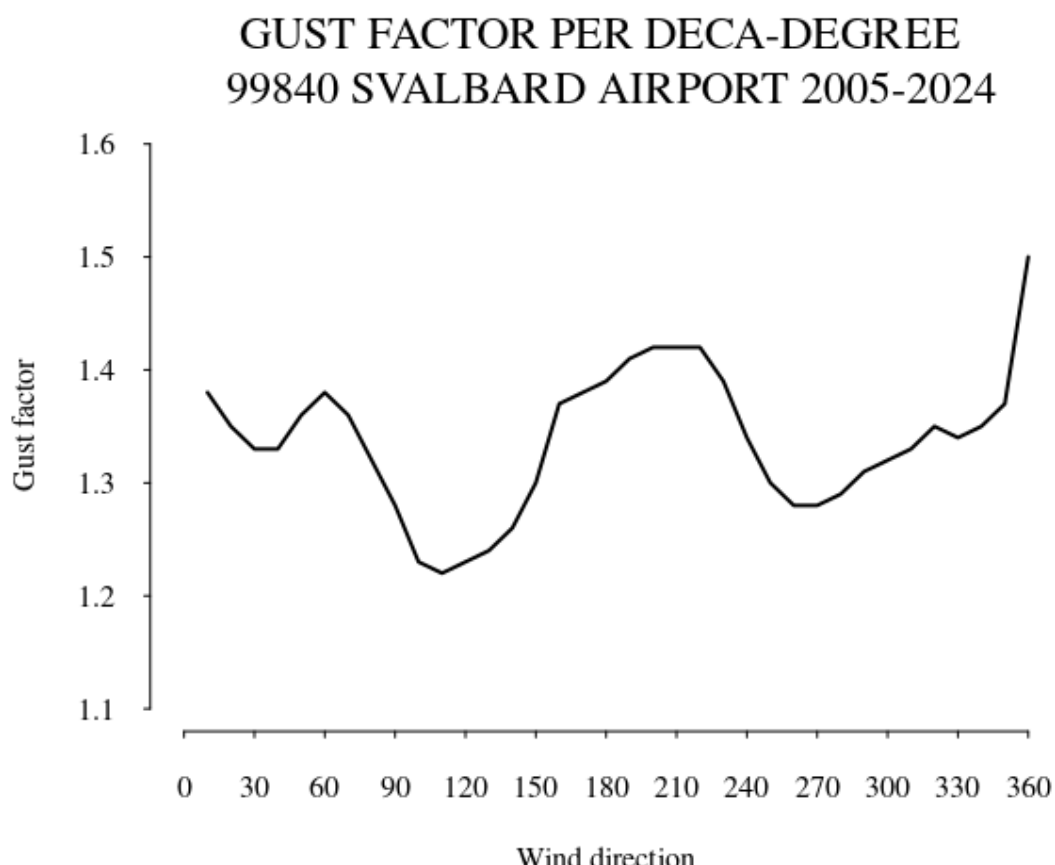


Figure 6.5.3.4.1. Gust factor per deca-degree at Svalbard airport.

It is also interesting to examine the strength of wind gusts that can occur with different wind directions. In Figure 6.5.3.4.2, both the average of the 25 strongest wind gusts and the single strongest gust recorded for each deca-degree are plotted.

The single strongest gust at Svalbard airport, 70 knots, was recorded 17 March 2022 with wind from 240 degrees. This wind direction has a gust factor of around 1.35, but the annual frequency for this wind direction is less than 5 percent.

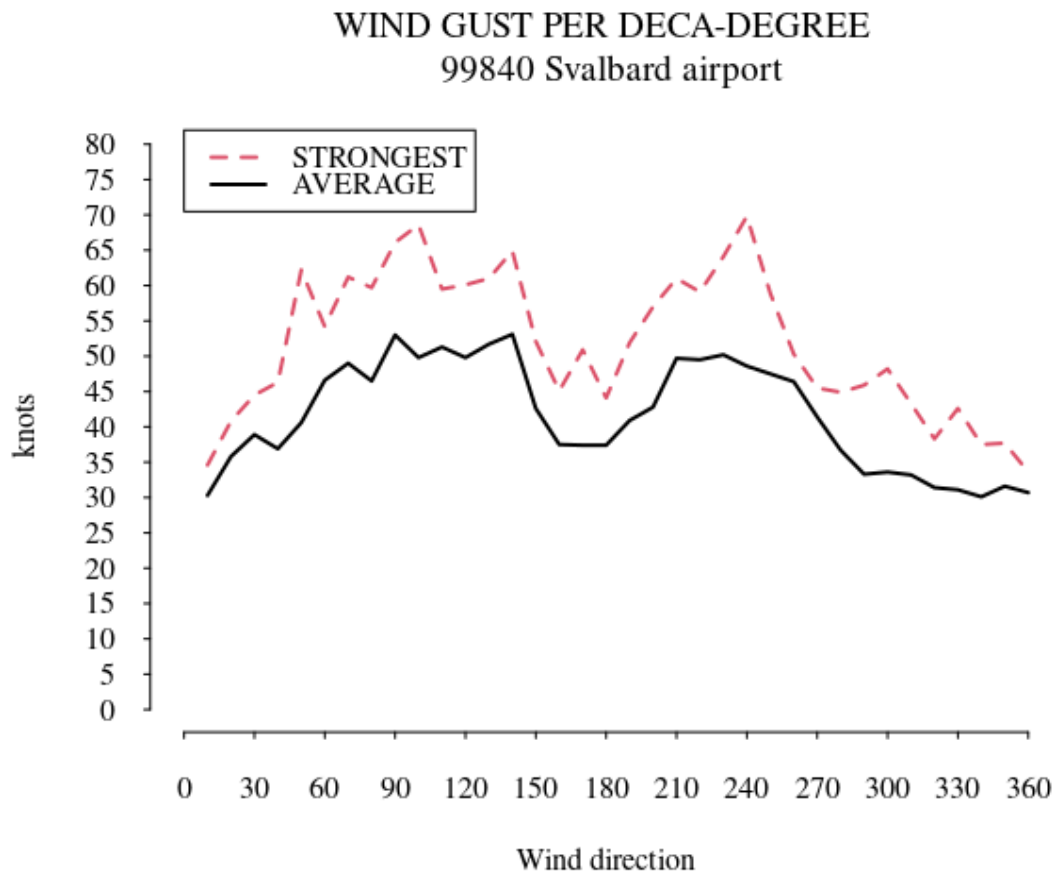


Figure 6.5.3.4.2. Strongest wind gusts and the average of the 25 strongest gusts per deca-degree at Svalbard airport.

6.5.3.5 Crosswind

Crosswinds at Svalbard airport are, as previously mentioned, at 180 and 360 degrees. Neither of these directions occur often. But strong winds from other directions can also give significant crosswind components. Table 6.5.3.5.1 shows the monthly frequencies of a crosswind component of more than 20 and 35 knots respectively. A 360 degree wind gust of 30 knots, gives, of course, a northerly component of 30 knots, while a 50 degree wind gust at 30 knots, gives a northerly component of 20 knots, still contributing to the total frequency. All strong winds from 180 and 360 degrees, will not contribute to any crosswind component.

We notice that southerly crosswinds occur more frequently than northerly crosswinds. The frequencies varies from 3 to 8 percent and 2 to 3.5 percent, respectively. Crosswind components of more than 35 knots occur very seldom, being 0.6 percent for southerly crosswind in January as highest.

Table 6.5.3.5.1. Frequency of crosswind components of 20 knots and 35 knots or more.

MONTH	Northerly >=20KT	Southerly =20KT	Northerly >=35KT	Southerly >=35KT
OCTOBER	2.0 %	3.3 %	0.0 %	0.1 %
NOVEMBER	1.9 %	5.9 %	0.0 %	0.1 %
DECEMBER	2.2 %	7.0 %	0.1 %	0.3 %
JANUARY	2.0 %	8.2 %	0.0 %	0.4 %
FEBRUARY	2.8 %	7.7 %	0.0 %	0.6 %
MARCH	3.5 %	5.8 %	0.0 %	0.3 %
APRIL	1.6 %	4.1 %	0.0 %	0.1 %
TOTAL	2.3 %	6.0 %	0.0 %	0.3 %

6.5.3.6 Trends for crosswind components

Figure 6.5.3.6.1 and 6.5.3.6.2 show the frequency of all wind gust observations giving a 180 or 360 degrees crosswind component larger than 20 and 35 knots respectively.

The frequency for southerly crosswinds stronger than 20KT varies from around 3 percent to almost 12 percent. The trend line shows a *decreasing* trend. If we look at figure 6.5.3.2.1 we see that the frequency of southeasterly wind has increased between the periods 2005-2014 and 2014-2024, giving fewer occurrences of crosswind from the south. Northerly crosswinds vary from 1 to 5 percent, and have a *slightly increasing* trend line.

Figure 6.5.3.6.2 shows the frequency of crosswind components stronger than 35 knots. The frequency for southerly crosswinds is about 1 percent at most. The figure shows a decreasing trend line. Strong northerly crosswinds occur very seldom. The highest frequency is only 0.2 % in 2023. The trend line is therefore omitted.

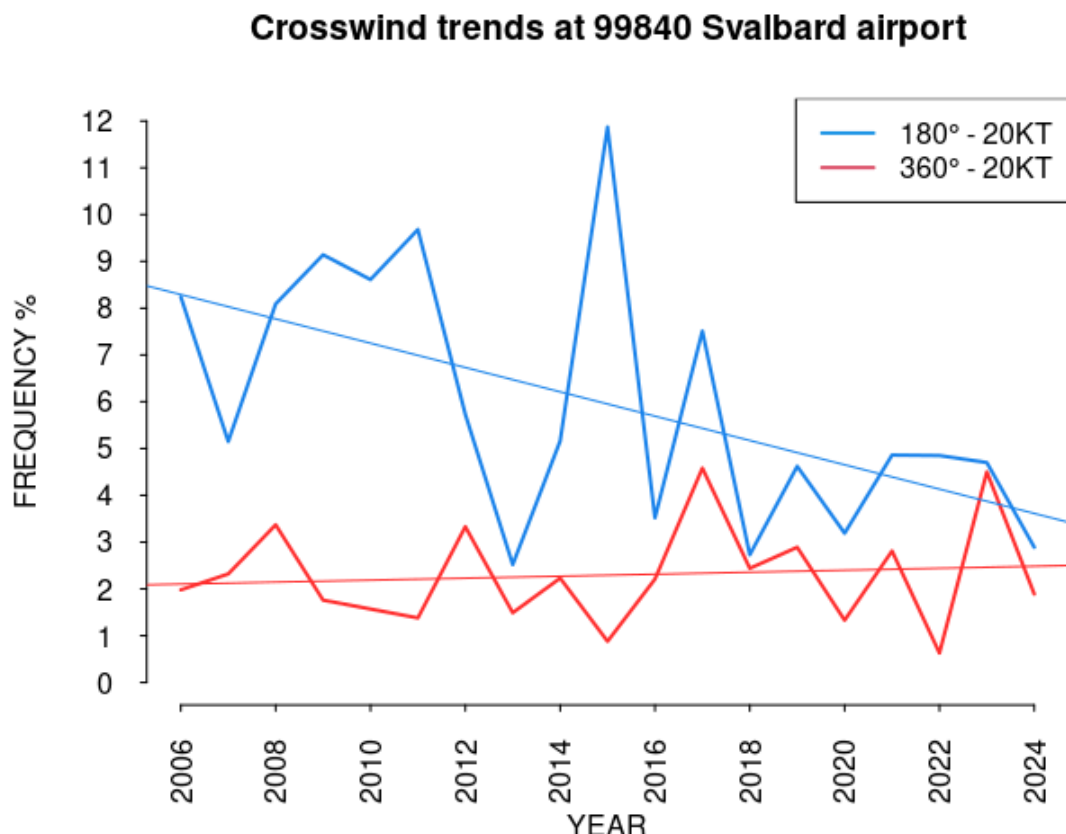


Figure 6.5.3.6.1. Frequency of crosswind components of 20 knots or more

Crosswind trends at 99840 Svalbard airport

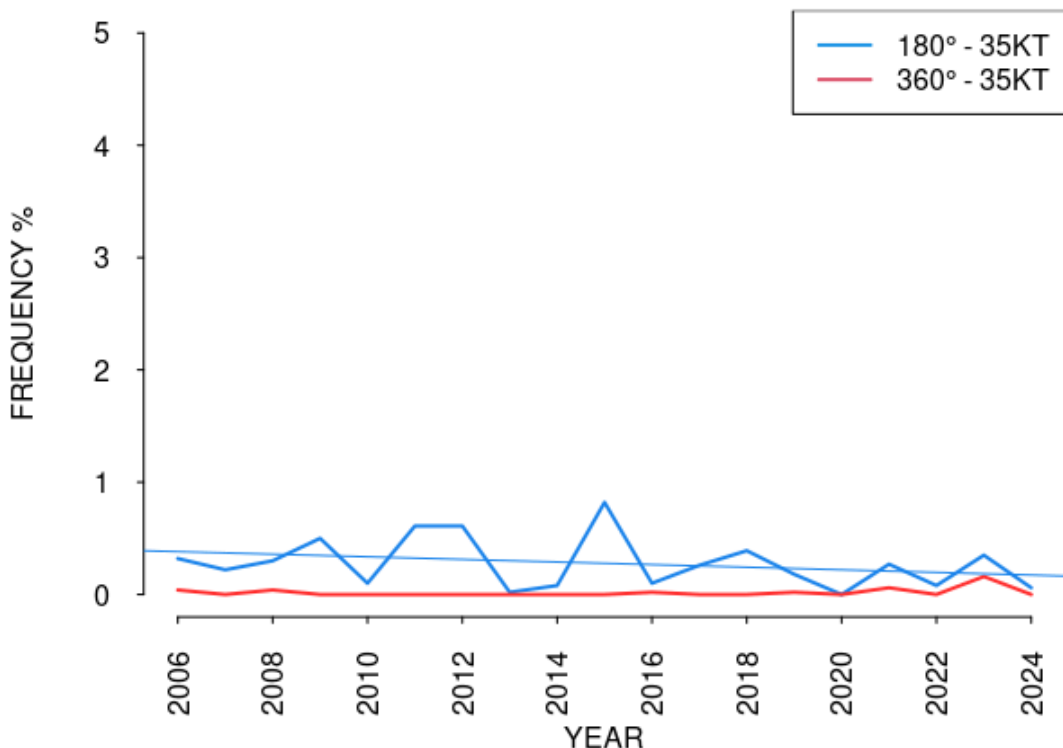


Figure 6.5.3.6.1. Frequency of crosswind components of 35 knots or more.

6.5.3.7 Crosswind of long duration

It is interesting to find occasions of crosswinds of long duration. The criteria used were cross wind components of 35 knots or more for more than 10 hours, though not necessarily consecutive (Table 6.5.3.7.1).

Table 6.5.3.7.1. Events of prolonged and strong crosswind at Svalbard airport.

START	END	DURATION (HOURS)	STRONGEST MEAN WIND (KNOTS)	STRONGEST CROSSWIND COMPONENT (KNOTS)
10.12.2008 11	10.12.2008 22	11	SW 37 (gale)	41
17.03.2011 13	18.03.2011 02	10 (not consecutive)	SW 45 (severe gale)	40
03.02.2015 15	04.02.2015 09	14 (not consecutive)	S 28 (near gale)	40

06.02.2023 22	07.02.2023 14	10 (not consecutive)	SSW 39 (gale)	55
---------------	---------------	----------------------	---------------	----

6.5.3.8 Trends for extreme wind

For this analysis “extreme wind” is defined as wind gusts of 60 knots or more. In the period 1 October 2005 to 30 April 2024 this has occurred 21 times. However, if we compute the crosswind components of these observations, only four of them are higher than 60 knots.

In many analyses the 99-percentile value is of special interest. The 99-percentile is the 1 % highest value of a dataset. For one year of hourly observations, which is 8760 hours in a normal year, this means the 88th highest ranked value. For the seven month period October to April, 5040 hours, it means the 51st highest value.

Figure 6.5.3.8.1 shows the 99-percentile wind gust speed for each year, i.e. the value for the 1 percent highest wind gust each year. The trendline shows a very *slight decrease*.

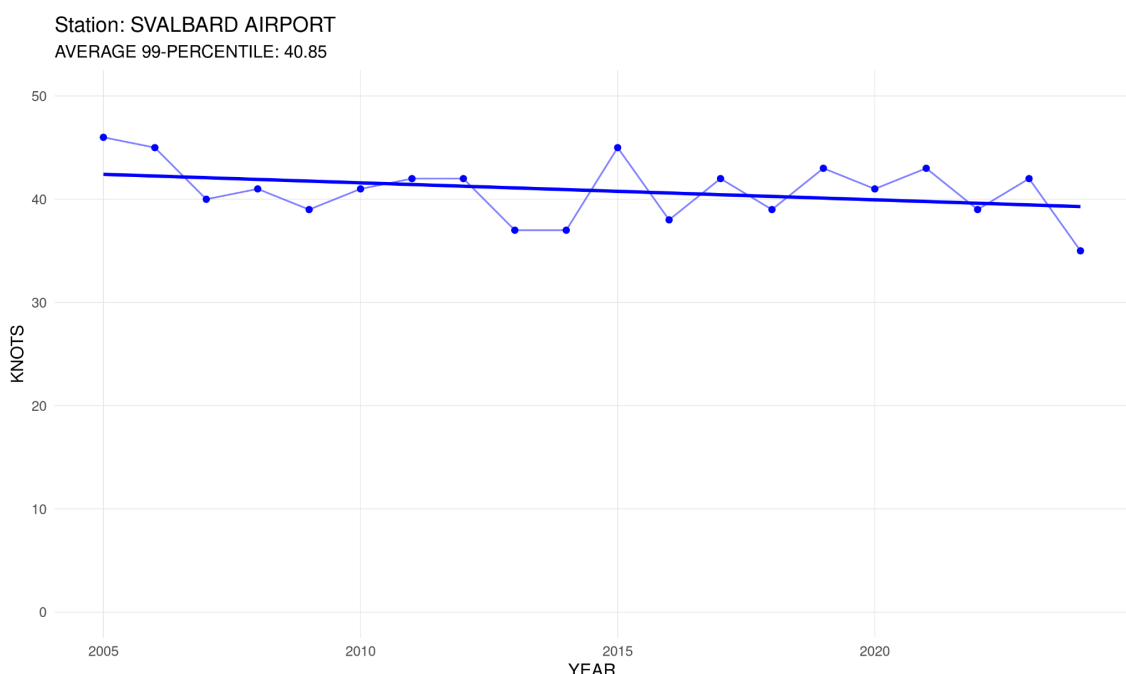


Figure 6.5.3.8.1. The annual value for the 99-percentile wind gust speed and the corresponding trend line.

6.5.4 Freezing precipitation at ground level

Freezing precipitation can be hazardous for aircraft operation. There are two main processes giving freezing precipitation: 1) Even if the temperature is less than 0 degrees Celsius, rain drops can exist as supercooled drops. They will momentarily freeze to ice when hitting the cold ground, buildings or vehicles. 2) Because cold air is heavier than warm air, it seeks to the lowest lying places. Rain drops, with a temperature above freezing, from warmer and lighter air aloft, will freeze when they are reaching the ground.

Figure 6.5.4.1 shows the annual frequency of both types of freezing precipitation at Svalbard in the period October to April. The highest value is 0.95 % in 2023. The trend line shows an increasing trend. It is reasonable to expect that higher winter temperatures also will give more occurrences of freezing precipitation.

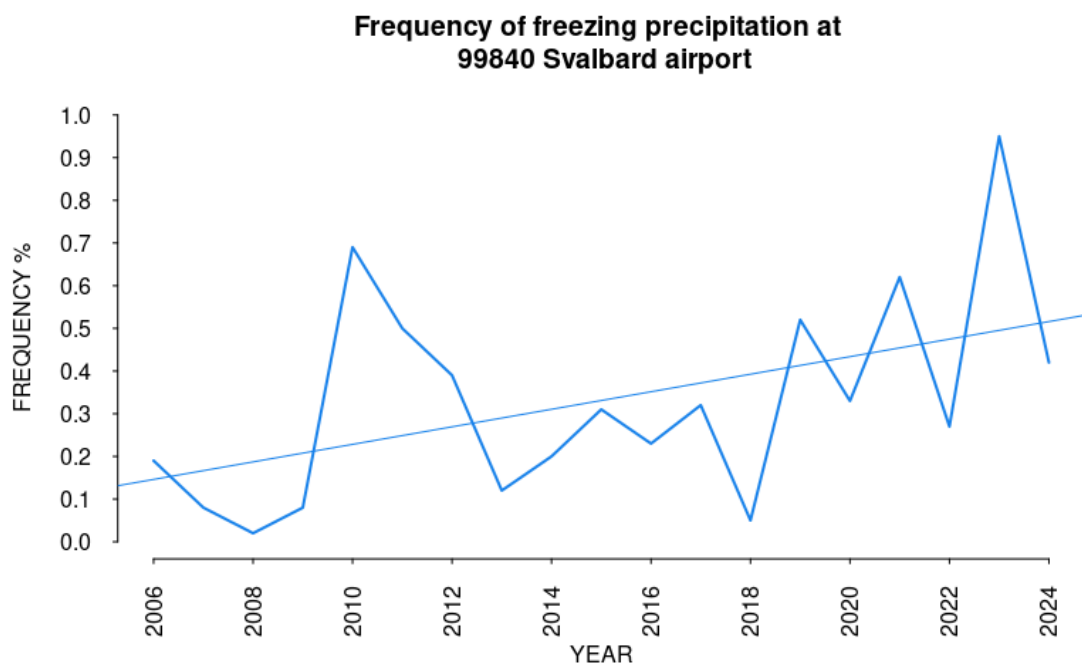


Figure 6.5.4.1. Frequency of freezing precipitation at Svalbard airport

6.5.5 Freeze/thaw events

Since temperatures around 0°C often are challenging for airport operations, and in particular for the runway conditions, the number of freeze/thaw events are analysed.

Figure 6.5.5.1 shows the number of days when the temperature during a day both has been below and above 0 degrees at Svalbard airport. This occurs typically on 30 to 70 days annually from 1 October to 30 April. The trend line is almost flat.

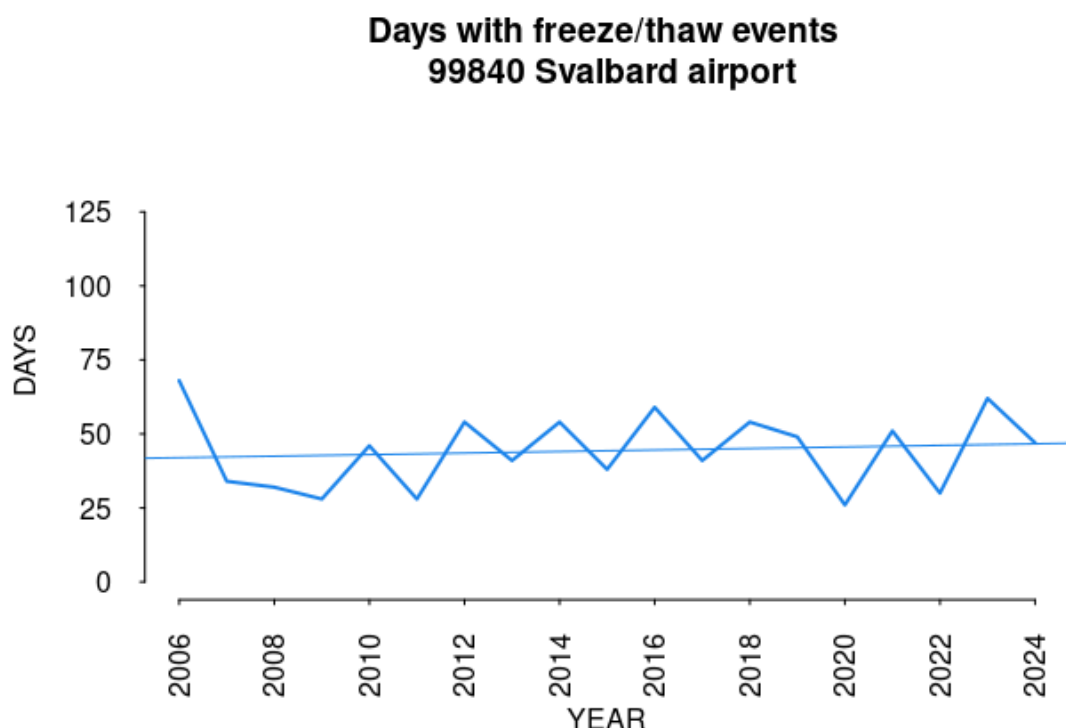


Figure 6.5.5.1. Annual number of days with temperature crossing 0 degrees Celsius

6.6 Evenes airport

6.6.1 Main findings

The analysis of hourly wind speed observations from 2005 to 2024 for the seven month period October to April, shows that the annual frequency of crosswind components of 20 knots or more, varies from 3 to 9 percent for westerly crosswind, and 1.5 to 6 percent for easterly crosswind. Both trendlines show a slightly *decreasing* trend. For crosswind components of 35 knots or more, the annual frequency is up to 1.5 percent for westerly crosswinds and around 0.5 percent for easterly crosswinds. The trend lines show a *slightly increasing* trend. The trend for the 99-percentile value, i.e. the 1 percent highest wind gust each year, shows a *slightly decreasing* trend.

6.6.2 Location

Evenes is located north of Ofotfjorden with hilly terrain with heights of 400-500 m 3-4 km from the runway on both sides of the airport. The runway is oriented in the direction 17/35. Consequently, winds from 80 and 260 degrees will result in crosswind at the airport. See figure 6.6.2.1.

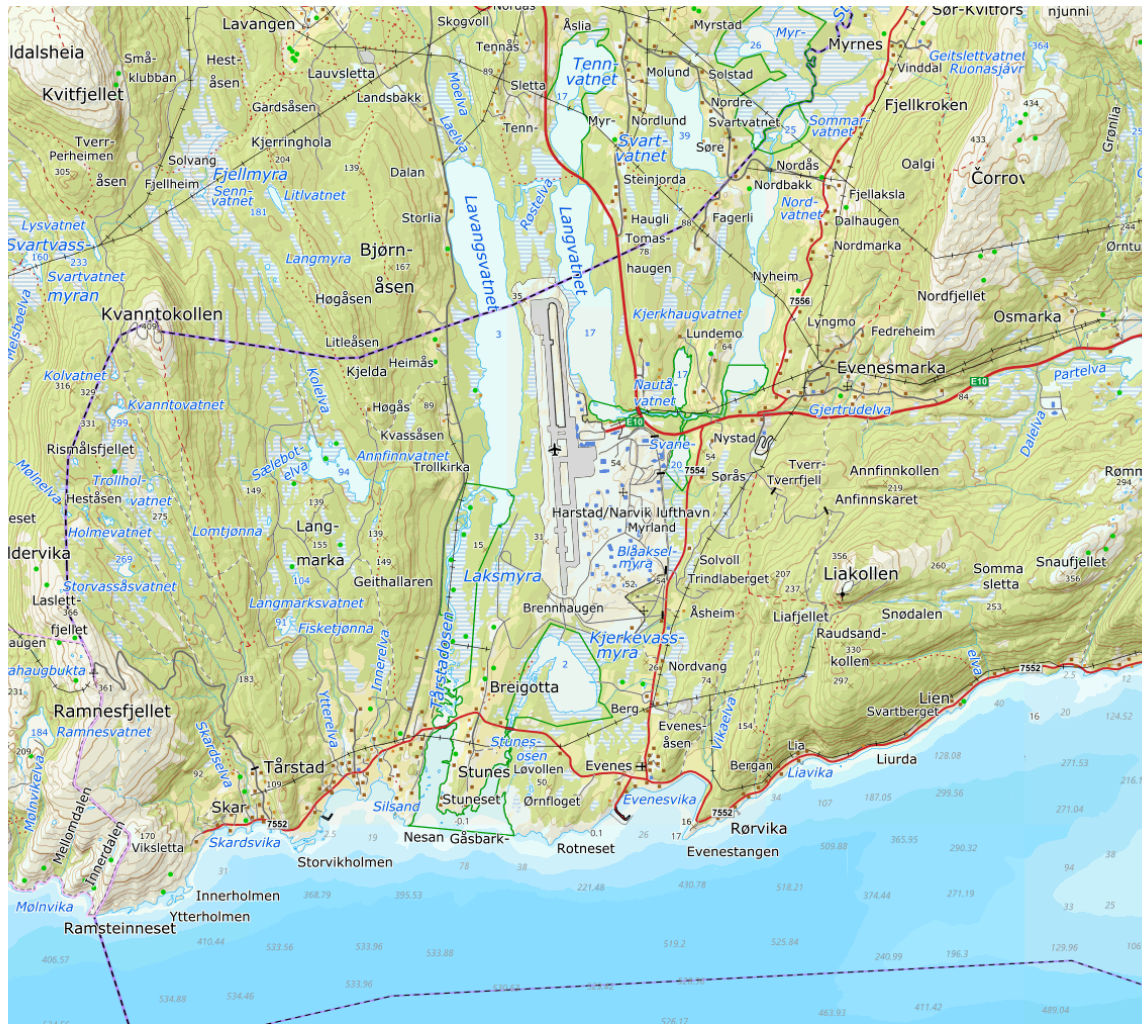


Figure 6.6.2.1. Evenes is located north of Ofotfjorden with hilly terrain on both sides of the airport. Source: The Norwegian Mapping Authority

6.6.3 Wind conditions

6.6.3.1 Mean wind speed

Evenes began weather observations in 1973. Hourly measurements of mean wind speed, strongest mean wind in the last hour, and strongest 3-second wind gusts in the last hour started in November 2004. These wind measurements have been used in the analysis.

The wind measurements, both METAR and SYNOP, are taken from an anemometer standing west of the threshold of runway 17. Wind observations are also taken northeast of the threshold of runway 35.

Figure 6.6.3.1.1 shows the average mean wind speed at Evenes over the seven-month period from October to April for the years 2005 to 2024. The year indications on the x-axis represent the end year of each period, so 2006 indicates the period from October 2005 to April 2006.

The average mean wind speed lies around 6-7 knots each year. A trendline has been added, showing a slightly negative trend.

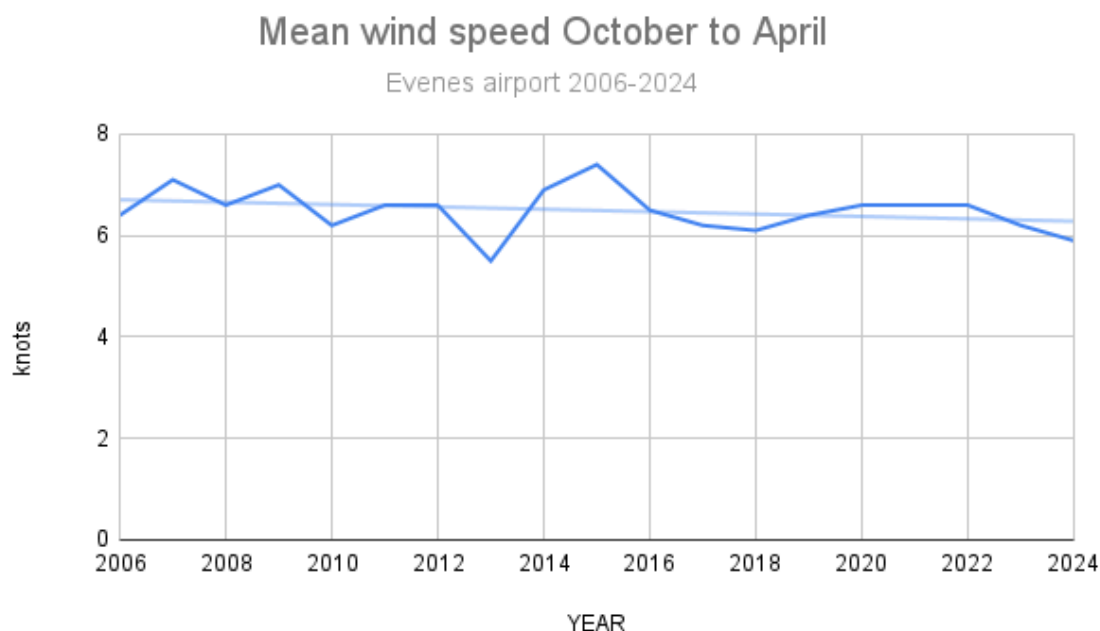


Figure 6.6.3.1.1. Average mean wind speed during the period from October to April.

6.6.3.2 Wind roses

Wind Rose for Evenes Lufthavn (SN84970) in period; 10.2005–4.2014. Months: 10,11,12,1,2,3,4
Calm (0.0–0.2 m/s) = 3 %

Wind Rose for Evenes Lufthavn (SN84970) in period; 10.2014–4.2024. Months: 10,11,12,1,2,3,4
Calm (0.0–0.2 m/s) = 2.4 %

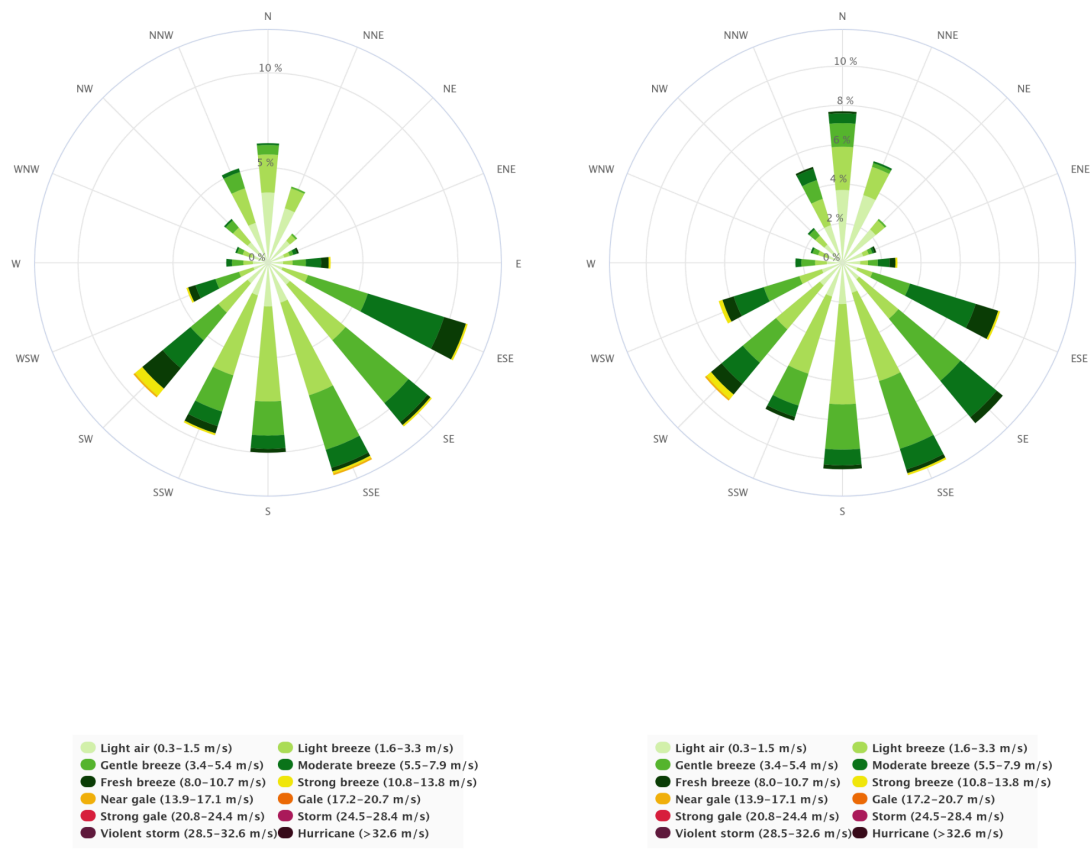


Figure 6.6.3.2.1. Wind roses for the period from October to April for the years 2005 to 2014 on the left and 2014 to 2024 on the right. Wind speed in m/s.

Visually, the wind roses in Figure 6.6.3.2.1 appear to be very similar. Wind in the sector ESE to SW has a total frequency of 63 % and 58 % in the two periods, respectively. Northerly winds occur slightly more often in the second period, 2014-2024, by having a total frequency of 19 % compared to 16 % for the first period, 2005-2014. For the crosswind directions WSW and ENE, the total frequencies are 8 % in the second period and 6 % in the first period.

6.6.3.3 Differences in wind in a mild and a cold winter month

There exists a relationship between monthly temperatures and wind: a mild month will usually have higher mean wind. Therefore, it would be interesting to compare the wind conditions in the mildest and the coldest winter months at Evenes.

February 2007 is the coldest winter month at Evenes in the period from 2005 to 2024, while December 2007 is the mildest. Figure 6.6.3.3.1 shows the wind roses for these two months, with February 2007 on the left and December 2007 on the right. The average wind speed was 3.2 m/s (5.9 knots) and 4 m/s (7.8 knots), respectively. We notice that SW, one of the crosswind directions, has a higher frequency in December 2007 than in February 2007, with 14 % and 6 %, respectively.

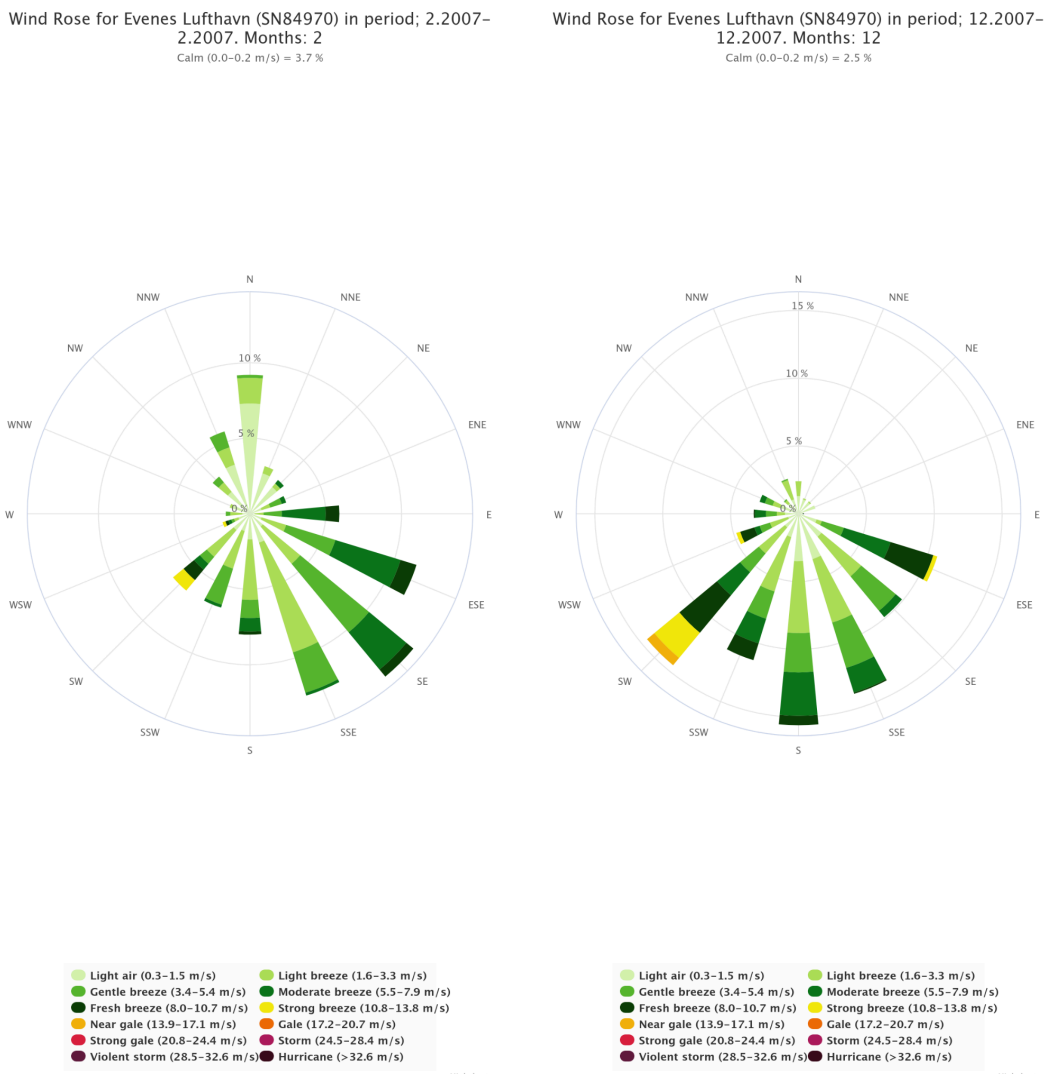


Figure 6.6.3.3.1 shows the wind roses for the cold February 2007 on the left and the mild December 2007 on the right. Wind speed in m/s.

6.6.3.4 Wind gusts

The terrain near an airport influences the wind locally, creating wind conditions that will be typical for the various wind directions experienced at the airport.

One way to assess these local conditions is to observe how the gust factor changes with wind direction. The gust factor is defined as FG_1/FX_1 , where FG_1 is the strongest 3-second wind gust in the last hour and FX_1 is the strongest mean wind in the last hour. At weather stations with relatively flat and uniform terrain around the station, the gust factor typically lies around 1.2. In highly rugged terrain, wind gusts can be more than double the mean wind speed.

Figure 6.6.3.4.1 shows the average gust factor for each 10th degree, deca-degree, at Evenes for the months from October to April throughout the measurement period from 2005 to 2024. With a runway going almost straight north/south and hilly terrain both west and east of the airport, it is not surprising that both westerly and easterly winds have the highest gust factors, up to 1.6. Winds from the south and north have the lowest, but still as high as around 1.5.

GUST FACTOR PER DECA-DEGREE 84970 EVENES 2005-2024

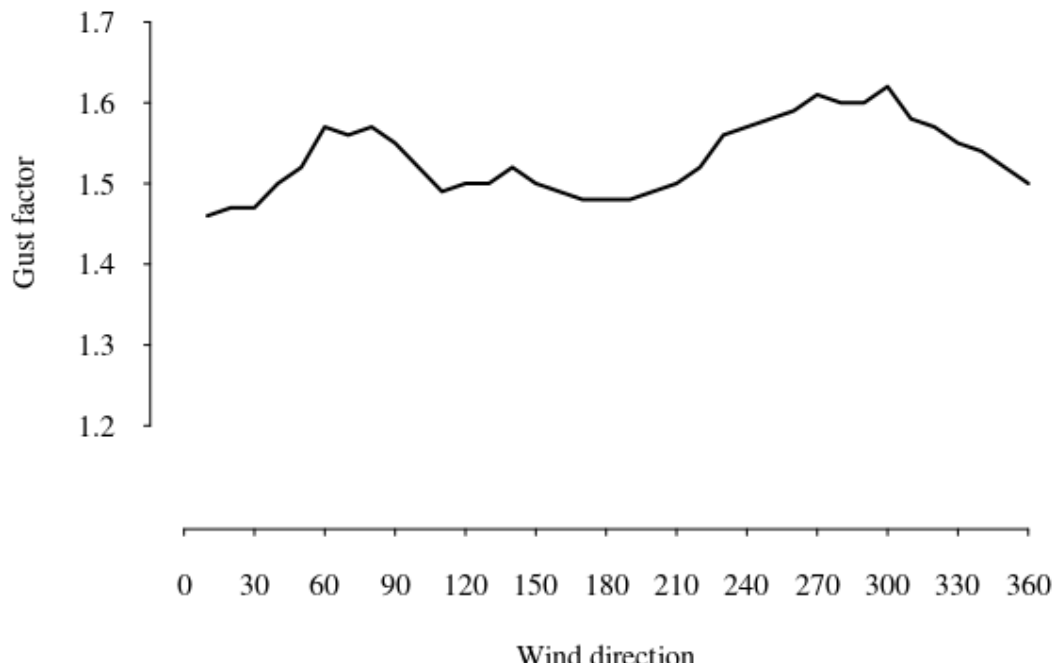


Figure 6.6.3.4.1. Gust factor per deca-degree at Evenes

Although wind from the crosswind directions WNW and ENE has high gust factors, the wind roses in figures 6.6.2.3.1 and 6.6.3.3.1 show that wind from these directions does not occur frequently. But in a mild month, wind from SW occurs more often. Therefore, it is interesting to examine the strength of wind gusts that can occur with different wind directions. In Figure 6.6.3.4.2, both the average of the 25 strongest wind gusts and the single strongest wind gust recorded for each deca-degree are plotted.

The single strongest wind gust at Evenes, 66 knots, was recorded with wind from 237 degrees in January 2024, giving a crosswind component of 60 knots.

WIND GUST PER DECA-DEGREE 84970 Evenes

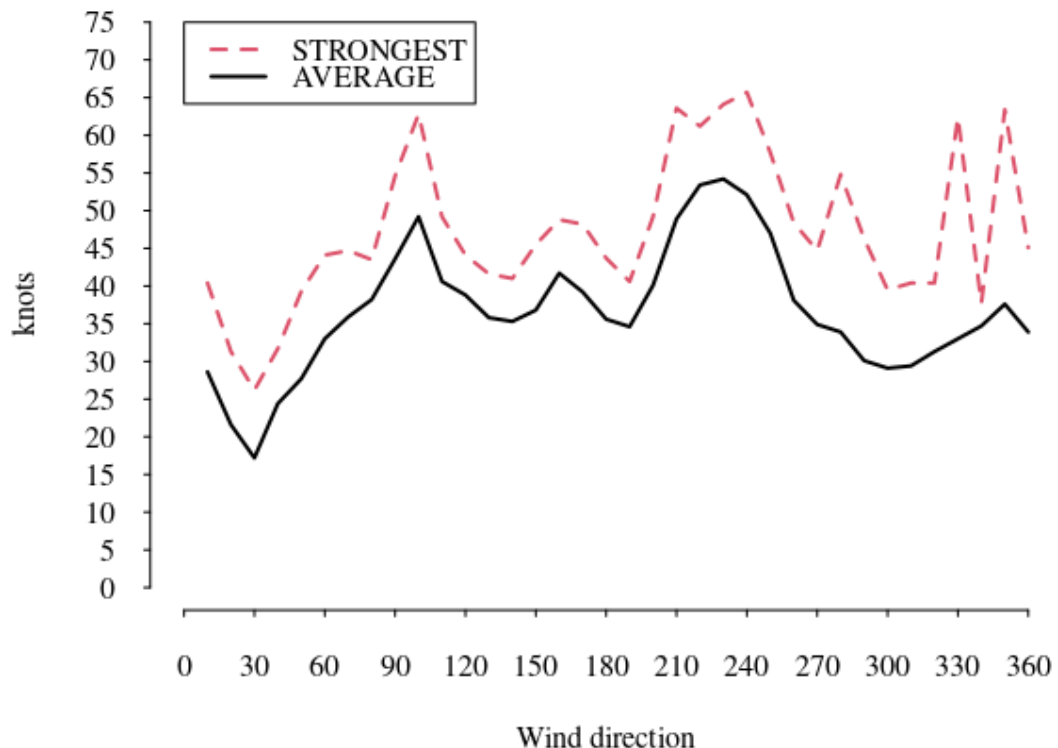


Figure 6.3.3.4.2. Strongest wind gust and the average of the 25 strongest gusts per deca-degree at Evenes

6.6.3.5 Crosswinds

Crosswinds at Evenes, as previously mentioned, are at 80 and 260 degrees. Wind from 80 degrees does not occur often. Wind from 230 degrees has the highest average, 56 knots, for the 25 strongest wind gusts from this direction.

But strong wind from other directions can also give significant crosswind components. Table 6.6.3.5.1 shows the monthly frequencies of a crosswind component of more than 20 and 35 knots respectively. A 260 degrees wind gust of 30 knots, gives, of course, a westerly component of 30 knots, while a 230 or 290 degrees wind gust at 30 knots, gives a westerly component of 26 knots. All strong winds from 160 and 340 degrees, will not contribute to any crosswind components at all.

Table 6.6.3.5.1. Monthly frequencies of crosswind component of 20 knots and 35 knots or more at Evenes airport

MONTH	Westerly >=20 knots	Easterly>=20 knots	Westerly>=35 knots	Easterly>=35 knots
OCTOBER	4.3%	3.2 %	0.3 %	0.0 %
NOVEMBER	3.6 %	3.3 %	0.3 %	0.1 %
DECEMBER	5.4 %	4.5 %	0.7 %	0.1 %
JANUARY	5.0 %	6.5 %	0.8 %	0.7 %
FEBRUARY	5.9 %	4.1 %	0.9 %	0.0 %
MARCH	7.2 %	2.4 %	1.0 %	0.0 %
APRIL	5.9 %	2.0 %	0.3 %	0.0 %
TOTAL	5.4 %	3.7 %	0.6 %	0.2 %

6.6.3.6 Trends for crosswind

Figure 6.6.3.6.1 and 6.6.3.6.2 show the frequency of all wind gust observations giving a 260 or 80 degrees wind component larger than 20 and 35 knots respectively.

The frequency for westerly crosswinds stronger than 20KT varies from around 2 percent to almost 10 percent annually. Easterly crosswinds occur from 1 to 6 percent annually. Both curves have a *decreasing* trend line.

Crosswind trends at 84970 Evenes

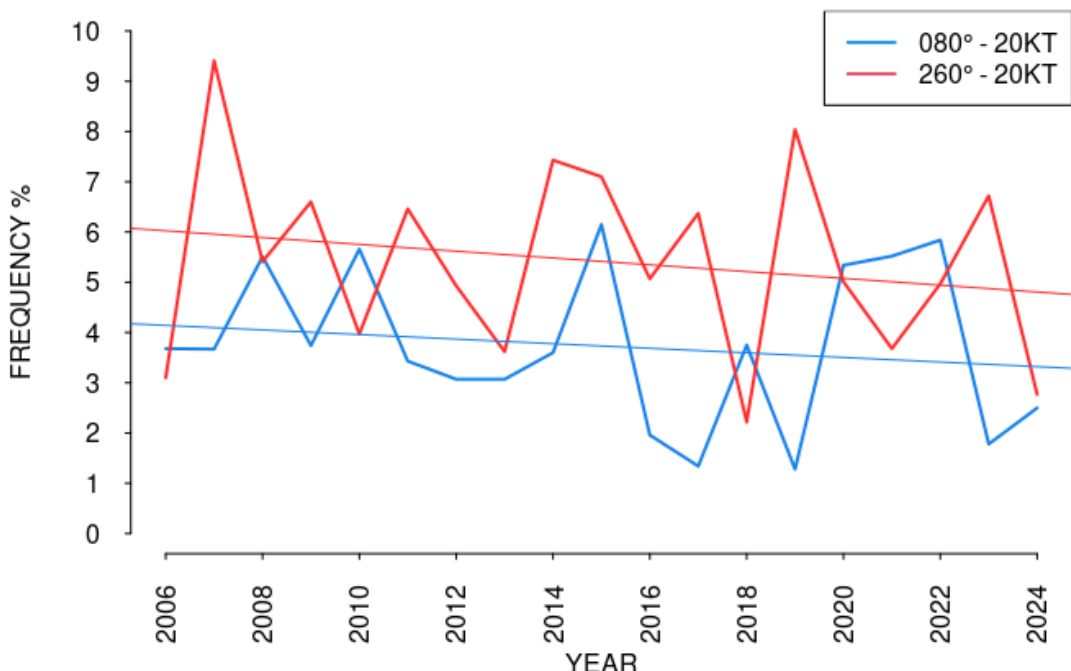


Figure 6.6.3.6.1. Annual frequency of crosswind components of 20 knots or more

Figure 6.6.3.6.2 shows the frequency of crosswind components stronger than 35 knots. The frequencies for easterly crosswinds vary from a few tens of a percent to up to 1.5 percent. Frequencies of westerly crosswinds vary from a few tens of a percent to 0.8 percent. Both trendlines show an *increasing* trend.

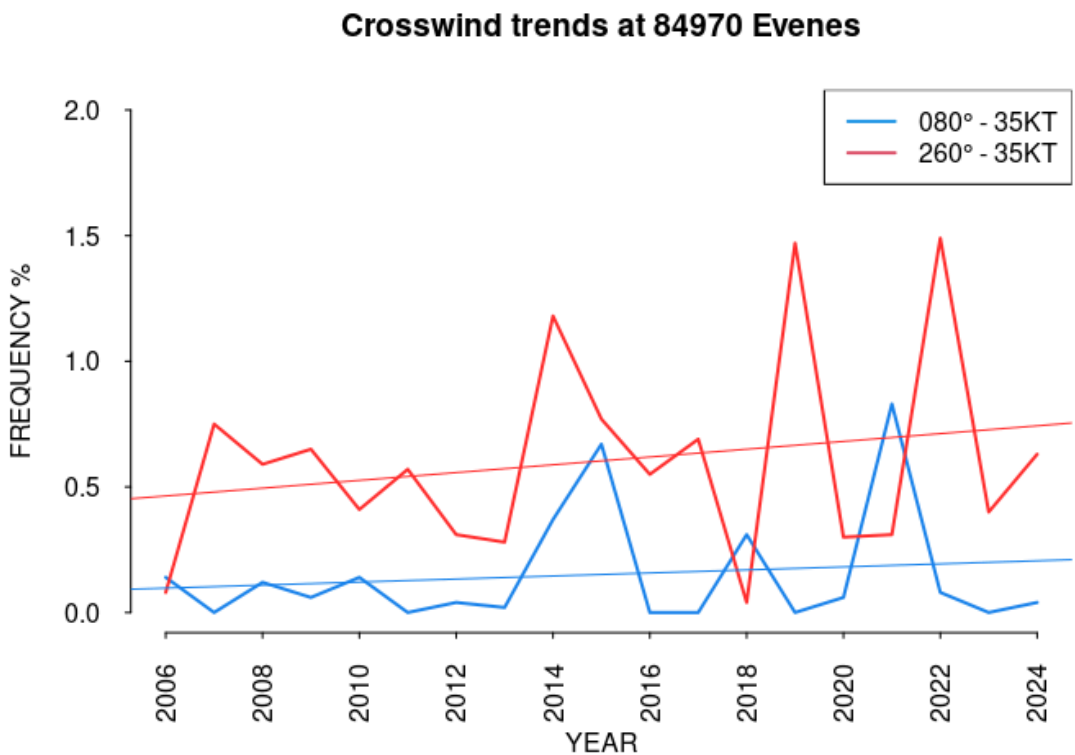


Figure 6.6.3.6.2. Frequency of crosswind components of 35 knots or more

6.6.3.7 Crosswind of long duration

It is interesting to find occasions of crosswinds of long duration. The criteria used in Table 6.6.3.7.1 are duration of more than 12 hours and a mean wind speed of 30 knots or more.

Table 6.6.3.7.1 Events of prolonged and strong crosswind at Evenes

START	END	DURATION (HOURS)	STRONGEST MEAN WIND (KNOTS)	STRONGEST CROSS WIND COMPONENT (KNOTS)
09.01.2014 06	10.01.2014 00	18	NE 30 (near gale)	45
09.03.2014 16	10.03.2014 09	16	SW 34 (near gale)	48
28.01.2015 23	30.01.2015 08	31 (not consecutive)	E 40 (gale)	60
01.11.2015 04	01.11.2015 19	14	SE 33 (near gale)	49

23.11.2017 09	24.11.2017 06	14 (not consecutive)	SSE 33 (near gale)	41
21.01.2021 14	23.01.2021 09	40 (not consecutive)	E 30 (near gale)	44
19.03.2022 16	20.03.2022 09	16	W 31 (near gale)	49
29.01.2024 04	29.01.2024 21	15	SW 38 (near gale)	60

6.6.3.8 Extreme wind

For this analysis “extreme wind” is defined as wind gusts of 60 knots or more. In the period 1 October 2005 to 30 April 2024 this has occurred 9 times. However, if we compute the crosswind components of these observations, only two of them are higher than 60 knots.

In many analyses the 99-percentile value is of special interest. The 99-percentile is the 1 % highest value of a dataset. For one year of hourly observations, which is 8760 hours in a normal year, this means the 88th highest ranked value. For the seven month period October to April, 5040 hours, it means the 51st highest value.

Figure 6.6.3.8.1 shows the 99-percentile wind gust speed for each year, i.e. the value for the 1 percent highest wind gust each year. The trendline shows a very *slight decrease*.

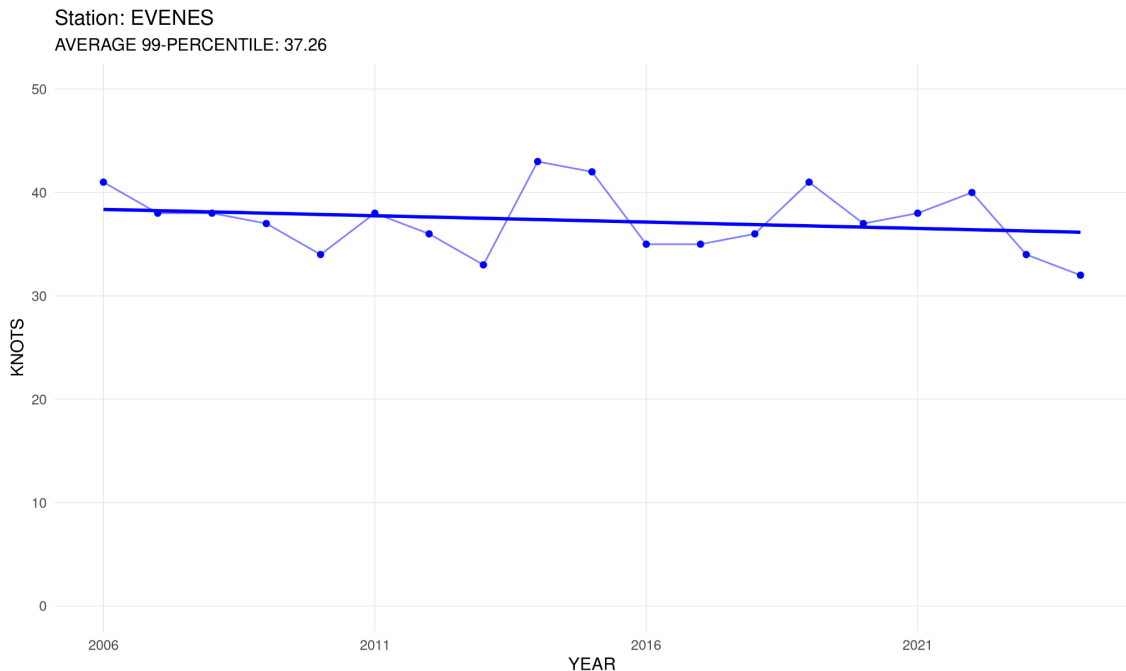


Figure 6.6.3.8.1. The annual value for the 99-percentile wind gust speed and the corresponding trend line.

6.6.4 Freezing precipitation

Freezing precipitation can be hazardous for aircraft operation. There are two main processes giving freezing precipitation: 1) Even if the temperature is less than 0 degrees Celsius, rain drops can exist as supercooled drops. They will momentarily freeze to ice when hitting the cold ground, buildings or vehicles. 2) Because cold air is heavier than warm air, it seeks to the lowest lying places. Rain drops, with a temperature above freezing, from warmer and lighter air aloft, will freeze when they are reaching the ground.

When the airport is closed for traffic, the weather observations are taken automatically. This is adequate for wind, temperature and humidity observations, but the instruments are not capable of detecting the type of precipitation. Inspecting the observation series for precipitation, it looks like the number of occurrences of freezing precipitation are overestimated by instruments compared to manual observations. Therefore the statistics for freezing precipitation at Evenes airport are omitted.

6.6.5 Freeze/thaw events

Since temperatures around 0°C often are challenging for airport operations, and in particular for the runway conditions, the number of freeze/thaw events are analysed.

Figure 6.6.5.1 shows the number of days when the temperature during a day both has been below and above 0 degrees at Evenes. This occurs typically on 70 to 110 days annually from 1 October to 30 April. The trend line is slightly decreasing.

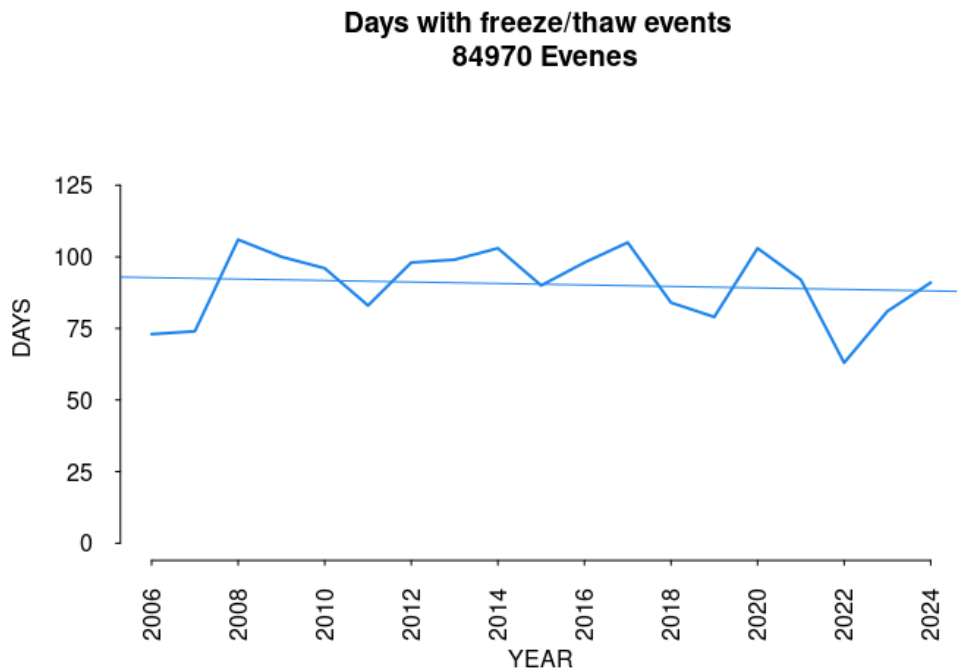


Figure 6.6.5.1. The number of days with freeze/thaw events for the period October to April

6.7 Andøya airport

6.7.1 Main findings

The analysis of hourly wind speed observations from 2005 to 2024 for the seven month period October to April, shows that the annual frequency of southwesterly crosswind components of 20 knots or more varies from 7 to 15 percent. The trendline shows a *decreasing* trend. For northeasterly crosswind components of 20 knots or more, the annual frequency lies between 2 to 8 percent, and shows an increasing trend. For southwesterly crosswind components of 35 knots or more the annual frequency varies from 0.5 to 3.5 percent, and also shows a decreasing trend. Northeasterly crosswind components of 35 knots or more usually have an annual frequency well below 1 percent, and show no significant trends. The trend for the 99-percentile value, i.e. the 1 percent highest wind gust each year, shows a *slightly decreasing* trend.

6.7.2 Location

Andøya airport is situated on very flat terrain on the northeast side of Andøya. The highest point within 5 km from the runway is the hill Røyken at 468 meters above sea level. See figure 6.7.2.1.

The runway is oriented in the direction 14/32, i.e. 140/320 degrees. Consequently, winds from 50 and 230 degrees will result in crosswind at the airport.

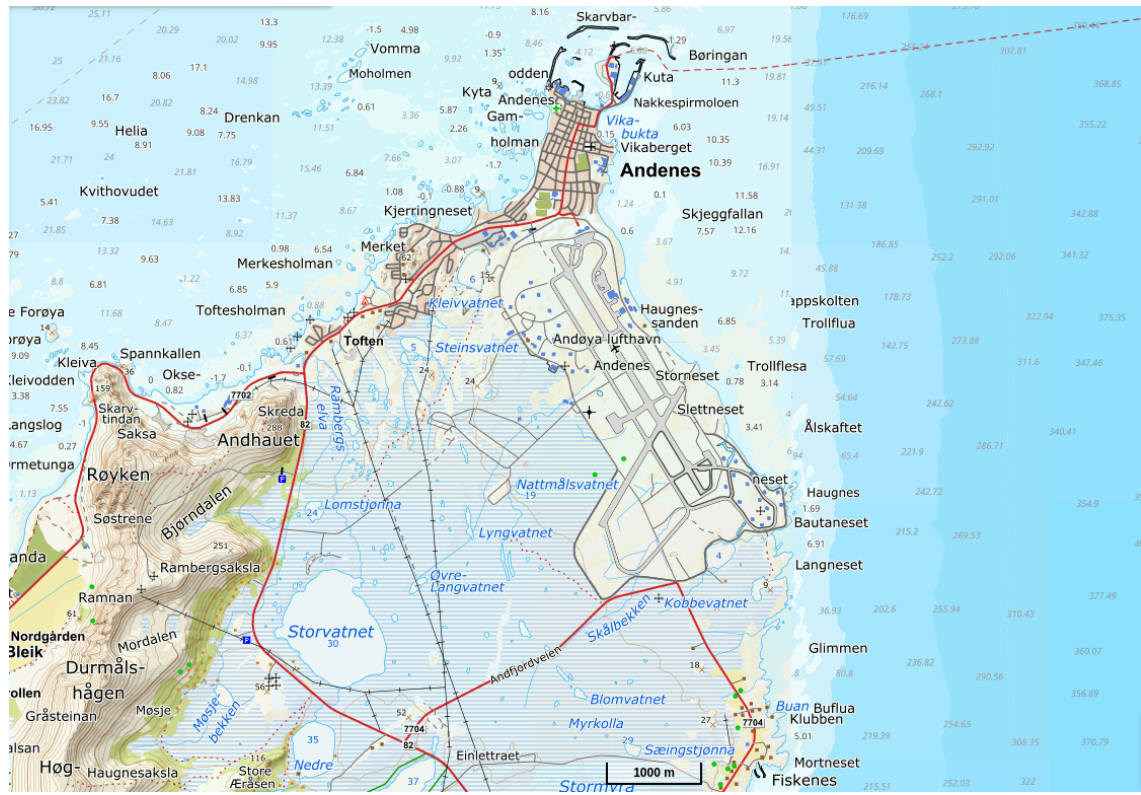


Figure 6.7.2.1. Andøya airport is located on the northeast side of Andøya. Source: The Norwegian Mapping Authority

6.7.3 Wind conditions

6.7.3.1 Mean wind speed

Andøya began weather observations in 1958. Hourly measurements of mean wind speed, strongest mean wind in the last hour, and strongest 3-second wind gusts in the last hour started in January 2004. Wind measurements since October 2005 have been used in this analysis.

The wind measurements, both METAR and SYNOP, are taken from an anemometer standing 250 m east of the threshold of runway 14. Wind observations are also taken 400 m west of runway 32.

Figure 6.7.3.1.1 shows the average mean wind speed at Andøya over the seven-month period from October to April for the years 2005 to 2024. The year indications on the x-axis represent the end year of each period, so 2006 indicates the period from October 2005 to April 2006.

The average mean wind speed lies typically around 12-14 knots each year. A trendline has been added, showing no trend.

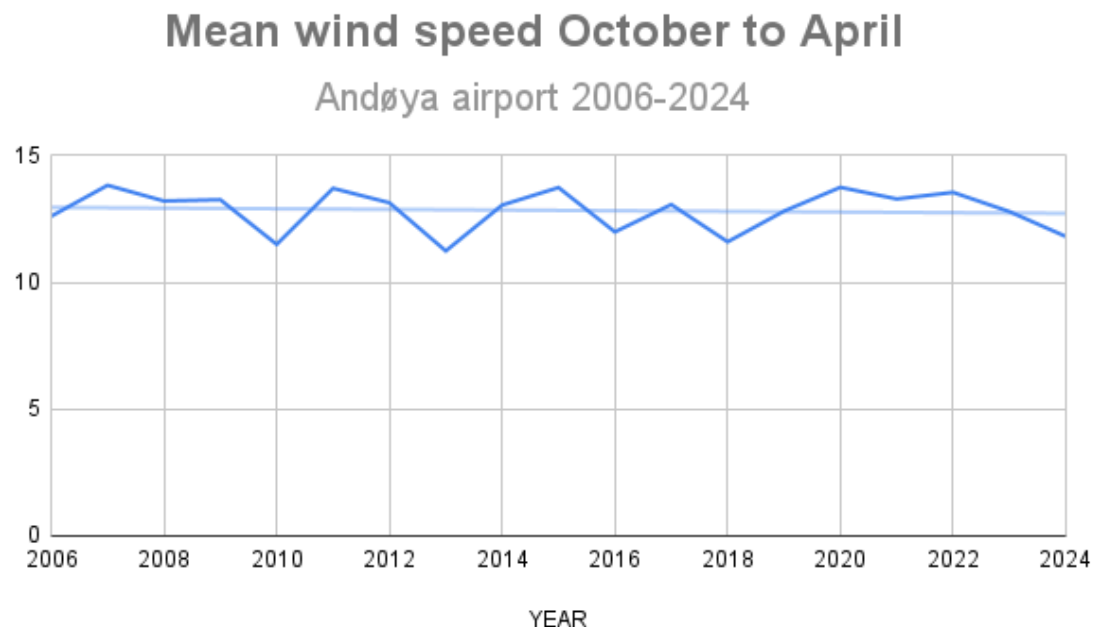


Figure 6.7.3.1.1. Average mean wind speed during the period from October to April.

6.7.3.2 Wind roses

Wind Rose for Andøya (SN87110) in period; 10.2005–4.2014.
Months: 10,11,12,1,2,3,4
Calm (0.0–0.2 m/s) = 0.3 %

Wind Rose for Andøya (SN87110) in period; 10.2014–4.2024.
Months: 10,11,12,1,2,3,4
Calm (0.0–0.2 m/s) = 0.2 %

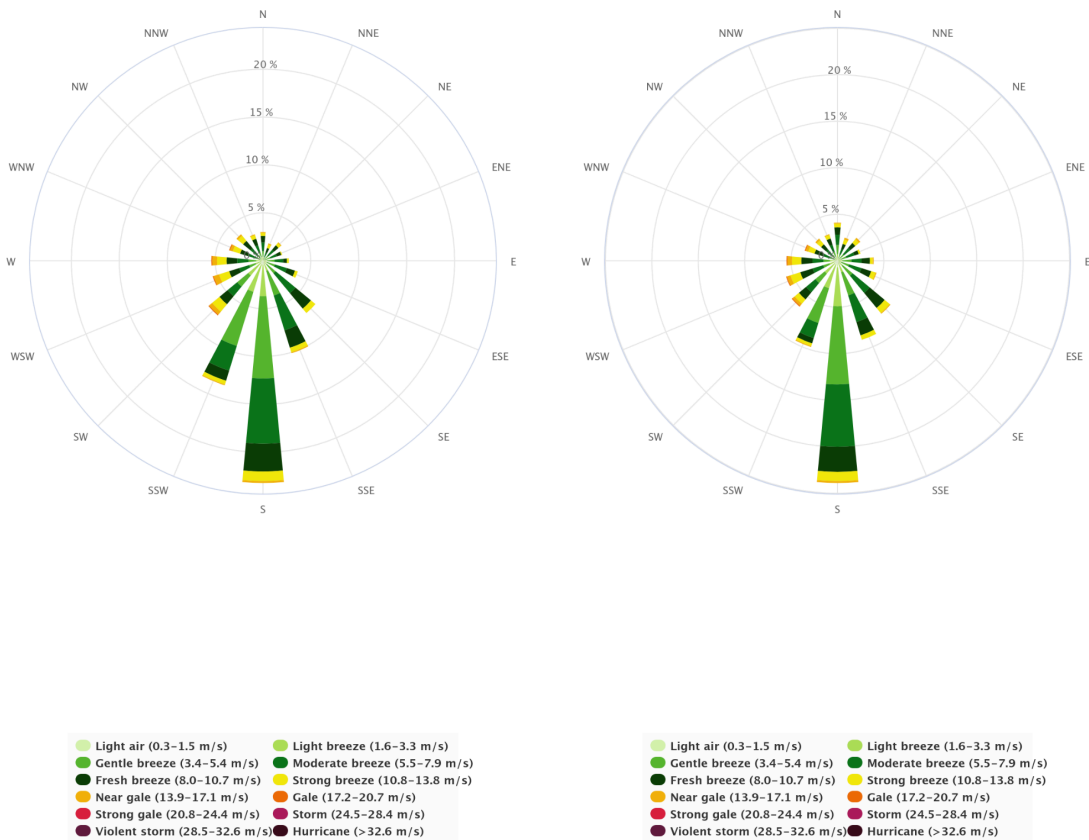


Figure 6.7.3.2.1. Wind roses for the period from October to April for the years 2005 to 2014 on the left and 2014 to 2024 on the right. Wind speed in m/s.

Visually, the wind roses in Figure 6.7.3.2.1 appear to be very similar. The three most frequent wind directions, SSE, S, and SSW, have frequencies of 47 % and 43 % in the two periods, respectively.

6.7.3.3 Differences in wind in a mild and a cold winter month

It is interesting to compare the wind conditions in a mild and a cold winter month.

December 2012 is one the coldest winter months at Andøya in the period from 2005 to 2024, while December 2007 is one of the mildest. Figure 6.7.3.3.1 shows the wind roses for these two months, with the cold 2012 on the left and the mild 2007 on the right. The average wind speed was 5.6 m/s (11 knots) and 8.2 m/s (16 knots), respectively. In December 2012 SSW was the most frequent wind direction with 26 %, while in December 2007 wind from S was dominating with 38 %. We also notice more westerly wind in a mild winter month.

Wind Rose for Andøya (SN87110) in period; 12.2012–12.2012.
Months: 12
Calm (0.0–0.2 m/s) = 0 %

Wind Rose for Andøya (SN87110) in period; 12.2007–12.2007.
Months: 12
Calm (0.0–0.2 m/s) = 0 %

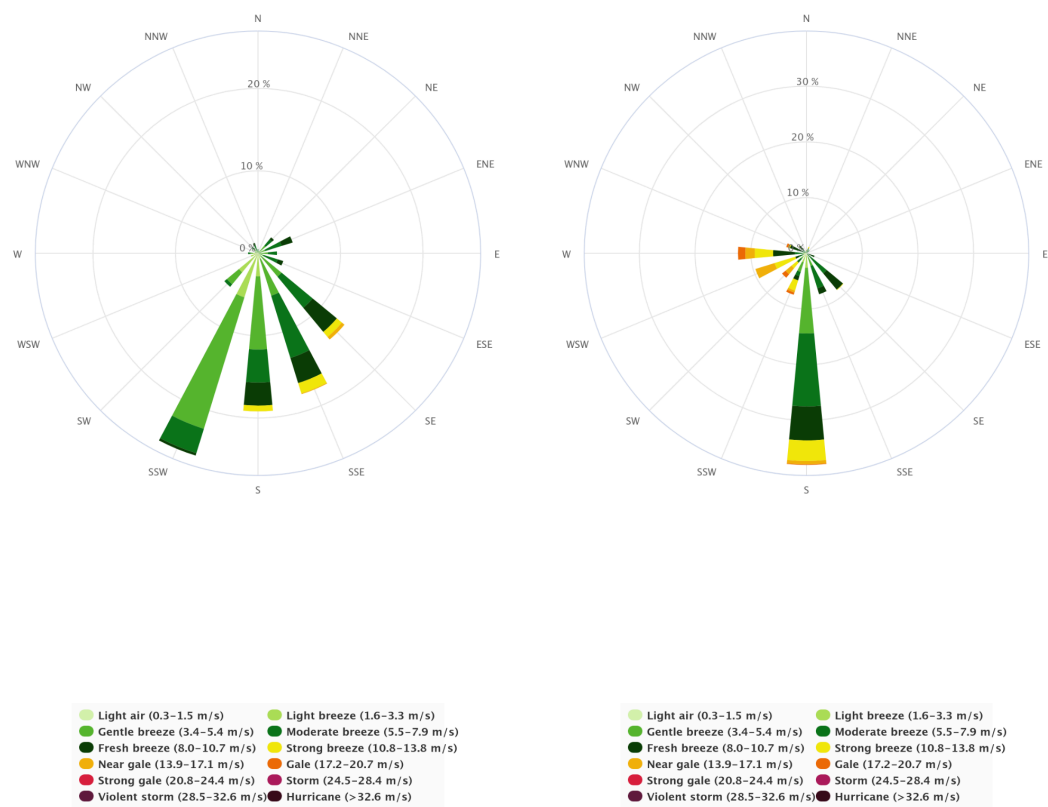


Figure 6.7.3.3.1 shows the wind roses for the cold December 2012 on the left and the mild December 2007 on the right. Wind speed in m/s.

6.7.3.4 Wind gusts

The terrain near an airport influences the wind locally, creating wind conditions that will be typical for the various wind directions experienced at the airport.

One way to assess these local conditions is to observe how the gust factor changes with wind direction. The gust factor is defined as FG_1/FX_1 , where FG_1 is the strongest 3-second wind gust in the last hour and FX_1 is the strongest mean wind in the last hour. At weather stations with relatively flat and uniform terrain around the station, the gust factor typically lies around 1.2. In highly rugged terrain, wind gusts can be more than double the mean wind speed.

Figure 6.7.3.4.1 shows the average gust factor for each 10th degree, deca-degree, at Andøya for the months from October to April throughout the measurement period from 2005 to 2024. Because the terrain near the airport is mainly flat, the gust factor does not vary so much, and lies mainly between 1.2 and 1.3. But wind from the southwest has a gust factor of 1.4. This is one of the crosswind directions.

GUST FACTOR PER DECA-DEGREE 87110 ANDØYA 2005-2024

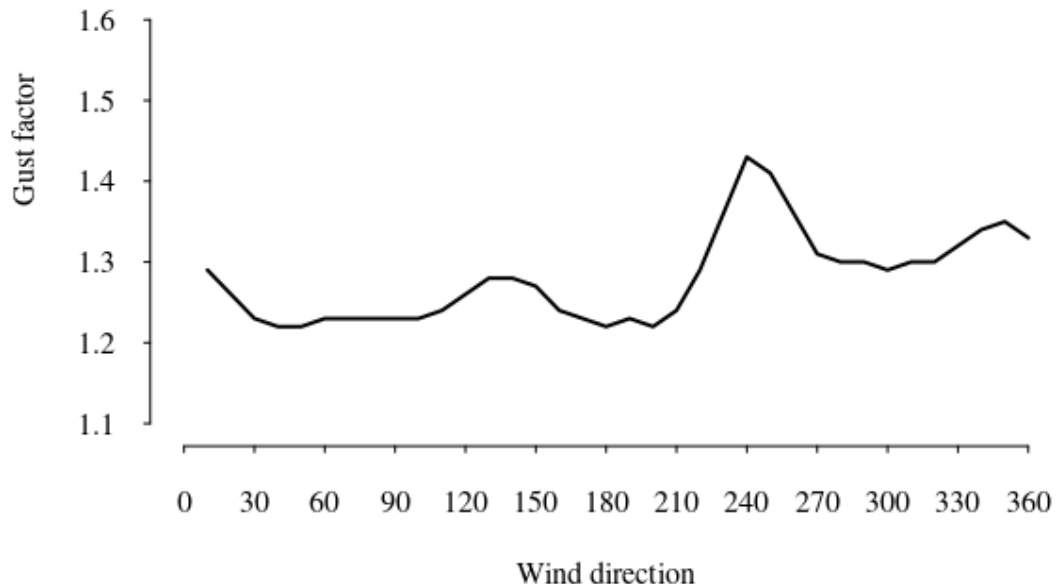


Figure 6.7.3.4.1. Gust factor per deca-degree at Andøya.

It is also interesting to examine the strength of wind gusts that can occur with different wind directions. In Figure 6.7.3.4.2, both the average of the 25 strongest wind gusts and the single strongest wind gust recorded for each deca-degree are plotted.

The single strongest wind gust, 83 knots, was recorded with wind from 240 degrees on 23 January 2022. The crosswind component was 82 knots.

WIND GUST PER DECA-DEGREE 87110 Andøya

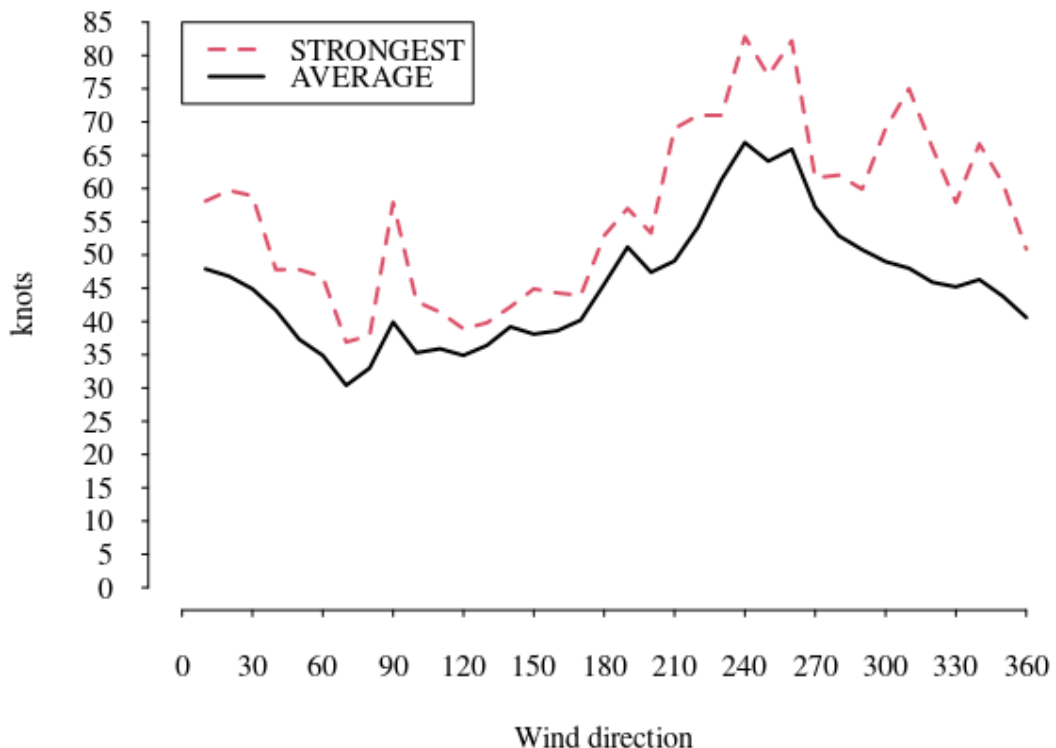


Figure 6.7.3.4.2. Strongest wind gust and the average of the 25 strongest gusts per deca-degree at Andøya.

6.7.3.5 Crosswind

Crosswinds at Andøya, as previously mentioned, are at 50 and 230 degrees.

But strong wind from other directions can also give significant crosswind components. Table 6.7.3.5.1 shows the monthly frequencies of a crosswind component of more than 20 and 35 knots respectively. A 230 degree wind gust of 30 knots, gives, of course, a southwesterly component of 30 knots, while a wind gust at 30 knots from 190 or 260 degrees, gives a southwesterly component of 26 knots. All strong winds from 140 and 320 degrees, will not contribute to any crosswind component at all.

Table 6.7.3.5.1. Frequency of crosswind component of 20 knots and 35 knots or more

MONTH	Southwesterly >=20 knots	Northeasterly >=20 knots	Southwesterly >=35 knots	Northeasterly >=35 knots
OCTOBER	9,5 %	6,1 %	1,4 %	0,3 %

NOVEMBER	9,3 %	3,5 %	1,3 %	0,2 %
DECEMBER	10,5 %	4,3 %	2,7 %	0,2 %
JANUARY	12,7 %	4,0 %	2,9 %	0,3 %
FEBRUARY	11,6 %	4,3 %	2,7 %	0,4 %
MARCH	14,2 %	6,9 %	3,0 %	0,4 %
APRIL	11,2 %	6,2 %	1,5 %	0,3 %
TOTAL	11,3 %	5,1 %	2,2 %	0,3 %

6.7.3.6 Trends for crosswind

Figure 6.7.3.6.1 and 6.7.3.6.2 show the frequency of all wind gust observations giving a 050 or 230 degrees wind component larger than 20 and 35 knots respectively.

The frequency for southwesterly crosswinds stronger than 20KT varies from around 2 percent to 8 percent annually. The trend line shows a *decreasing* trend. Northeasterly crosswinds have a frequency up to 0.8 percent in 2022, but usually lies well below this figure. The curve has a *slightly increasing* trend line.

Crosswind trends at 87110 Andøya airport

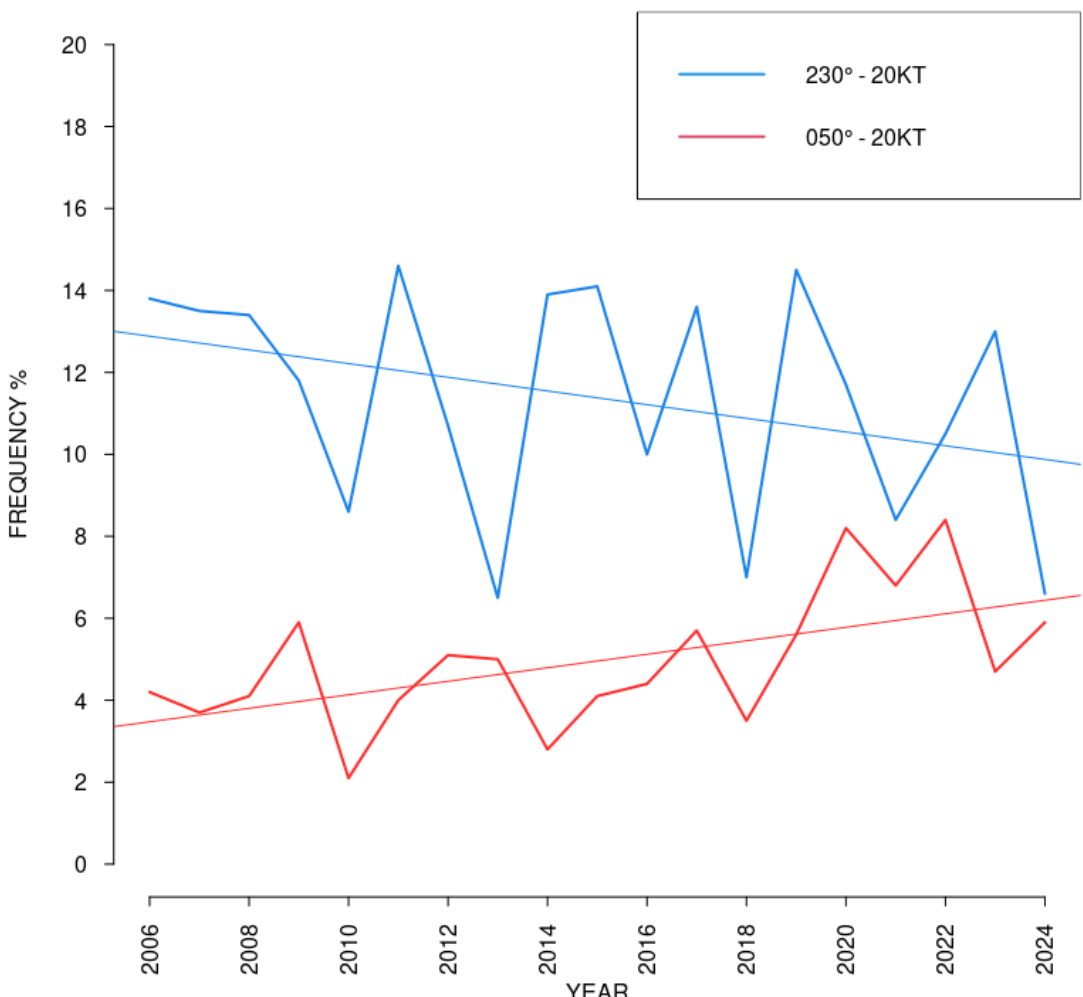


Figure 6.7.3.6.1. Frequency of crosswind of 20 knots or more

Figure 6.7.3.6.2 shows the frequency of crosswind components stronger than 35 knots. The frequency for southwesterly crosswinds varies from 0.5 percent to 3.5 percent. The corresponding trend line is decreasing. Northeasterly crosswinds stronger than 35 knots have an annual frequency of typically only a few tenths of a percent. The trend line is almost flat.

Crosswind trends at 87110 Andøya airport

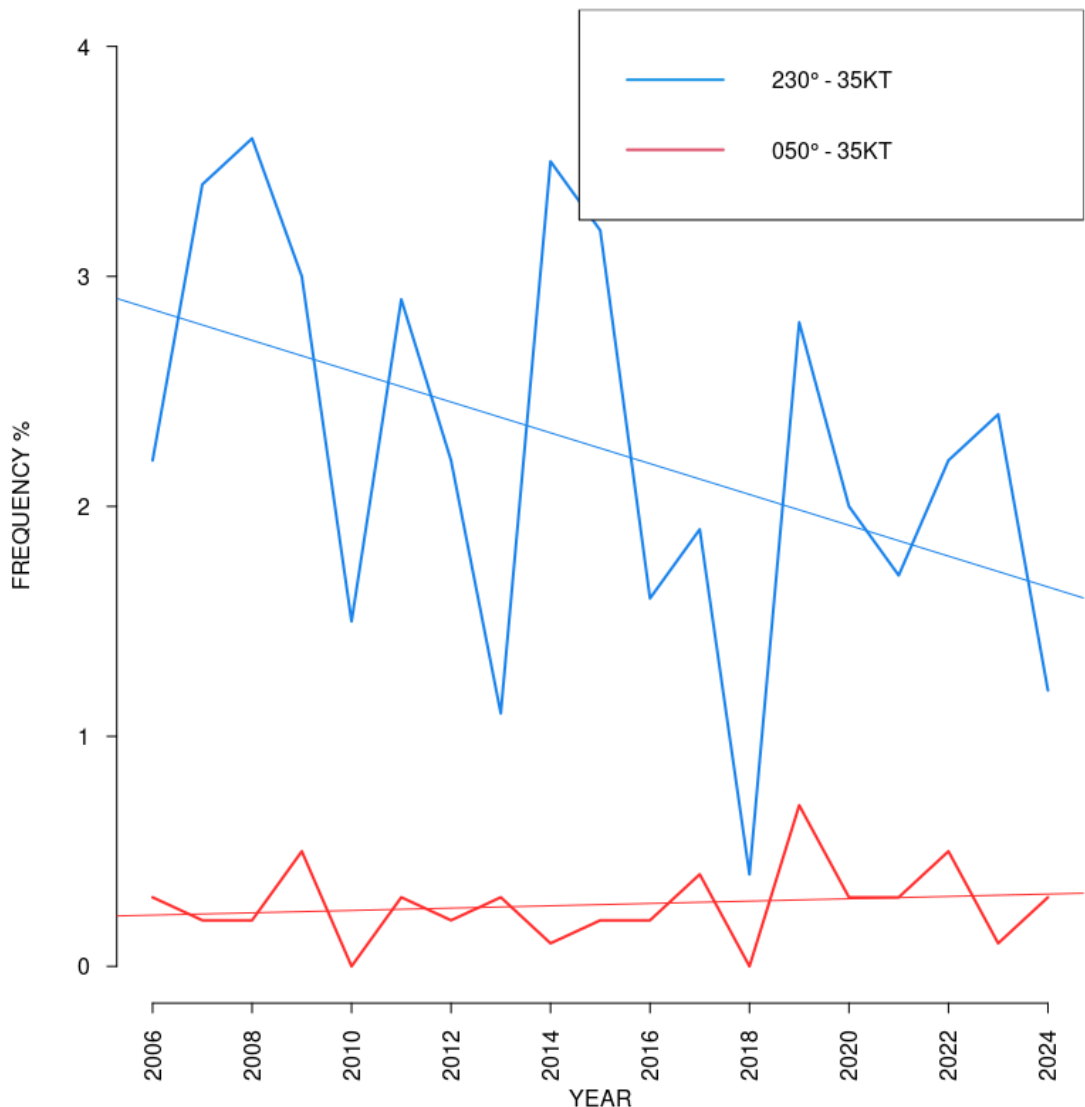


Figure 6.7.3.6.2. Frequency of crosswind components 35 knots or more

6.7.3.7 Crosswind of long duration

Andøya has the highest frequency of crosswind events of long duration. The criteria used were wind mean wind speed above 35 knots and crosswind components of more than 35 knots.

Table 6.7.3.7.1 Events of prolonged and strong wind from the west at Andøya

START	END	DURATION (HOURS)	STRONGEST MEAN WIND (KNOTS)	STRONGEST CROSS WIND COMPONENT (KNOTS)
2010.01.09 07	2010.01.10 12	29	SW 37	52
2010.11.01 05	2010.11.01 20	15	SW 55	72
2010.12.01 22	2010.12.02 15	17	SW 35	53
2013.02.25 00	2013.02.26 02	26	SW 38	54
2014.03.09 16	2014.03.10 13	21	SW 42	62
2014.03.13 15	2014.03.14 12	21	SW 47	62
2014.04.18 20	2014.04.19 22	26	SW 35	51
2015.03.07 22	2015.03.09 11	37	SW 36	61
2015.03.12 05	2015.03.12 22	17	SW 45	60
2015.11.01 04	2015.11.02 00	20	SW 46	67
2022.01.18 08	2022.01.18 23	15	SW 41	61
2022.01.22 21	2022.01.24 02	29	SW 53	82
2023.01.23 05	2023.01.24 14	33	SW 46	71
2023.02.07 18	2023.02.07 20	26	SW 44	69
2023.02.12 05	2023.02.13 02	21	W 51	76
2024.01.29 01	2024.01.30 04	27	W 51	73

6.7.3.8 Extreme wind

For this analysis “extreme wind” is defined as wind gusts of 60 knots or more. In the period 1 October 2005 to 30 April 2024 this has occurred 102. times. If we compute the crosswind components of these observations, 62 of them are higher than 60 knots.

In many analyses the 99-percentile value is of special interest. The 99-percentile is the 1 % highest value of a dataset. For one year of hourly observations, which is 8760

hours in a normal year, this means the 88th highest ranked value. For the seven month period October to April, 5040 hours, it means the 51st highest value.

Figure 6.7.3.8.1 shows the 99-percentile wind gust speed for each year, i.e. the value for the 1 percent highest wind gust each year. The trendline shows a very *slight decrease*.

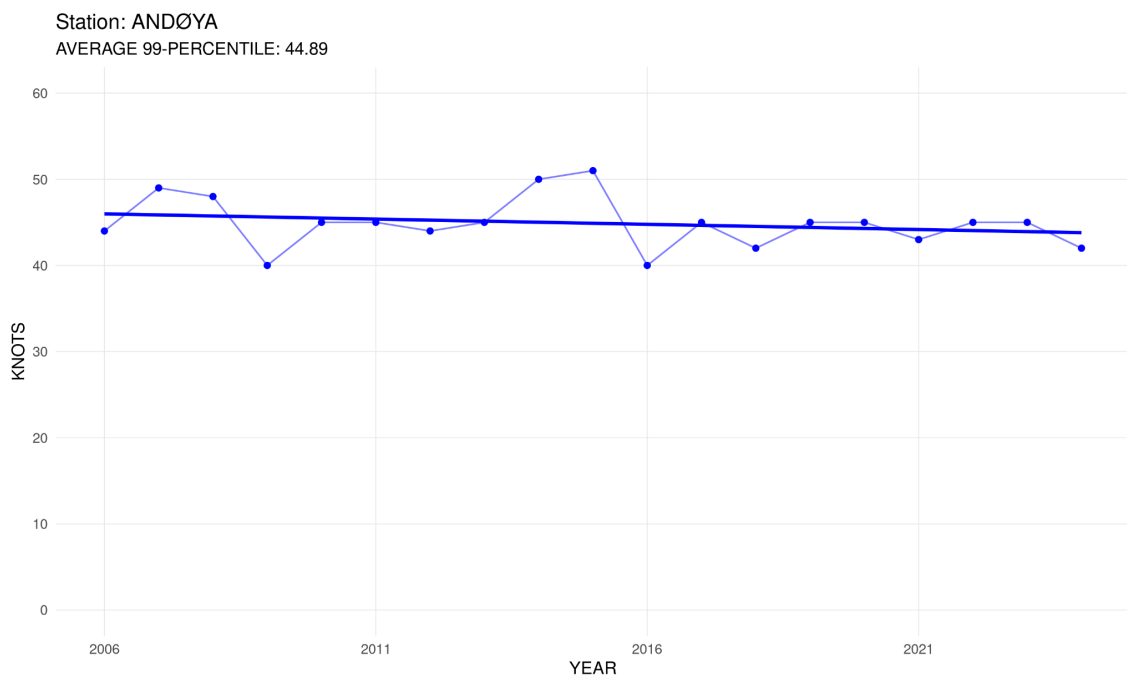


Figure 6.7.3.8.1. The annual value for the 99-percentile wind gust speed and the corresponding trend line.

6.7.4 Freezing precipitation

Freezing precipitation can be hazardous for aircraft operation. There are two main processes giving freezing precipitation: 1) Even if the temperature is less than 0 degrees Celsius, rain drops can exist as supercooled drops. They will momentarily freeze to ice when hitting the cold ground, buildings or vehicles. 2) Because cold air is heavier than warm air, it seeks to the lowest lying places. Rain drops, with a temperature above freezing, from warmer and lighter air aloft, will freeze when they are reaching the ground.

When the airport is closed for traffic, the weather observations are taken automatically. This is adequate for wind, temperature and humidity observations, but the instruments are not capable of detecting the type of precipitation. Inspecting the observation series

for precipitation, it looks like the number of occurrences of freezing precipitation are overestimated by instruments compared to manual observations. Therefore the statistics for freezing precipitation at Andøya are omitted.

6.7.5 Freeze/thaw events

Since temperatures around 0°C often are challenging for airport operations, and in particular for the runway conditions, the number of freeze/thaw events are analysed.

Figure 6.7.5.1 shows the number of days when the temperature during a day both has been below and above 0 degrees at Evenes. This occurs typically on 70 to 110 days annually from 1 October to 30 April. The trend line is slightly decreasing.

**Days with freeze/thaw events
87110 Andøya airport**

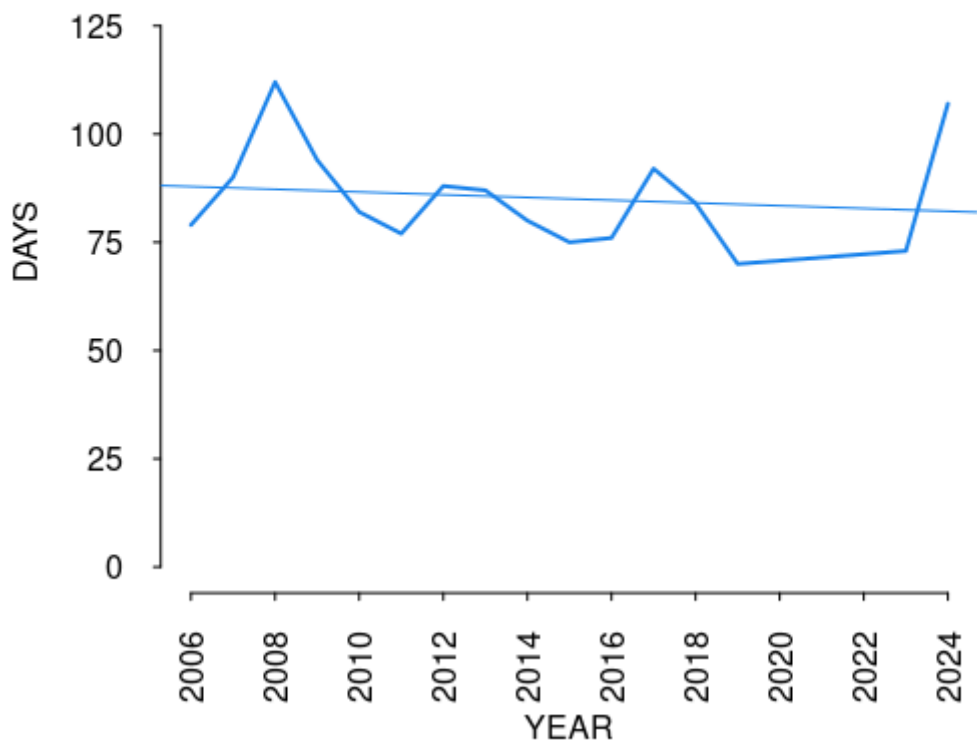


Figure 6.7.5.1. The number of days with freeze/thaw events for the period October to April

6.8 Bardufoss airport

6.8.1 Main findings

The analysis of hourly wind speed observations from 2005 to 2024 for the seven month period October to April, shows that the trend line for the 99-percentile value, i.e. the 1 percent highest wind gust each year, is *slightly increasing*. The trend line for freeze/thaw events is also *slightly increasing*. There is a flat trend line for southerly crosswinds, with annual frequencies from 0.5 to 2.5 percent.

6.8.2 Location

Bardufoss airport is located on flat, low-lying terrain between the river Målselva and the lake Andsvatnet. The terrain around the airport is hilly. Rustafjellet, 415 masl, is the highest within 3 km of the airport. See figure 6.8.2.1.

The runway is oriented in the direction 10/28, i.e. 100/280 degrees. Consequently, winds from 10 and 190 degrees will result in crosswind at the airport.

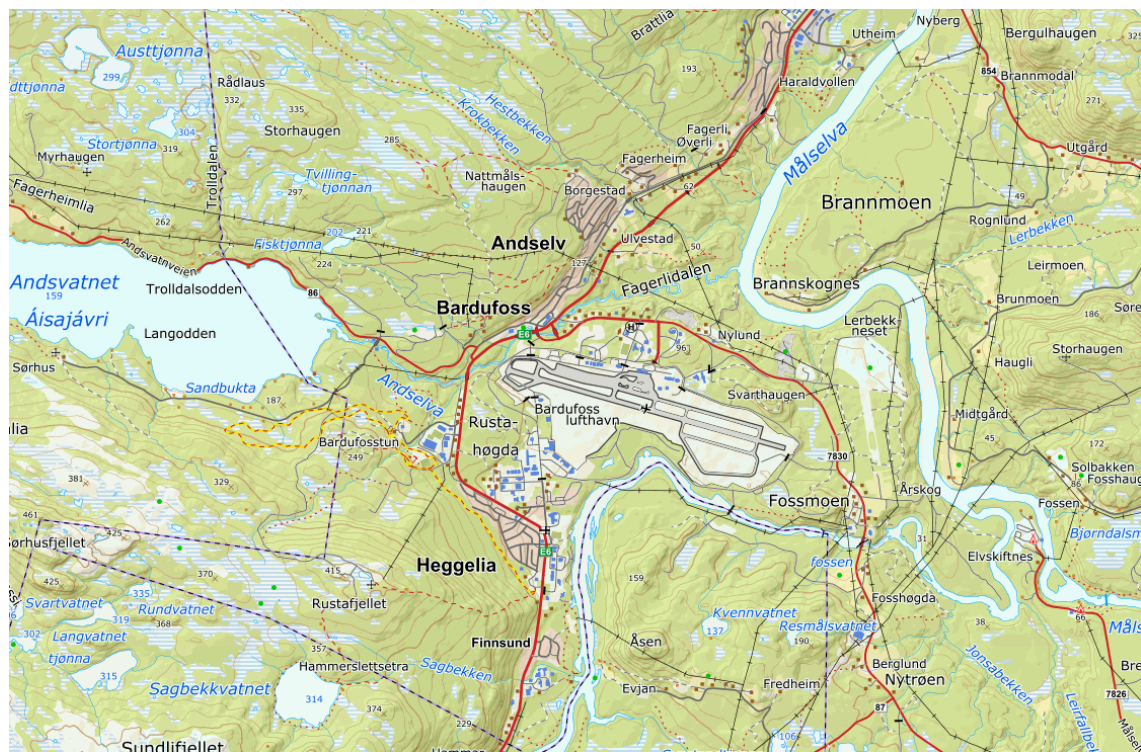


Figure 6.8.2.1 Bardufoss airport is located between the river Målselva and the lake Andsvatnet. Source: The Norwegian Mapping Authority

6.8.3 Wind conditions

6.8.3.1 Mean wind speed

Bardufoss began weather observations in 1946. Hourly measurements of mean wind speed, strongest mean wind in the last hour, and strongest 3-second wind gusts in the last hour started in January 2010. These wind measurements have been used in the analysis.

The wind measurements, both METAR and SYNOP, are taken from an anemometer standing 350 m southeast of the threshold of runway 10. Wind observations are also taken 330 m west of the threshold of runway 28.

Figure 6.8.3.1.1 shows the average mean wind speed at Bardufoss over the seven-month period from October to April for the years 2005 to 2024. The year indications on the x-axis represent the end year of each period, so 2006 indicates the period from October 2005 to April 2006.

The average mean wind speed lies typically around 3-5 knots each year. A trendline has been added, showing a slightly decreasing trend.

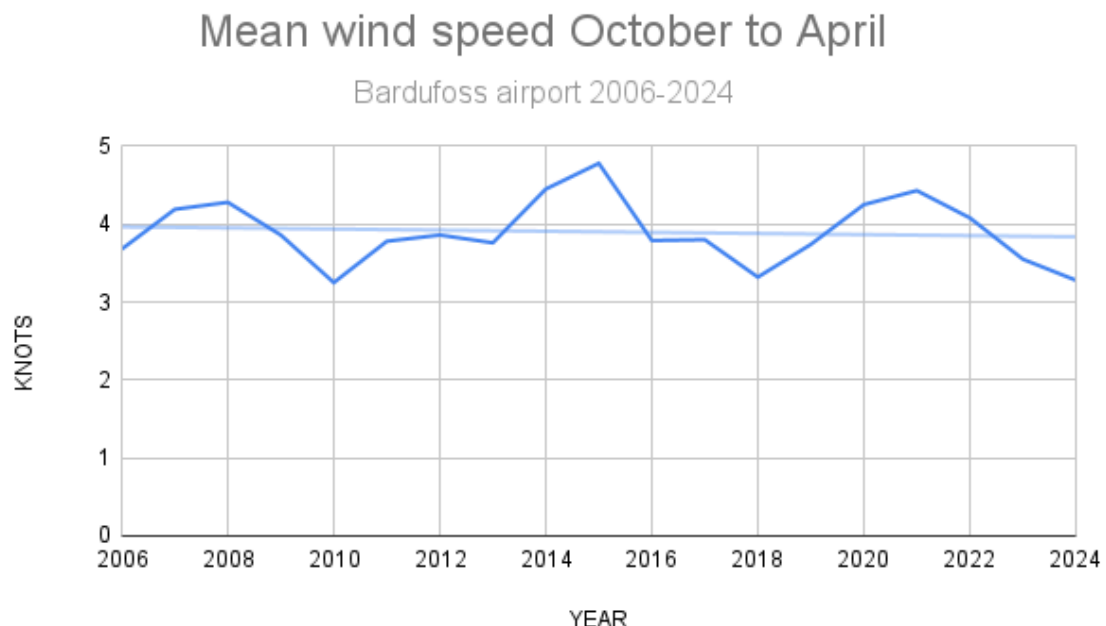


Figure 6.8.3.1.1. Average mean wind speed during the period from October to April.

6.8.3.2 Wind roses

Figure 6.8.3.2.1 shows wind roses for the months October to April for the two periods 2005-2014 and 2014 to 2024.

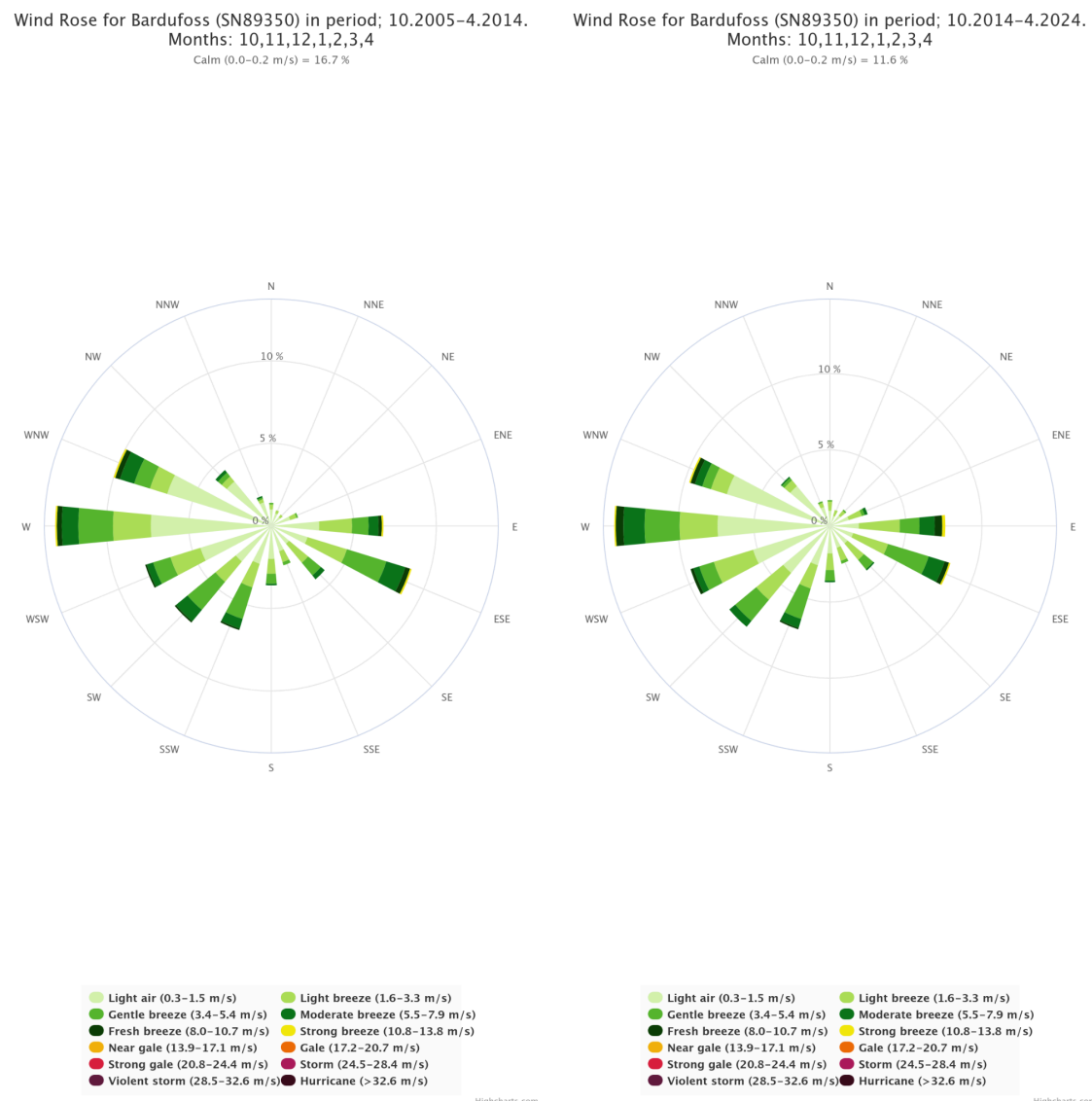


Figure 6.8.3.2.1. Wind roses for the period from October to April for the years 2005 to 2014 on the left and 2014 to 2024 on the right. Wind speed in m/s.

Visually, the wind roses in Figure 6.8.3.2.1 appear to be very similar. The three most frequent wind directions, WSW, W and WNW occur 31 and 34 percent of the time in the two periods October 2005 to April 2014 and October 2014 to April 2024, respectively.

6.8.3.3 Differences in wind in a mild and a cold winter month

February 2018 is the coldest winter month at Bardufoss in the period 2005 to 2024, while February 2023 is the mildest. Figure 4 shows the wind roses for these two months, with 2018 on the left and 2023 on the right. The average wind speed was 1.2 m/s (2.3 knots) and 2.3 m/s (4.5 knots), respectively. In February 2018, winds between WSW and WNW occurred in 44 percent of cases. In February 2023, the corresponding figure was 34 percent. Winds between S and SW occurred 13 percent in 2018 and 27 percent in 2023.

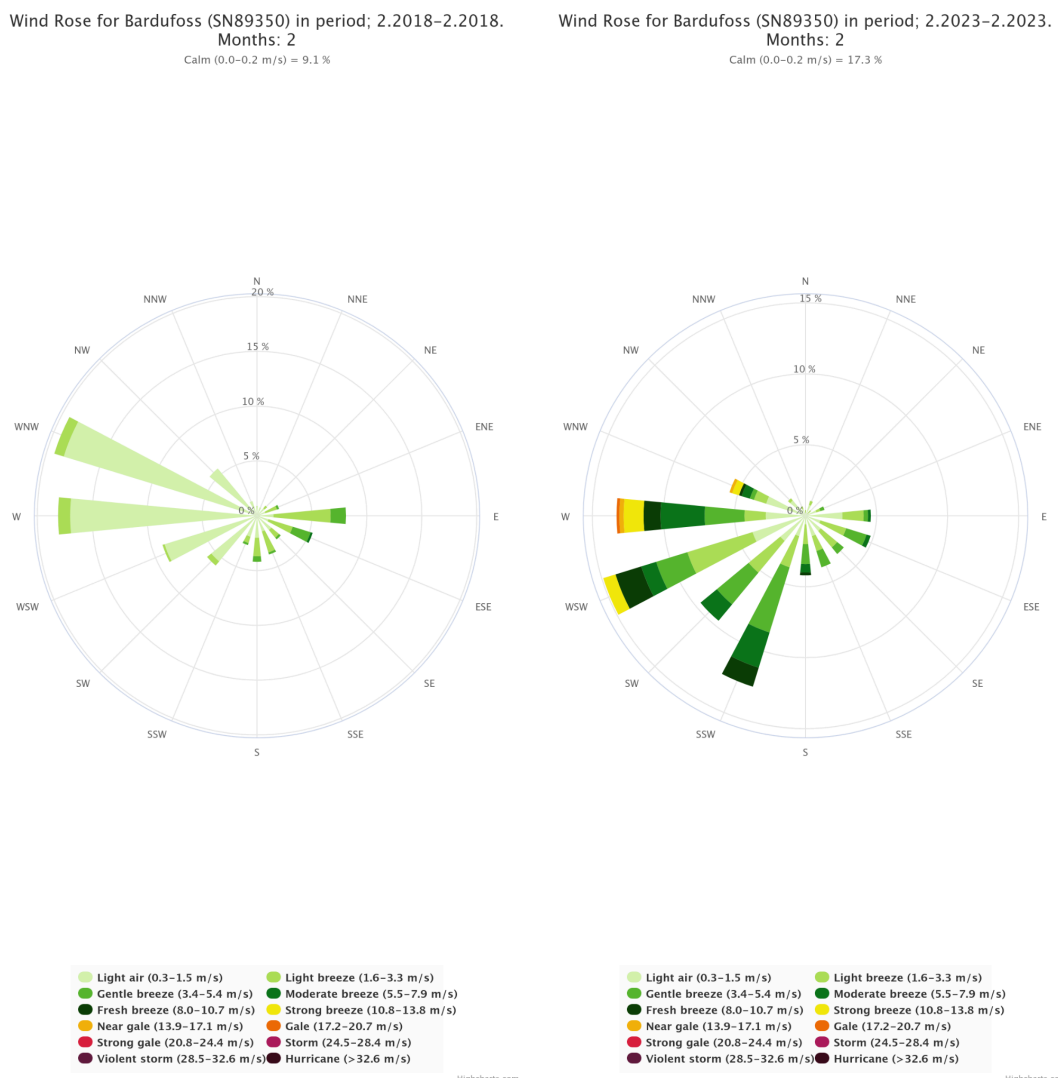


Figure 6.8.3.3.1 shows the wind roses for the cold February 2018 on the left and the mild February 2023 on the right. Wind speed in m/s.

6.8.3.4 Wind gusts

The terrain near an airport influences the wind locally, creating wind conditions that will be typical for the various wind directions experienced at the airport.

One way to assess these local conditions is to observe how the gust factor changes with wind direction. The gust factor is defined as FG_1/FX_1 , where FG_1 is the strongest 3-second wind gust in the last hour and FX_1 is the strongest mean wind in the last hour. At weather stations with relatively flat and uniform terrain around the station, the gust factor typically lies around 1.2. In highly rugged terrain, wind gusts can be more than double the mean wind speed.

Figure 6.8.3.4.1 shows the average gust factor for each 10th degree, deca-degree, at Bardufoss for the months from October to April throughout the measurement period from 2005 to 2024. Wind from the northeast, south and northwest all have the highest gust factor, around 1.6, while wind from the east and west, which mainly coincide with the runway direction, has the lowest, below 1.5.

GUST FACTOR PER DECA-DEGREE 89350 BARDUFOSS 2005-2024

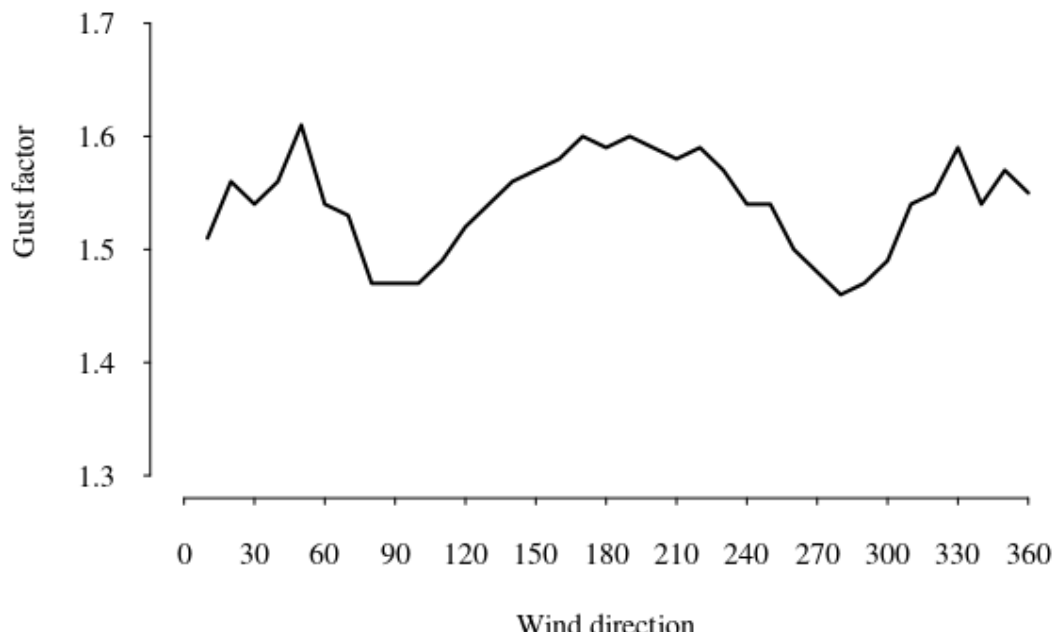


Figure 6.8.3.4.1. Gust factor per deca-degree at Bardufoss.

It is also interesting to examine the strength of wind gusts that can occur with different wind directions. In Figure 6, both the average of the 25 strongest wind gusts and the single strongest wind gust recorded for each deca-degree are plotted.

The single strongest wind gust, 63 knots, was recorded with wind from 321 degrees during the extreme weather event *Ole* in February 2015.

WIND GUST PER DECA-DEGREE 89350 Bardufoss

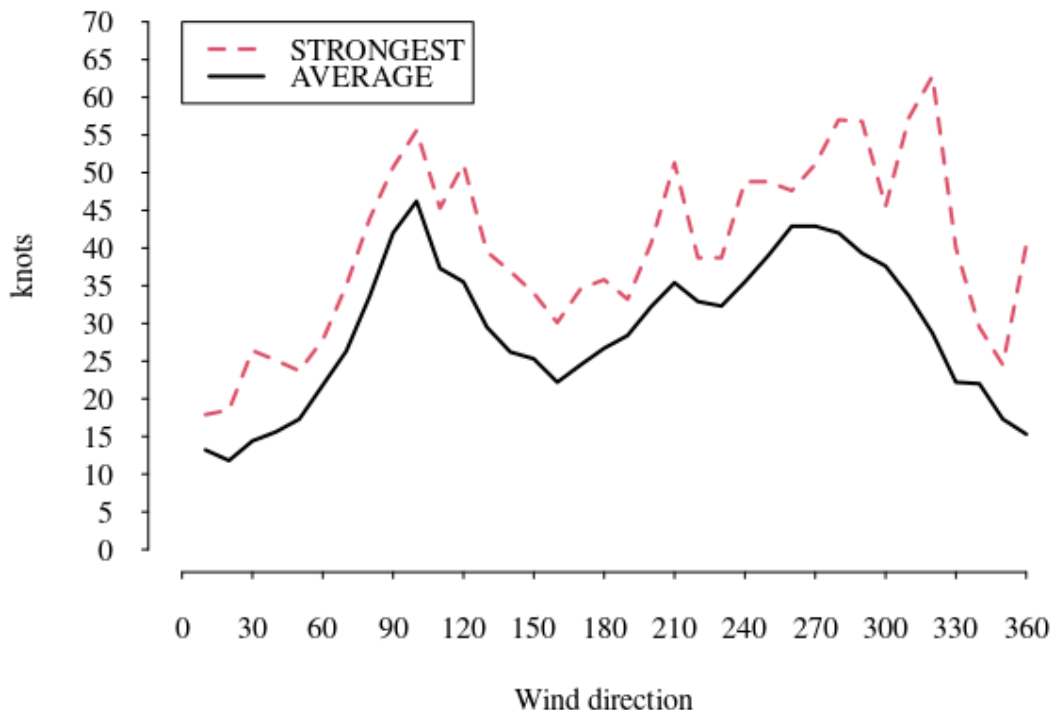


Figure 6.8.3.4.2 Strongest wind gust and the average of the 25 strongest gusts per deca-degree at Bardufoss.

6.8.3.5 Crosswind

Crosswinds at Bardufoss, as previously mentioned, are at 010 and 190 degrees, which are directions that do not occur so often.

But strong wind from other directions can give significant crosswind components. Table 1 shows the monthly frequencies of a crosswind component of more than 20 and 35 knots respectively. A 190 degree wind gust of 30 knots, gives, of course, a southsouthwesterly component of 30 knots, while a 230 og 160 degree wind gust at 30 knots, gives a southsouthwesterly component of 26 knots. All strong winds from 100 and 280 degrees, will not contribute to a crosswind component at all.

Table 6.8.3.5.1. Frequency of crosswind components of 20 knots and 35 knots or more

MONTH	SSW >=20 knots	NNE>=20 knots	SSW>=35 knots

OCTOBER	0.5 %	0.1 %	0.01 %
NOVEMBER	0.9 %	0.1 %	0.00 %
DECEMBER	1.0 %	0.1 %	0.00 %
JANUARY	1.9 %	0.0 %	0.03 %
FEBRUARY	1.8 %	0.1 %	0.05 %
MARCH	2.9 %	0.1 %	0.04 %
APRIL	0.9 %	0.0 %	0.02 %
TOTAL	1.4 %	0.1%	0.03 %

6.8.3.6 Trends for crosswind

Figure 6.8.3.6.1 shows the frequency of all wind gust observations giving a 010 or 190 degrees crosswind component larger than 20 knots.

The frequency for SSW crosswinds stronger than 20KT varies from around 0.5 percent to 2 percent annually. The trend line is almost flat. NNE crosswind occurs only a few tens of a percent at most.

SSW crosswinds of 35 knots or more occur occasionally, but the annual frequency is only 0.03 percent, and the highest value is 0.05 percent in February. See table 6.8.3.5.1.

Crosswind trends at 89350 Bardufoss airport

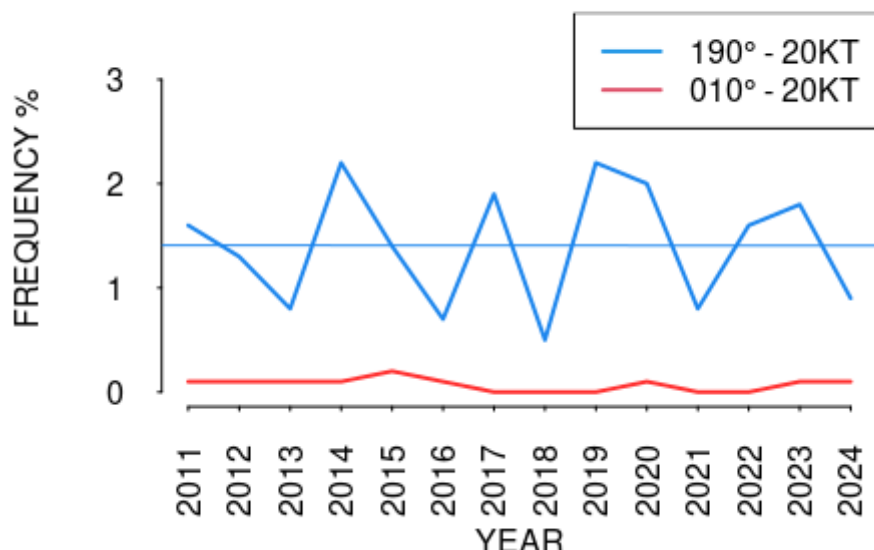


Figure 6.8.3.6.1. Frequency of crosswind of 20 knots or more

6.8.3.7 Crosswind of long duration

The longest duration of crosswinds of more than 35 knots is not more than 2 hours, from 8 February 2023 09 UTC to 11 UTC, but at the same event crosswinds of 20 knots or more lasted for 17 hours, from 07 UTC to 24 UTC.

6.8.3.8 Extreme wind

For this analysis “extreme wind” is defined as wind gusts of 60 knots or more. In the period 1 October 2005 to 30 April 2024 this has occurred only once. The crosswind component was 41 knots with wind from 321 degrees.

In many analyses the 99-percentile value is of special interest. The 99-percentile is the 1 % highest value of a dataset. For one year of hourly observations, which is 8760 hours in a normal year, this means the 88th highest ranked value. For the seven month period October to April, 5040 hours, it means the 51st highest value.

Figure 6.8.3.8.1 shows the 99-percentile wind gust speed for each year, i.e. the value for the 1 percent highest wind gust each year. The data goes back to October 2010. The trendline shows a very *slight increase*.

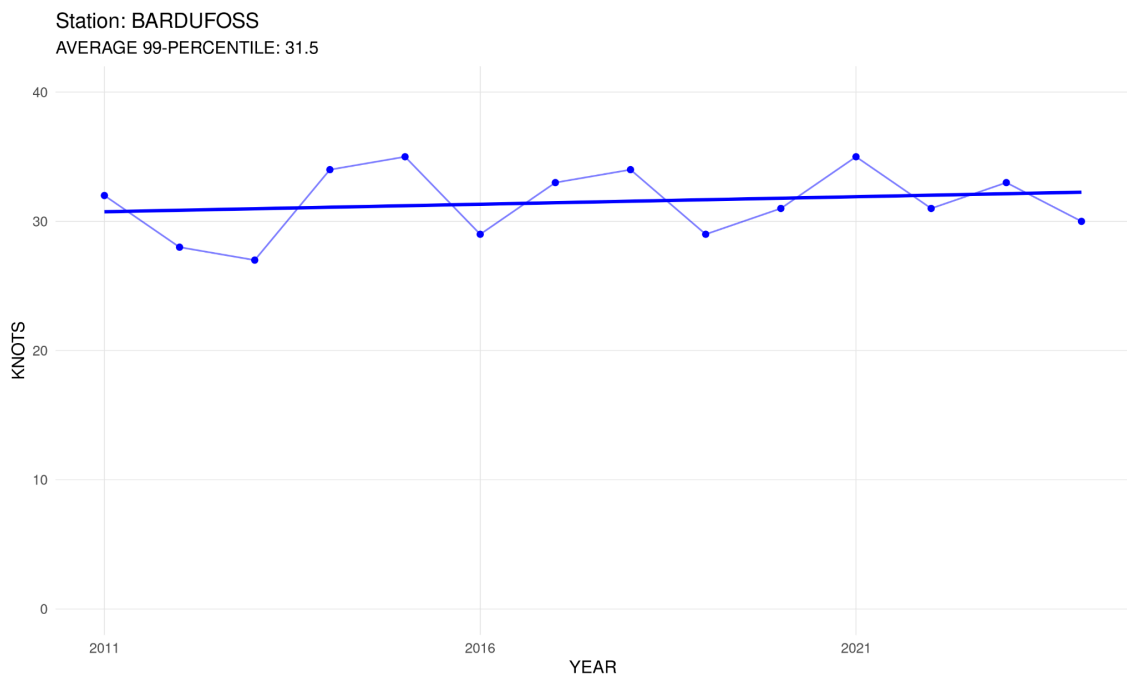


Figure 6.8.3.8.1. The annual value for the 99-percentile wind gust speed and the corresponding trend line.

6.8.4 Freezing precipitation

Freezing precipitation can be hazardous for aircraft operation. There are two main processes giving freezing precipitation: 1) Even if the temperature is less than 0 degrees Celsius, rain drops can exist as supercooled drops. They will momentarily freeze to ice when hitting the cold ground, buildings or vehicles. 2) Because cold air is heavier than warm air, it seeks to the lowest lying places. Rain drops, with a temperature above freezing, from warmer and lighter air aloft, will freeze when they are reaching the ground.

When the airport is closed for traffic, the weather observations are taken automatically. This is adequate for wind, temperature and humidity observations, but the instruments are not capable of detecting the type of precipitation. Inspecting the observation series for precipitation, it looks like the number of occurrences of freezing precipitation are overestimated by instruments compared to manual observations. Therefore the statistics for freezing precipitation at Bardufoss are omitted.

6.8.5 Freeze/thaw events

Since temperatures around 0°C often are challenging for airport operations, and in particular for the runway conditions, the number of freeze/thaw events are analysed.

Figure 6.8.5.1 shows the number of days when the temperature during a day both has been below and above 0 degrees at Bardufoss airport. This occurs typically on 60 to 100 days annually from 1 October to 30 April. The trend line is slightly increasing.

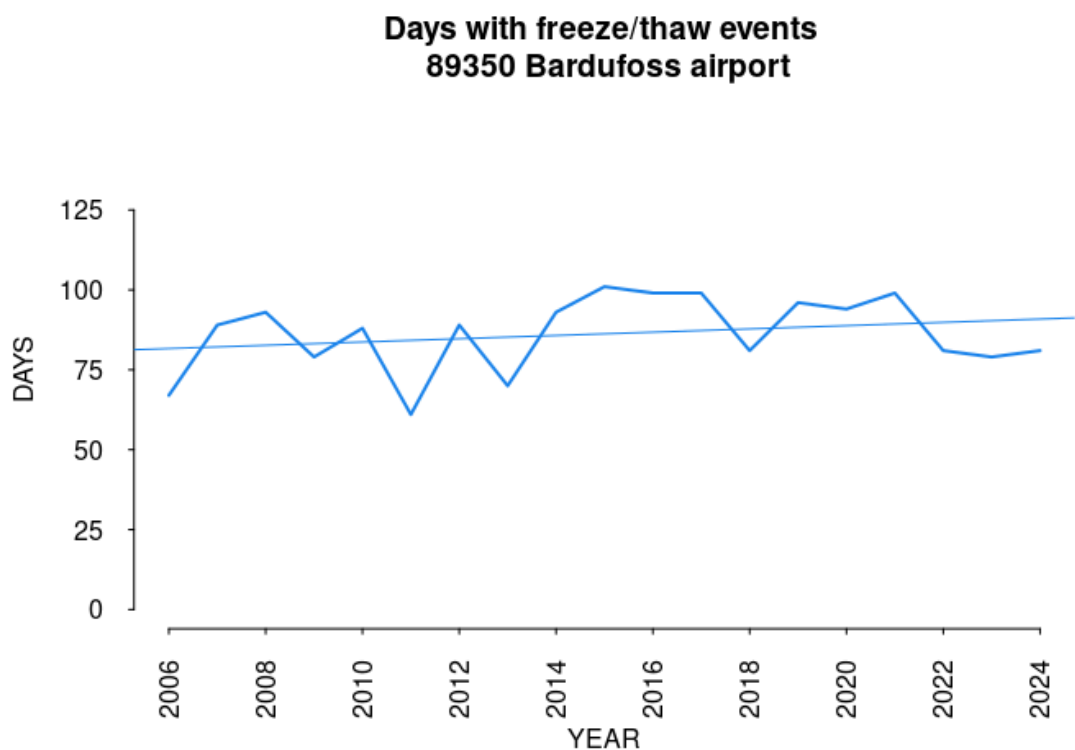


Figure 6.8.5.1. The number of days with freeze/thaw events for the period October to April

6.9 Alta airport

6.9.1 Main findings

The analysis of hourly wind speed observations from 2005 to 2024 for the seven month period October to April, shows that the annual frequency of SSW crosswind components of 20 knots or more varies from 1.5 to 5 percent. The trendline shows a *decreasing* trend. NNE crosswind components of 20 knots or more have an annual frequency of up to almost 3 percent, and show a *slightly increasing* trend. The trend for the 99-percentile value, i.e. the 1 percent highest wind gust each year, shows a *slightly decreasing* trend.

6.9.2 Location

Alta airport is situated in the innermost part of Altafjord. The highest point within 2.5 km from the runway is Komsa in NW, with a height of 200 masl. See figure 6.9.2.1.

The runway is oriented in the direction 11/29, i.e. 110/290 degrees. Consequently, winds from 20 and 200 degrees will result in crosswind at the airport.



Figure 6.9.2.1. Alta airport is located in the innermost part of Altafjord. Source: The Norwegian Mapping Authority

6.9.3 Wind conditions

6.9.3.1 Mean wind speed

Alta airport began weather observations in 1963. Hourly measurements of mean wind speed, strongest mean wind in the last hour, and strongest 3-second wind gusts in the last hour started in November 2004. These wind measurements have been used in the analysis.

The wind measurements, both METAR and SYNOP, are taken from an anemometer standing 70 m south of the threshold of runway 11. Wind observations are also taken 120 m north of the threshold of runway 29. Komsa also has an ultrasonic wind sensor.

Figure 6.9.3.1.1 shows the average mean wind speed at Alta airport over the seven-month period from October to April for the years 2005 to 2024. The year indications on the x-axis represent the end year of each period, so 2006 indicates the period from October 2005 to April 2006.

The average mean wind speed varies around 7-8 knots each year. A trendline has been added, showing no trend.

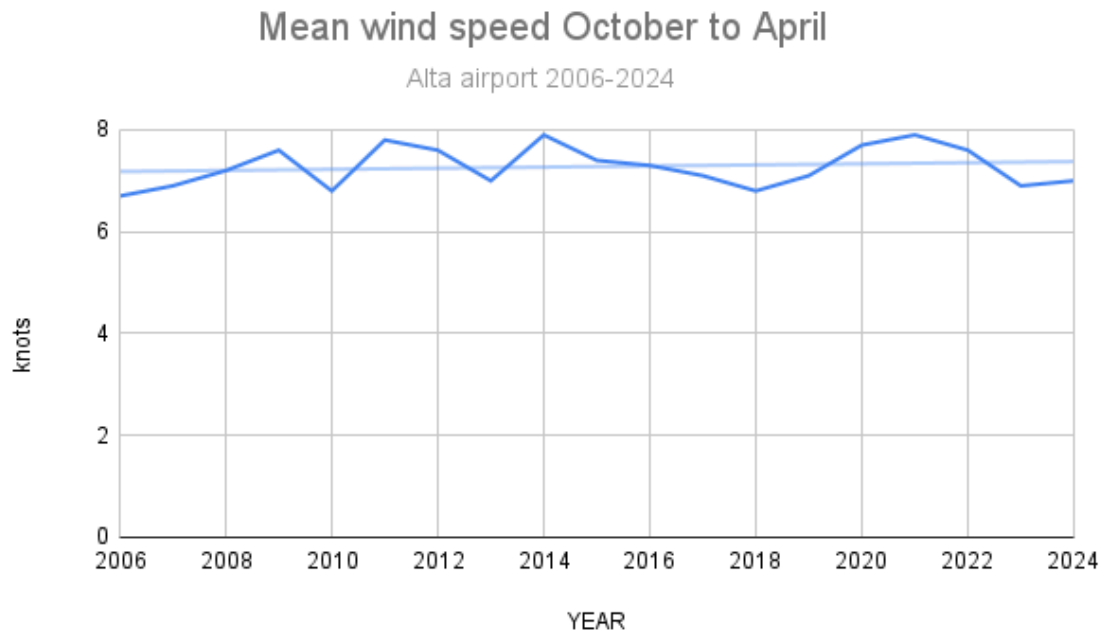


Figure 6.9.3.1.1. Average mean wind speed during the period from October to April.

6.9.3.2 Wind roses

Figure 6.9.3.2.1 shows wind roses for the months October to April for the two periods 2005-2014 and 2014 to 2024.

Wind Rose for Alta Lufthavn (SN93140) in period; 10.2005–4.2014.
 Months: 10,11,12,1,2,3,4
 Calm (0.0–0.2 m/s) = 2.2 %

Wind Rose for Alta Lufthavn (SN93140) in period; 10.2014–4.2024.
 Months: 10,11,12,1,2,3,4
 Calm (0.0–0.2 m/s) = 1 %

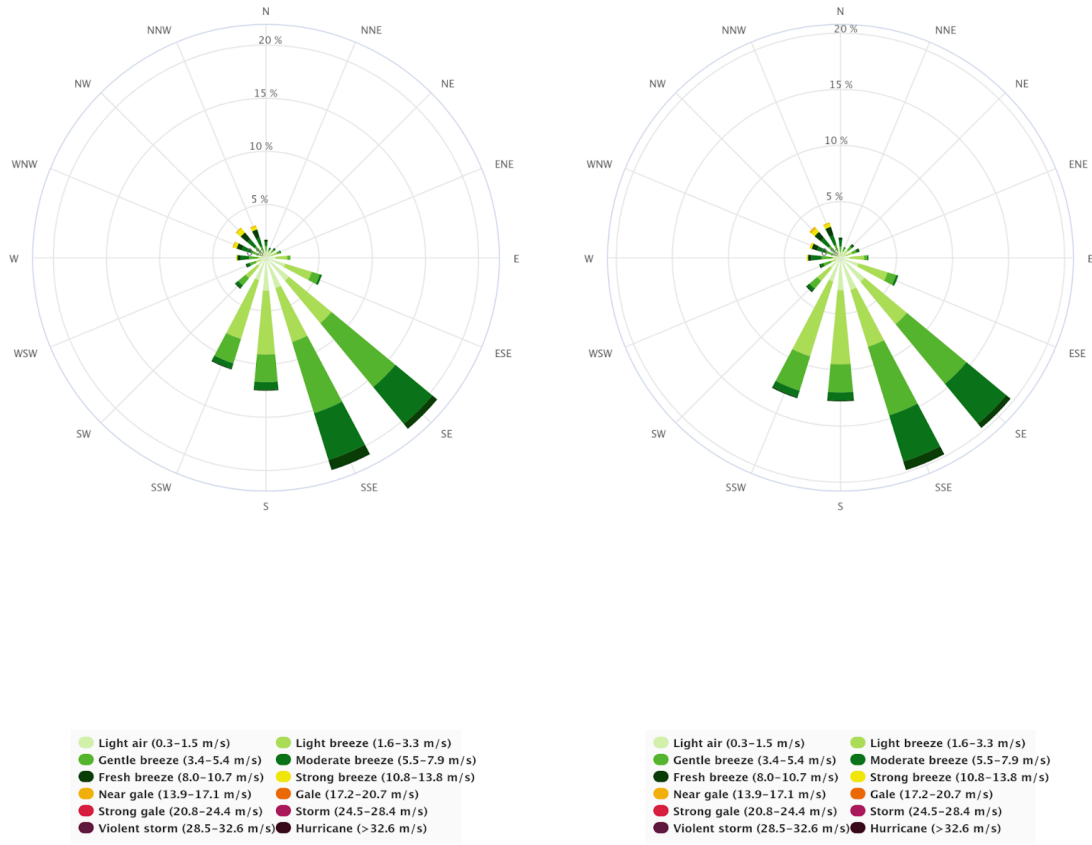


Figure 6.9.3.2.1 Wind roses for the period from October to April for the years 2005 to 2014 on the left and 2014 to 2024 on the right. Wind speed in m/s.

Visually, the wind roses in Figure 3 appear to be very similar. The two most frequent wind directions, SE and SSE, have total frequencies of 42 % and 40 % in the two periods, respectively. The frequency for the crosswind direction SSW has increased from 11 to 13 %, but this applies most to the weaker winds from this direction.

6.9.3.3 Differences in wind in a mild and a cold winter month

There exists a relationship between monthly temperatures and wind: a mild month will usually have higher mean wind. Therefore, it would be interesting to compare the wind conditions in the mildest and the coldest winter months at Alta airport.

February 2007 is the coldest winter month in Alta in the period from 2005 to 2024, while December 2007 is the mildest. Figure 6.9.3.3.1 shows the wind roses for these two months, with February 2007 on the left and December 2007 on the right. The average wind speed was 3.5 m/s (6.7 knots) and 4.5 m/s (8.8 knots), respectively. In the cold February 2007 wind from SE and SSE had a frequency of 54 %, compared to only 41 % in December 2007. On the other hand, wind from W and WNW had a total frequency of only 4 % in February 2007, but as high as 15 % in December 2007. The total frequencies of the crosswind directions NNE and SSW were 11 % in February 2007 and 8 % in December 2007.

Wind Rose for Alta Lufthavn (SN93140) in period; 2.2007–2.2007.
Months: 2
Calm (0.0–0.2 m/s) = 1.9 %

Wind Rose for Alta Lufthavn (SN93140) in period; 12.2007–
12.2007. Months: 12
Calm (0.0–0.2 m/s) = 1.9 %

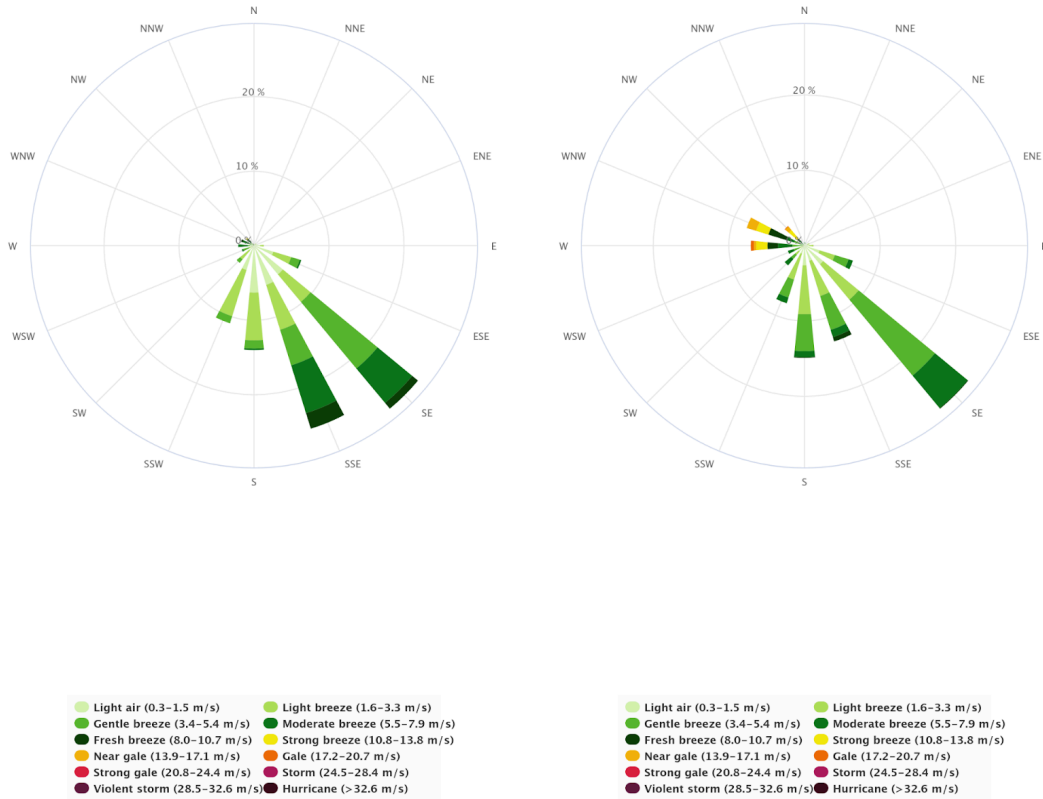


Figure 6.9.3.3.1 shows the wind roses for the cold February 2007 on the left and the mild December 2007 on the right. Wind speed in m/s.

6.9.3.4 Wind gusts

The terrain near an airport influences the wind locally, creating wind conditions that will be typical for the various wind directions experienced at the airport.

One way to assess these local conditions is to observe how the gust factor changes with wind direction. The gust factor is defined as FG_1/FX_1 , where FG_1 is the strongest 3-second wind gust in the last hour and FX_1 is the strongest mean wind in the last hour. At weather stations with relatively flat and uniform terrain around the

station, the gust factor typically lies around 1.2. In highly rugged terrain, wind gusts can be more than double the mean wind speed.

Figure 6.9.3.4.1 shows the average gust factor for each 10th degree, deca-degree, at Alta airport for the months from October to April throughout the measurement period from 2005 to 2024. Winds from the north have the highest gust factor, around 1.5, which includes the crosswind direction NNE, while wind from the northwest has the lowest, near 1.3. The other crosswind direction, SSW, has a gust factor around 1.4.

GUST FACTOR PER DECA-DEGREE 93140 ALTA AIRPORT 2005-2024

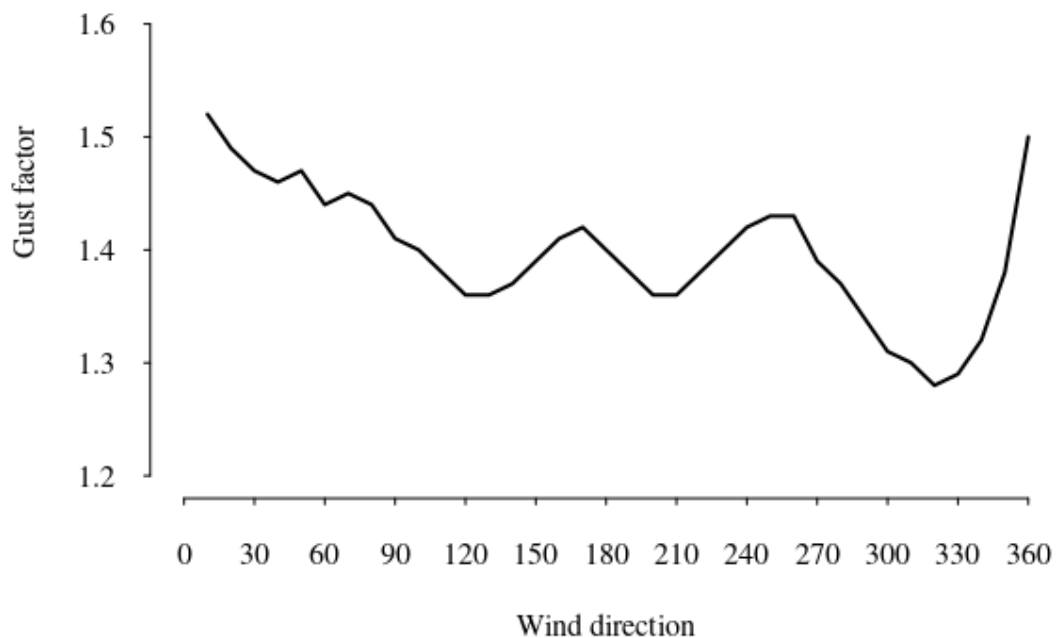


Figure 6.9.3.4.1. Gust factor per deca-degree at Alta airport.

Although wind from the north has the highest gust factor, the wind roses in Figures 6.9.3.2.1 and 6.9.3.2.2 show that wind from this direction does not occur frequently. Therefore, it is also interesting to examine the strength of wind gusts that can occur

with different wind directions. In Figure 6.9.3.4.2, both the average of the 25 strongest wind gusts and the single strongest wind gust recorded for each deca-degree are plotted.

The single strongest wind gust, 59 knots, was recorded on 8 March 2014 with wind from 316 degrees, here rounded up to 320 degrees, during the extreme weather event *Jorun*. As can be seen from figure 5, the gust factor for this wind direction is one of the lowest at 1.3. 316 degrees is only 26 degrees from the runway direction of 290 degrees, so the crosswind component was not more than 26 knots.

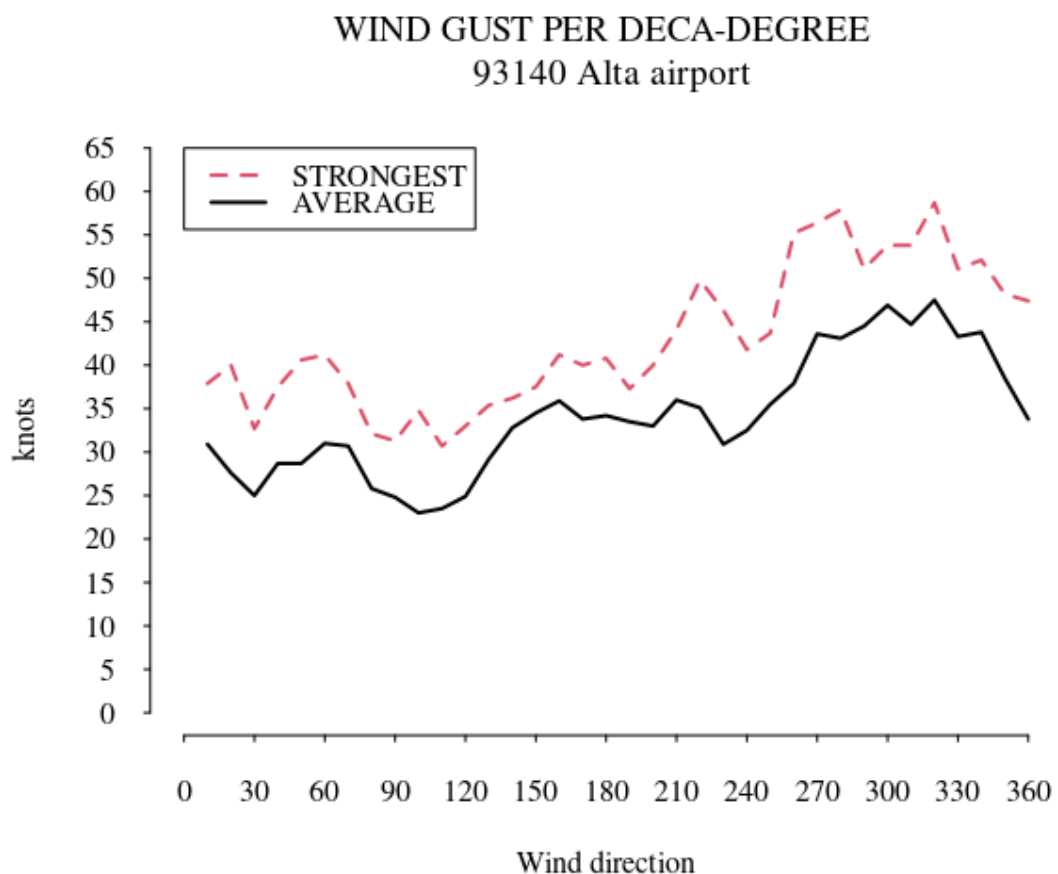


Figure 6.9.3.4.2 Strongest wind gust and the average of the 25 strongest gusts per deca-degree at Alta airport.

6.9.3.5 Crosswind

The crosswind directions at Alta airport are, as previously mentioned, 20 and 200 degrees. But strong wind from other directions can also give significant crosswind components. Table 6.9.3.5.1 shows the monthly frequencies of a crosswind component of more than 20 and 35 knots respectively. A 200 degree wind gust of 30 knots, gives, of course, a southsouthwesterly component of 30 knots, while a 170 or 230 degree wind gust at 30 knots, gives a crosswind component of 26 knots. All strong winds from 110 and 290 degrees, will not contribute to a crosswind component at all.

Table 6.9.3.5.1. Frequency of crosswind component of 20 knots and 35 knots or more

MONTH	SSW >=20 knots	NNE >=20 knots	SSW >=35 knots	NNE >=35KT
OCTOBER	1.9 %	1.7 %	0.0 %	0.0 %
NOVEMBER	2.1 %	1.6 %	0.0 %	0.0 %
DECEMBER	2.3 %	1.2 %	0.0 %	0.2 %
JANUARY	3.5 %	1.8 %	0.0 %	0.0 %
FEBRUARY	3.0 %	1.1 %	0.1 %	0.0 %
MARCH	3.5 %	1.9 %	0.0 %	0.0 %
APRIL	1.2 %	1.1 %	0.1 %	0.0 %
TOTAL	2.5 %	1.5 %	0.0 %	0.0 %

6.9.3.6 Trends for crosswind

Figure 6.9.3.6.1 and 6.9.3.6.2 show the frequency of all wind gust observations giving a 20 or 200 degrees crosswind component equal to or larger than 20 and 35 knots, respectively.

The frequency for SSW crosswinds stronger than 20KT varies from around 1.5 percent to 5 percent annually. The trend line shows a *decreasing* trend. NNE crosswinds of 20

knots or more occur up to almost 3 % in some years, but usually lies well below this figure. The curve has a *slightly increasing* trend line.

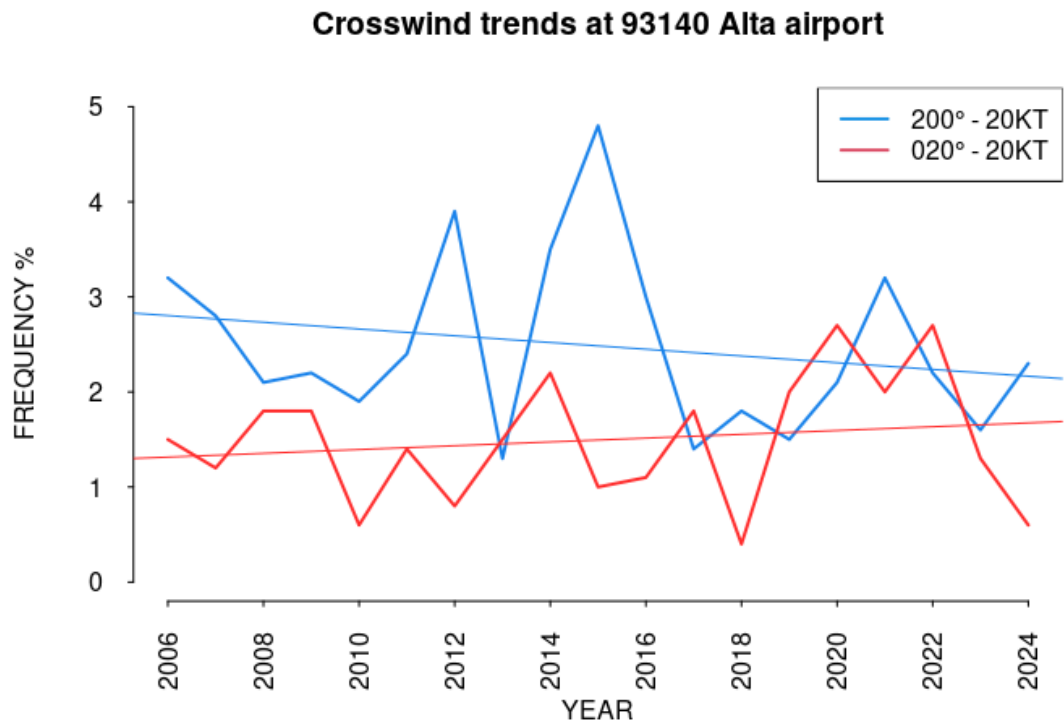


Figure 6.9.3.6.1. Frequency of crosswind of 20 knots or more

Figure 6.9.3.6.2 shows the frequency of crosswind components stronger than 35 knots. The frequencies are typically a few tens of a percent. The trend lines are omitted.

Crosswind trends at 93140 Alta airport

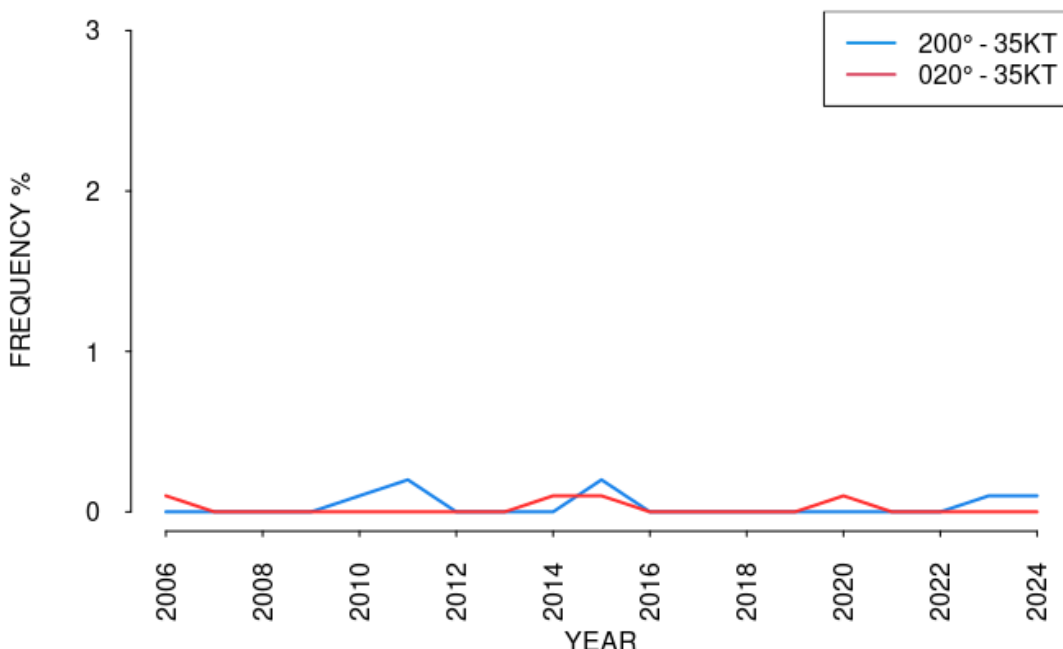


Figure 6.9.3.6.2. Frequency of crosswind components of 35 knots or more

6.9.3.7 Crosswind of long duration

Not applicable for Alta airport

6.9.3.8 Extreme wind

For this analysis “extreme wind” is defined as wind gusts of 60 knots or more. There has never been such a high value at Alta airport. The highest recorded wind gust is 59 knots from 316 degrees, giving a crosswind component of 26 knots.

In many analyses the 99-percentile value is of special interest. The 99-percentile is the 1 % highest value of a dataset. For one year of hourly observations, which is 8760 hours in a normal year, this means the 88th highest ranked value. For the seven month period October to April, 5040 hours, it means the 51st highest value.

Figure 6.9.3.8.1 shows the 99-percentile wind gust speed for each year. The trendline is slightly decreasing.

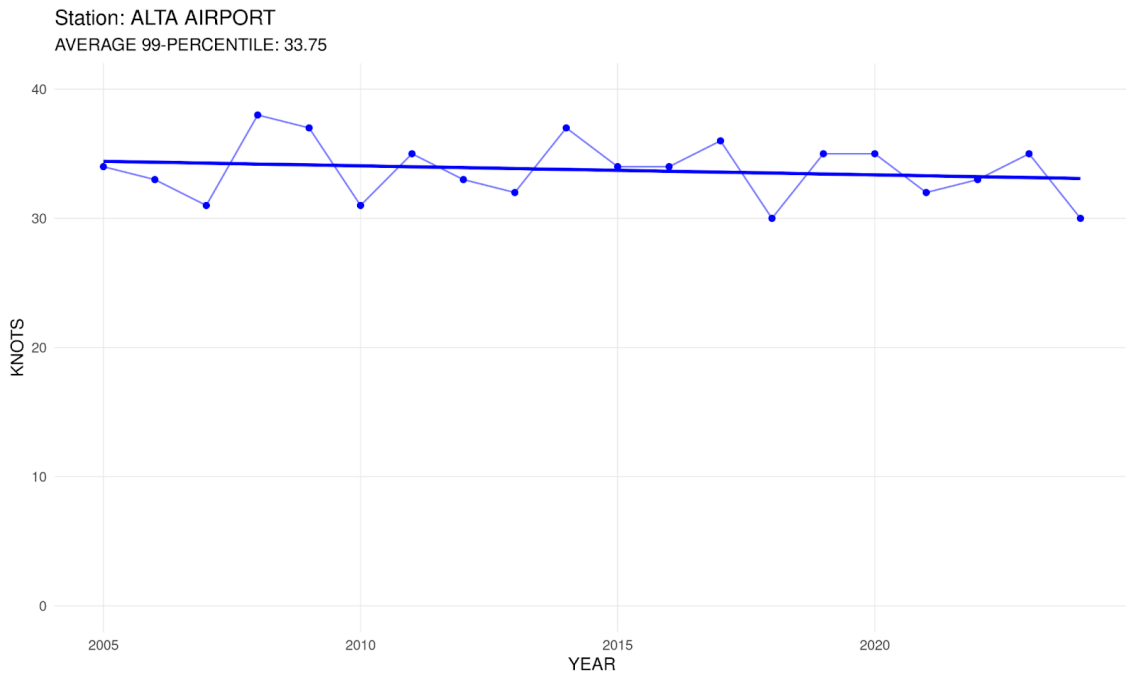


Figure 6.9.3.8.1. The annual value for the 99-percentile wind gust speed and the corresponding trend line.

6.9.4 Freezing precipitation

Freezing precipitation can be hazardous for aircraft operation. There are two main processes giving freezing precipitation: 1) Even if the temperature is less than 0 degrees Celsius, rain drops can exist as supercooled drops. They will momentarily freeze to ice when hitting the cold ground, buildings or vehicles. 2) Because cold air is heavier than warm air, it seeks to the lowest lying places. Rain drops, with a temperature above freezing, from warmer and lighter air aloft, will freeze when they are reaching the ground.

When the airport is closed for traffic, the weather observations are taken automatically. This is adequate for wind, temperature and humidity observations, but the instruments are not capable of detecting the type of precipitation. Inspecting the observation series for precipitation, it looks like the number of occurrences of freezing precipitation are overestimated by instruments compared to manual observations. Therefore the statistics for freezing precipitation at Alta airport are omitted.

6.9.5 Freeze/thaw events

Since temperatures around 0°C often are challenging for airport operations, and in particular for the runway conditions, the number of freeze/thaw events are analysed.

Figure 6.9.5.1 shows the number of days when the temperature during a day both has been below and above 0 degrees at Alta airport. This occurs typically on 60 to 90 days annually from 1 October to 30 April. The trend line is slightly increasing.

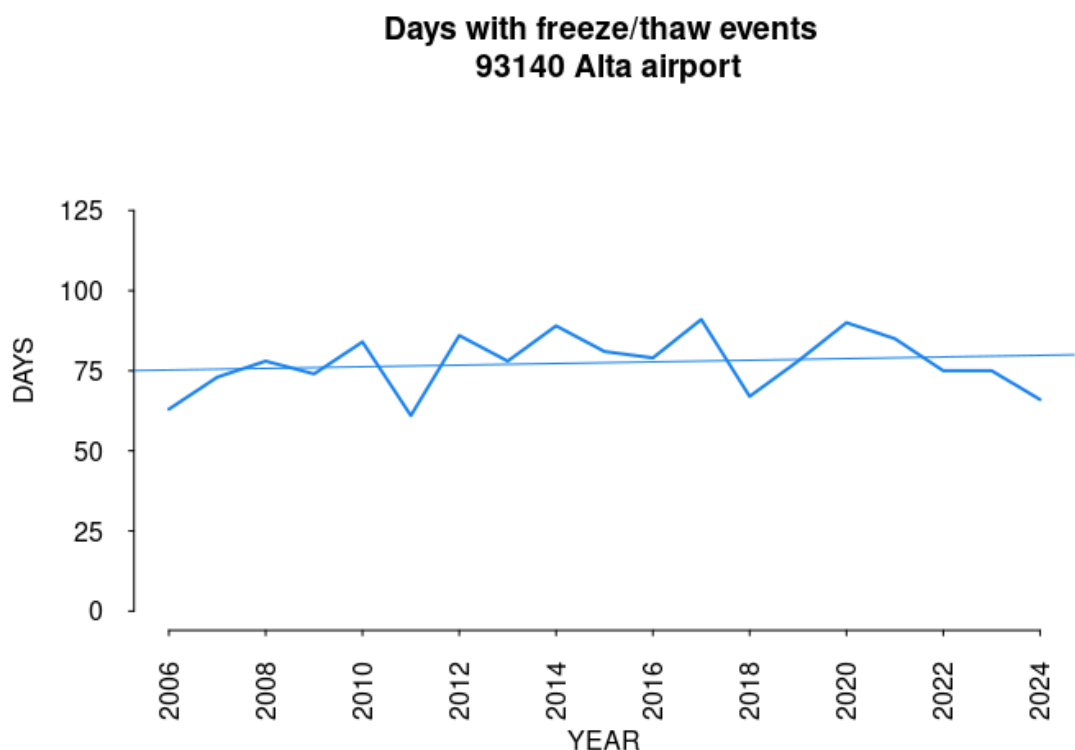


Figure 6.9.5.1. The number of days with freeze/thaw events for the period October to April

6.10 Banak airport

6.10.1 Main findings

The analysis of hourly wind speed observations from 2005 to 2024 for the seven month period October to April, shows that the annual frequency of westerly crosswind components of 20 knots or more varies from 5 to 11 percent. The trendline shows an *increasing* trend. For westerly crosswind components of 35 knots or more the annual frequency lies between 1 and 3 percent, and also shows an increasing trend.

6.10.2 Location

Banak is located in the innermost part of the Porsanger fjord, east of a 600-650 m hilly terrain. See figure 6.10.2.1 The runway is oriented in the direction 16/34, i.e. 160/340 degrees. Consequently, winds from 70 and 250 degrees will result in crosswinds at the airport.



Figure 6.10.2.1. Banak is located in the innermost part of the Porsanger fjord. Source: The Norwegian Mapping Authority

6.10.3 Wind conditions

6.10.3.1 Mean wind speed

Banak began weather observations in 1957. Hourly measurements of mean wind speed, strongest mean wind in the last hour, and strongest 3-second wind gusts in the last hour started in January 2005. These wind measurements have been used in the analysis.

The wind measurements, both METAR and SYNOP, are taken from an anemometer standing 400 m southeast of the threshold of runway 16. Wind observations are also taken 340 m northeast of the threshold of runway 34.

Figure 6.10.3.1.1 shows the average mean wind speed at Banak over the seven-month period from October to April for the years 2005 to 2024. The year indications on the

x-axis represent the end year of each period, so 2006 indicates the period from October 2005 to April 2006.

The average mean wind speed varies around 10-12 knots each year. A trendline has been added, showing an almost flat trend.

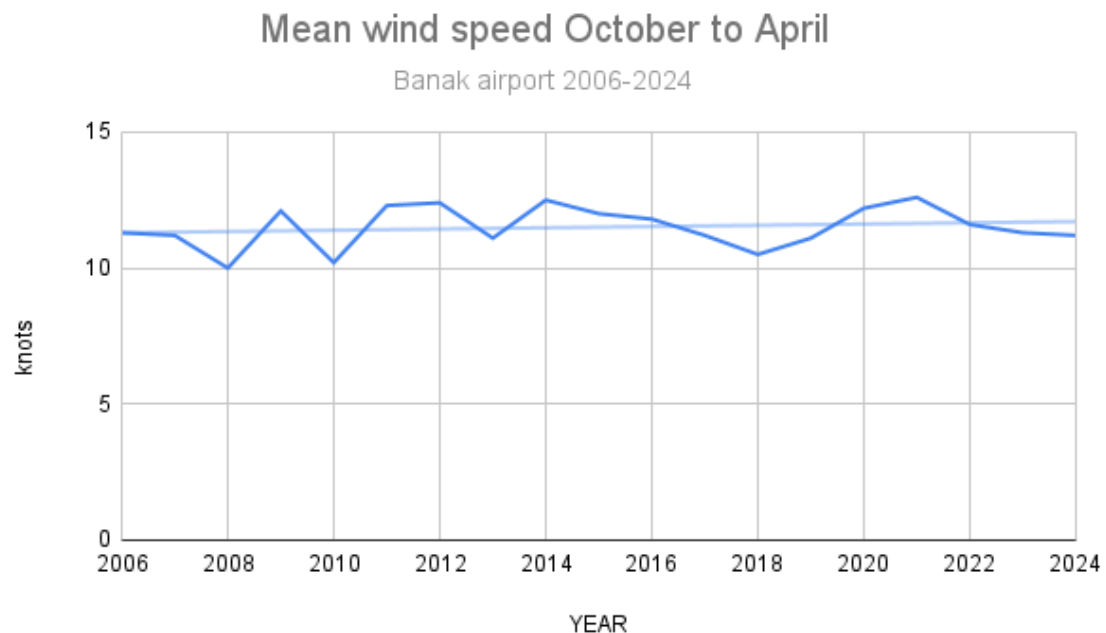


Figure 6.10.3.1.1. Average mean wind speed during the period from October to April.

6.10.3.2 Wind roses

Figure 6.10.3.2.1 shows wind roses for the months October to April for the two periods 2005-2014 and 2014 to 2024.

Wind Rose for Banak (SN95350) in period; 10.2005–4.2014.
 Months: 10,11,12,1,2,3,4
 Calm (0.0–0.2 m/s) = 2.5 %

Wind Rose for Banak (SN95350) in period; 10.2014–4.2024.
 Months: 10,11,12,1,2,3,4
 Calm (0.0–0.2 m/s) = 1.1 %

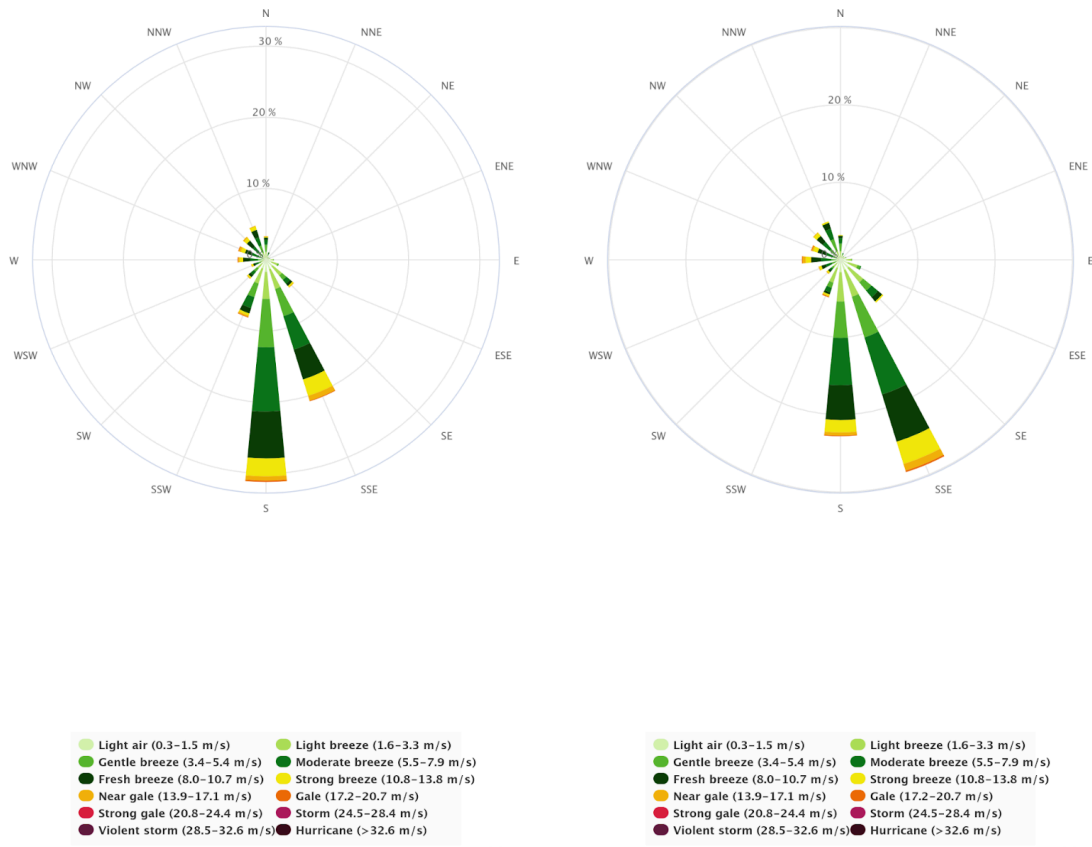


Figure 6.10.3.2.1 Wind roses for the period from October to April for the years 2005 to 2014 on the left and 2014 to 2024 on the right. Wind speed in m/s.

In both periods the most frequent wind directions are S and SSE, having an almost equal total frequency of 52 %, but in the first period wind from S occurs most often, while in the second period SSE winds dominate. The main crosswind directions WSW and ENE have a total frequency of 10 % in both periods.

6.10.3.3 Differences in wind in a mild and a cold winter month

There exists a relationship between monthly temperatures and wind: a mild month will usually have higher mean wind. Therefore, it would be interesting to compare the wind conditions in the mildest and the coldest winter months at Banak.

February 2010 is the coldest winter month at Banak in the period from 2005 to 2024, while February 2014 is the mildest. Figure 6.10.3.3.1 shows the wind roses for these two months, with 2010 on the left and 2014 on the right. The average wind speed was 3.9 m/s (7.6 knots) and 7.5 m/s (14.6 knots), respectively. In February 2010, southerly winds had a frequency of 40 %, while in February 2014 SSE winds occurred 56 % of the time. The frequencies of the crosswind directions WSW and ENE occurred less than 2 % in both periods.

Wind Rose for Banak (SN95350) in period; 2.2010–2.2010.
Months: 2
Calm (0.0–0.2 m/s) = 7.7 %

Wind Rose for Banak (SN95350) in period; 2.2014–2.2014.
Months: 2
Calm (0.0–0.2 m/s) = 0.2 %

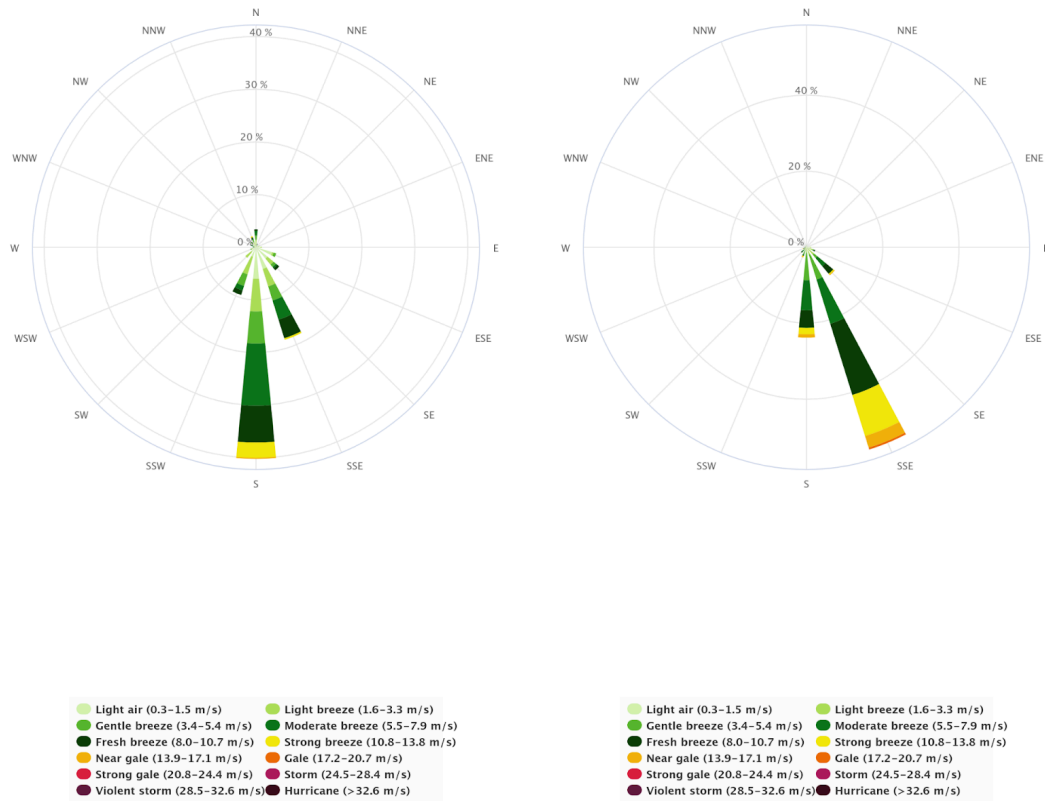


Figure 6.10.3.3.1 shows the wind roses for the cold February 2010 on the left and the mild February 2014 on the right. Wind speed in m/s.

6.10.3.4 Wind gusts

The terrain near an airport influences the wind locally, creating wind conditions that will be typical for the various wind directions experienced at the airport.

One way to assess these local conditions is to observe how the gust factor changes with wind direction. The gust factor is defined as FG_1/FX_1 , where FG_1 is the strongest 3-second wind gust in the last hour and FX_1 is the strongest mean wind in the last hour. At weather stations with relatively flat and uniform terrain around the

station, the gust factor typically lies around 1.2. In highly rugged terrain, wind gusts can be more than double the mean wind speed.

Figure 6.10.3.4.1 shows the average gust factor for each 10th degree, deca-degree, at Banak for the months from October to April throughout the measurement period from 2005 to 2024. Wind from 50 and 250 degrees, which are close to the crosswind directions, has the highest gust factor, around 1.5, while wind from 170 and 350 degrees, almost along the runways, has the lowest, around 1.25.

GUST FACTOR PER DECA-DEGREE 95350 BANAK 2005-2024

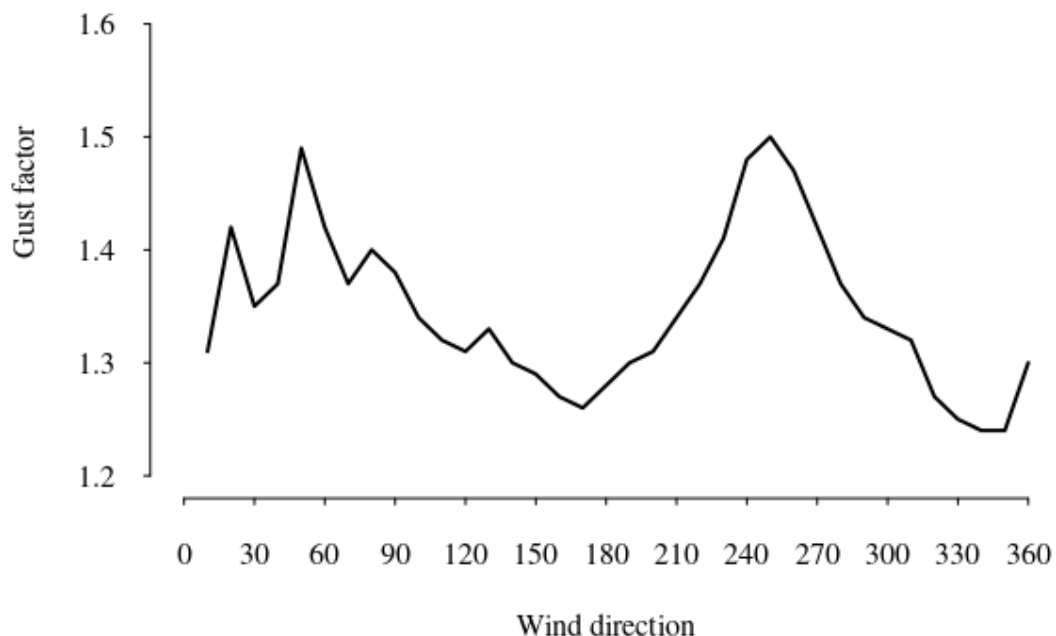


Figure 6.10.3.4.1. Gust factor per deca-degree at Banak.

Wind from both crosswind directions, 70 and 250 degrees, have rather high gust factors, the wind roses in Figures 6.10.3.2.1 and 6.10.3.2.2 show that wind from these directions do not occur frequently, but the southwesterly wind could occasionally be

very strong. It is also interesting to examine the strength of wind gusts that can occur with different wind directions. In Figure 6.10.3.4.2, both the average of the 25 strongest wind gusts and the single strongest wind gust recorded for each deca-degree are plotted. We notice that wind gusts above 60 knots have been observed in a wide sector from 160 to 320 degrees, with the highest gusts in the sector 260 to 320 degrees.

The single strongest wind gust, 88 knots, was recorded with wind from 280 degrees on 27 December 2006, giving a crosswind component of 74 knots.

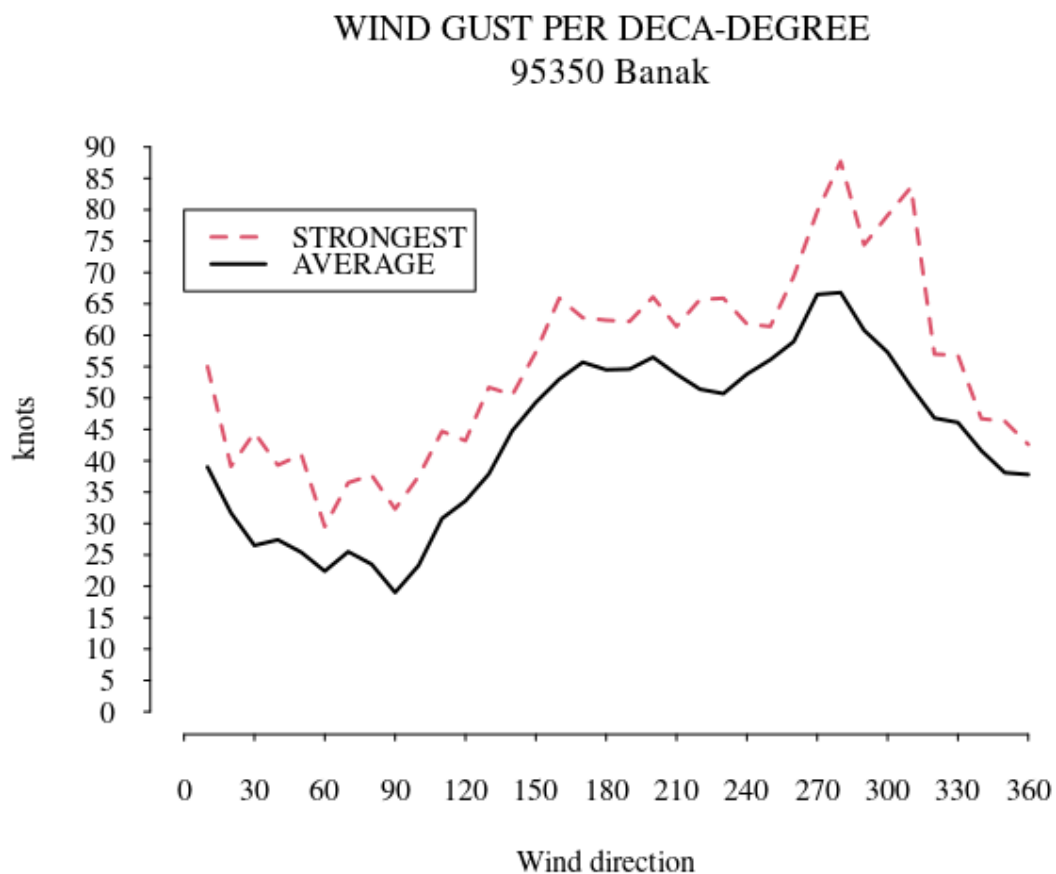


Figure 6.10.3.4.2 Strongest wind gust and the average of the 25 strongest gusts per deca-degree at Banak.

6.10.3.5 Crosswind

Crosswinds at Banak, as previously mentioned, are at 70 and 250 degrees. But strong wind from other directions can also give significant crosswind components. Table 1 shows the monthly frequencies of a crosswind component of more than 20 and 35 knots respectively. A 250 degree wind gust of 30 knots, gives, of course, a southwesterly component of 30 knots, while a 220 or 280 degree wind gust at 30 knots, gives a southwesterly component of 26 knots. All strong winds from 160 and 340 degrees, will not contribute to any crosswind component at all.

Table 6.10.3.5.1 Frequency of crosswind components of 20 knots and 35 knots or more

MONTH	Westerly >=20 knots	Easterly>=20 knots	Westerly>=35 knots	Easterly>=35 knots
OCTOBER	5,77 %	0,38 %	0,42 %	0,01 %
NOVEMBER	6,79 %	0,23 %	1,51 %	0,01 %
DECEMBER	6,61 %	0,30 %	1,71 %	0,00 %
JANUARY	7,19 %	0,12 %	1,84 %	0,01 %
FEBRUARY	7,37 %	0,16 %	1,59 %	0,00 %
MARCH	12,83 %	0,19 %	2,80 %	0,01 %
APRIL	10,24 %	0,35 %	1,86 %	0,01 %
TOTAL	8,15 %	0,25 %	1,68 %	0,01 %

6.10.3.6 Trends for crosswind

Figure 6.10.3.6.1 and 6.10.3.6.2 show the frequency of all wind gust observations giving a 250 or 70 degrees wind component larger than 20 and 35 knots respectively.

The frequency for southwesterly crosswinds stronger than 20KT varies from around 5 percent to 11 percent annually. The trend line shows a *increasing* trend. Northeasterly crosswind occurs up to around one percent in some years, but usually lies well below this figure.

Crosswind trends at 95350 Banak

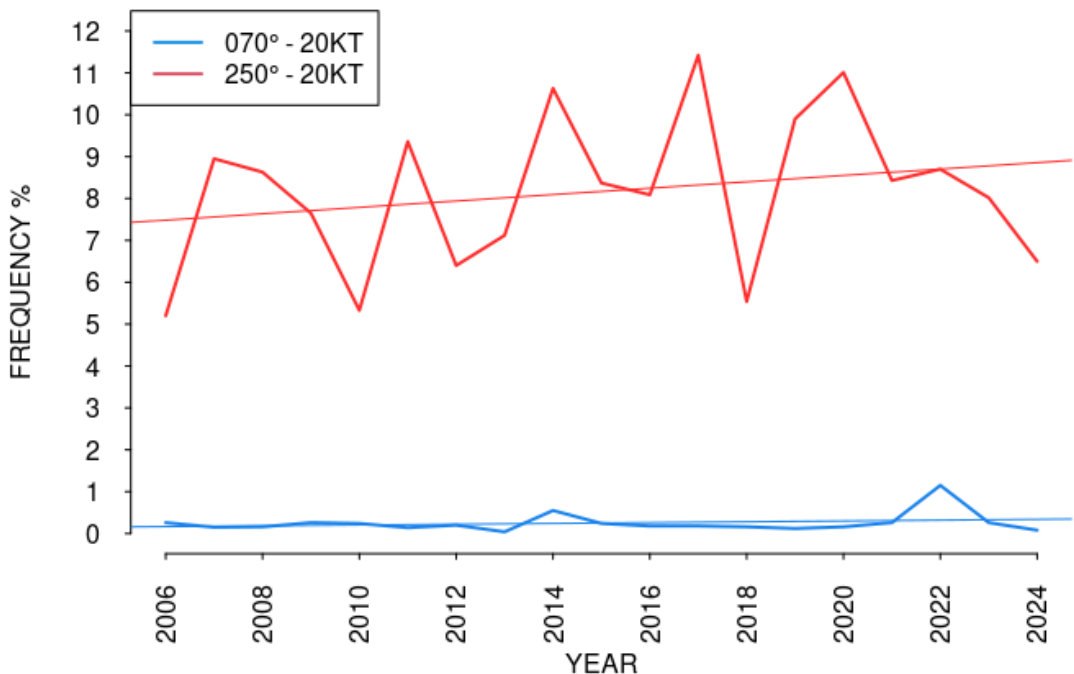


Figure 6.10.3.6.1 Frequency of crosswind of 20 knots or more

Figure 6.10.3.6.2 shows the frequency of a southwesterly crosswind component stronger than 35 knots. The frequency varies from 1 percent to up to almost 3 percent. The corresponding trend line shows an increasing trend. Strong northeasterly crosswinds occur very rarely.

Crosswind trends at 95350 Banak

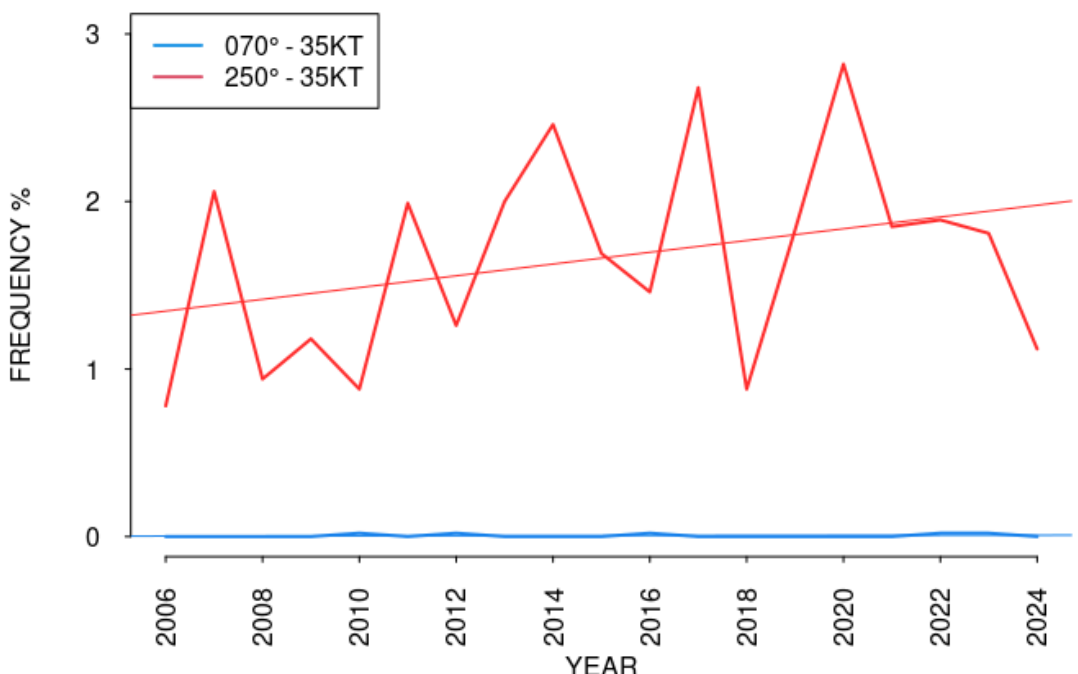


Figure 6.10.3.6.2 Frequency of crosswind of 35 knots or more

6.10.3.7 Crosswind of long duration

It is interesting to find occasions of crosswinds of long duration. The criteria used were strongest mean wind 40 knots or more, cross wind components of 35 knots or more for more than 12 hours, though not necessarily consecutive.

Table 6.10.3.7.1 Events of prolonged and strong wind from the west at Banak

START	END	DURATION (HOURS)	STRONGEST MEAN WIND (KNOTS)	STRONGEST CROSSWIND GUST (KNOTS)
26.12.2006 10	27.12.2006 09	22	W 51 (storm)	74
01.11.2010 17	02.11.2010 12	17 (not consecutive)	SW-W 42 (severe gale)	57

08.03.2014 12	09.03.2014 03	13	W 41 (severe gale)	49
26.12.2015 00	26.12.2015 17	13 (not consecutive)	W 53 (storm)	67
15.03.2016 09	16.03.2016 02	16 (not consecutive)	W-NW 45 (severe gale)	55
12.02.2017 14	13.02.2017 16	20 (not consecutive)	W 45 (severe gale)	54
29.03.2019 15	30.03.2019 06	14	SW 41 (severe gale)	59
30.11.2019 01	30.11.2019 17	16	W 44 (severe gale)	61
29.03.2019 15	30.03.2019 06	14	SW 41 (severe gale)	61
09.01.2020 23	10.01.2020 12	12	W 41 (severe gale)	60

6.10.3.8 Extreme wind

For this analysis “extreme wind” is defined as wind gusts of 60 knots or more. In the period 1 October 2005 to 30 April 2024 this has occurred 103 times, giving a frequency of 0.11 %. If we compute the crosswind components of these observations, 41 of them, a frequency of 0.04 %, are 60 knots or higher.

In many analyses the 99-percentile value is of special interest. The 99-percentile is the 1 % highest value of a dataset. For one year of hourly observations, which is 8760 hours in a normal year, this means the 88th highest ranked value. For the seven month period October to April, 5040 hours, it means the 51st highest value.

Figure 6.10.3.8.1 shows the 99-percentile wind gust speed for each year, i.e. the value for the 1 percent highest wind gust each year. The trendline is almost flat.

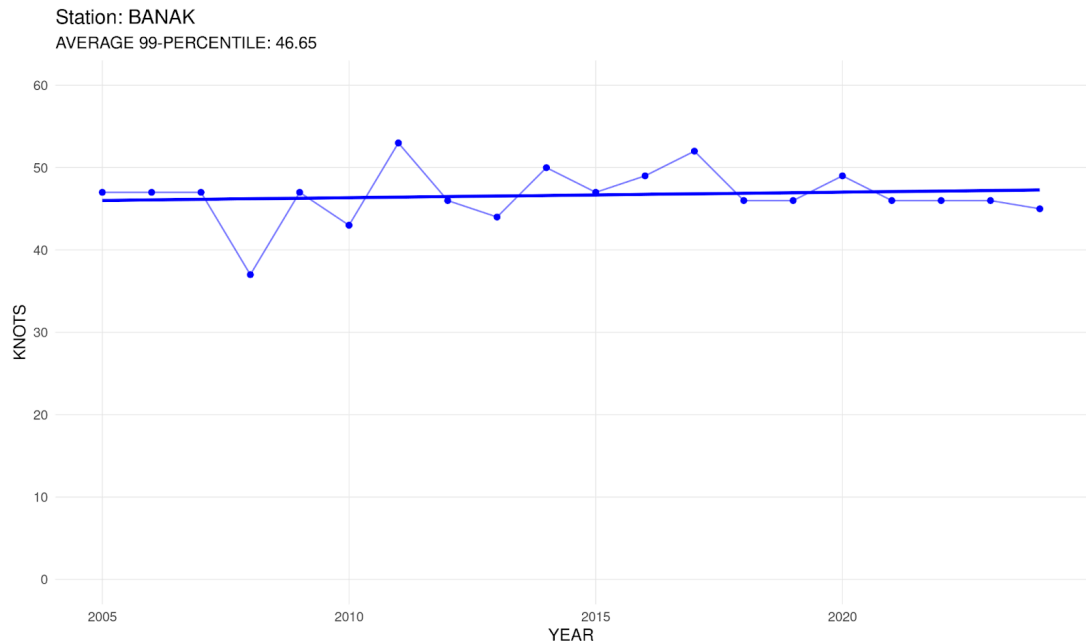


Figure 6.10.3.8.1 The annual value for the 99-percentile wind gust speed and the corresponding trend line.

6.10.4 Freezing precipitation

Freezing precipitation can be hazardous for aircraft operation. There are two main processes giving freezing precipitation: 1) Even if the temperature is less than 0 degrees Celsius, rain drops can exist as supercooled drops. They will momentarily freeze to ice when hitting the cold ground, buildings or vehicles. 2) Because cold air is heavier than warm air, it seeks to the lowest lying places. Rain drops, with a temperature above freezing, from warmer and lighter air aloft, will freeze when they are reaching the ground.

When the airport is closed for traffic, the weather observations are taken automatically. This is adequate for wind, temperature and humidity observations, but the instruments are not capable of detecting the type of precipitation. Inspecting the observation series for precipitation, it looks like the number of occurrences of freezing precipitation are overestimated by instruments compared to manual observations. Therefore the statistics for freezing precipitation at Banak are omitted.

6.10.5 Freeze/thaw events

Since temperatures around 0°C often are challenging for airport operations, and in particular for the runway conditions, the number of freeze/thaw events are analysed.

Figure 6.10.5.1 shows the number of days when the temperature during a day both has been below and above 0 degrees at Banak. This occurs typically on 65 to 95 days annually from 1 October to 30 April. The trend line is slightly increasing.

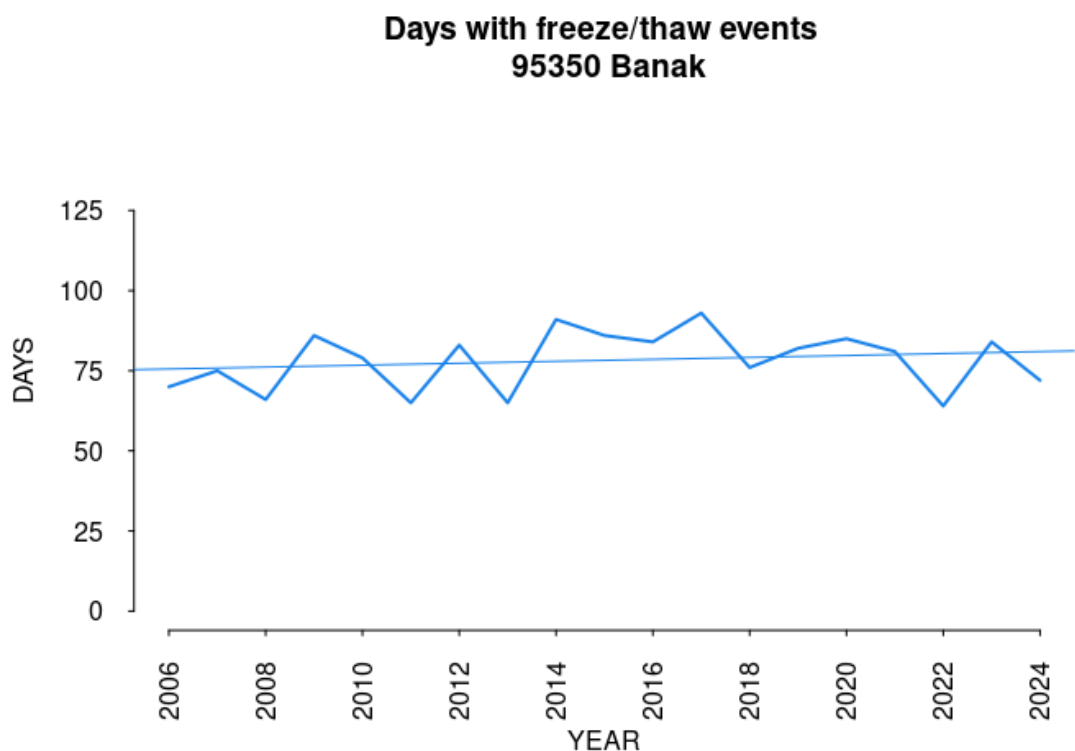


Figure 6.10.5.1. The number of days with freeze/thaw events for the period October to April

7. Meteorological Analysis of Reported Weather

Related Events & Historical and Future Trends in Large-scale Aviation Weather

7.1 Wind and Turbulence

Summary: The frequency of experienced aircraft turbulence and wind shear incidents varies both regionally and seasonally. Relative to flight activity, turbulent incidents are most frequent at Svalbard and in Nordland and Troms during winter (DJF).

In terms of the 1991-2023 winter climatology (October-April), a maximum in the 99%-tile of the 10 m mean wind speed is found in the mountainous terrain of Nordland, Troms and Spitsbergen with values of more than 42 knots. In general, a maximum in the 99%-tile climatology of the \sqrt{TKE} (square root of the turbulent kinetic energy) and downdrafts (vertical velocity) is found on both sides of the mountainous and complex terrain from Vesterålen and southwards depending on the wind direction.

In terms of the difference between the 1991-2006 and the 2008-2023 period, the 10 m mean wind speed and ‘turbulence’ parameters show a modest reduction in the 99%-tile values. In general, the highest reduction is found in the mountainous area of the mainland and in the western parts of Spitsbergen.

The results on turbulent conditions presented relate quite well with the changes in storm track and convective activity for the 1991-2023 period. Due to a further reduction in storm track and convective activity (thermal/convective turbulence) it is likely that future turbulent conditions will be less frequent during the winter season in Northern Norway.

The scientific literature suggests that the Clear Air Turbulence (CAT) in the midlatitudes has increased in recent decades and that it most likely will continue to increase in the coming future, including in Northern Norway and at Svalbard.

Aircraft turbulence occurs when an aircraft enters into an area of irregular air motion characterised by chaotic changes in air pressure and flow velocity. There are four main categories of turbulence: 1) Mechanical turbulence, due to the friction between the air and the ground, e.g low level turbulence and mountain waves (MTW) generated by

wind passing complex terrain, 2) Thermal/Convective turbulence due to downdrafts associated with CB activity, 3) Frontal turbulence, due friction between two opposing air masses and 4) Wind Shear, due to a change in wind direction and/or speed over a specific horizontal or vertical distance, e.g. Clear Air Turbulence (CAT).

The analysis in this report is mainly focusing on low and medium level turbulent conditions. Due to the recent global focus on CAT, often associated with wind shear near the jet stream at higher levels, available scientific literature is studied in order to describe any potential future trends in the CAT pattern for Northern Norway and at Svalbard.

Wind shear and turbulent conditions are reported by pilots in so-called AIREPs. Despite several limitations with these observations (see discussion in data section), they are a valuable source for producing larger data samples of turbulent conditions. In the period from 2015-2023, in total 845 events of turbulent conditions were reported in Northern Norway and at Svalbard. Due to the fact that many of the AIREPs in Nordland are reported at cruising level (above FL200, mainly due to CAT and MTW) and the flight activity is linked to the number of landings, the distribution of reported turbulence events per region and season listed in Figure 7.1.1 only include reports between SFC and FL200, in total 464 reports. Relative to flight activity, turbulence seems to be most frequent at Svalbard and in Nordland and Troms during winter (DJF), and least frequent in Finnmark. In general the least number of reports are found during summer (JJA).

Mechanical turbulence (strong wind over complex terrain) is usually the main cause of the turbulent conditions below FL200, whereas CAT, mountain waves propagating at high levels and convective turbulence near the CB top more often cause turbulent conditions above FL 200. In Table 7.1.1 the total number of AIREPs are listed based on flight level intervals and year. The Table shows an annual variation in the number of reports, and approximately 45% of the reports are made above FL200, 37% above FL300.

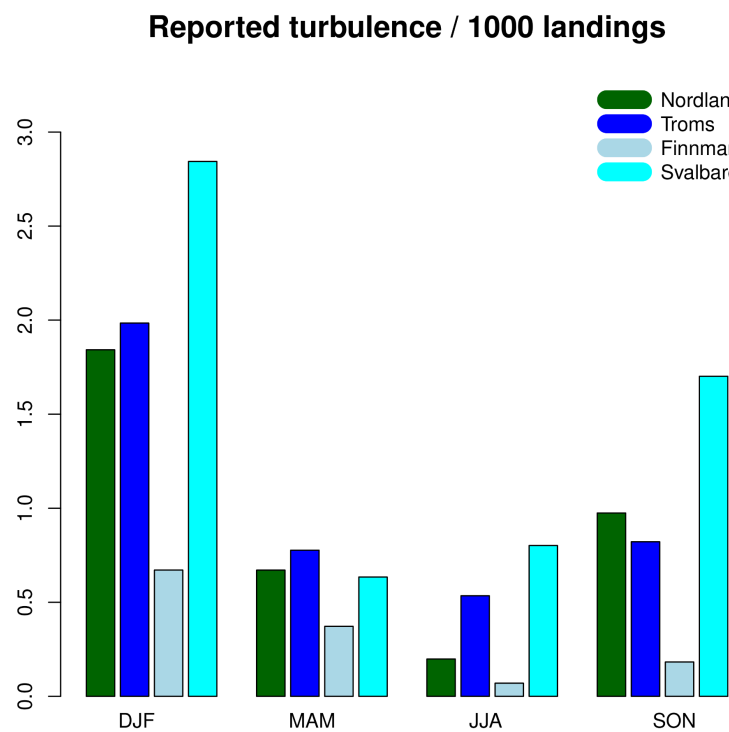


Figure 7.1.1 Reported cases of turbulence in Nordland, Troms, Finnmark and Svalbard per 1000 landings to an airport in the region per season (2015-2023). Only heights below FL200 are included (in total 464 AIREPs).

Table 7.1.1. Number of reported cases with turbulence for Northern Norway and Svalbard for different height intervals and years.

Reported turbulence	2015	2016	2017	2018	2019	2020	2021	2022	2023	Total
Surface - FL100	39	41	62	37	31	49	45	52	40	396
FL100 - FL 200	11	5	10	8	6	3	7	11	7	68
FL200 - FL 300	6	8	6	12	5	10	7	10	4	68
Above FL300	24	33	61	53	48	20	20	32	22	313
Total	80	87	139	110	90	82	79	105	73	845

In order to better understand under which atmospheric conditions turbulence is reported, a MSLP composite distinguishing between reports from the four regions are

shown in Figure 7.1.2. Note that for these composites only AIREPs below FL200 are included since the main focus in this analysis is for low and medium level turbulence. Although the MSLP for each individual case varies significantly from case to case, the composites show some evident patterns. The average location of the low pressure centre and the associated wind field during these reported events differ slightly regional wise as shown in Figure 7.1.2. For Nordland, the low pressure centre on average is located in the Norwegian Sea, halfway between Jan Mayen and Lofoten, setting up a strong southeasterly to southerly wind field over the complex and mountainous terrain in Nordland. Be aware that the wind is not fully geostrophic (wind direction parallel with the isobars) in the lower level of the atmosphere, but has a certain angle/component towards the low pressure. For Troms, the low pressure centre on average is located further northeast (just southwest of Bjørnøya), setting up a strong southeasterly - southwesterly wind field over the mountainous terrain in Troms. For the reported turbulent events in Finnmark the location of the low pressure centre on average seems to be west of Bjørnøya, setting up a strong southeasterly to southerly wind field, blowing outwards the valleys and fjords and potentially creating turbulent conditions. The number of reported events from Svalbard during the 2015-2023 is quite sparse, but on average the location of the low pressure centre during these events is just southwest of Bjørnøya, setting up a strong northeasterly to southeasterly wind field (prevailing wind direction during the winter season) over the archipelago. Due to these prevailing easterlies, the western and central area of Spitsbergen will be most frequently exposed to turbulence.

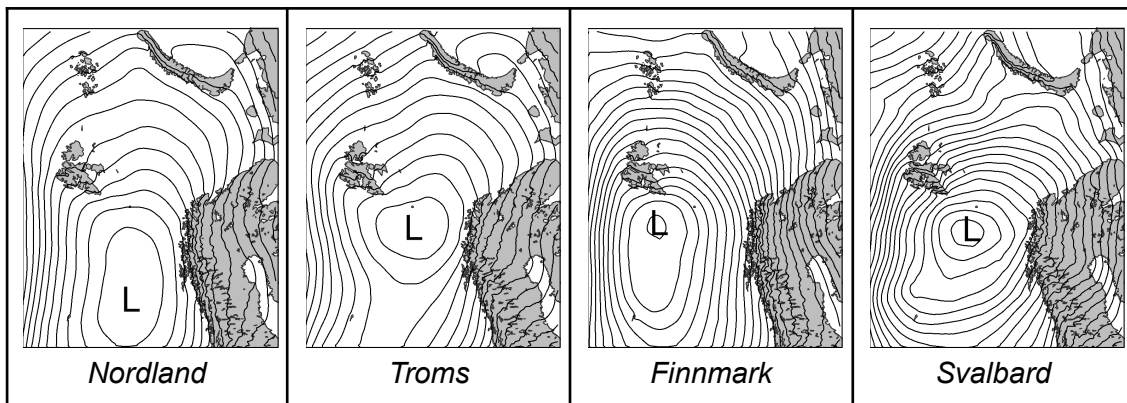


Figure 7.1.2 MSLP composites for reported AIREPs below FL200 in Nordland (189), Troms (131), Finnmark (47) and at Svalbard (12) for ONDJFMA.

In this study **reanalysis data is applied in order to estimate historical turbulence conditions and changes**. From the CARRA data set, the 10 m mean wind speed, the square root of the Turbulent Kinetic Energy (\sqrt{TKE}) and downdrafts (vertical velocity) are applied for analysing and detecting areas with turbulence. The maximum value of \sqrt{TKE} , which usually is most predominant near the surface (SFC), is analysed between the surface and 2000 ft. In operational aviation weather forecasting, thresholds for

determining the turbulence severity level are defined as: FBL (1-2), MOD (2-3.5) and SEV (> 3.5). In order to analyse the turbulence at medium/high levels, the maximum downdraft (minimum vertical velocity, w) between 750 and 500 hPa is applied by using the operational thresholds: FBL (1-1.75), MOD (1.75-3) and SEV (> 3).

What is the climatology of turbulent conditions and the recent historical changes based on the reanalysis? A maximum in the 99%-tile climatology of the 10 m mean wind speed from CARRA is found in the mountainous terrain of Nordland, Troms and Spitsbergen with values of more than 42 knots (Figure 7.1.3a). The lowest mean wind speed on average is found on the Swedish and Finnish side of the Norwegian border.

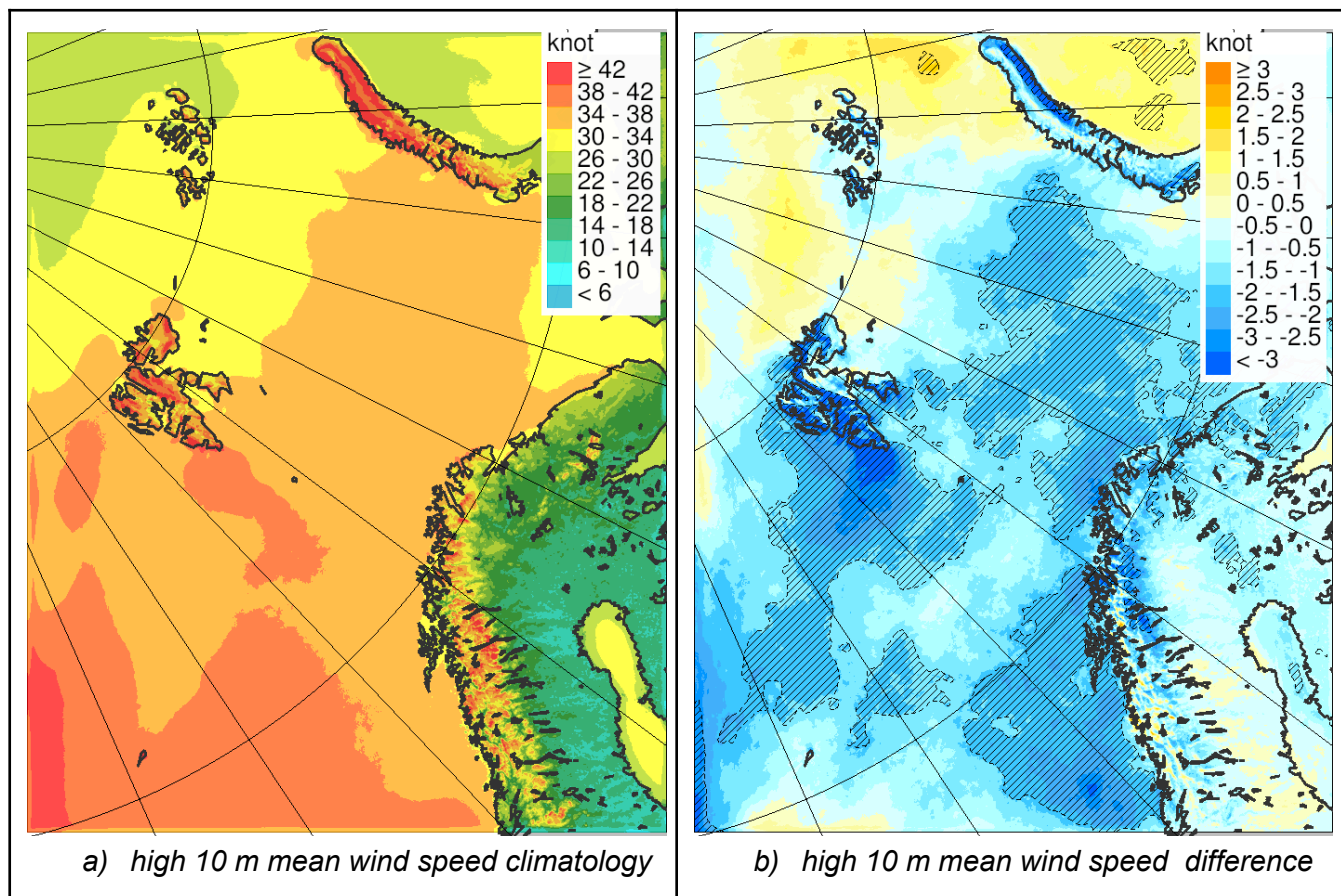


Figure 7.1.3 Climatology for 1991-2023 (left side) and difference between last 15 years (2008-2023) and first 15 years (1991-2006) (right side) for high 10 m mean wind speed. a,b) Yearly 99%-tile of 10m mean wind speed. Data from CARRA. Differences in regions marked with thin black lines are significant with a 90% confidence interval.

The MSLP composites of the annual (ONDJFMA) 99%-tile of the 10 m mean wind speed at ENBO, ENTC, ENKR and ENSB (Figure 7.1.4) help us to better understand the average large scale circulation pattern during the most 'extreme' events, critical for

the generation of wind shear and low level turbulence in general and at the individual airports. For ENBO, we find the strongest 10 m mean wind speed associated with an intense low pressure system located northwest of Lofoten, accompanied by a strong southwesterly wind field in Nordland and in the ENBO-area. For ENTC the pattern is quite similar, but with a slightly more northerly shift in the location of the low pressure centre. For ENKR, the low pressure centre is located north of Øst-Finnmark, setting up a strong southwesterly to westerly wind flow (offshore wind). For ENSB and Spitsbergen, we find the average location of the low pressure centre southwest of the archipelago, setting up a strong southeasterly to northeasterly wind field over Spitsbergen.

For the 'high' (99%-tile) 10 m mean wind speed from CARRA, an overall, modest reduction is seen from the 1991-2006 to the 2008-2023 period (Figure 7.1.3b). The highest, significant reduction is found in the mountainous area north of Lofoten, over large ocean areas and in the western parts of Spitsbergen. The maximum reduction is more than 3 knots (approximately 5%). On the mainland south of Salten the reduction is less evident, and even showing some patches of an increase in the 'high' 10 m mean wind speed. However, the differences in this area are not significant.

Due to the fact that turbulent conditions also are heavily dependent on the wind direction (flow over complex terrain with a significant perpendicular wind component) and not only the wind speed itself, we will see some minor differences in the composites of the 10 m mean wind speed compared with the composites of the downdrafts and \sqrt{TKE} (see below). The two latter parameters are in general better turbulence predictors.

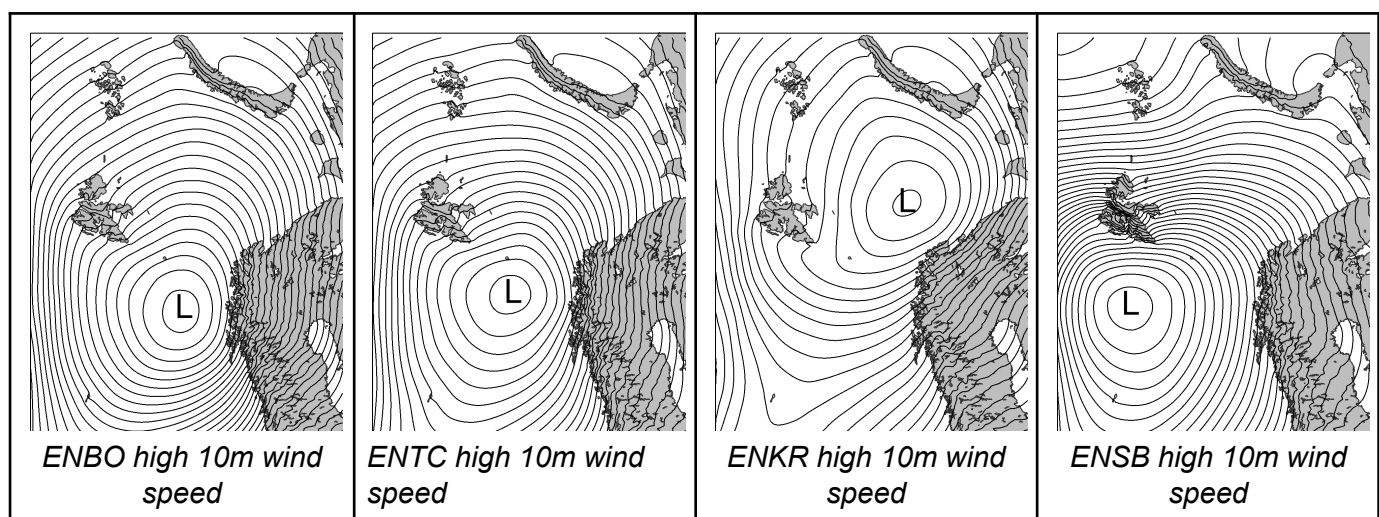


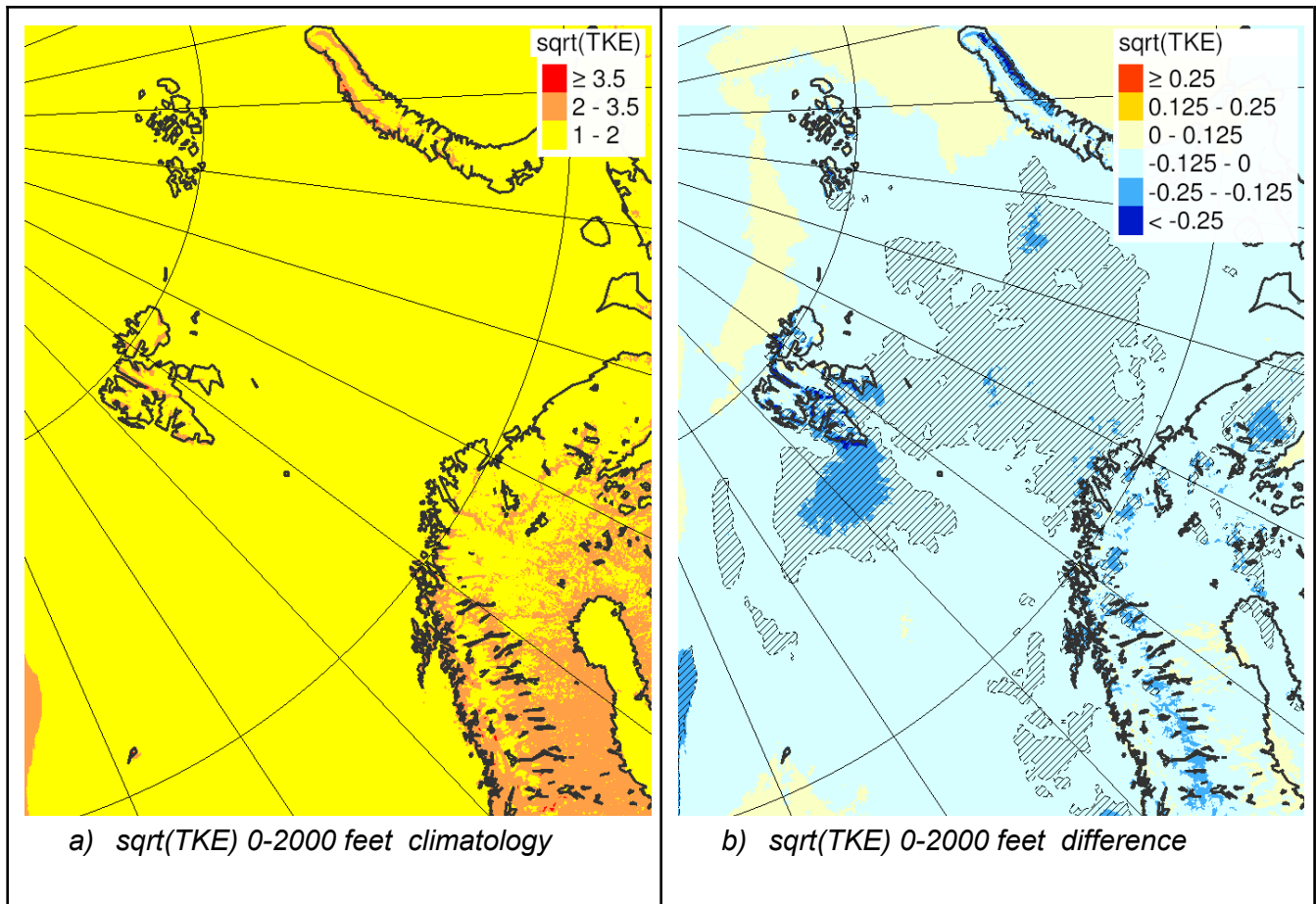
Figure 7.1.4 MSLP composites of the 99%-tile of 10 m mean wind speed at ENBO, ENTC, ENKR and ENSB. Isobar line per 1 hPa. For 10 m mean wind speed the %-tile is calculated for the airport itself.

\sqrt{TKE} is usually a good indicator for detecting turbulence (mainly mechanical turbulent conditions) at lower levels, while downdrafts, e.g. associated with mountain waves (MTW), is a good indicator for detecting turbulence at medium to higher levels. It should also be noted that the atmospheric stability is an important parameter in order to separate between different forms of turbulence, e.g. distinguishing between pure mechanical low level turbulence and mountain waves propagating at higher levels. However, a detailed analysis of the atmospheric stability during these turbulent events are not elaborated any further in this section. In the following, we study the climatology and historical changes of the 99%-tile for the maximum \sqrt{TKE} below 2000 ft (Figure 7.1.5.a,b) and the 99%-tile of the maximum downdraft between 750 and 500 hPa (Figure 7.1.5.c,d).

A maximum in the 99%-tile climatology of the \sqrt{TKE} is found on both sides of the mountainous and complex terrain from Vesterålen and southwards depending on the wind direction (events with onshore and offshore wind) with widespread areas of moderate turbulence (MOD TURB) and a few patches of severe turbulence (SEV TURB). In general, Finnmark is not as mountainous as Nordland and Troms. On average, we find widespread areas with feeble/light turbulence (FBL TURB) and patches of moderate turbulence in this area in parallel with the valleys and fjords due to the predominant offshore winds during the winter season in this region. As for Finnmark, we find fewer 'extreme' turbulent events at Svalbard with widespread areas of feeble turbulence and patches of moderate turbulence on the lee side of the mountainous area on the central and western side of Spitsbergen due to the predominant easterlies at Svalbard during the winter season. In terms of the 99%-tile climatology of the downdrafts (Figure 7.1.5c), we find a quite similar pattern. However, the maximum values seem to be more related to the areas where we find the highest mountains and where mountain waves are more common, e.g. in Nordland and Troms.

In general, we find some evident similarities between the MSLP composites of the reported turbulent conditions from the AIREPs (Figure 7.1.2) and from the MSLP composites of the downdrafts and \sqrt{TKE} (Figure 7.1.6), demonstrating that the reanalysis are capable of describing important mechanisms of observed aircraft turbulent events. Particularly for the downdraft composites for ENBO (Nordland), ENTC (Troms) and ENSB (Svalbard) we find similarities with the AIREP composites in terms of the location of the low pressure centre. However, for ENKR (Finnmark), we find a significant difference in the location of the low pressure centre when comparing the composites of the AIREPs with the composites of the downdrafts and \sqrt{TKE} . This can

be due to a diversity in the situations favourable for turbulent conditions related to lower mechanical turbulence (\sqrt{TKE} as the pronounced parameter) at ENKR and for the generation of mountain waves (downdraft as the pronounced parameter). In the \sqrt{TKE} composite for ENKR, the location of the low pressure centre is northeast of Finnmark, setting up a southwesterly to northwesterly wind field, favourable for generation of low level mechanical turbulence in this area. In the downdraft composite for ENKR, however, the composite is much more in line with the composite for Finnmark of the reported turbulent conditions from the AIREPs, where generation of mountain waves are more favourable due to the predominant offshore winds blowing outwards of the valleys and fjords (south- and southeasterlies).



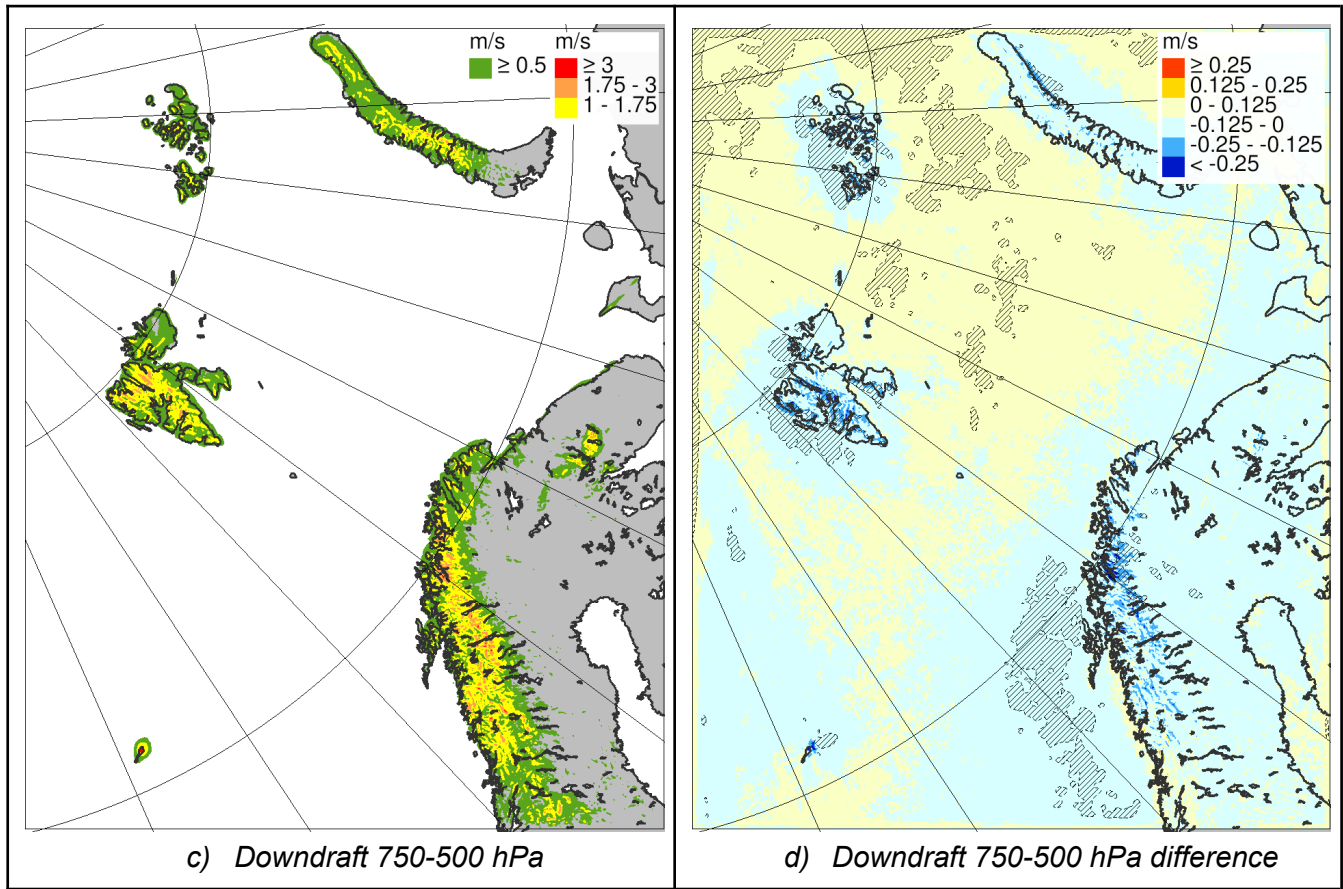


Figure 7.1.5. Climatology for 1991-2023 (left side) and difference between last 15 years (2008-2023) and first 15 years (1991-2006) (right side) for atmospheric $\sqrt{\text{TKE}}$ (upper row) and downdrafts (bottom row). a,b) Yearly 99%-tile of maximum $\sqrt{\text{TKE}}$ in the atmospheric layer 0-2000 feet. c,d) Yearly 99%-tile of maximum downdrafts in the atmospheric layer 750-500 hPa. Colour scales in the climatology equals thresholds for fbl turbulence (yellow), moderate turbulence (brown) and severe turbulence (red). Data are based on CARRA pressure levels. Differences in regions marked with thin black lines are significant with a 90% confidence interval.

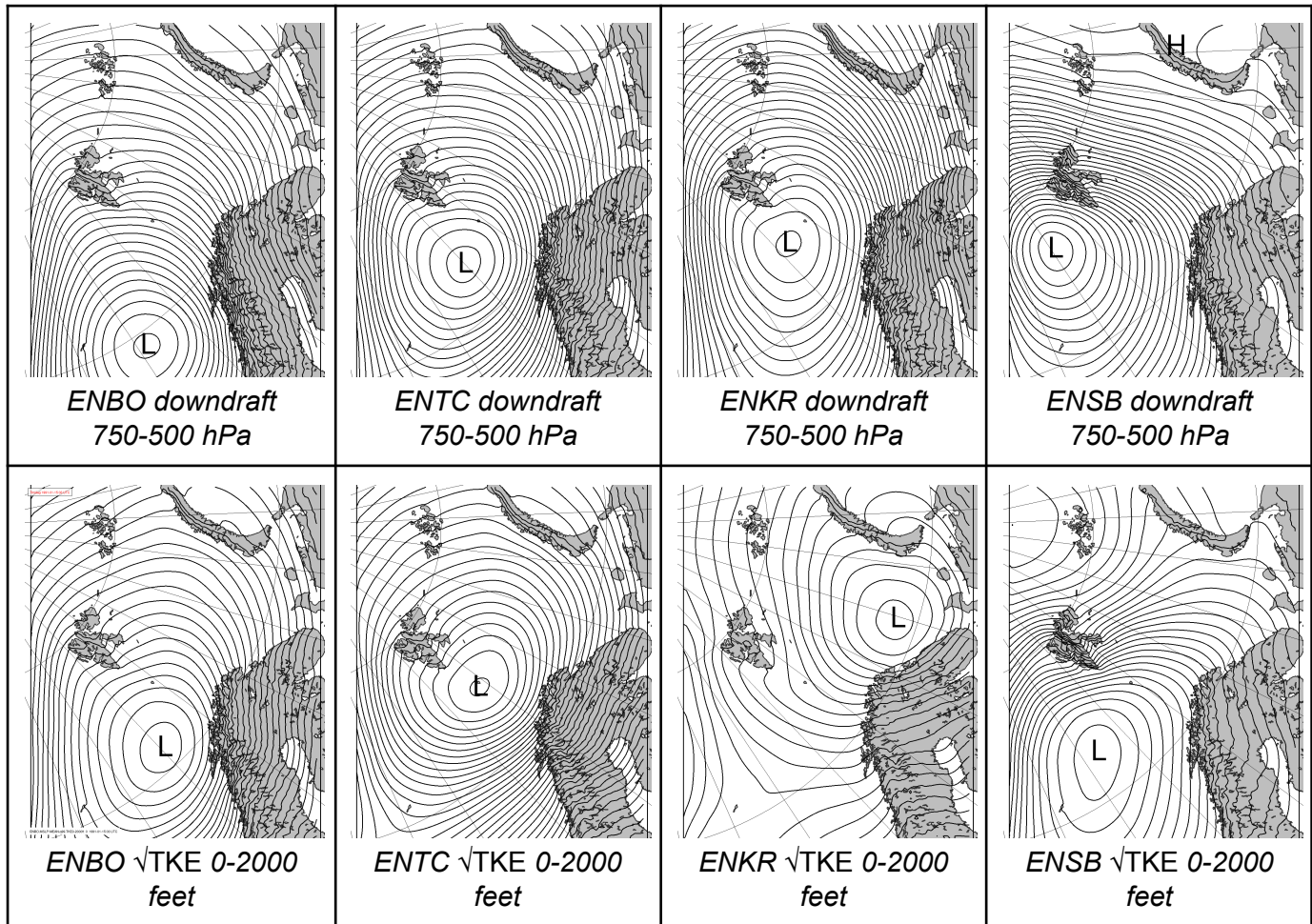


Figure 7.1.6 MSLP composites of the 99%-tile of maximum downdrafts for ENBO, ENTC, ENKR, ENSB for the 750-500 hPa levels (row 1), the 99%-tile of maximum \sqrt{TKE} for ENBO, ENTC, ENKR, ENSB for levels between 0 and 2000 feet (row 2). Isobar line per 1 hPa. For downdrafts and \sqrt{TKE} the %-tile is calculated for a maximum point within 25 km from the airport.

In general, the differences in \sqrt{TKE} and the downdrafts between the 1991-2006 and the 2008-2023 period (Figure 7.1.5 b and d) follow the same pattern as for the 10 m mean wind speed. The highest reduction is seen in the inner mountainous area on the mainland close to the Norwegian border and in the western parts of Spitsbergen (as for the 10 m mean wind speed).

The results on turbulent conditions presented here relate quite well with the changes in storm track activity for the same period (see section 5). It is likely that less storm track activity reduces the number of strong wind events and hence a reduction in the turbulent conditions. Perhaps the modest (but not significant) increase in downdrafts between the two periods (Figure 7.1.5d) seen over Trøndelag could be due to a modest increase in storm track activity over Southern Norway during the winter season,

increasing the turbulent conditions on the lee side (offshore winds) of the mountains in this area?

How do the presented results fit with the scientific literature and what about the future? With the exception of Clear Air Turbulence (CAT), the impact climate change has on aircraft turbulent conditions is not well studied (Storer et al., 2019). However, due to a reduction in both the storm track activity and convective activity (see section on convective activity) between the two examined periods, as well as a further modest reduction in storm track activity towards the end of the century, it is likely that future turbulent conditions will be less frequent in Northern Norway.

CAT is relatively well studied in the context of climate change. Burbidge et al. (2024) summarised the existing knowledge and concluded that it is likely, on average, that climate change will increase the strength and frequency of CAT. Prosser et al. (2023) found that CAT in general has increased over the past four decades by examining reanalysis data. In their study this is in particular seen around the midlatitudes, e.g. in the North Atlantic, at typical aircraft cruising levels. However, no specific indication of a recent change was found over Northern Norway and Svalbard in the existing scientific literature.

For the future projections, Williams and Storer (2022) showed that climate models reasonably well describe relevant CAT information and can be applied for future scenarios. By applying output from climate models, Storer et al. (2017) find a significant increase in CAT from pre-industrial time to 2050-2080, in particular for the midlatitudes, but also seen further north to include Northern Norway and Svalbard during autumn and winter. This is also supported by Williams (2017), concluding that the Transatlantic wintertime CAT will increase, seen in their Figure 4-6. It is also likely that this includes Northern Norway and Svalbard for the frequency of light/feeble and moderate CAT. The available literature seems to be relatively consistent regarding the link between climate change and CAT. However there are still a number of sources of uncertainty, particularly related to the actual future emission scenarios.

Methodology: In order to investigate the changes in historical aviation weather conditions (in this section for wind and turbulence), the annual 99%-tile for the ‘winter’ months October, November, December, January, February, March and April is calculated for selected parameters (assuming that the 99%-tile provides difficult or severe aviation weather conditions). The average of the annual values of the two periods, 1991-2006 and 2008-2023, are compared. Note that 2007 is not included in the analysis when comparing the two periods. This is due to the fact that we want two equally long periods to compare. In order to decide on the statistical significance, a two sided student t-test with a 90% confidence interval is applied.

From the CARRA data set, the 99%-tile ('high') of the 10 m mean wind speed (surface wind) is analysed. The square root of the Turbulent Kinetic Energy ($\sqrt{\text{TKE}}$) is applied for analysing and detecting areas with low level turbulence. The $\sqrt{\text{TKE}}$ is usually most predominant between the surface (SFC) and 2000 ft. In operational aviation weather forecasting, thresholds for determining the turbulence severity level are defined, such as FBL (1-2), MOD (2-3.5) and SEV (> 3.5). In order to analyse the turbulence at higher levels, the downdraft (vertical velocity, w) is applied by using the operational thresholds - FBL (1-1.75), MOD (1.75-3) and SEV (> 3).

7.2 Icing

Summary: *The frequency of experienced aircraft icing incidents varies both regionally and seasonally. Relative to flight activity, icing incidents are most frequent in Svalbard in autumn, winter and spring. On the mainland, icing incidents are reported more often in Nordland than in Troms and Finnmark. A diversity is found in situations where icing conditions are present, but often icing is associated with strong onshore air flow with the potential to lift moist air masses to produce clouds with supercooled liquid water. The presence of high amounts of supercooled liquid water was slightly reduced in the 2008-2023 period compared to the 1991-2006 period in Northern Norway, most likely due to the reduction in storm track activity. In the future, it is likely that the icing conditions will be less frequent due to a likely reduction in storm track activity during the winter season. However, since warmer air has the potential to transport more moisture, it is uncertain whether each event will have the potential to be more severe or not.*

Aircraft icing happens when an aircraft flies into a cloud with supercooled water droplets. Supercooled droplets are water that remain in a liquid phase even at freezing temperatures and are common in a temperature range of -20°C to 0°C and may under favourable conditions go down to -40°C . Clouds with supercooled droplets can form under various processes. The potential icing severity depends on the amount of liquid water content, the size of the droplets and the ambient air temperature (Cao et al., 2018), in addition to the characteristics of the aircraft.

Icing conditions are reported by pilots in so-called AIREPs. Despite many limitations with these observations (see discussion in data section), they are a valuable source for producing larger data samples of icing conditions. In the period from 2015-2023, in total 465 events of icing conditions were reported near airports in Northern Norway - for Nordland (233), Troms (149), Finnmark (53) and Svalbard (30). Figure 7.2.1 shows the distribution for the different regions and seasons relative to flight activity. In terms of icing per flight, icing is most frequent at Svalbard, and in particular in the transition

seasons - MAM and SON, but also during DJF. For the mainland regions, icing occurs more often in Nordland than in Troms and Finnmark. Seasonally there are more icing events in DJF and less in JJA. The interannual variability is substantial, for example with twice as many icing reports in 2020 than in 2016. In general, icing is reported on all heights vertically below FL250 with a median value of approximately 6000-7000 feet (FL070) in winter and slightly above 10000 feet (FL100) in summer.

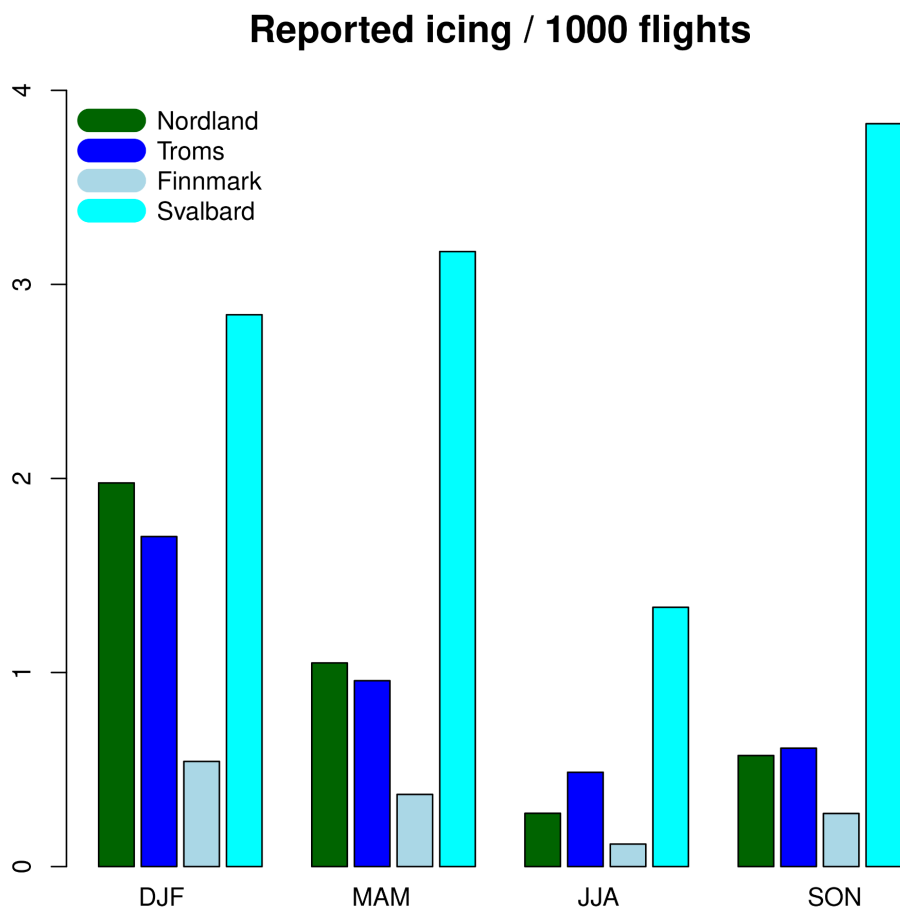


Figure 7.2.1 Number of reported cases of icing in Nordland, Troms, Finnmark and Svalbard per 1000 landings to an airport in the region per season (period 2015-2023).

In order to better understand under which atmospheric conditions icing is reported, a Mean Sea Level Pressure (MSLP) composite distinguishing between reports from the four regions are shown in Figure 7.2.2. Although an analysis of the MSLP in each individual case reveals large variations from case to case within each region and season, the composites show some clear patterns. The low pressure systems set up a strong onshore air flow, forcing the moist air masses to be lifted by the coastal mountains, reaching sub-zero temperatures, hence potentially producing supercooled liquid water. This is in particular evident for Nordland and Troms, while the MSLP gradients in the composite for Svalbard and Finnmark are slightly weaker. If these less

evident composites for Finnmark and Svalbard are due to a larger variety of the large-scale conditions during icing events or due to a smaller data sample leading to a higher uncertainty, is unclear.

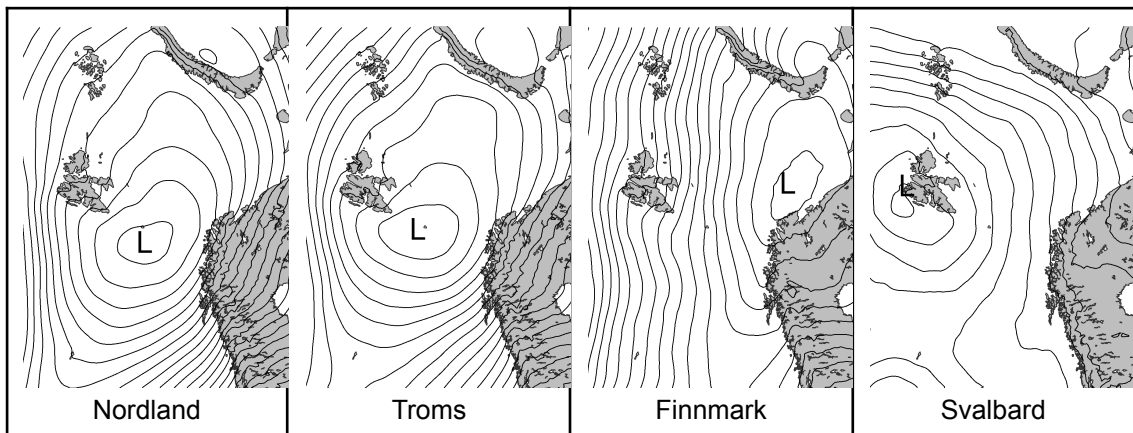


Figure 7.2.2 MSLP composites (average MSLP) for reported AIREPs with icing near airports in Nordland (233), Troms (149), Finnmark (53) and Svalbard (30). Isobars 1 hPa.

We apply **reanalysis data to analyse historical pilot, incident and weather reports**:

When do severe aviation conditions occur? What is the role of large-scale low pressure systems on icing conditions and changes. As mentioned above, the main ingredients for icing conditions are supercooled liquid water. From CARRA we apply the supercooled Specific Cloud Liquid Water Content (SCLWC) above ~1000 feet, and from ERA5 the total column of supercooled liquid water (TCSLW). Data from two different reanalysis help us to better understand some of the uncertainty associated with the estimation of these in-cloud parameters in the reanalysis (for more details, see description of methodology below and in the section on data).

What is the climatology of icing conditions in the reanalysis? The climatology of the annual (ONDJFMA) 99%-tile values of TCSLW from ERA5 (Figure 7.2.3) and supercooled SCLWC above 1000 feet from CARRA (Figure 7.2.4) shows similar large-scale patterns. An icing maximum is found over the topography in Nordland, with decreasing values northward along the Norwegian coast. In addition, an east-west gradient is seen over Svalbard with higher values in the western part. The most evident difference between CARRA and ERA5 is the much more detailed small scale pattern associated with the high-resolution CARRA data set over the local topography. The overall similarities in the icing pattern from the two data sets strengthen our trust in the usefulness of the reanalysis data for the purpose of providing a qualitative analysis of the icing conditions.

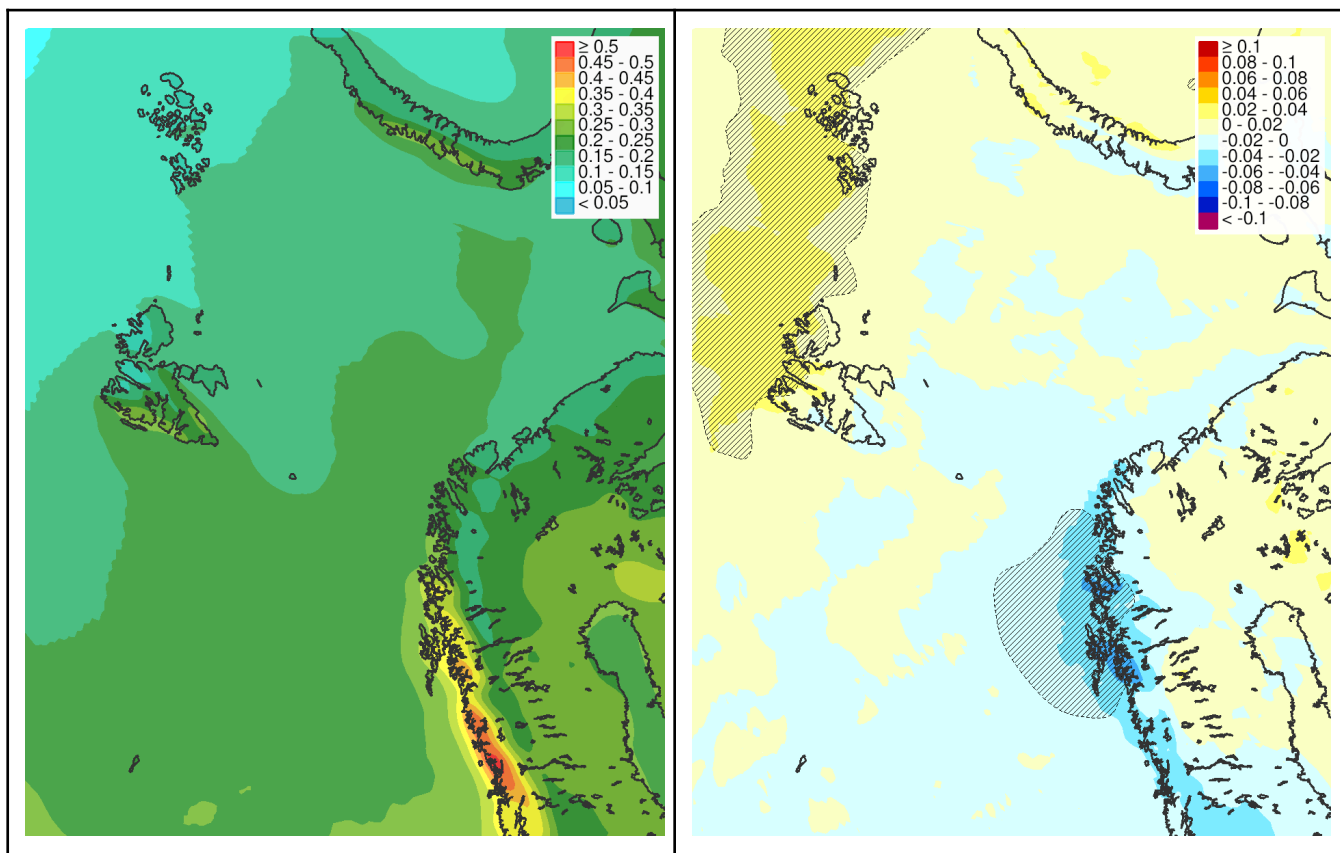


Figure 7.2.3 Climatology for 1991-2023 (left side) and difference between last 15 years (2008-2023) and first 15 years (1991-2006) (right side) for total integrated supercooled liquid water in ERA5. a,b) Yearly 99%-tile. Differences in regions marked with thin black lines are significant with a 90% confidence interval.

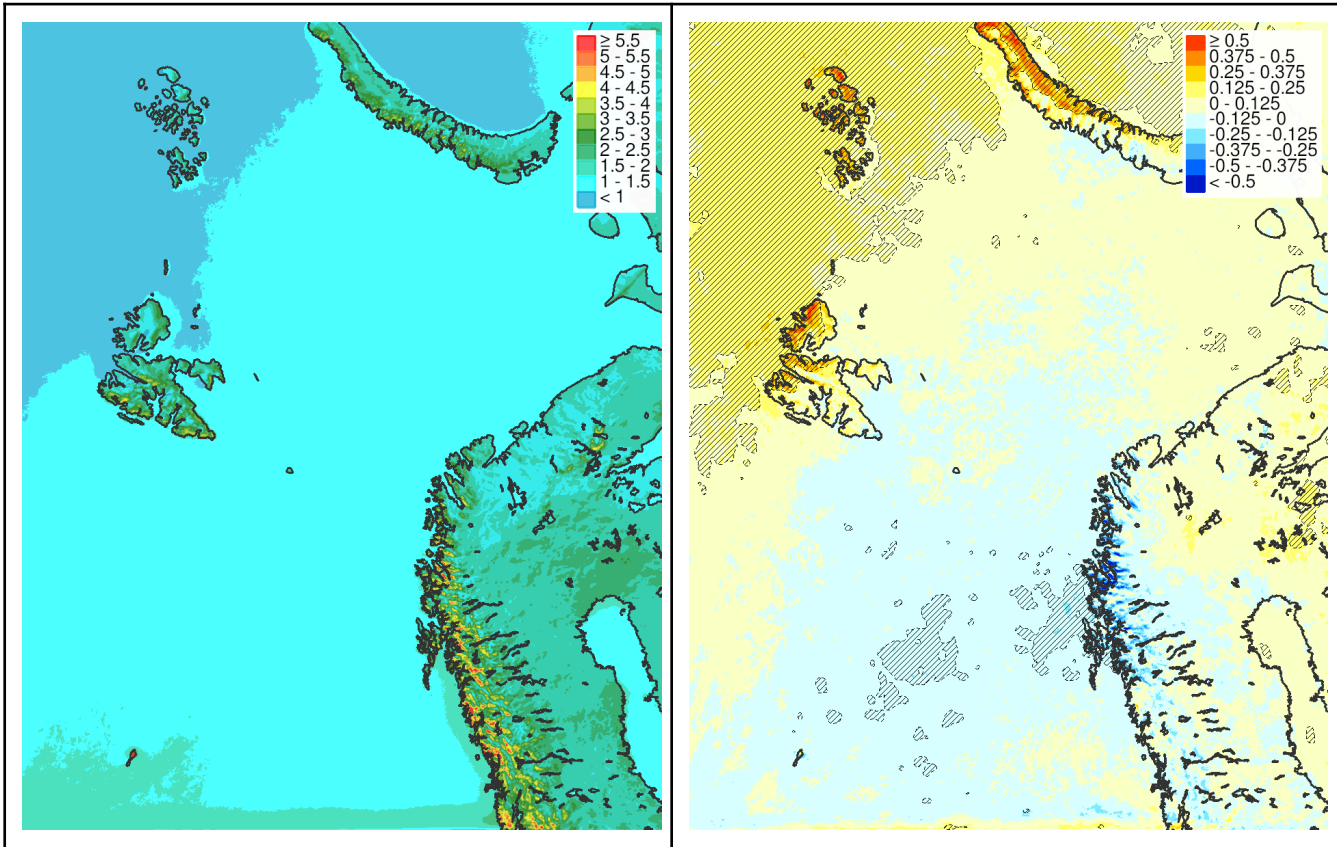


Figure 7.2.4. Climatology for 1991-2023 (left side) and difference between last 15 years (2008-2023) and first 15 years (1991-2006) (right side) for total integrated supercooled liquid water in CARRA above 1000 feet [g/kg]. a,b) Yearly 99%-tile. Differences in regions marked with thin black lines are significant with a 90% confidence interval.

The MSLP composites of the annual (ONDJFMA) 99%-tile for “a climatological icing maxima point” near the airports ENBO, ENTC, ENKR and ENSB (Figure 7.2.5) help us to better understand the connection between the icing conditions and the large scale circulation. For all regions, the large-scale weather conditions on average indicate a strong onshore flow with the potential of transporting and lifting moist air towards the complex coastal terrain. For ENBO, ENTC and ENSB the flow has a strong southerly component while for Finnmark the maximum icing events seem to be associated with a northerly flow ‘behind’ the location of the low pressure centre. We also find that there are some evident similarities between the MSLP composites of the reported icing conditions from the AIREPs (Figure 7.2.2) and from supercooled SCLWC, demonstrating that the reanalysis are capable of describing important mechanisms of observed aircraft icing events. The main difference is seen in the slightly different location of the low pressure systems for Svalbard and Finnmark. This can be due to a diversity in the situations favourable to icing conditions, or indicating that the MSLP composites represent reports (AIREPs) for the entire region versus a point near the

main airports (CARRA). The reason for the diversity could also be a sampling issue due to relatively few icing reports in these two regions.

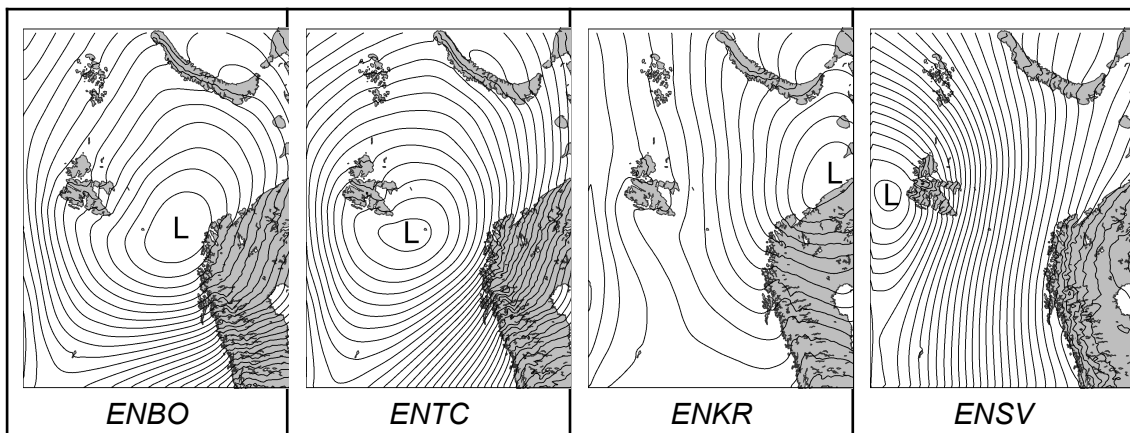


Figure 7.2.5 MSLP composites of annual (ONDJFMA) 99%-tile of supercooled liquid water above 1000 feet in CARRA data near ENBO, ENTC, ENKR and ENSV. Isobars 1 hPa.

What are the recent historical changes in icing conditions based on reanalysis?

In 99%-tile of TCSLW from ERA5 a modest reduction is seen from the 1991-2006 to the 2008-2023 period along the Norwegian coast (Figure 7.2.3). The reduction is up to 5%, but only significant from south of Lofoten to the western part of Finnmark. In addition, an increase of up to 25% is found in the north- and northeastern parts of Svalbard. However, we see that the climatological icing values in this area are much smaller than for mainland Norway. The changes in the 99%-tile of supercooled SCLWC from CARRA is in general similar to the pattern seen for TCSLW from ERA5, but with some minor differences, in particular showing much more local details related to topography (Figure 7.2.4). The results on icing conditions presented here relate well with the changes in storm track activity for the same periods (see section 5). It is likely that less storm track activity reduces the number of strong onshore wind events and hence a reduction in icing conditions.

Northern Norway icing situations typically happen when warm and moist air is transported into the region, e.g. by low pressure systems, and that the air masses are lifted towards topography and reach freezing. We have therefore investigated how common temperatures above 0°C are at different vertical levels. Here we show the results from model level 55 in CARRA (approximately 1000 feet) during ONDJFMA, and the change in frequency between the two periods 2008-2023 and 1991-2006 (Figure 7.2.6). Over Northern Norway there are small and non-significant changes. It is likely that a reduced storm track activity leads to a reduced number of cases, and cancels out the impact of any general increase in atmospheric temperature. Around Svalbard and in the Barents Sea a clear and significant increased frequency is seen

and can most likely be attributed to the strong local warming due to increased Sea Surface Temperatures and reduced sea ice cover in the region. The spatial patterns in the changes are similar for the entire lower atmosphere, but the magnitude of the differences are larger closer to the surface than higher up (not shown).

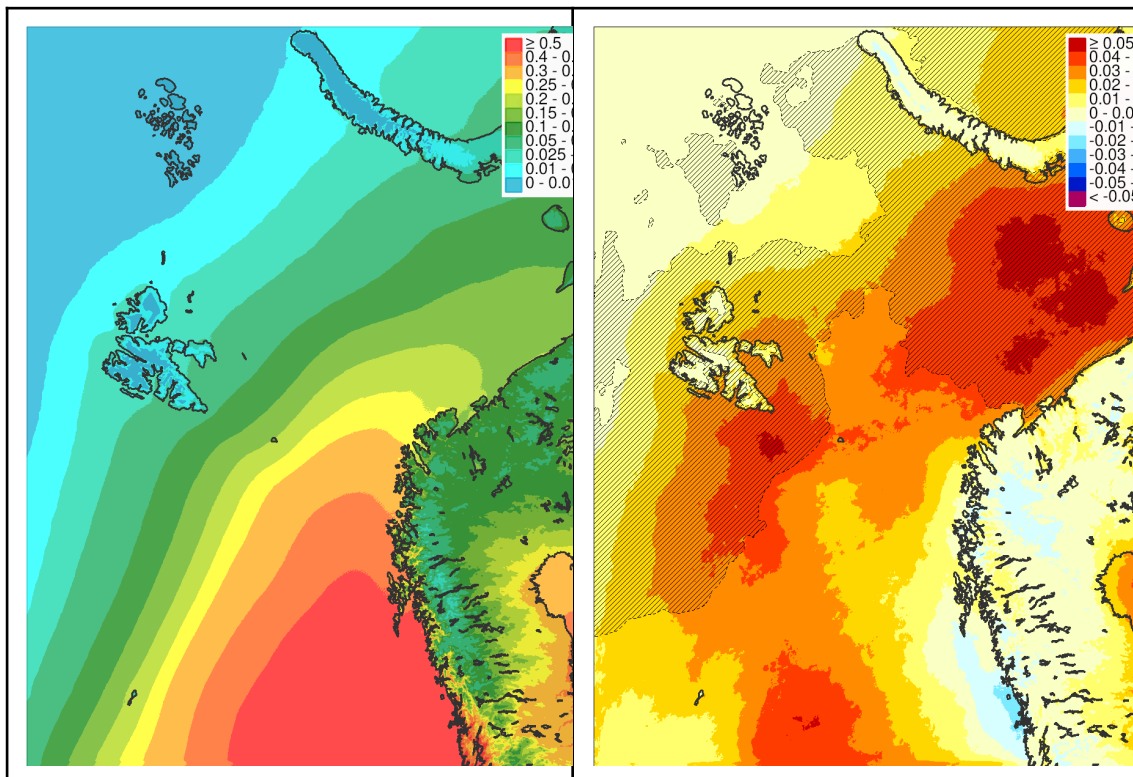


Figure 7.2.6 Frequency for 1991-2023 (left side) and difference between last 15 years (2008-2023) and first 15 years (1991-2006) (right side) for temperatures above 0°C at model level 55 in CARA (approximately 1000 feet) for ONDJFMA. Differences in regions marked with thin black lines are significant with a 90% confidence interval.

How do the presented results fit with the scientific literature and what about the future? The impact climate change has on aircraft icing conditions is not well studied in the scientific literature. It is assumed that the impact will vary regionally and seasonally, and it has been assumed that an increase in the air temperature and moisture content can contribute to a strengthened icing level (Burbridge et al., 2024). The close connection between low pressure systems and icing conditions suggests that at least part of the reduction in high values of supercooled liquid water content from the 1991-2006 period to the 2008-2023 period can be explained by the reduction in storm track activity. An unknown in the results is that icing in stratiform clouds (smaller droplets and possibly less LWC) and in convective clouds (larger droplets and potential for larger LWC) are not distinguished. However, there is a reduction in both the storm track and convective activity (see section on convective activity) between the two

examined periods. With a further modest reduction in storm track activity towards the end of the century, it is likely that future icing conditions will be less frequent in Northern Norway. However, since warmer air can transport more moisture, it is a possibility that the icing potential in each individual event can be higher than in the present-day climate.

Methodology. Since parameters like liquid water content and droplet size often are associated with a high uncertainty in meteorological models, a range of different icing algorithms are applied in weather forecasting for aviation. Typically temperature, liquid cloud water content, other types of hydrometers and measures of humidity from numerical weather prediction models are used (Gultepe et al. 2019). However, the basic requirement for icing is the availability of supercooled liquid water, which we therefore have used as the key parameter in our study of the reanalysis data. Since the main focus in our analysis is the spatial distribution (to describe spatial patterns in the climatology) and the relative changes between the two periods (to describe changes in icing conditions), the exact amount of supercooled liquid water content is less important (opposite to operational aviation weather forecasting). Therefore the analysis is limited to the study of supercooled liquid water content. From CARRA, the Specific cloud liquid water content (SCLWC) and temperature is extracted from all model levels above 1000 feet chosen to represent relevant heights. A further break up in multiple heights added very little information. The total and accumulated value of SCLWC in the column is the sum of the SCLWC from each model level, given that the temperature in each level is below 0°C (as supercooled SCLWC). From the ERA5 data set the output variable 'Total column supercooled liquid water (TCSLW)' is applied, i.e. it represents the full vertical column of the atmosphere. Information of droplet size is not available in the reanalysis.

To investigate the changes in historical aviation weather conditions, the annual 99%-tile for the 'winter' months October, November, December, January, February, March and April is calculated for selected parameters (assuming that the 99%-tile provides difficult or severe aviation weather conditions). The average values from the two periods, 1991-2006 and 2008-2023, are then compared. Note that 2007 is not included in the analysis when comparing the two periods. This is because we want two equally long periods to compare. In order to decide on the significance of the differences, a two sided student t-test with a 90% confidence interval is used.

7.3 Convective activity

Summary: *Observations show that the occurrence of convection in coastal areas of Northern Norway in winter is as frequent, or more frequent, than in summer. Wintertime convection is strongly associated with an onshore wind pattern steered by the large scale conditions and strong vertical temperature gradients.*

Over the 1991-2023 period, a general reduction in both the onshore wind speed and the vertical instability is found. However, the change in the vertical instability shows regional differences in sign and amplitude for the cases with the strongest onshore wind components. The latter makes the interpretation of changes in convective activity complex and not straightforward for some regions.

The scientific literature anticipates in general a future reduction in offshore wintertime convection. This is supported by the close connection between the large-scale low pressure systems and convection found in our analysis and the likely reduction of storm track activity shown in section 5.

Wintertime convection in Northern Norway forms, develops and grows over the ocean. When reaching the coast the convection is further reinforced due to convergence of the air masses and lifting towards steep topography. However, when moving further inland during wintertime, the convection is losing its energy source of heat and moisture rapidly. Hence, wintertime convection is an offshore and coast phenomenon and is very rarely seen in the inland areas. Favourable conditions for the creation of convection in the Norwegian and Barents Sea are cold, dry air outbreaks from the Arctic, strong winds and/or storm activity. Convection can therefore be present both as individual convective cells, typically in Cold Air Outbreaks (CAO, see section 3.7 and Figure 3.7.1), organised into meso-scale phenomena, such as polar lows, embedded in large-scale low pressure systems or in the flow behind large-scale systems (example in Figure 3.6.1). A long fetch over the relatively warm water gives the convection enough time to form, develop and intensify. The strong up- and downdrafts associated with convection create problems for aviation by generating turbulence, wind shear, microbursts, lightning, icing and could impact the visibility and produce heavy precipitation.

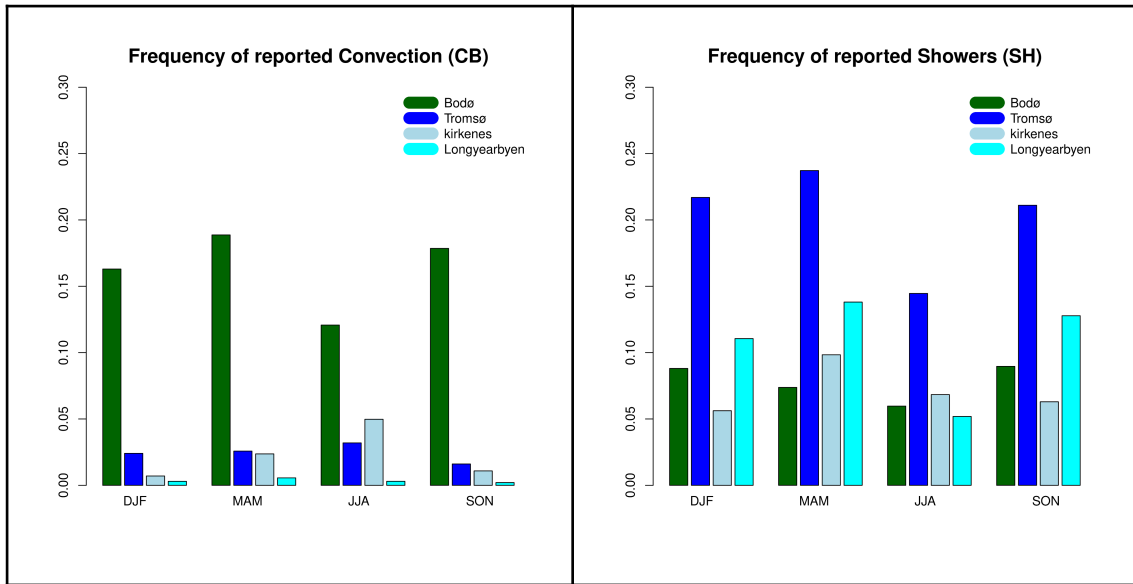


Figure 7.3.1 Observed frequency of convective weather in METAR observations between 09 and 18 UTC from airports in Bodø, Tromsø, Kirkenes and Longyearbyen for the period 2003-2023. Reports of clear convective activity (CB, TCU, TS, GR, GS) to the left, and reports with only showers (SH) reported, which can be an indication of convective activity.

The frequency of convection at airports can be estimated from METAR observations. However, there are a number of issues with the METAR observations (see data section), hence the interpretation should be done with care. In Figure 7.3.1, the frequency of convection related observations (i.e. CB, TCU, TS, GR, GS) for the airports in Bodø, Tromsø, Kirkenes and Longyearbyen are shown. The METAR data can also include observations of showers (SH) if none of the above categories are reported. This can be an indication of convection, but not necessarily. The frequency of showers is therefore plotted separately. Only observations between 09 and 18 UTC are applied in order to avoid the darkest and most difficult conditions for when the visual observations are taken.

The known issues with the METAR observations make the comparison of airport sites and seasons difficult. However, some key features can be identified. Convection is frequently observed in Bodø (~15% of the time), and more often in winter than summer. In contrast to this, an annual cycle with slightly more reports in summer than winter is seen for Tromsø, Kirkenes and Longyearbyen. However, this is not a robust result, since the differences between the seasons are minor, and it is reasonable to believe that the visual observations are underreporting convection during the dark winter. In addition, a higher frequency of showers is found in winter than summer for Tromsø and Longyearbyen. An interpretation of the results is therefore that convection is more

common in winter than summer for Bodø, and most likely the same or equally common between winter and summer for Tromsø and Longyearbyen. In Kirkenes it seems like convection occurs more often in summer than winter.

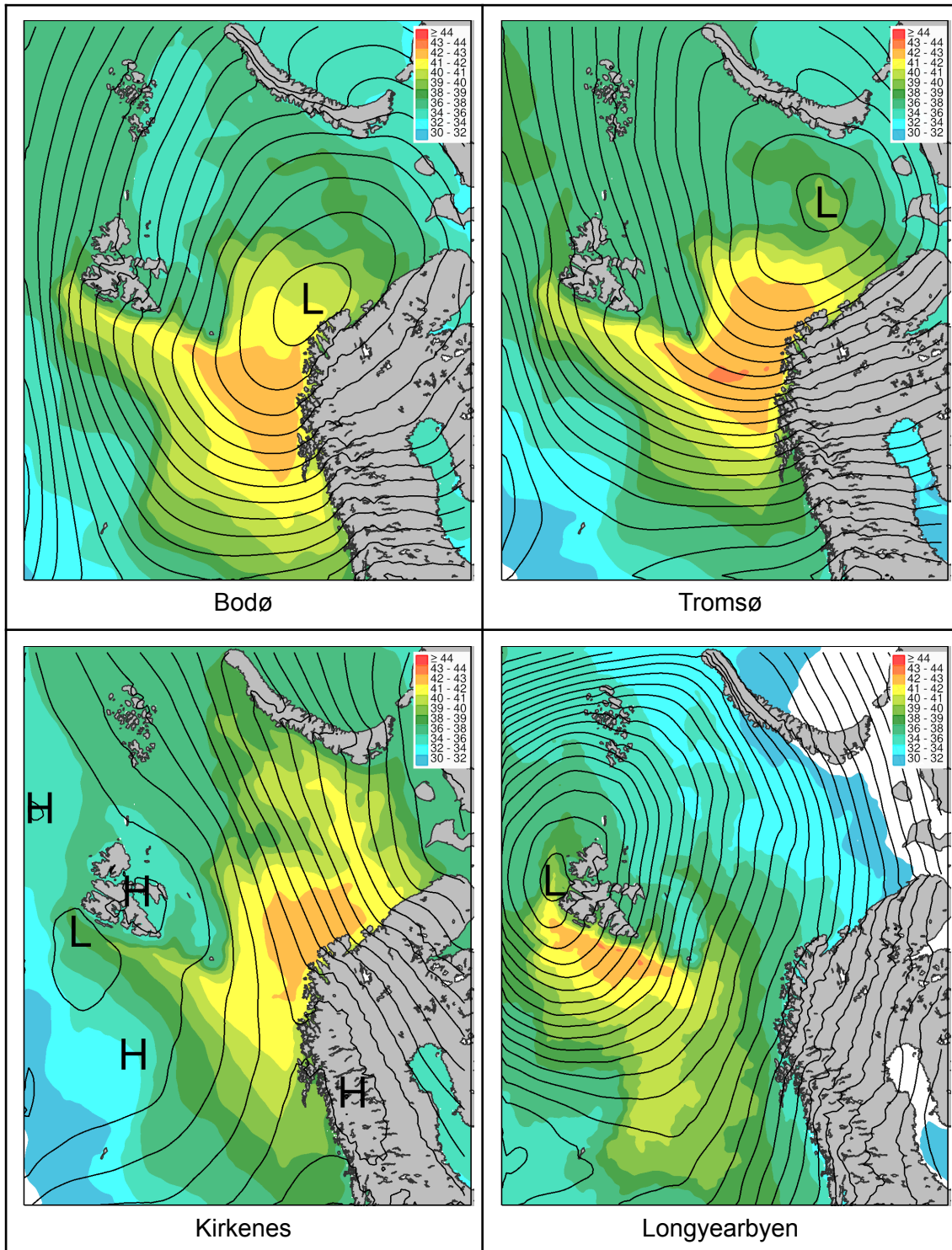


Figure 7.3.2 Composites of MSLP and temperature differences (SST-T500hPa) when convection (CB, TCU, TS, GR/GS) is observed in Bodø, Tromsø, Kirkenes or Longyearbyen (ONDJFMA).

Typical weather conditions under which wintertime convection is observed is presented in Figure 7.3.2. Composites of MSLP and the temperature difference between the Sea Surface Temperature (SST) and the temperature at 500 hPa (T500hPa) when convection is observed in Bodø, Tromsø, Kirkenes and Longyearbyen are shown. On average, all regions show a strong onshore wind component, typically with air masses with an Arctic origin and steered by a pronounced large-scale low pressure system. A strong vertical temperature difference (SST-T500hPa) is found in the vicinity of the respective regions, indicating less stable conditions. However, it should be noted that compared to the 99%-tile of the vertical temperature gradient in all cases (Figure 7.3.3), the vertical temperature gradients in Figure 7.3.2 are weaker. Hence, a strong onshore wind component set up by the MSLP pattern, is not necessarily always combined with an extreme instability and the depth and intensity of the generated convection can vary for similar MSLP situations.

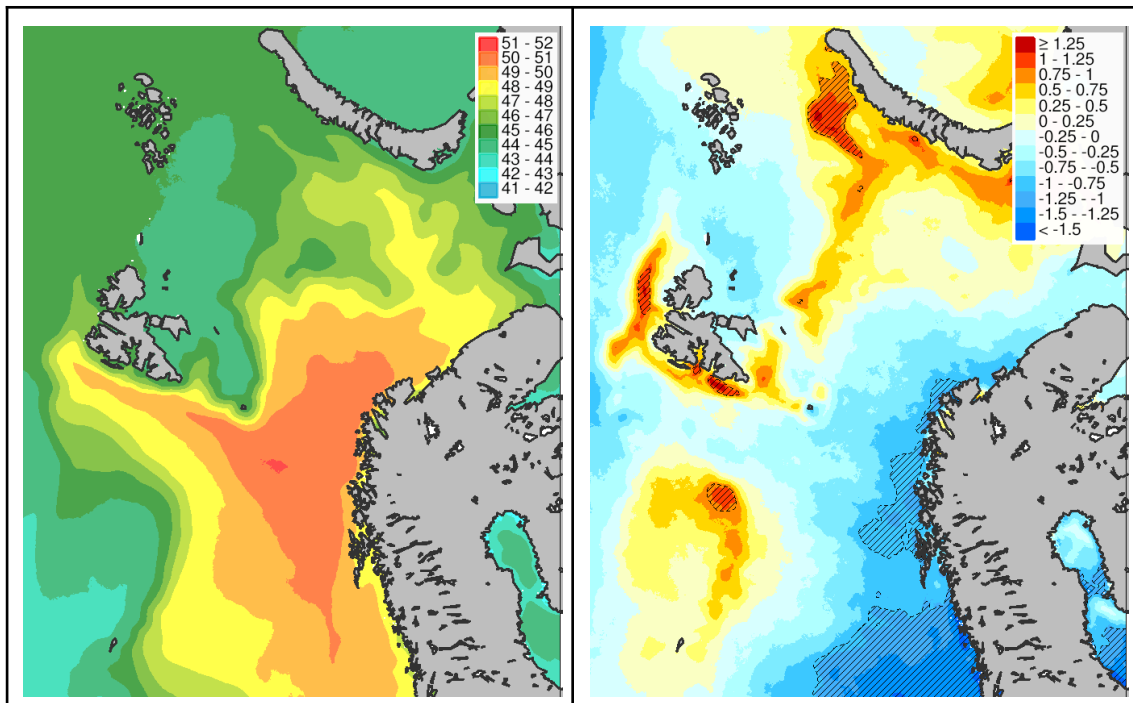


Figure 7.3.3 Climatology for 1991-2023 (left side) and difference between last 15 years (2008-2023) and first 15 years (1991-2006) (right side) for the 99%-tile of the vertical temperature difference (SST-T500hPa). Data are based on CARRA pressure and surface levels. Differences in regions marked with thin black lines are significant with a 90% confidence interval.

Offshore atmospheric vertical stability and strong onshore winds are essential ingredients for wintertime convection along the Norwegian coast. We therefore show the climatology and changes over the 1991-2023 period for these quantities. In Figure 7.3.3, the average of the 99%-tile of the annual (ONDJFMA) temperature difference between SST and T500hPa is shown. Higher values indicate more favourable conditions for convection. The patterns of the climatology reflect the location of the warm ocean currents from the south which is split into two branches south of Svalbard, one going into the Fram Strait and one into the Barents Sea. Apparently, the vertical instability reaches slightly higher values just off the coast of Troms and western parts of Finnmark than in Nordland and Svalbard.

The plot with changes in the vertical temperature gradient from 1991-2006 to 2008-2023 shows a decrease in the instability in the Norwegian Sea and along the Norwegian coast. However, in the Fram Strait, North of Svalbard, between Jan Mayen and Svalbard, and between Svalbard and Novaja Semlja, an increased instability is found. The latter regions have experienced a strong reduction in the sea ice cover and an increase in the SST over the same period (Isaksen et al., 2022).

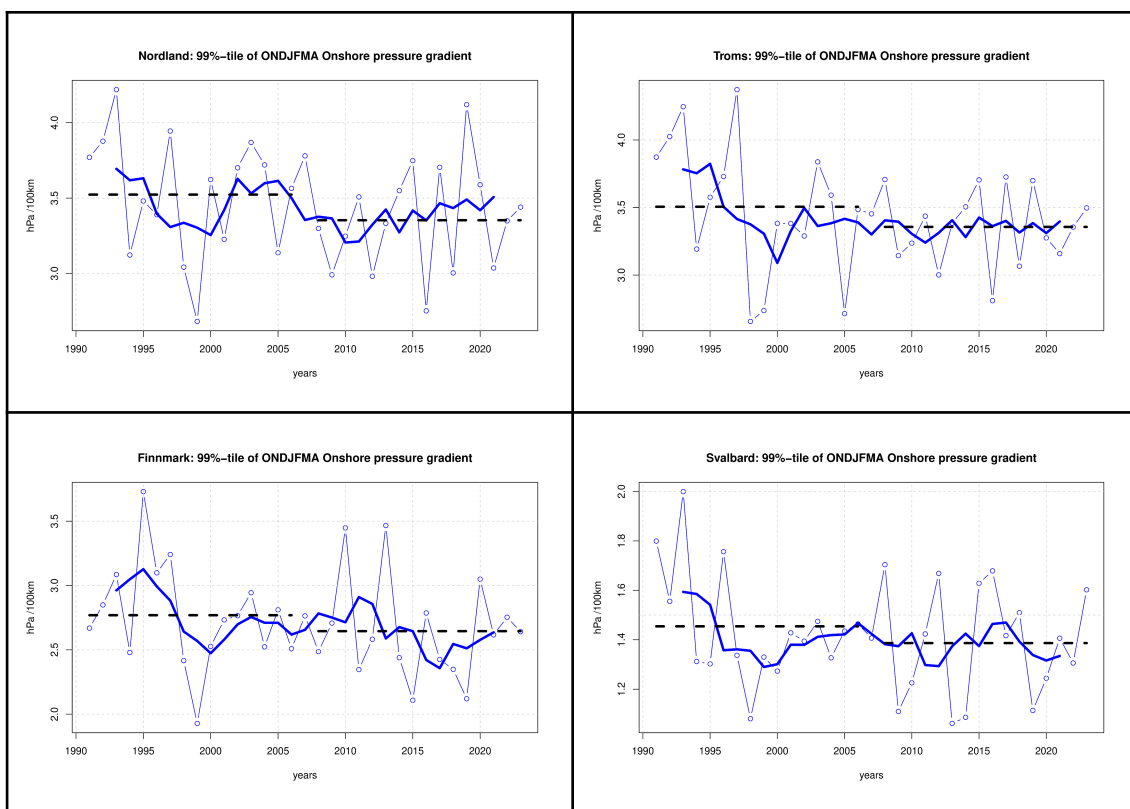


Figure 7.3.4 Time series of 99%-tile of yearly (ONDJFMA) MSLP gradients across regions indicating strong onshore wind speeds. Yearly values in thin blue lines and dots, 5 year running mean in thick blue line and mean value of 1991-2006 and 2008-2023 in dashed grey lines.

The strength of the onshore wind component is decided by the pressure gradient in parallel with the coast line, e.g. for Nordland, meaning the pressure difference between the northern and southern parts of the region. We therefore define an index for Nordland, Troms, Finnmark and Svalbard separately by calculating the MSLP gradient over the length of the coastline for each region. Figure 7.3.4 shows the yearly (ONDJFMA) 99%-tile values of this index and the average values of the 1991-2006 and 2008-2023 periods. A noticeable year-to-year variability is seen for all regions. The average value is lower for the 2008-2023 period than for the 1991-2006 period for all regions. However, this is in particular due to higher values for the first 5-10 years, while during the last 20-25 years the curve with the running mean is not showing any particular trends. Another feature to note is that while Nordland and Troms have similar MSLP gradients per 100 km, Finnmark shows weaker gradients, and even more substantially weaker at Svalbard. Hence the potential in Nordland and Troms is higher than in Finnmark and at Svalbard.

Both the changes in the 99%-tile of vertical stability and MSLP gradients, indicate a reduced convective activity along the Norwegian coast. However, it is the coincidence of strong onshore wind and instability that have the potential to produce the most intense convection. By taking a representative ocean point for each region, we calculate the change in the temperature gradient given that the onshore wind forcing is strong (equal to or above the 99%-tile of the MSLP-gradient index). When doing this, we find that for both Nordland and Troms a decreased vertical stability is found ($\sim 1^{\circ}\text{C}$) for the strong onshore wind events, but not for Finnmark. The complexity of these results make it difficult to interpret, and to fully understand the findings in a physically consistent way. However, a possible interpretation could be that we experience a general trend towards less wintertime convection, but that a reduction in the onshore wind strength may be counteracted by an increased vertical instability in some cases.

Cold air outbreaks (CAO) create favourable conditions for convection in the Norwegian and Barents Sea and have gained attention in the scientific literature. We apply a CAO index from Terpstra et al. (2021), also used in a number of other studies. The index is defined as the difference between surface skin potential temperature and the potential temperature at 850 hPa. Larger values indicate more intense cold air outbreaks. The main difference from the vertical temperature gradient used in Figure 7.3.3 is that the CAO index focuses on the more shallow surface near parts of the atmosphere. This is complementary to the results presented in Figure 7.3.3 because the convection over the ocean during CAO initiated events is shallow near the sea ice, before it gradually grows as it is transported southwards and the air masses are reformed. Figure 3.7.1 shows how the convection cells grow with distance from the sea ice. An additional important feature associated with CAOs is polar lows, which are short-lived intense small marine mesoscale weather systems that develop during

CAOs. Terpstra et al. (2021) found that about two thirds of CAOs also develop polar lows.

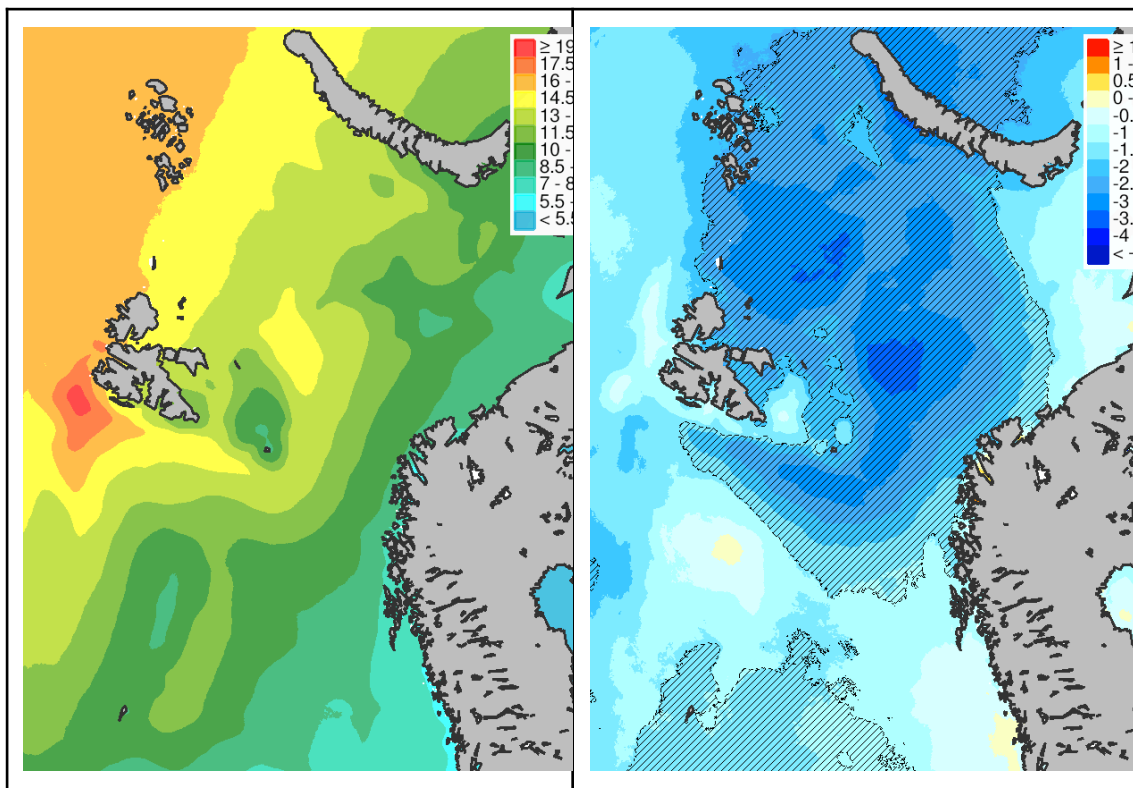


Figure 7.3.5 Climatology for 1991-2023 (left side) and difference between last 15 years (2008-2023) and first 15 years (1991-2006) (right side) for the CMAO index (difference in potential temperature at sea level and 850hPa). Data are based on CARRA pressure levels. Differences in regions marked with thin black lines are significant with a 90% confidence interval.

The climatology of the 99%-tile of the CAO index is shown in Figure 7.3.5 together with the changes over the 1991-2023 period. A reduced CAO-index is seen in most of the Barents Sea and from Lofoten to Finnmark, while the changes are small and not significant at the coast of Nordland. Similar results are also reported elsewhere. Dahlke et al. (2022) found substantial interannual variability in CAO and a decreasing trend in December and January, but an increase in March. Smith and Sheridan (2020) also found a reduction in CAOs in the North Atlantic over the last 40 years.

Future changes in CAOs, Polar Lows and Convection are reported in a number of studies. Kanno and Iwaski (2019) found that CAOs by the end of the century in general will decrease significantly. Related to this, Lin et al. (2024) anticipate a decrease in polar low intensity. Landgren et al. (2019) found that it is likely that the regions of polar low genesis move northward with the sea ice retreat. They further predicted a reduced

number of polar lows in the beginning of the season, but an increase in occurrence of polar lows for February-April. Furthermore, Iversen et al. (2023) report on a substantial decrease in convective precipitation over the Norwegian sea. The close connection between storms and wintertime convection presented here, together with a potential reduced future storm track activity as reported in section 5 also suggests that a reduction in future wintertime convection is likely. It should be noted that, in contrast to this, the scientific literature agrees on a potential increase in future convective activity in summer.

Methodology. In order to investigate the changes in historical aviation weather conditions (in this section for convection), the annual 99%-tile for the ‘winter’ months October, November, December, January, February, March and April is calculated for selected parameters (assuming that the 99%-tile provides difficult or severe aviation weather conditions). The average of the annual values of the two periods, 1991-2006 and 2008-2023, are compared. Note that 2007 is not included in the analysis when comparing the two periods. This is due to the fact that we want two equally long periods to compare. In order to decide on the statistical significance, a two sided student t-test with a 90% confidence interval is applied.

From the CARRA data set, the 99%-tile (‘high’) of the temperature difference between the Sea Surface Temperature and 500 hPa is analysed. Similar analysis is also done for a CAO index, namely the difference between the potential temperature at the surface and at 850 hPa.

7.4 Lightning

Summary: *The climatology of lightning in North Norway shows a pronounced annual cycle. Most lightning strikes occur at inland locations during summer, while wintertime lightning strikes are fewer and only happen offshore and at the coast. In contrast to this, most triggered lightning to aircraft happens in wintertime in the proximity of coastal airports.*

The observations of lightning are inconsistent in time and can not be used for trend analysis. A study of defining lightning indicators and analysing their climatology and changes from the applied reanalysis data set has been beyond the scope of this work. However, several other studies provide indications of an increased historical frequency of lightning in the Arctic, but not necessarily in North Norway and most of these studies focus on the warm season.

Although the results on future changes in lightning activity in the scientific literature vary in terms of both sign and magnitude a common pattern is the reduction of lightning activity in the tropics and a shift northward in favourable lightning conditions. However,

most studies have focused on the warm season and only a few studies also include or specify wintertime changes. It should be noted that even if some studies report large changes in percent, the baseline from which the percent is calculated is very small for Arctic regions and in particular wintertime.

Lightning is an electrical discharge between different areas in a cloud, between the cloud and the surface, or between the cloud and an aircraft or other obstacles, occurring when the electrical potential becomes large relative to their distance. The build up of electrical charged areas in the atmosphere depends on strong vertical motion, typical in a convective environment. Different types of hydrometers (e.g. ice, snow, graupel, water droplets) that co-exist collide and exchange electrical charge between their surfaces. Due to their differences in density, mass and shape, regions with differences in electrical charge can form since different kinds of hydrometeors are transported differently in up- and downdrafts, resulting in e.g. light snow crystals aloft and heavier graupel at lower altitude. When these areas start to form, they are reinforced by multiple other charging processes. However, the complete set of charging processes in thunderclouds are not fully understood. It should be noted that also aircraft become charged (e.g. Pavan et al., 2020, Salmela et al., 2013) making them exposed to lightning.

Lightning happens due to a combination of large and small-scale atmospheric phenomena, where the latter is not resolved or explicitly described in reanalysis, weather forecasting or climate models. In practice, this means that the large-scale weather situation in terms of the lightning potential often is predictable in weather forecasting, while the exact location and intensity of lightning events is not. A detailed description of lightning in weather and climate models is dependent on so-called parameterization schemes (i.e. small-scale processes are described based on the resolved large-scale weather) or simply based on large scale stability indices which describe the conditions under which lightning might form based on vertical stability and on the availability of moisture. While the first approach can vary from a simple relationship to more complex and sophisticated physics (more common in later years), the latter has its origin based on the interpretation of relatively simple diagnostics from soundings (vertical profiles) and has been used for many years.

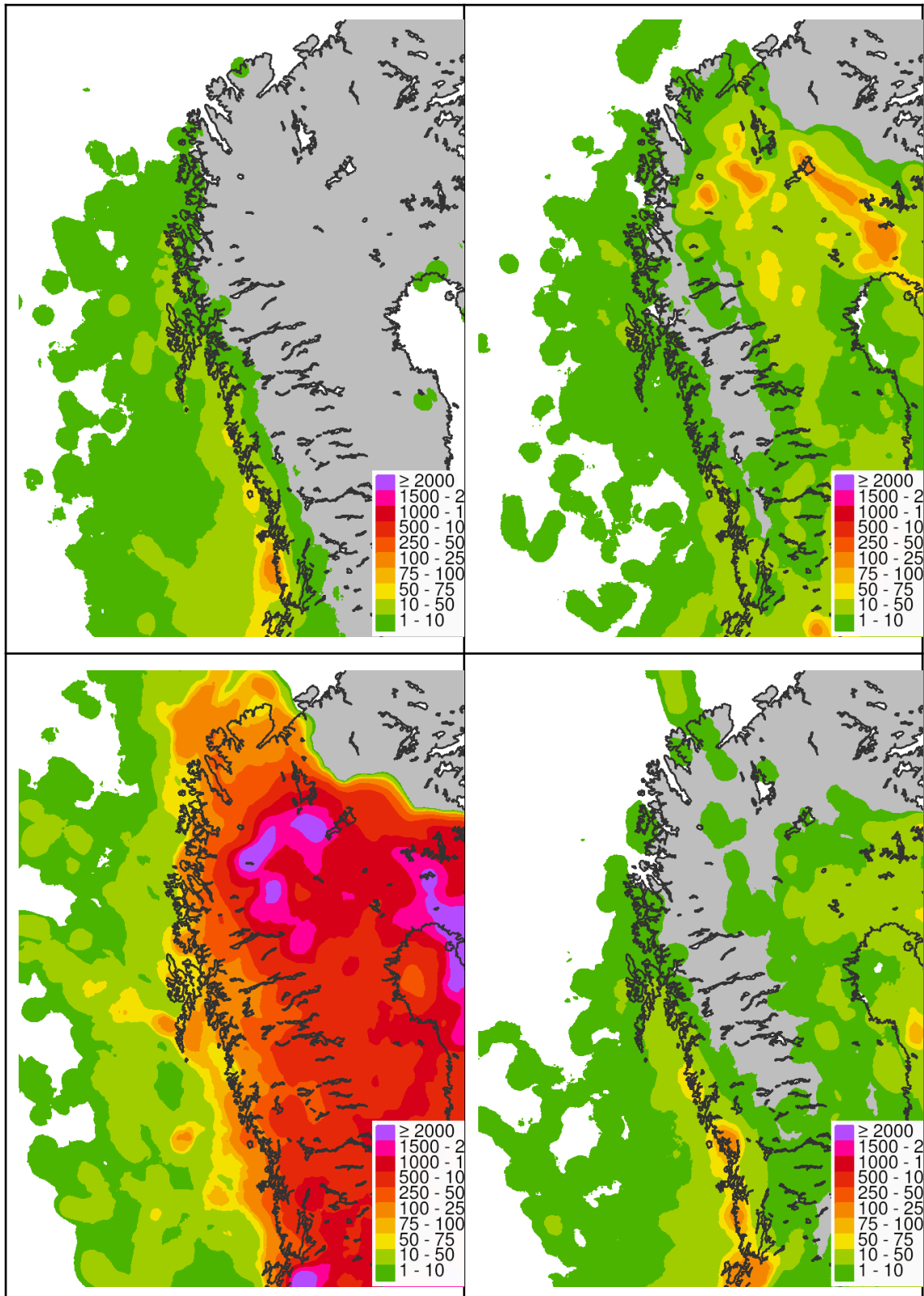


Figure 7.4.1 Maps of the number of observed lightning strikes within a distance of 25 km per year averaged over 2013-2023 for DJF (top left), MAM (top right), JJA (bottom left) and SON (bottom right). Data from the MET-Norway lightning archive.

Spatial and seasonal distribution of lightning in Northern Norway observed between 2013 and 2023 is shown in Figure 7.4.1. Most lightning strikes are observed during summer (JJA) with a maximum in the inland parts, e.g. Finnmarksvidda, Sweden and Finland. At Finnmarksvidda, areas with an annual average of more than 2000 observed lightning strikes within a radius of 25 km are seen, whereas the number of lightning strikes along the coast in Northern Norway typically is between 50 and 250 during the summer season (JJA). Lightning during the summer season often occurs due to an inland, continental convective activity, usually more frequently seen further south. During winter (DJF), lightning strikes are only observed along the coast and over the ocean, with decreasing numbers northwards. In total, the numbers are small compared to summer. In some parts of southern Nordland in winter, more than 50 lightning strikes (within 25 km) are seen, whereas winter lightning in Eastern Finnmark is a rare event. Winter time lightning often develops over the ocean due to a relatively cold air mass flowing over a relatively warm ocean, initiating convection. This can occur either during a cold air outbreak (CAO) or in the northerly flow behind or embedded in large scale low pressure systems. The pattern for spring (MAM) and autumn (SON) shows a mix from both the winter and summer characteristics. The spatial and seasonal patterns of lightning activity in the presented data set are qualitatively similar to what is reported in other lightning climatologies based on other data sets (e.g. Enno et al., 2020, Taszarek et al., 2019)

Kępski & Kubicki (2022) found a distinct difference between the daily cycle during winter and summer, with an afternoon peak in the latter. They also found that winter days with lightning are associated with positive air temperatures and often accompanied by strong low-pressure anomalies. Enno et al. (2020) further found that severe lightning events may occur even in regions with a low climatological frequency.

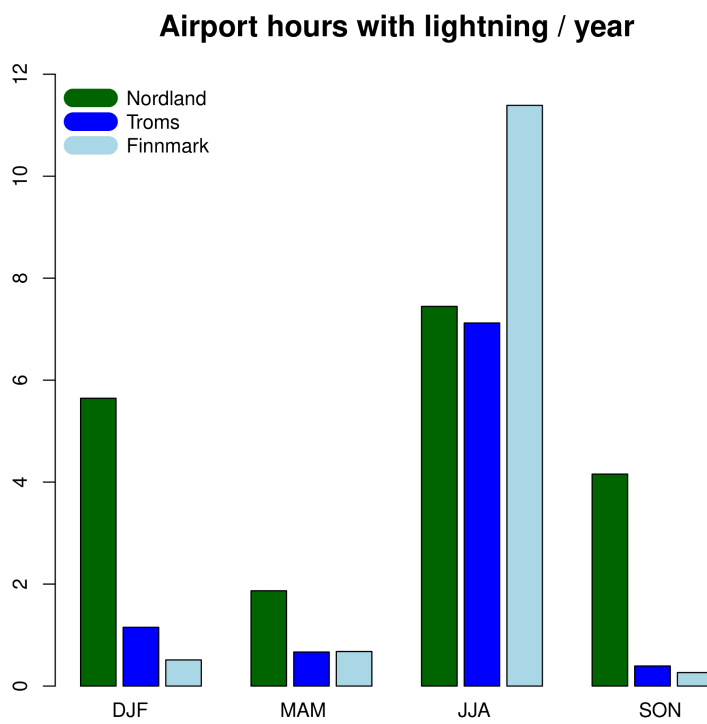


Figure 7.4.2 Hours with lightning strikes per airport within a radius of 25 km in Nordland, Troms and Finnmark.

Total hours of lightning strikes close to airports for different regions and seasons for 2013-2023 are summarised in Figure 7.4.2. The Figure underlines that lightning strikes are more frequent in summer than during the other seasons, and shows that lightning near airports is a relatively rare event. The maximum frequency is seen in Finnmark during the summer (JJA) with 12 hours on average per airport, which equals approximately 0.5% of the time. Interestingly for Nordland, and opposite for Troms and Finnmark, the difference between summer and winter is modest. The numbers for each airport are listed in Table 7.4.1 together with the average number of lightning strikes per hour. The variability is significant between the different airports and the time period is most likely too short in order to make a clear conclusion about detailed geographical differences. However, in general there are more lightning hours for “inland” airports than airports located along the coast in summer, and with an opposite pattern in winter. In winter, Brønnøysund has the highest number of lightning hours (128). In Vadsø and Kirkenes not a single hour of lightning is observed during the same period. However, during summer most lightning hours are observed in Kirkenes (235), Alta (179) and Mosjøen (177), but a few hours at Røst (23), Andøya (29) and Værøy (34). The number of lightning strikes per hour is on average much higher during summer than winter.

Table 7.4.1. Number of hours (2013-2023) with lightning within a 25 km radius for airports in Nordland, Troms and Finnmark. Numbers in brackets are the average observed lightning strikes per hour.

Region	Airport	winter (DJF)	spring (MAM)	summer (JJA)	autumn (SON)
Nordland	Brønnøysund	128 (8)	29 (11)	154 (14)	93 (14)
Nordland	Leknes	48 (5)	19 (5)	46 (20)	37 (9)
Nordland	Bodø	106 (6)	36 (6)	63 (11)	72 (7)
Nordland	Andøya	32 (5)	20 (4)	29 (18)	8 (14)
Nordland	Sandnessjøen	109 (10)	37 (5)	111 (20)	88 (28)
Nordland	Værøy	40 (7)	12 (5)	34 (20)	32 (5)
Nordland	Røst	34 (5)	13 (3)	23 (13)	29 (10)
Nordland	Svolvær	75 (5)	15 (5)	51 (25)	41 (8)
Nordland	Mo i Rana	22 (8)	8 (12)	142 (13)	23 (6)
Nordland	Mosjøen	64 (5)	28 (6)	177 (19)	64 (16)
Nordland	Evenes	25 (10)	9 (3)	71 (13)	16 (4)
Troms	Tromsø	33 (10)	14 (9)	55 (16)	10 (10)
Troms	Bardufoss	1 (11)	4 (12)	105 (11)	2 (5)
Troms	Sørkjosen	4 (20)	4 (20)	75 (11)	1 (6)
Finnmark	Mehamn	3 (7)	5 (10)	80 (9)	2 (24)
Finnmark	Banak	2 (25)	10 (8)	190 (14)	0 (-)
Finnmark	Honningsvåg	4 (14)	3 (16)	58 (15)	1 (2)
Finnmark	Berlevåg	5 (6)	3 (8)	103 (13)	4 (3)
Finnmark	Vadsø	0 (-)	12 (3)	174 (10)	1 (2)
Finnmark	Vardø	2 (25)	8 (2)	128 (10)	3 (2)
Finnmark	Kirkenes	0 (-)	14 (12)	235 (14)	0 (-)
Finnmark	Båtsfjord	4 (12)	5 (10)	130 (9)	6 (9)
Finnmark	Alta	2 (5)	4 (10)	179 (13)	1 (12)
Finnmark	Hasvik	28 (10)	12 (7)	48 (16)	11 (15)
Finnmark	Hammerfest	12 (12)	6 (6)	53 (15)	3 (4)

The strength of the lightning strikes is not investigated in this study. However, this was previously done by Køltzow et al. (2018) for the period 2004-2016. They found that for Northern Norway the average yearly lightning strength was 10 kA, which is slightly higher than 9 kA in the southeastern parts of Norway, but substantially lower than 15 kA at the Norwegian west coast. However, during the cold season in Northern Norway the lightning strength is higher than the annual average, with an average of 15 kA. In general, winter lightning in Norway has more energy than lightning in summer.

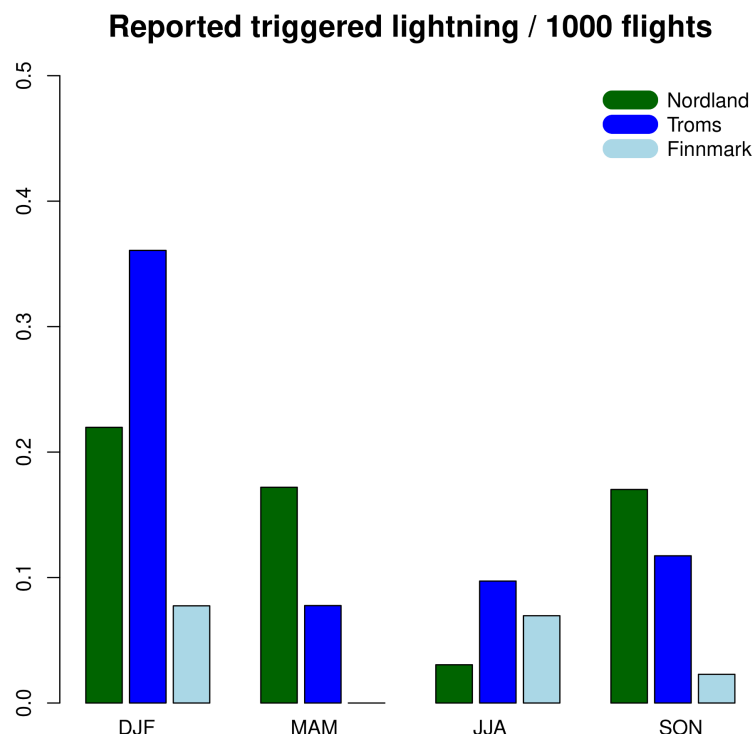
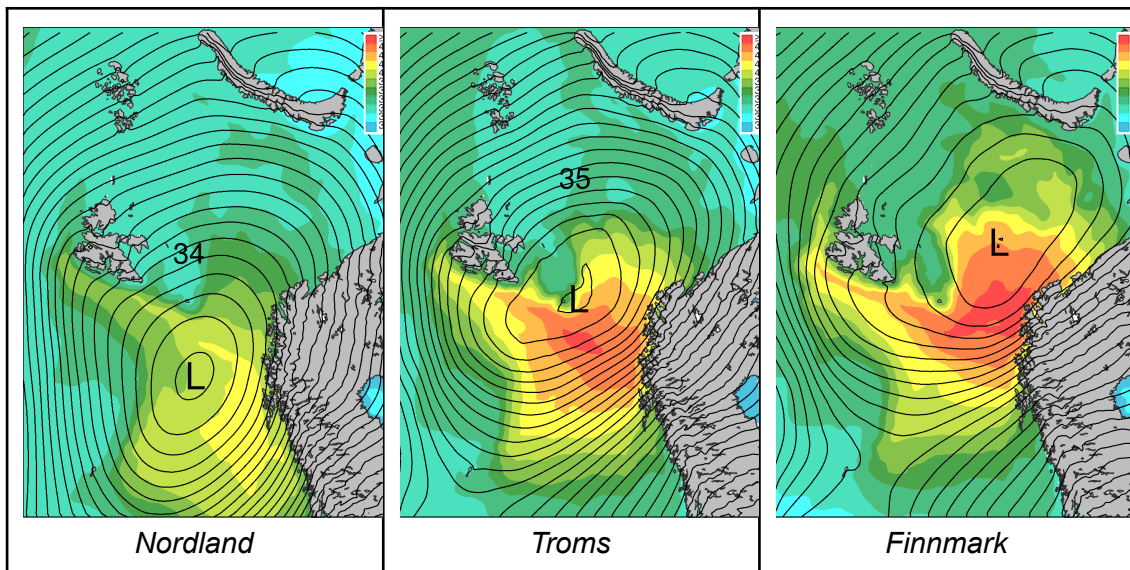


Figure 7.4.3 Triggered lightning in Nordland, Troms, Finnmark

Triggered lightning by aircraft and other objects are well documented as a challenge to safe operations and properties (e.g. Mäkelä et al., 2013, Wilkinson et al., 2013, Montanyà et al., 2014). In Norway this is reported for both fixed wing aircraft and helicopters (Langvatn, 2020). In Figure 7.4.3 the number of reported lightning strikes of aircraft for each season and region is given per 1000 flights. The numbers are low, and well below 1 event per 2000 flights for all seasons and regions. It is most frequently reported during winter in Troms. Usually aircraft experience lightning either on departure or approach from/to an airport when they are forced to fly through an atmospheric area between -15°C and 0°C, where the maximum electrical charging occurs. In winter, these charged areas are closer to the surface and the aircraft have

less possibilities to circumvent the convective activity in connection with departure and approach. This is most likely the reason why triggered lightning strikes of aircraft are more frequent in winter than summer, even if lightning strikes in general are a more common summer phenomena.

In order to understand under what circumstances lightning strikes typically occur during the extended winter (ONDJFMA), composite maps of MSLP are presented in Figure 7.4.4 of when lightning strikes are observed in the vicinity of the airports in Nordland, Troms and Finnmark. Pronounced low pressure systems offshore are seen for all three regions with an onshore southerly wind component at the Norwegian coast. Similar MSLP composites are presented for the cases of triggered aircraft lightning strikes. The composites show similarities, but the location of the low pressure centre is slightly shifted northwards for all three regions for the triggered lightning strikes. However, due to relatively few cases, in particular for Finnmark, the composites should be interpreted and compared with care.



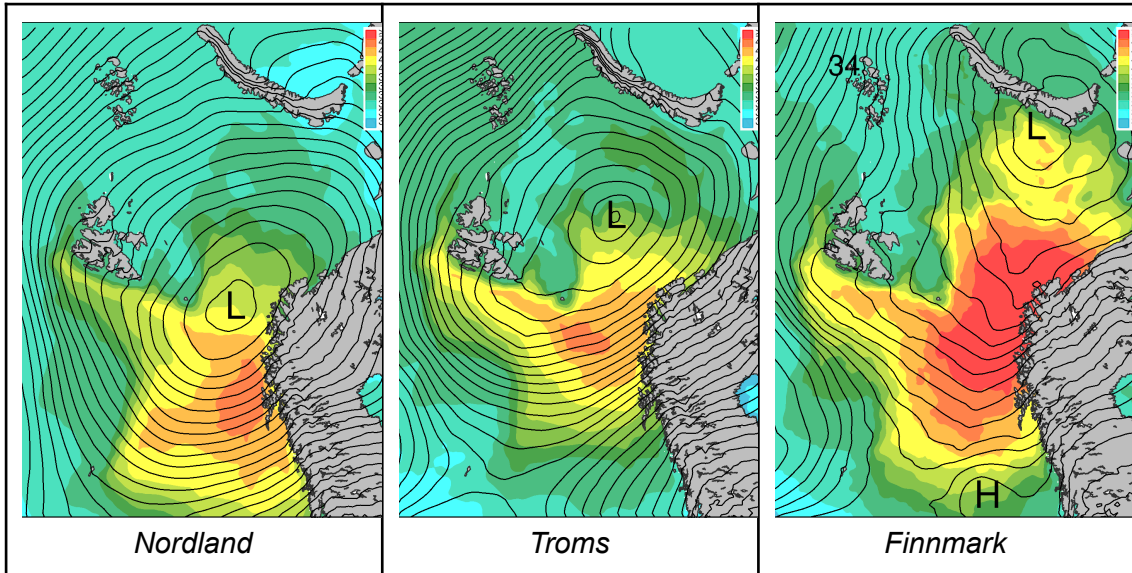


Figure 7.4.4. MSLP composites of observed natural lightning in the vicinity of airports in Nordland, Troms, Finnmark and Svalbard for ONDJFMA (row 1), MSLP composites of triggered lightning of aircraft reported in Nordland (29 cases), Troms (19 cases) and Finnmark (4 cases) for ONDJFMA (row 2).

Three different flights approaching Tromsø Langnes were hit by lightning within an hour on the 12. February. Noticing the MSLP in Figure 4.2.3 we find a similar pattern as in Figure 7.4.4 with a strong onshore wind component in Troms. A severe aircraft accident related to lightning happened in December 2003 on the approach to Bodø. A Widerøe aircraft was first hit by lightning east of Bodø resulting in a needed damage repair for one week. Just a few minutes later, a Kato Airline aircraft was hit east-northeast of Bodø resulting in an emergency landing with severe damage (<https://havarikommisjonen.no/Luftfart/Avgitte-rapporter/2007-23-eng>). The large scale weather situation and the all observed lightning strikes are shown in Figure 7.4.5. Again, the general pattern shows a strong low pressure system over the sea northwest of Lofoten, accompanied by a strong onshore and almost coast parallel wind in Nordland. Even if the low pressure centre location and the wind direction is somewhat different than for the average case, the main “ingredients” are similar to the ones in Figure 7.4.4. A close inspection of the observation record reveals that the two lightning strikes to the aircraft most likely are observed (registrations at the approximately same location and time as reported). The registration of the strength of the lightning strike hitting the Kato Airline aircraft was 98kA, which is 5-6 times higher than the lightning hitting the Widerøe aircraft a few minutes earlier and for the average lightning strength reported by Køltzow et al (2018) for winter time lightning in Northern Norway. In both examples mentioned here, multiple aircraft were hit by lightning, hence the lightning might strike twice or more in the same region when the conditions are favourable. This is also supported by Makela et al. (2013) reporting that 10 and 3 aircraft were hit by

lightning during two separate days in October and December near Helsinki. Therefore, if an aircraft reports a lightning strike, other aircraft nearby should be careful.

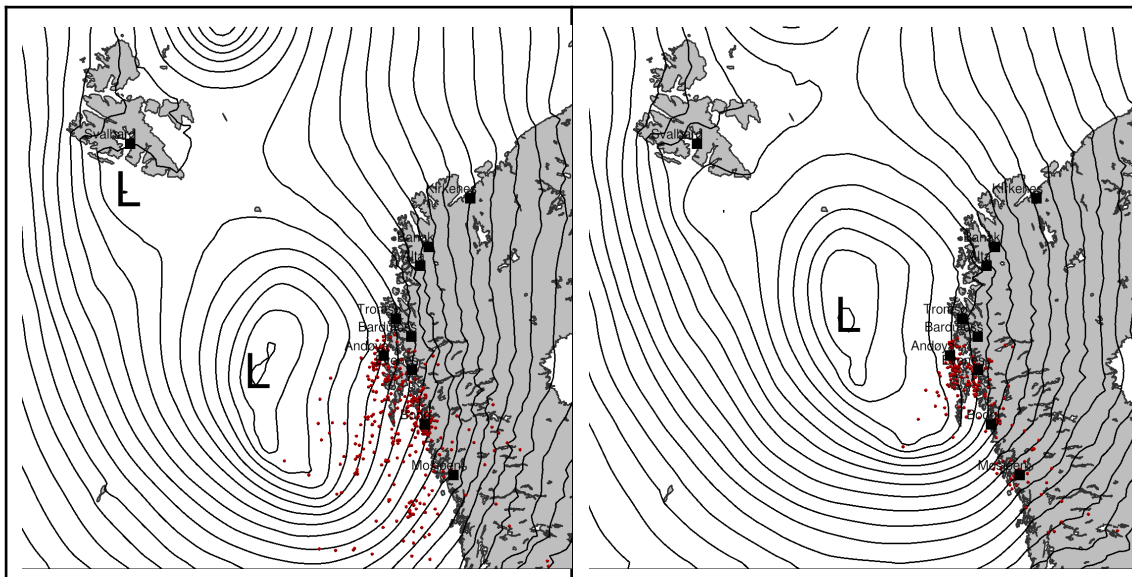


Figure 7.4.5. MSLP on 06 UTC 4. December 2003 with observed lightning strikes within 1.5 hours (left) and at 09 UTC (right).

There are several studies investigating recent and historical changes in lightning activity. However, due to problems with the availability of long, homogenous observation records they are often based on model simulations or lightning proxies from reanalysis. This is also the case for the lightning observation data set in Norway (see section on data) and it should not be used to investigate trends in lightning due to substantial changes over time. Therefore, we need to rely on what is reported in the scientific literature. Battaglioli et al. (2024) investigated changes in lightning based on logistic models using ERA5 reanalysis data from 1950-2021 as input. They found for Norway, south of Lofoten, a significant, but minor positive trend in the annual lightning of approximately 1-2 lightning hours per decade throughout all seasons, but with the main contribution during the summer season (JJA). In general, the decadal trend in lightning hours is larger in Southern Norway and further south in Europe. Michibata (2024) applied a climate model and found an increase in the global lightning activity from the pre-industrial to the present day climate of approximately 7%. Other studies, such as , Kaplan and Lau (2022) did not find any global trend in lightning activity over a recent 10 year period (2010-2021), using global lightning observations. However, regional changes are reported. Holzworth et al. (2021) reported a substantial increase in observed lightning strokes during JJA over the 2010-2020 period in the Arctic (north of N65). Kępski & Kubicki (2022) found an increase in lightning activity in parts of the Arctic, including Alaska, Canada and Russia, but found a reduction in Southern Norway

based on manual surface observations (SYNOP) over the 2000-2019 period. Bienik et al. (2020) also reported an increase in summer lightning activity in Alaska based on climate model output. In summary, a global, minor positive trend in lightning activity in recent decades is likely. However there is little evidence that this is a pronounced trend in Northern Norway.

Future changes in lightning activity are also investigated in a number of studies, but mostly for summer conditions. The results vary, depending on region, season and how the lightning process is described in the applied model tools. Both future increasing and decreasing trends in lightning activity are reported. A traditional approach has been to solely study changes in convective activity and precipitation. However, this approach neglects the effect of in-cloud ice and ice-flux which is a key to producing electrical charge. Hence, changes in lightning activity are sensitive to changes in convective activity and the height of the 0°C isotherm (potential for in-cloud ice). It is therefore believed that more sophisticated parameterization schemes are needed in climate models in order to provide more accurate estimates (or even signs of changes) of future trends in lightning activity.

Finney et al. (2018) compared the outcome from two methods; the first one applying a more traditional, simple approach, and the second one applying a more sophisticated and complex approach including the cloud-ice in a global climate model. The simplified approach predicted a future increase in lightning activity almost everywhere, while the more sophisticated approach predicted a reduction in lightning activity in the Tropics and near the Equator and an increase at the mid- and high latitudes. Michibata (2024) predicts a strong increase in lightning activity in the Norwegian Sea, Northern Norway and even at Svalbard per Kelvin degree of warming (as high as an increase of 30-40% / K in some regions, shown in their Figure 3). This change is for the entire Arctic, distributed over the full annual cycle. Even if the percentage change is high, it should be noted that the number of lightning strikes in the present-day climate is low for most regions, and in particular in winter (as seen e.g. in Figure 1). Also Rädler et al. (2019) reports similarly with an increase in wintertime lightning. Having in mind the potential future reduction in storm track activity and Cold Air Outbreaks, partly explaining the generation of winter convection and lightning, the reported increase in lightning is not that straightforward to interpret.

Chen et al. (2021) reports a doubling in summer lightning over areas with permafrost. A doubling of the summer lightning activity by the end of the century was also found by Bienik et al. (2020) for Alaska. Kahraman et al. (2022) performed a regional study with a high resolution regional model system over Europe south of 60N. A future northward shift in favourable weather regimes (for lightning), increases the lightning frequency at higher latitudes, e.g. more thunderstorms over the Alps, but with a decrease in lightning over lower terrain elsewhere and over the sea. In summary, studies suggest that it is

likely with an increase in the lightning activity in Northern Norway during summer, while the potential change during winter is uncertain.

Methodology. The current accessible, lightning observation data set in Norway is unfortunately not homogeneous in time. Therefore, it is not suitable to be used for investigations of potential trends. However, the observations provide insight on differences in spatial and seasonal patterns and thereby help us to better understand lightning in the present-day climate. To describe and understand historical and future trends in lightning activity, a literature review is applied.

7.5 Other Aviation Weather Related Parameters

In this section, a brief analysis of other aviation weather related parameters is conducted; 2-m air temperature (T2m), 0°C conditions, precipitation (rain, snow) and 2-m relative humidity (RH2m).

In summary; The trend of the 2-m air temperature (T2m) during the winter season for Northern-Norway the last 120 years is a shift towards a warmer climate, particularly since 1990. In the Arctic, including Svalbard and the Barents area, an exceptional ongoing warming is well documented of up to 2.7°C per decade. On average, the coldest winters are getting less cold and the frequency of 'warm' winters is increasing (most predominant at Svalbard).

Temperatures around 0°C and 0°C-crossings are often challenging for airport operations, in particular for the runway conditions. During the last 30 years (1991-2023), there has been a minor increase (about 2-4%) in the number of 0°C condition events, where many of the airports are located. In the coastal and outer areas of Nordland and Troms, a future decrease in the number of days with 0°C-crossings is expected (more often on the "warm" side), while an increase in Finnmark and in the inner parts of Nordland and Troms is expected.

During the last 120 years, an increase in the number of "wet" winters after 1990 is seen, however still with annual fluctuations. Even if no or only minor changes in the winter precipitation in Northern Norway is found during the last 30 years, we find that the precipitation amount during this period on average is higher than before 1990. Future projections show a modest increase in winter precipitation, but these predictions are very uncertain. In the future, more of the winter precipitation in Northern Norway and even at Svalbard will come as rain, rather as snow.

A high 2-m relative humidity (RH2m) at an airport, in particular accompanied by below zero temperatures, can impact the aviation weather in different ways, such as slippery

runway conditions, poor visibility (freezing fog, fog, mist) and freezing fog impacting aircraft and other objects. In general, a minor, negative trend of high values of relative humidity is found during winter the last 30 years where the majority of the airports in Northern Norway are located.

7.5.1 2-m Air Temperature (T2m)

The overall change in the 2-m air temperature (T2m) for Northern-Norway the last 120 years shows a shift towards a warmer climate, including for the winter season (DJF) as shown in Figure 7.5.1.1. The deviation in the temperature (DJF) is relative to the 1991-2020 reference period for Northern-Norway (Svalbard not included). From 1900 until 1988 the temperature was approximately 1.5 °C lower than for the 1991-2020 reference period, with a short 'warm' period during the 1930s. After 1988, there is a positive trend in the temperature during DJF, but still with significant annual fluctuations. The coldest winters are less cold and the frequency of 'warm' winters is increasing.

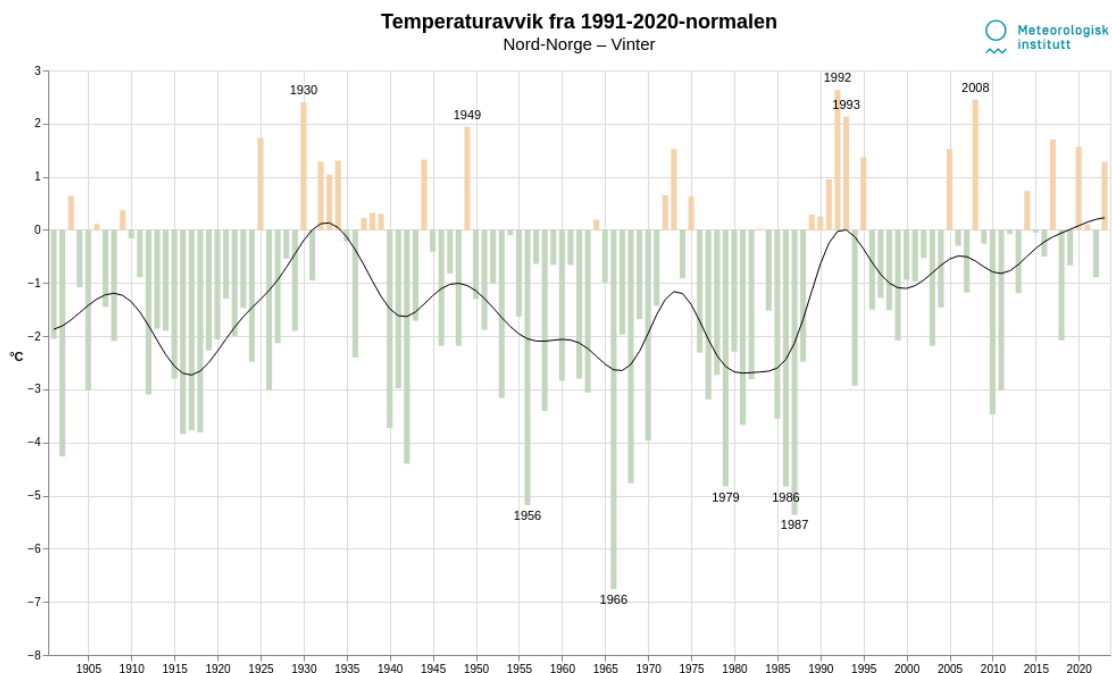


Figure 7.5.1.1. Observed 2-m Air Temperature deviation from the 1991-2020 reference period for Northern-Norway (Svalbard not included) between 1900-2023 for DJF. Black solid line represents the running mean. Source: Met Norway.

At Svalbard and in the Barents area, an exceptional ongoing warming is well documented. Isaksen et al (2022), studied the warming in this region over the past

20-40 years, and identified a statistically significant record-high annual warming of up to 2.7°C per decade, with a maximum in autumn of up to 4.0°C. The warming pattern is primarily consistent with the seen reduction in sea ice cover.

Reanalysis data is applied in order to estimate the regional patterns in T2m climatology for October until April (ONDJFMA) over the last 30 years and the related changes. In Figure 7.5.1.2, the climatology of the mean T2m for ONDJFMA for the 1991-2023 period (left side) is shown. The lowest temperatures on average are seen on Svalbard and in particular in the northeastern parts (-20 to -10°C). On the mainland, the lowest temperatures on average are seen in the inner and/or mountainous areas in Northern Norway (-12 to -8°C). The highest temperatures on average are seen over the ocean west of the mainland (2 to 7°C).

The difference between the last 15 years (2008-2023) and first 15 years (1991-2006) is shown on the right hand side in Figure 7.5.1.2. A major increase in T2m is seen in the northeastern parts of the Barent Sea, including on Svalbard (in particular in the eastern parts). A difference of 3-6°C in this area between the two 15 year periods is quite dramatic. One of the main reasons for the major warming east of Svalbard is due to a significant reduction in the sea ice cover in this area during ONDJFMA. On the mainland the difference is not as evident when comparing the 1991-2006 with the 2008-2023 period. As seen in Figure 7.5.1.1, the year to year fluctuations of the temperature are quite significant. Therefore, it is important to keep this in mind when analysing the difference between the two periods. On average, it seems to be a minor non-significant (except for most coastal regions north of Lofoten), positive trend of 0 - 1.2°C on the mainland.

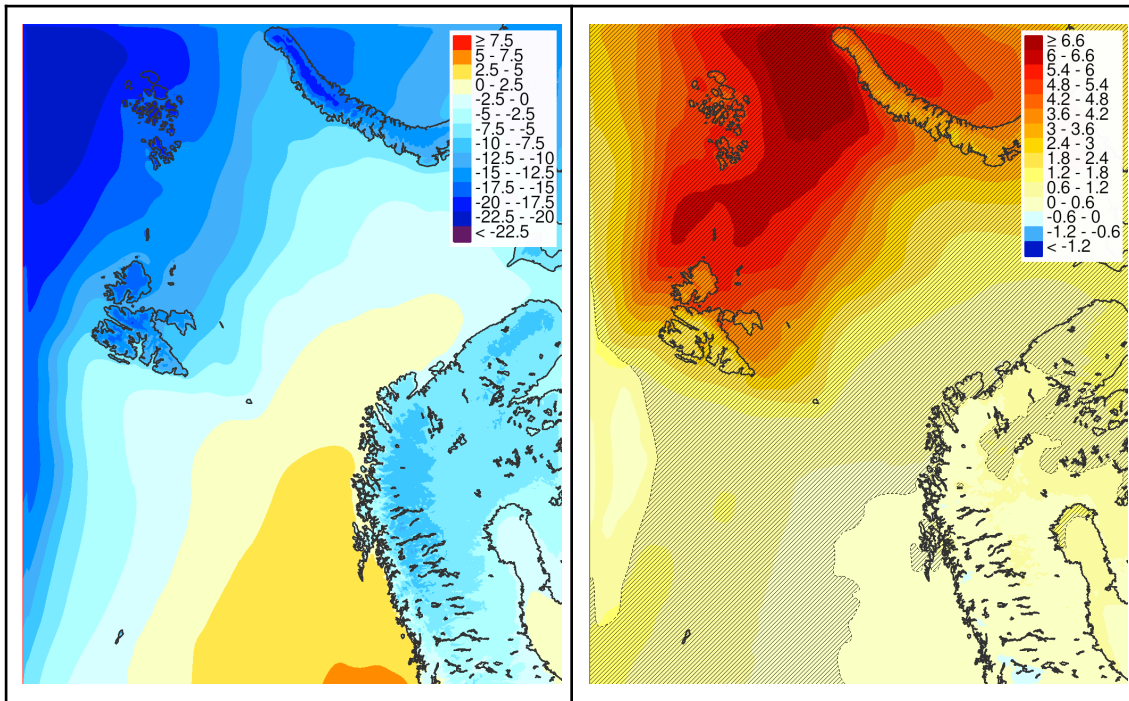


Figure 7.5.1.2. Climatology for 1991-2023 (left side) and difference between last 15 years (2008-2023) and first 15 years (1991-2006) (right side) of the mean T2m in CARRA for October until April (ONDJFMA). Differences in regions marked with thin black lines are significant with a 90% confidence interval.

In order to study the ‘extremes’, the 1%-tile of T2m from the CARRA data set (the 1% coldest temperatures) and the 99%-tile (the 1% warmest temperatures) are applied (Figure 7.5.1.3 and 7.5.1.4). In terms of the climatology of the 1%-tile (the coldest temperatures), the spatial pattern is quite similar to the climatology of the mean temperature in Figure 7.5.1.2, but indeed with much lower temperatures (below -30°C in some areas). The difference between the last 15 years (2008-2023) and first 15 years (1991-2006) is shown on the right hand side in Figure 7.5.1.3. Again, Svalbard and the northeastern parts of the Barents Sea experience the most dramatic warming. The coldest periods become less cold, and in some areas the difference between the two periods is more than 8°C. For vast areas of the mainland, a positive trend of 1 - 3°C is seen. However, also a few patches with a decrease in the lowest temperatures are seen (blue colour), e.g. in the inner parts of Trøndelag. It is also important to keep in mind that different patterns during autumn, winter and spring might impact the overall analysis of the months October until April (ONDJFMA) combined.

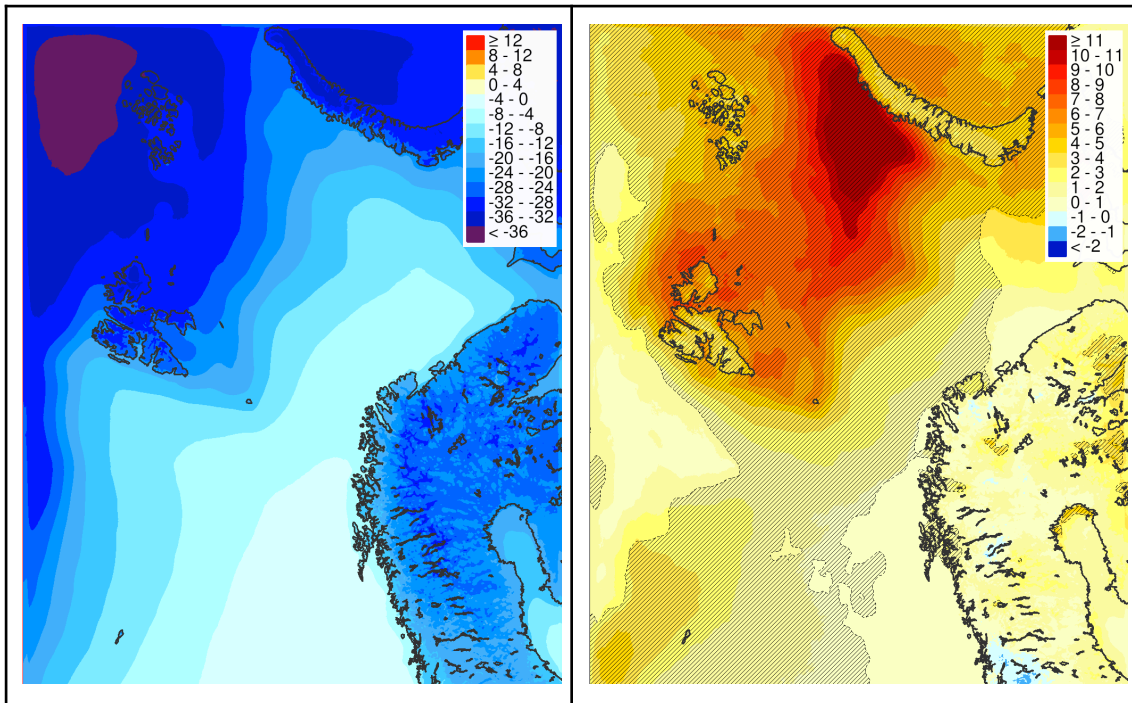


Figure 7.5.1.3. Climatology for 1991-2023 (left side) of the coldest (1%-tile) T2m from CARRA and difference between last 15 years (2008-2023) and first 15 years (1991-2006) (right side) for October until April (ONDJFMA). Differences in regions marked with thin black lines are significant with a 90% confidence interval

In terms of the climatology of the 99%-tile (the warmest temperatures) in Figure 7.5.1.4, the spatial pattern is quite similar to the climatology of the mean temperature in Figure 7.5.1.2, but in this case with much higher temperatures (more than 8-10°C in some areas). The difference between the last 15 years (2008-2023) and first 15 years (1991-2006) is shown on the right hand side in Figure 7.5.1.4. Again, the Svalbard region and the northeastern parts of the Barents Sea experience the most significant changes, hence the warmest periods have become even warmer. However, the relative positive trend of the 99%-tile is not as dramatic as for the 1%-tile. This means that the trend in “extreme” low temperatures is much more dramatic than the trend in “extreme” high temperatures. For the mainland, a minor, positive, non-significant trend is seen (less than 1°C).

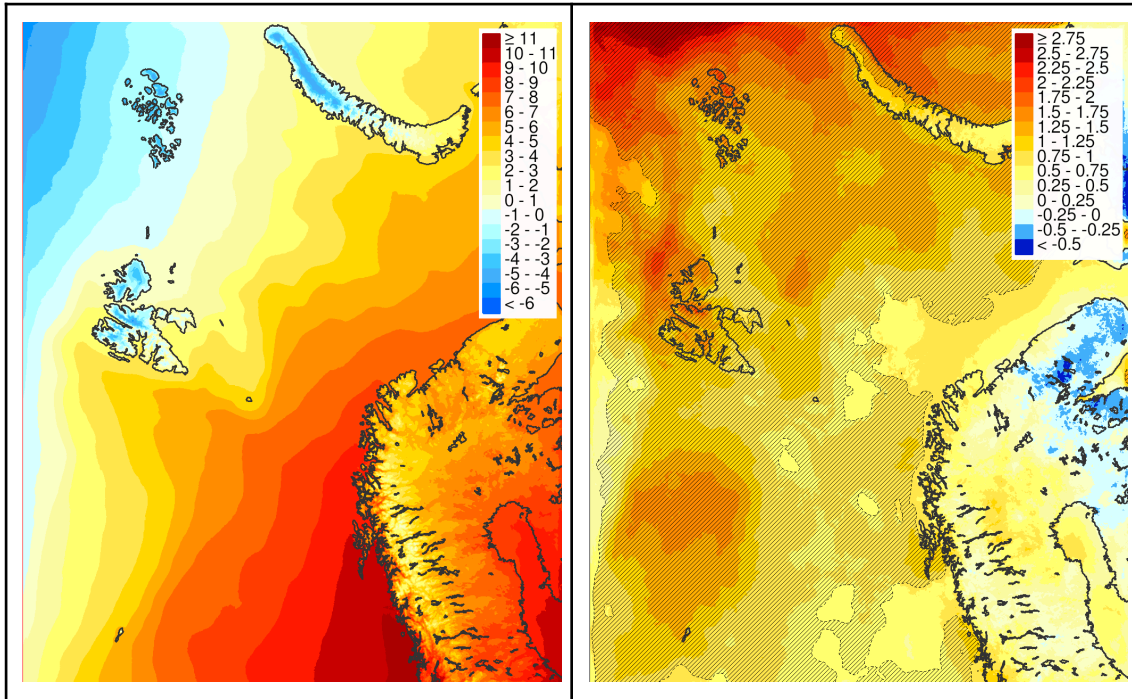


Figure 7.5.1.4. Climatology for 1991-2023 (left side) of the warmest (99%-tile) T2m from CARRA and difference between last 15 years (2008-2023) and first 15 years (1991-2006) (right side) for October until April (ONDJFMA). Differences in regions marked with thin black lines are significant with a 90% confidence interval.

Since temperatures around 0°C, often are challenging for airport operations and in particular for the runway conditions, a potential trend in the frequency of temperatures between -3 to 3°C is analysed. In Figure 7.5.1.5, the frequency for 1991-2023 (left side) and the difference between the last 15 years (2008-2023) and first 15 years (1991-2006) (right side) for temperatures between -3 and 3 °C for ONDJFMA is shown. From the climatology, the ocean areas between Jan Mayen and the southeastern parts of the Barents Sea have the highest frequency of temperatures around 0°C, including in the coastal areas north of Lofoten. At Svalbard, the frequency is low since the average temperature still is on the “cold” side (below -3°C). Over the ocean west of Nordland, the frequency is also quite low, due to temperatures on the “warm” side (more than 3°C). When comparing the two 15 year periods, we find a minor, non-significant increase (about 2-4%) in the number of 0°C condition events where many of the airports in the region are located.

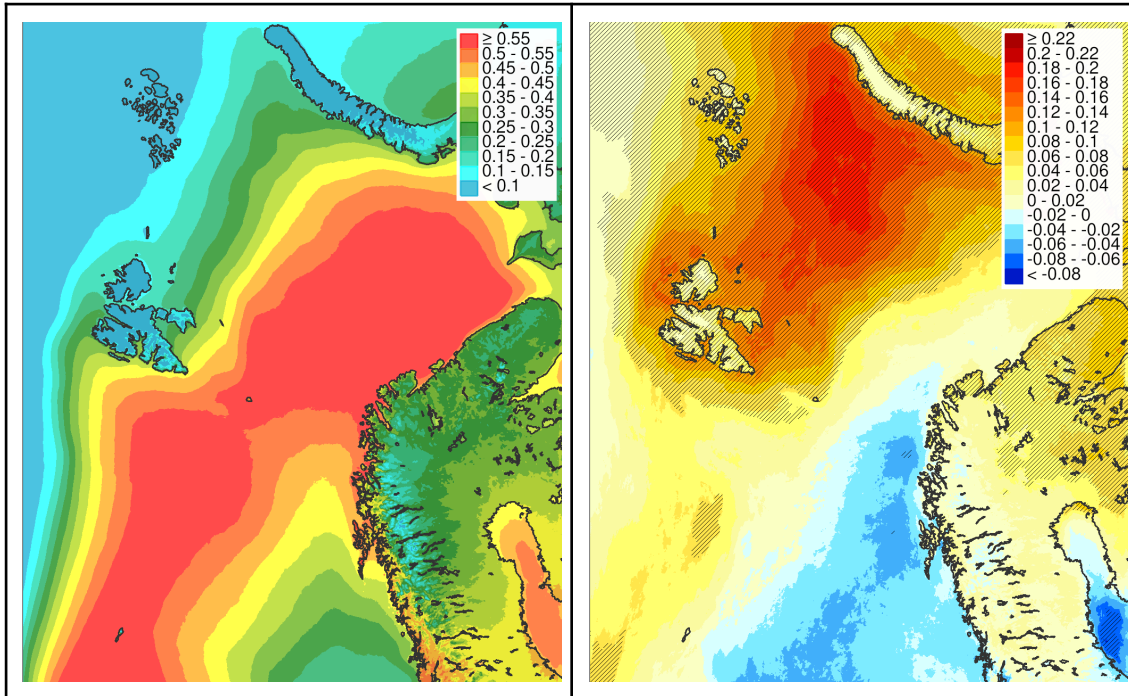


Figure 7.5.1.5. Frequency for 1991-2023 (left side) and difference between last 15 years (2008-2023) and first 15 years (1991-2006) (right side) for temperatures between -3 and +3 °C in CARRA for ONDJFMA. Differences in regions marked with thin black lines are significant with a 90% confidence interval.

What about the future trend in temperature?

A future scenario of the 2-m air temperature during the winter season (DJF), as a deviation (°C) from the 1971-2000 reference period for Troms, is shown in Figure 7.5.1.6. The black curve represents observational data, smoothed in order to illustrate variations on a 30-year scale. The coloured curve shows the median value for a number of RCM (Regional Climate Models) simulations. Shaded area indicates the spread between a low and high climate scenario (10 and 90 percentiles). Projections for Nordland and Finnmark could also be found at Norsk Klimaservicesenter, but not shown here, since the predicted pattern is quite similar to the scenario for Troms. A future increase in the 2-m air temperature for the winter season (DJF) is expected in Northern Norway. By 2050, the winter temperature on average could be 2.5 - 4.5 degrees higher than the reference temperature (1971-2000).

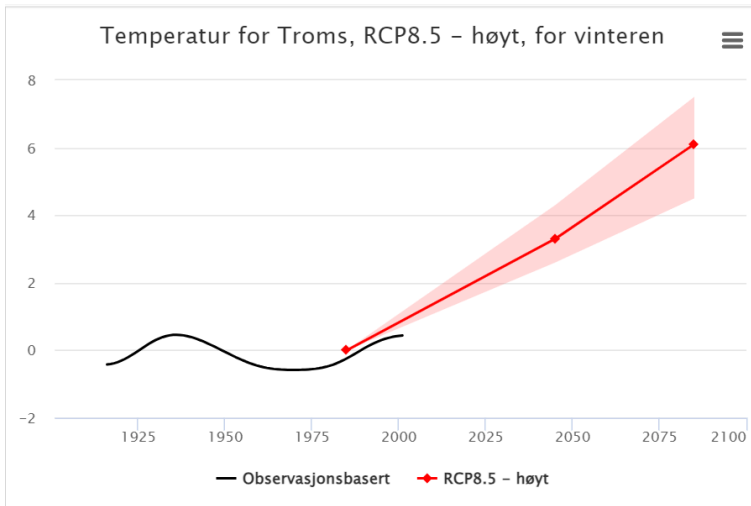


Figure 7.5.1.6: Future potential development (RCP8.5) of the temperature during the winter season (DJF) as a deviation ($^{\circ}\text{C}$) from the 1971-2000 reference period for Troms. (Source: Norwegian Climate Service Center)

In Figure 7.5.1.7, the change in the number of days with 0°C -crossings from the period 1971-2000 (reference period) to 2031-2060 and 2071-2100 is shown. As mentioned, a high number of 0°C -crossings might be challenging for aviation, in particular for the runway conditions. In the coastal and outer areas of Nordland and Troms, a future decrease in the number of days with 0°C -crossings is expected (more often on the “warm” side), while an increase in Finnmark and in the inner areas of Nordland and Troms is expected. The airports in Finnmark and in the inner parts of Troms seem to be more exposed for difficult runway conditions due to the increased frequency of 0°C -crossings during the winter season in the near and far future, while the overall runway conditions most likely will improve at the other airports since they more often will experience temperatures above 0°C .

Also Dyrrdal et al (2020) have studied changes in winter weather known to potentially cause access disruptions in Troms for the present and future climate. In terms of changes in 0°C -crossings, a clear increase is found in all of Troms during 1958-2017, with large parts being dominated by significant positive trends, reflecting increasing temperatures over the period. Projected changes in 0°C -crossings for two future periods (2041-2070 and 2071-2100) also showed an increase in many areas, reflecting that temperatures will rise to the 0°C threshold for a longer period. However, they also show that in the mildest areas along the coast, where the mean winter temperatures already are close to 0°C in the present climate, these crossings will become less frequent.

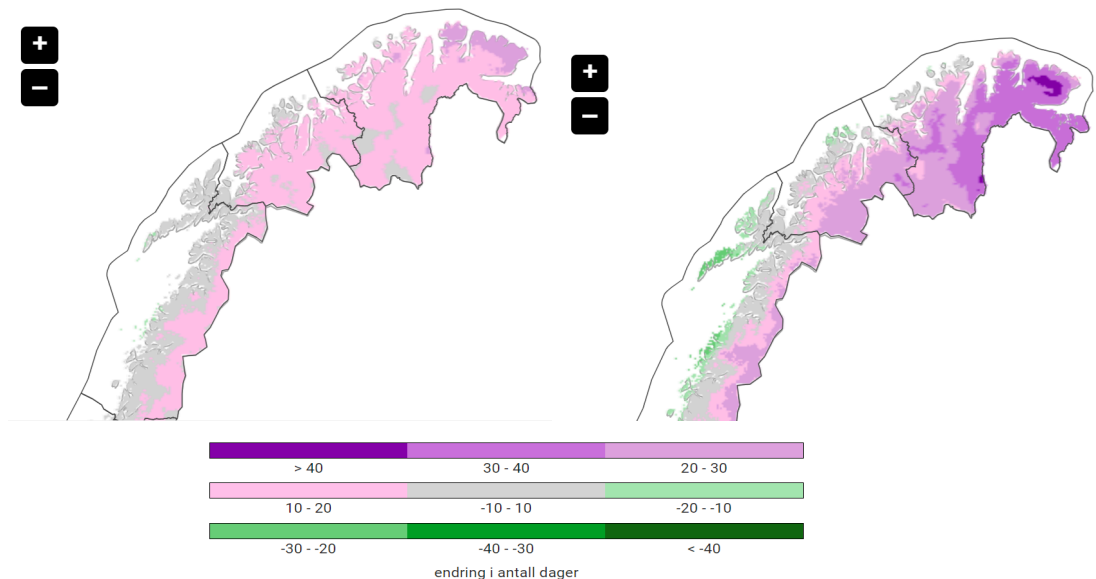


Figure 7.5.1.7: Change in the number of days with 0°C-crossings between the 1971-2000 period (reference period) and 2031-2060 (left side), 2071-2100 (right side). Source: Norwegian Climate Service Center.

Methodology:

From the CARRA data set, the ONDJFMA climatology (1991-2023) of the mean 2-m air temperature (T2m), the 1%-tile (the coldest temperatures), the 99%-tile (the warmest temperatures) and temperatures around zero (-3 to 3°C) are applied. In order to analyse the T2m changes and trends during the last 30 years, the 1991-2006 and 2008-2023 period are compared. In order to decide on the statistical significance, a two sided student t-test with a 90% confidence interval is applied. The future scenarios are from Norsk Klimaservicesenter.

7.5.2 Precipitation

The overall historical trend in precipitation for Northern Norway during the last 120 years for the winter season (DJF) is shown in Figure 7.5.2.1. The annual deviation is relative to the 1991-2020 reference period for Northern Norway (Svalbard not included). In general, we find an increase in the number of “wet” years after 1988 when comparing with the earlier period, however still with annual fluctuations. The increased

frequency of “wetter” years after 1988 could partly be due to the temperature rise after 1988 (Figure 7.5.1.1), since warm air contains more moisture than cold air, and thereby increasing the potential precipitation amounts.

Lutz et al (2024), investigates the changes in precipitation patterns in Norway, focusing on the comparison between the standard normal periods 1961-1990 and 1991-2020 as defined by the World Meteorological Organization (WMO). Overall, Norway experienced a 7% increase in the average annual precipitation from 1961-1990 to 1991-2020, however with significant spatial and seasonal variations. The precipitation rise is influenced by an increase in both the number of days with precipitation and the average precipitation on these days, primarily attributed to rising temperature and relative humidity.

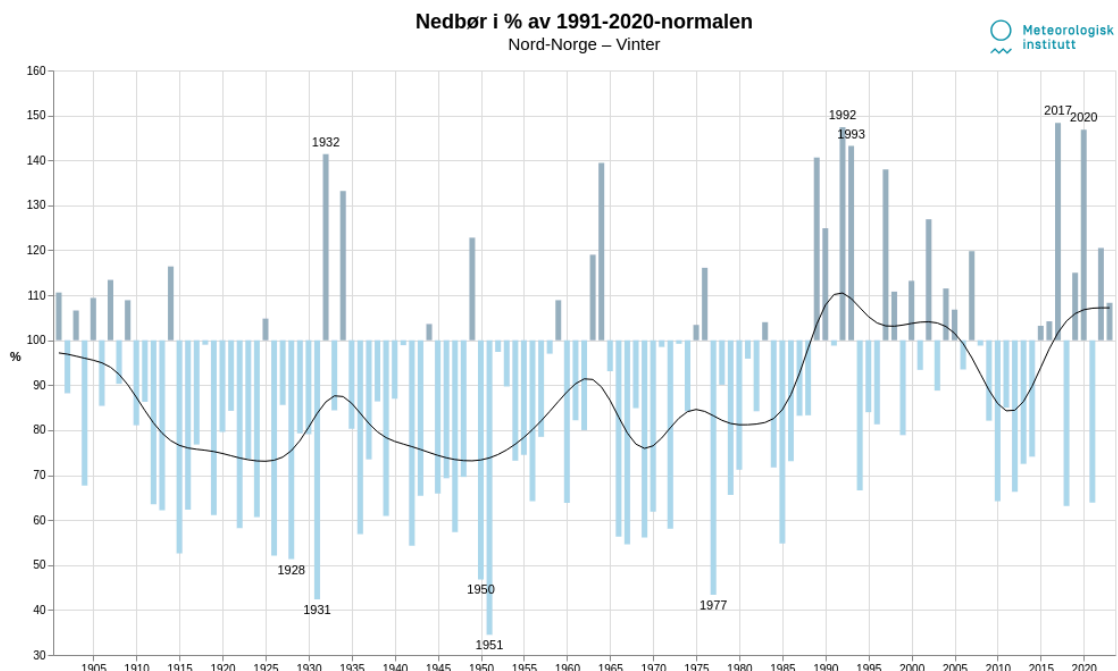


Figure 7.5.2.1. Observed deviation in annual precipitation from the 1991-2020 reference period for Northern-Norway (Svalbard not included) between 1900-2020 for DJF. Source: Met Norway.

In the following, **reanalysis data is applied in order to estimate the regional patterns in the precipitation climatology during ONDJFMA the last 30 years and related changes**. In Figure 7.5.2.2, the 1991-2023 climatology of the mean daily precipitation for ONDJFMA is shown (left side). The maximum mean daily precipitation amounts during the winter season are found in the outer parts of Nordland (more than 10 mm/day on average), supported by topographic lifting of relative warm, moist air.

The precipitation amounts are decreasing as moving further north and northeastwards on the mainland. On Svalbard, the mean daily precipitation amounts are less than for the mainland, with maximum precipitation in the southernmost parts.

The difference in precipitation amounts between the last 15 years (2008-2023) and first 15 years (1991-2006) is shown on the right hand side in Figure 7.5.2.2. In general, small changes in precipitation amounts are seen when comparing the two periods. However, a modest, but significant decrease is found in the coastal and outer parts of Troms and Finnmark (western parts), which might be due to the decrease in the low pressure tracking activity (see section 5). On Svalbard, a significant increase in the precipitation amount is found in the northernmost parts, likely due to less sea ice cover and an increase in the availability of moisture.

When investigating the change in the precipitation pattern of the last 30 years, we need to keep in mind the longer historical trends (last 100 years), as seen above. Even if we find no or minor changes in the winter precipitation in Northern Norway during the last 30 years, we note that the precipitation amounts during the winter season for the last 30 years on average are higher than before 1990 (Figure 7.5.2.1).

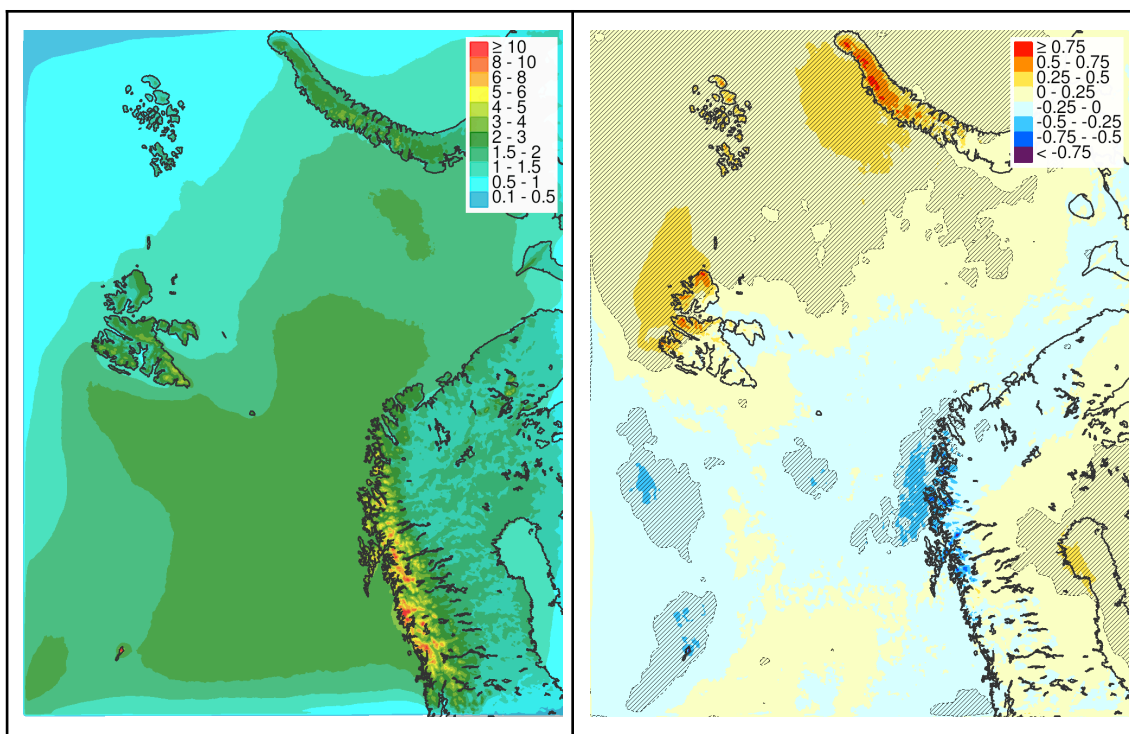


Figure 7.5.2.2. Climatology for 1991-2023 (left side) of the 24h precipitation mean value from CARRA and difference between last 15 years (2008-2023) and first 15 years (1991-2006) (right side) for October until April (ONDJFMA). Differences in regions marked with thin black lines are significant with a 90% confidence interval.

In order to study the ‘extremes’, the 99%-tile of the daily precipitation amounts is applied (Figure 7.5.2.3). The spatial pattern is quite similar to the climatology of the mean daily precipitation in Figure 7.5.2.2, but of course with much higher precipitation amounts (more than 70 mm/day in parts of Nordland). The difference between the last 15 years (2008-2023) and first 15 years (1991-2006) is shown on the right hand side in Figure 7.5.2.3. Again, a modest decrease is found in the coastal and outer areas of Nordland, Troms and Vest-Finnmark, while a significant increase is found in the northernmost areas of Svalbard.

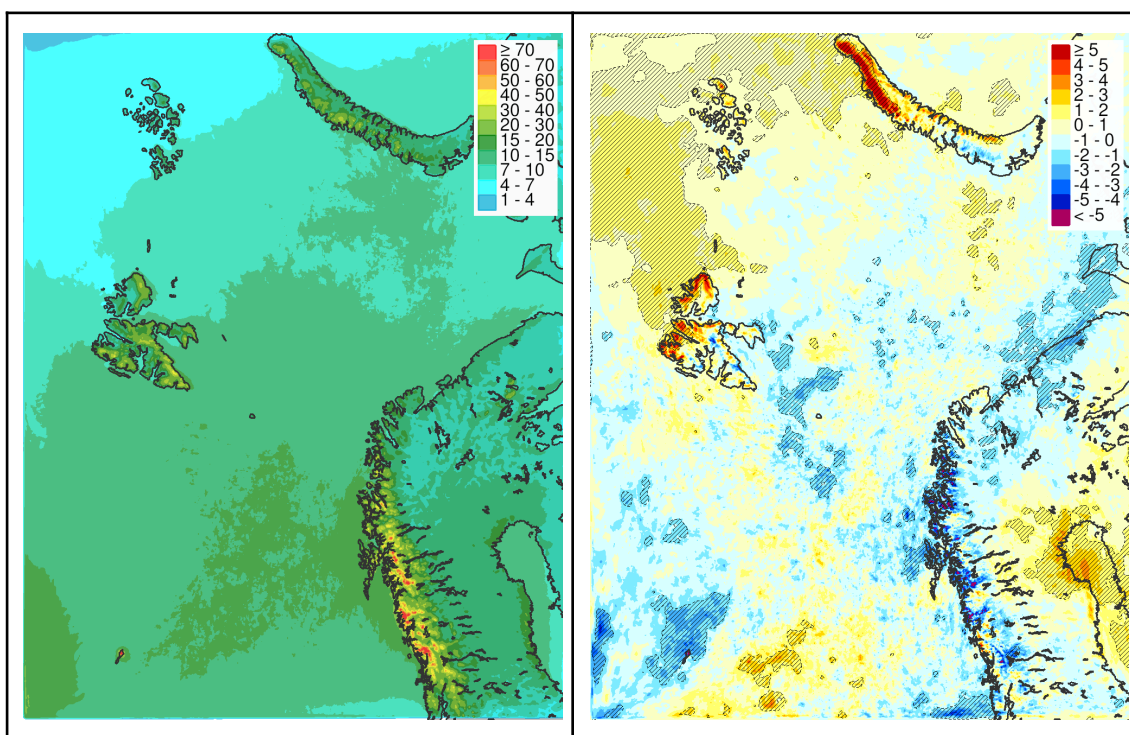


Figure 7.5.2.3. Climatology for 1991-2023 (left side) of the 99%-tile value of the 24h precipitation from CARRA and difference between last 15 years (2008-2023) and first 15 years (1991-2006) (right side) for October until April (ONDJFMA). Differences in regions marked with thin black lines are significant with a 90% confidence interval.

What about the future trend in precipitation?

A future scenario of the precipitation amount during the winter season (DJF), as a deviation (°C) from the 1971-2000 reference period for Troms, is shown in Figure 7.5.2.4. Projections for Nordland and Finnmark could also be found at Norsk Klimaservicesenter, but are not shown here, since the predicted pattern is quite similar to the scenario for Troms. The black curve represents observational data, smoothed to

illustrate variations on a 30-year scale. The coloured curve shows the trend in the median value for a number of RCM (Regional Climate Models) simulations, up to 2031-2060 and 2071-2100. Shaded area indicates a spread between low and high climate projection (10 and 90 percentiles). On average, the simulations indicate a future increase in the precipitation amount during the winter season, but as seen, the spread between the 10 and 90 percentile is large (-5 to 30% decrease/increase into the far future), indicating a significant uncertainty with these projections.

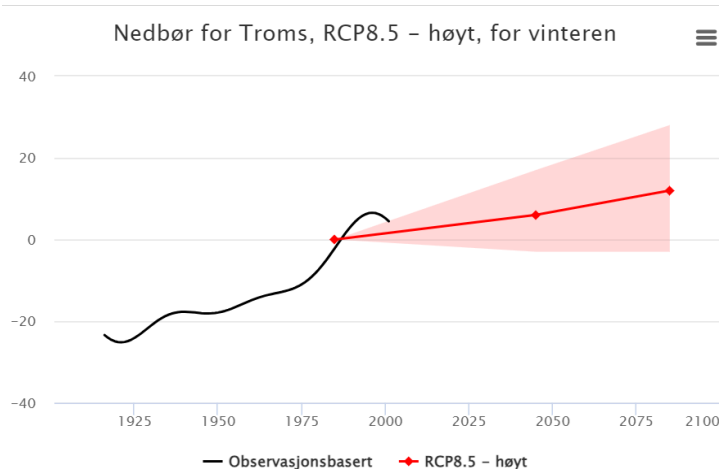


Figure 7.5.2.4: Future potential development (RCP8.5) during the winter season of precipitation as a deviation (%) from the 1971-2000 reference period for Troms. Source: Norwegian Climate Service Center.

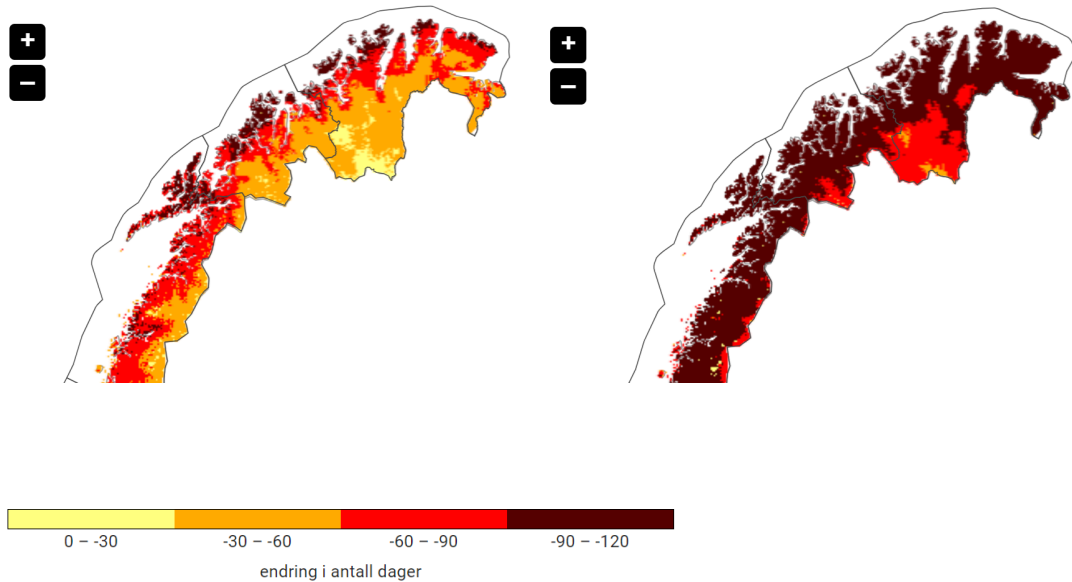


Figure 7.5.2.5: Future trend (RCP8.5) in the number of days with a snow cover on the ground between 1971-2000 (reference period) and 2031-2060 (left), 2071-2100 (right). Source: Norsk Klimaservicesenter.

The maps in Figure 7.5.2.5 show the change in the number of days with a snow cover on the ground between 1971-2000 and 2031-2060 (left), between 1971-2000 and 2071-2100 (right).

As anticipated, there is a strong link between the changes in the snow cover and the future temperature trend in this region. More of the future precipitation as rain and less as snow is expected in the region as a whole. For 2031-2060, the strongest, negative trend is predicted in the coastal and outer parts, with a reduction in days with snow cover of 60 to 120 days. The less reduction for the inner parts is due to the fact that the temperatures in this region on average still are below freezing during this period. In the far future (2071-2100), an increased negative trend is now also impacting the inner parts due to a further predicted temperature rise (more often temperatures above freezing) during the winter season in these parts.

Dyrrdal et al (2020) found that events of heavy rain during winter are rather infrequent in the present winter climate of Troms, but show that these events are likely to occur much more often in Troms in the future.

Methodology:

From the CARRA data set, the ONDJFMA climatology (1991-2023) of the mean daily precipitation and the 99%-tile (the 1% wettest days) are applied. In order to analyse the precipitation changes during the last 30 years, the 1991-2006 and 2008-2023 period are compared. In order to decide on the statistical significance, a two sided student t-test with a 90% confidence interval is applied. The future scenarios are from Norsk Klimaservicesenter.

7.5.3 Relative Humidity (RH2m)

Relative humidity refers to the moisture content (water vapor) of the atmosphere, expressed as a percentage of the amount of moisture that can be retained by the atmosphere at a given temperature and pressure without condensation. A high relative humidity near the surface at 2m height (RH2m) , e.g. more than 95%, can impact the aviation weather in different ways, in particular accompanied by freezing temperatures, such as slippery runway conditions, poor visibility (freezing fog, fog, mist) and freezing fog impacting aircraft (need of deicing etc) and other objects at the airport.

Reanalysis data is applied in order to estimate the regional patterns of RH2m climatology during ONDJFMA the last 30 years and the related changes. In Figure 7.5.3.1, the 1991-2023 climatology of the mean RH2m for ONDJFMA is shown (left side). Due to the fact that relative humidity is very temperature dependent, the highest mean values of RH2m are usually seen in the coldest areas during the winter season, such as inner parts of Nordland, Troms and Finnmark (e.g. Finnmarksvidda) and at Svalbard. The lowest mean RH2m values are found over the ocean and in the coastal area. Note that this does not mean that the total amount of water vapor (total/specific humidity) is less in these areas (often on the contrary), but is due to the fact the mean temperature is much higher and hence lowering the RH2m value in these areas. RH2m is still an interesting parameter to analyse more in detail since it is the high values (more than 95%) that might have an impact on the aviation weather.

The difference in the mean RH2m amounts between the last 15 years (2008-2023) and first 15 years (1991-2006) is shown on the right hand side in Figure 7.5.3.1. A minor decrease (-1 to -3 % points) in RH2m is seen in the coastal areas of Northern Norway and on the west coast of Spitsbergen, which might be due to the decrease in the low pressure tracking activity (see section 5) and increased temperatures in this region . In the northeastern parts of Svalbard, a statistical significant rise in RH2m (up to 5% points) is found in the northernmost parts, likely due to less sea ice cover and an increase in the availability of moisture in this area.

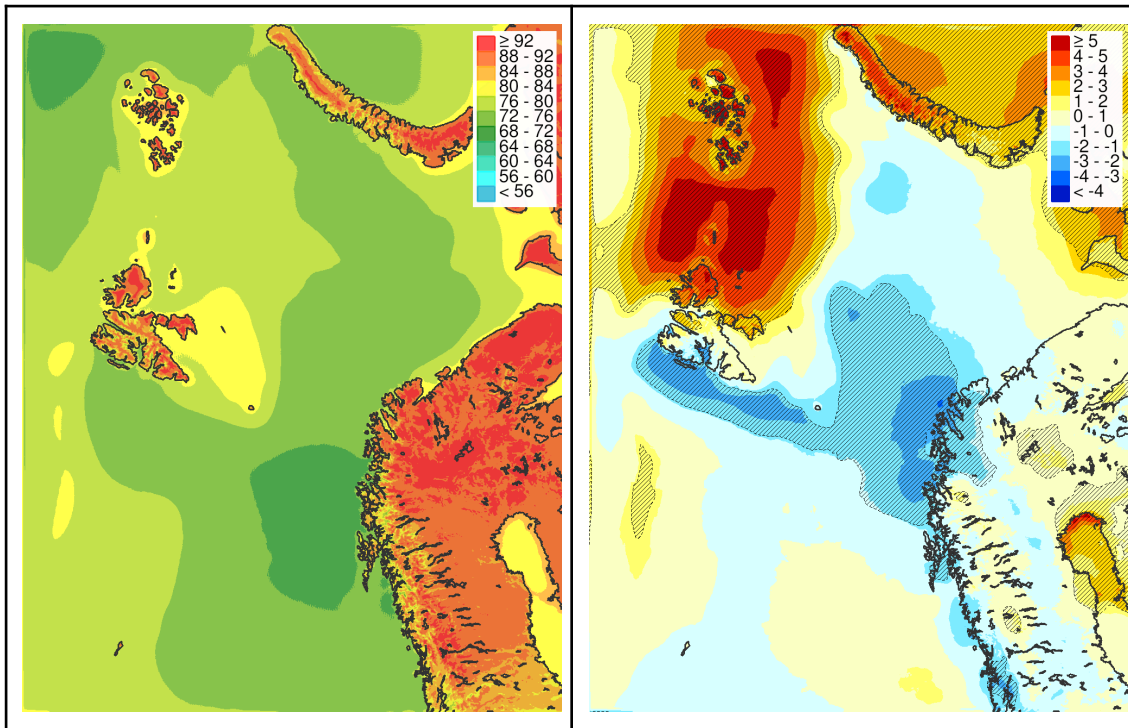


Figure 7.5.3.1. Climatology for the 1991-2023 (left side) of relative humidity (RH2m) mean value from CARRA and difference between last 15 years (2008-2023) and first 15 years (1991-2006) (right side) for October until April (ONDJFMA). Differences in regions marked with thin black lines are significant with a 90% confidence interval.

Since it usually is the highest values of relative humidity that are impacting aviation weather, as described above, the frequency of RH2m exceeding 99% is shown in Figure 7.5.3.2 (left side). Again, it seems to be the innermost parts of Nordland, Troms and Finnmark (e.g. Finnmarksvidda) that have the highest frequency (between 20-40% of the time) of RH2m exceeding 99% during the winter season (ONDJFMA). The difference between the last 15 years (2008-2023) and first 15 years (1991-2006) is shown on the right hand side in Figure 7.5.3.2. As for the mean RH2m values, a minor decrease is found in the coastal and outer areas of Northern Norway and in the western parts of Spitsbergen. A statistical significant increase is found in the northeastern parts of Svalbard and in the Barent Sea, as for the mean value. Also note the increase in the frequency of RH2m exceeding 99% in the northern parts of Sweden and Finland, which might be due to an increased frequency of onshore winds (the change in the low pressure tracking activity) from the Gulf of Bothnia, transporting more moisture into these areas from the sea.

To summarise, we find that there is a minor, negative trend of high values of RH2m during winter the last 30 years in the regions where the majority of the airports in Northern Norway are located.

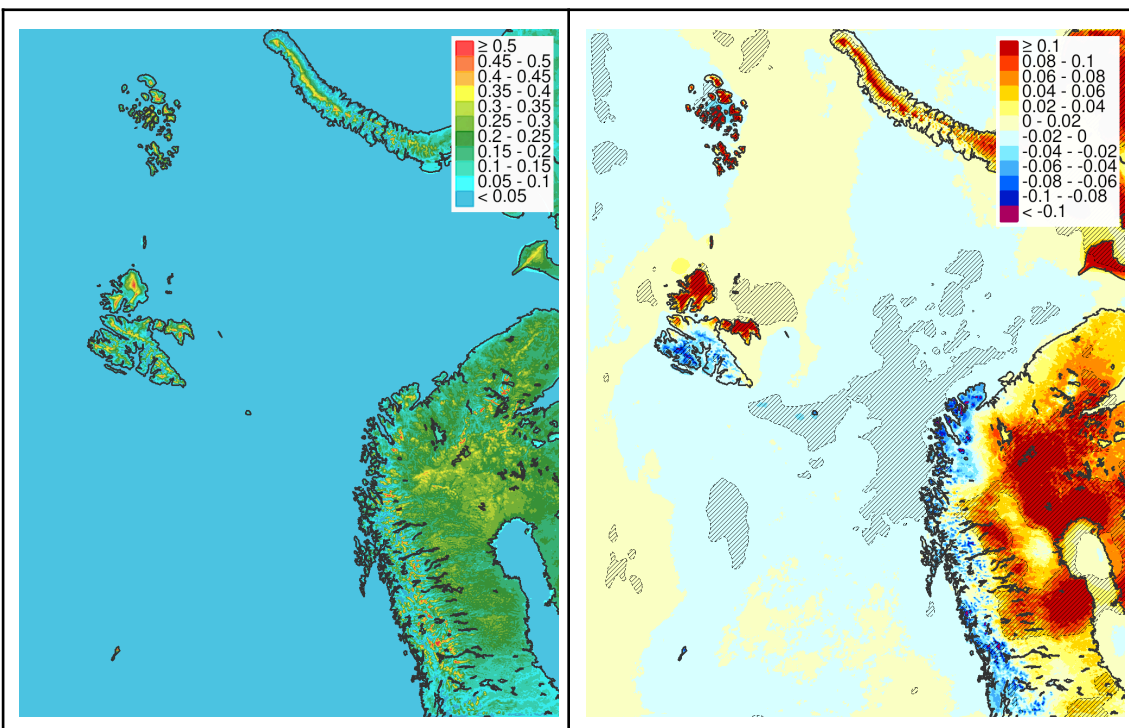


Figure 7.5.3.2. Climatology for the 1991-2023 (left side) of the frequency of relative humidity (RH2m) exceeding 99% from CARRA and difference between last 15 years (2008-2023) and first 15 years (1991-2006) (right side) for October until April (ONDJFMA). Differences in regions marked with thin black lines are significant with a 90% confidence interval.

8. Takeaways for the Meteorological Operational Community

During the working process of this report, many interesting results and learning points have emerged that will be useful to share with the operational aviation meteorological community and other operators in order to strengthen awareness and to share knowledge among the forecasters. In the long term some of these takeaways may potentially provide better services.

Some of the main takeaways:

- **Understanding of local weather patterns after an event:** The current resolutions of the operational NWP models in use at Met Norway is 2.5km (regional models) and 9km (global model from ECMWF). After severe aviation weather events, running NWP models with a higher resolution (e.g. on 300m or 500m) might be beneficial in order to in a better way capture areas with a complex terrain. The results from these model runs can provide added value, more details and a better understanding of the local pattern in a specific weather situation for the forecasters and will help to strengthen the capacity for the operational community. High resolution simulations of the 12. February 2023 event have shown more details and could provide a better understanding of the local pattern for specific weather elements, such as icing and turbulence. To some extent, this is already done today, but could be further extended and explored in the coming years.
- **Detailed ‘on-demand’ high resolution model runs in advance:** Currently there is a discussion at Met Norway to run ‘on-demand’ high resolution models for a given, selected domain in advance of challenging weather events, including for aviation weather. These results might provide added value, in particular of the local effects, for the operational community, but may also be distributed to other operators (for instance as a push notification). How this might be accomplished and adapted in the best possible manner needs to be further discussed in more detail with the users and operational community.
- **Access to ‘event data’:** The analysis of pilot reports (AIREPs) and other relevant ‘event data’ in this project have proven to be very useful. Pilot reports are also desired by the aviation weather forecasters in order for them to better understand the weather situation and to support in the decision making process of whether to issue an aviation weather warning or not, as well as supporting

the evaluation of a specific weather situation. Met Norway will continue with archiving of AIREPs for further future analysis. It should be noted that while this work has explored these data sets, the full potential for learning is not extracted.

- **Capacity building for the operational community:** As mentioned, 'event data' (AIREP, METAR, lightning observations) have been collected and applied in the analysis for a number of aviation weather phenomena. Composite maps of the average location and intensity of the low pressure systems during these events are generated per county and phenomena (turbulence, icing, convection and lightning). These composite maps will be a useful tool for the forecasters in order to strengthen the awareness and understanding of under which situations there is a potential of severe aviation weather conditions. These maps can be included as a part of a general knowledge sharing and in training sessions, both for new and more experienced forecasters.
- **Local aerodrome weather knowledge:** The general analysis of the different weather phenomena and the statistical analysis of the observations at a specific airport will also be very useful to study in more detail for the operational community and other operators in order to better understand and to strengthen the capacity of the local aviation weather conditions at the airports in Northern Norway.

The scope of this report is to study aviation weather trends during the winter season in Northern Norway. Many of the recommendations will likely also apply if similar analyses are conducted for Southern Norway and during the summer season.

9. Summary and Conclusion

The objective of this work has been to investigate aviation weather conditions in Northern Norway and Svalbard with focus on winter (October to April) during 1991-2023. A key incident for the work was severe aviation weather conditions on the 12 February 2023 with reports of icing, wind shear, turbulence and triggered lightning to aircraft. The weather condition during this particular event is analysed in detail. The focus was then broadened to analyses of storm track activity and phenomena like convection, lightning, icing, turbulence and high wind speeds for the last 3 decades. The aim of the analyses has been to answer 1) under which conditions these phenomena commonly occur, and 2) if there has been changes in their frequency and intensity over the period. The results have also briefly been discussed in the context of long-term trends extending backwards in time before 1991. Finally, potential future changes in the aviation weather have been discussed based on the results derived from analysis of storm track activity and a review of existing scientific literature.

The performed analysis has been done by applying a wide range of data; e.g. pilot reports, in-situ observations, METAR observations, lightning observations, reanalysis and climate model data. The different data sets have both strengths and weaknesses, but combined, and when taking these strengths and weaknesses into account, they provide a comprehensive picture of (severe) aviation weather in the analysed region.

On 12 February 2023, a large-scale low pressure system was located west and northwest of Tromsø. The low pressure system set up a strong and “direct” westerly onshore wind field at the coast of Tromsø, with a long fetch over the ocean favourable for the air masses to absorb moisture and heat, developing strong convection which was further reinforced when reaching the coast. This resulted in a strong westerly wind with a substantial crosswind component at Tromsø/Langnes, and heavy convection with favourable conditions for icing, turbulence and triggered lightning in the region. The long duration of this strong westerly wind event was rare and only 8 similar events were observed over the last 16 years.

Analysis of pilot reports, flight activity data, METAR and lightning observations reveals with what frequency and spatial pattern severe aviation weather conditions has been reported or occurred in recent years. In general, there is a strong seasonal variation, with more severe weather conditions related to icing, turbulence, convection and triggered lightning in winter than in summer. However, while reports on triggered lightning are more frequent in winter, the general lightning activity is higher in summer. Also some spatial patterns are revealed, with more turbulence and icing events reported relative to flight activity at Svalbard than on the mainland. In contrast,

wintertime convection and (triggered) lightning events occur more frequently in Nordland and Troms, than in Finnmark and at Svalbard.

By combining the event data with reanalysis data, we can identify in which situations severe aviation weather conditions typically happen during winter. Although there is substantial variability, there are also some common patterns in the large-scale conditions. On average, convection, icing, turbulence and (triggered) lightning happen in conditions largely steered by large-scale weather conditions like the presence of an offshore synoptic low pressure system. These large-scale systems are often accompanied by (strong) onshore winds, transporting moist air masses towards the coast. The weather conditions are further intensified by coast convergence, and forced lifting against the topography.

A detailed analysis of local airport climatology and historical changes over the period with hourly wind observations was done for wind conditions and freezing precipitation. Details of mean wind speed and direction, wind gust and its directional dependency, cross wind component and freezing rain are some of the information provided. All parameters show a large interannual variability, and they also vary largely between the airports. On average, the strongest observed wind speeds are observed in Bodø and the weakest wind at Bardufoss. Years with high frequencies of strong (cross)wind can often be traced back to single extreme weather events, e.g. as for Bodø in 2006 with the extreme weather 'Narve'. The trends are modest, but often towards less strong (cross)winds rather than more windy conditions. For example, the trend of the strongest wind speed is slightly decreasing in Bodø, Kirkenes and at Svalbard Airport, but slightly increasing in Tromsø, Evenes and Bardufoss. A modest increase in the frequency of freezing rain is seen in Bodø, Tromsø and Svalbard airport.

Due to the connection between severe aviation weather conditions and the large-scale low pressure systems (location and intensity), a more detailed analysis of the climatology, historical changes, and future scenarios of storm track activity in the Norwegian Sea, the Barents Seas and adjacent areas was performed. The storm track activity is at its highest on the eastern coast of North America (~ 50N) where many of the low pressure systems are initially developed before they travel eastwards, mainly towards Iceland and often further into the Norwegian and Barents Sea. During the 1991-2023 period there has been, on average, a tendency towards a slightly more zonal path of the storm track activity in December, January and February, resulting in a small reduction in storm track activity in our region of interest. It should be underlined that the vast majority of the low pressure systems will still enter the Norwegian and Barents Sea region. For March, April and May a slight increase in the same northern regions are seen. The reported changes over the recent decades can partly be due to a natural decadal variability or as a combination of this natural variability and a changing climate. Future climate scenarios suggest a modest decrease in storm track

activity in the Norwegian and Barents Sea. The potential future changes are sensitive to the climate forcing (e.g. the level of greenhouse gas emissions). In this report a high-end emission scenario is applied. Based on the analysis of storm track activity there are therefore no indications that the severe future aviation weather will be more frequent than in the present aviation weather. However, as described below, the answer to how the different weather phenomena may change in a future climate is complex. Anticipated changes are uncertain and may vary by season, in space, amplitude and even in the direction of change.

An analysis of the climatology and historical and future changes for different phenomena on a regional scale is done by applying reanalysis data supplemented by a review of the scientific literature;

- Icing; the largest amount of supercooled liquid water, which is necessary for icing to occur on aircraft, is found over regions with a complex topography and with strong wind accompanied by transport of maritime moist air masses. In general, favourable icing conditions are reduced northwards. Over the 1991-2023 period a small reduction in supercooled liquid water is found along the Norwegian coast, and in particular in Troms where the changes are statistically significant. On the northern part of Svalbard there has been a significant increase in the supercooled liquid water content related to the reduced sea ice cover. With a reduction in storm track activity, it is anticipated that the frequency of icing events will be slightly reduced in the future, but since warmer air has the potential to carry more moisture, it is uncertain if each event will be more severe or not. In regions and during seasons where the sea ice cover disappears, there might be an increase in the icing conditions due to the increased availability of moisture.
- Turbulence: Incidents with low level turbulence, and strong wind speeds near the surface are related to the mountainous and complex terrain of the different regions. Although there are local differences, and the changes over the 1991-2023 period in many places are not statistically significant, the general pattern shows a slight reduction in challenging near-surface wind speed and low level turbulence conditions over Northern Norway, Svalbard and the adjacent ocean areas. Due to a likely further reduction in the storm track activity, it is likely that the future frequency of low level turbulent conditions will be further reduced. Clear Air Turbulence (CAT, high level turbulence) has not been analysed in this work, but differs from the low level turbulence by its connection to the jet-stream and mountain waves propagating at high altitude. Several recent scientific studies suggest that the CAT will increase in the future, including in our region of interest.

- Convection; In general, convection in the coastal areas of Northern Norway is common, and more frequent during winter than summer. During winter, convection develops over the ocean and is transported towards the coast by the atmospheric flow. During wintertime the convection occurs only over the ocean and at the coast, and with a reduction in frequency northwards. The intensity is steered by the strength of the onshore wind component and the vertical instability (vertical temperature gradient) of the atmosphere. Over the 1991-2023 period, a modest reduction is found in both the onshore wind strength and the vertical instability. However, an increase in the vertical instability is found during the strongest events with onshore wind components. It is therefore uncertain whether the convection intensity for the most intense cases has changed over the period. The scientific literature anticipates a future reduction in offshore wintertime convection, which is also supported by the likely reduced storm track activity and reduced vertical temperature gradients in the region.
- Lightning shows a pronounced spatial and seasonal pattern in its climatology. Most lightning strikes occur inland during summer, while wintertime lightning strikes are less frequent and only occur offshore and in the coastal area. In contrast to this, most triggered lightning to aircraft happens in wintertime and in the proximity of airports near the coast. While there is no clear indication of a historical change of wintertime lightning in Northern Norway, most studies suggest a possible future increase in wintertime lightning, but there is uncertainty associated with these estimates.
- Other parameters;
 - Near-surface temperature; For the near surface temperature, a historical shift towards a warmer winter climate is well documented, and in particular after 1990. In the high Arctic, including Svalbard and in the Barents region, an exceptional warming is seen of up to 2.7°C per decade. Related to this, a minor increase (~2-4%) in temperatures around freezing is seen in areas on the mainland where many of the airports are located. In the future, the near-surface temperature is anticipated to further increase and the coastal and outer areas of Nordland and Troms can expect a decrease in the number of days with 0°C-crossings, while an increase in Finnmark and in the inner areas of Nordland and Troms is expected.
 - Precipitation; In the long historical records, a general increase in wintertime precipitation is seen. However, for the 1991-2023 period the changes are neutral and in certain areas even a reduction is seen. Future projections of winter precipitation show a modest increase, but

these predictions are uncertain. In the future, more of the winter precipitation in Northern Norway and at Svalbard will come as rain, rather than as snow.

- Near-surface relative humidity; In general, a minor, negative trend of high values of relative humidity is found during winter the last 30 years where the majority of the airports in Northern Norway are located. This means that changes in relative humidity can have contributed to less slippery runway conditions, less poor visibility and less freezing fog over the 1991-2023 period. How relative humidity will change in the future is uncertain.

It should be noted that the interannual variability in the frequency and intensity of severe aviation weather conditions is high. Therefore, independent of existing trends, the aviation weather conditions during the coming years will continue to vary, some years with a high frequency of poor conditions, other years with a low frequency.

The main strength of the performed analysis in this report is the holistic approach to a range of severe aviation weather conditions, such as the large-scale analysis of storm-track activity, regional conditions of severe weather, analysis of local conditions at specific airports and how all these analyses are connected. This makes it possible to provide a general overview, to understand the different weather conditions and their potential trends relative to each other. The analysis has been combined with a scientific literature review of relevant work by others. However, some important limitations should also be mentioned. It has been beyond the scope of this work to investigate all details of severe aviation conditions, e.g. while the favourable main large-scale conditions for icing have been investigated, the full variability in icing conditions has not been studied. Furthermore, for the future scenarios the analysis is based on changes in storm track activity and not directly on the relevant parameter itself.

It should be underlined that this work has focused on wintertime aviation weather conditions (October to April) in the region of Northern Norway and at Svalbard. Even if a number of international studies on how climate change impacts aviation weather are made, these rarely focus on winter conditions and our region of interest. It should also be noted that the details, and sometimes even the sign of historical trends, can be sensitive to the choice of the historical time period. Hence, the trends of historical periods can vary somewhat with the choice of period. There are also indications that the historical changes, or anticipated future changes, may differ for different parts of the defined wintertime in our study (ONDJFMA), and therefore the changes in early, mid and late winter can differ.

The main conclusion of this work is that severe wintertime aviation weather conditions in Northern Norway and at Svalbard often are steered by the location and intensity of the large-scale low pressure systems entering the Norwegian and Barents Sea region. There is in general no historical trend towards a worsening of the aviation weather conditions during the recent 3 decades, but a significant interannual variability in the frequency and severity of the weather conditions is seen. There is further no general trend towards a worsening in the wintertime aviation weather conditions in the future, but some anticipated differences between different weather elements and between specific airports and regions are expected.

References

Battaglioli, F., P. Groenemeijer, T. Púčik, M. Taszarek, U. Ulbrich, and H. Rust, 2023: Modeled Multidecadal Trends of Lightning and (Very) Large Hail in Europe and North America (1950–2021). *J. Appl. Meteor. Climatol.*, 62, 1627–1653, <https://doi.org/10.1175/JAMC-D-22-0195.1>.

Burbidge, Rachel, Christopher Paling & Rachel M. Dunk (2024) A systematic review of adaption to climate change impacts in the aviation sector, *Transport Reviews*, 44:1, 8-33, DOI: 10.1080/01441647.2023.2220917

Bieniek, P. A., and Coauthors, 2020: Lightning Variability in Dynamically Downscaled Simulations of Alaska's Present and Future Summer Climate. *J. Appl. Meteor. Climatol.*, 59, 1139–1152, <https://doi.org/10.1175/JAMC-D-19-0209.1>.

Chen, Y., Romps, D.M., Seeley, J.T. et al. Future increases in Arctic lightning and fire risk for permafrost carbon. *Nat. Clim. Chang.* 11, 404–410 (2021). <https://doi.org/10.1038/s41558-021-01011-y>

Dahlke, S., Solbès, A., & Maturilli, M. (2022). Cold air outbreaks in Fram Strait: Climatology, trends, and observations during an extreme season in 2020. *Journal of Geophysical Research: Atmospheres*, 127, e2021JD035741. <https://doi.org/10.1029/2021JD035741>

Dyrrdal Anita V., Ketil Isaksen, Jens Kristian Steen Jacobsen and Irene Brox Nilsen (2020). Present and future changes in winter climate indices relevant for access disruptions in Troms, Northern Norway, *Natural Hazards and Earth System Sciences*, <https://nhess.copernicus.org/articles/20/1847/2020/>

Engdahl, B. J. K., T. Carlsen, M. Køltzow, and T. Storelvmo, 2022: The Ability of the ICE-T Microphysics Scheme in HARMONIE-AROME to Predict Aircraft Icing. *Wea. Forecasting*, 37, 205–217, <https://doi.org/10.1175/WAF-D-21-0104.1>.

Enno, S-E., Sugier, J., Alber, R., Seltzer, M., 2020, Lightning flash density in Europe based on 10 years of ATDnet data, *Atmospheric Research*, V 235, <https://doi.org/10.1016/j.atmosres.2019.104769>

Eyring, V., Bony, S., Meehl, G. A., Senior, C. A., Stevens, B., Stouffer, R. J., and Taylor, K. E.: Overview of the Coupled Model Intercomparison Project Phase 6 (CMIP6) experimental design and organization, *Geosci. Model Dev.*, 9, 1937–1958, <https://doi.org/10.5194/gmd-9-1937-2016>, 2016.

Finney, D.L., Doherty, R.M., Wild, O. et al. A projected decrease in lightning under climate change. *Nature Clim Change* 8, 210–213 (2018). <https://doi.org/10.1038/s41558-018-0072-6>

Hersbach H, Bell B, Berrisford P, et al. The ERA5 global reanalysis. *Q J R Meteorol Soc.* 2020; 146: 1999–2049. <https://doi.org/10.1002/qj.3803>

Køltzow, M., Dobler, A., Eide, S.S., 2018, Lightning in Norway under a future climate, MET-Norway report available from: <https://www.met.no/publikasjoner/met-report/met-report-2018>

Holzworth, R. H., Brundell, J. B., McCarthy, M. P., Jacobson, A. R., Rodger, C. J., & Anderson, T. S. (2021). Lightning in the Arctic. *Geophysical Research Letters*, 48, e2020GL091366, doi: 10.1029/2020GL091366

Isaksen, K., Nordli, Ø., Ivanov, B. et al. Exceptional warming over the Barents area. *Sci Rep* 12, 9371 (2022). <https://doi.org/10.1038/s41598-022-13568-5>

Iversen, E. C., Hodnebrog, Ø., Seland Graff, L., Nygaard, B. E., & Iversen, T. (2023). Future winter precipitation decreases associated with the North Atlantic warming hole and reduced convection. *Journal of Geophysical Research: Atmospheres*, 128, e2022JD038374. <https://doi.org/10.1029/2022JD038374>

Kahraman, A. et al 2022 *Environ. Res. Lett.* 17 114023. DOI 10.1088/1748-9326/ac9b78

Kanno, Y., & Iwasaki, T. (2020). Future reductions in polar cold air mass and cold air outbreaks revealed from isentropic analysis. *Geophysical Research Letters*, 47, e2019GL086076. <https://doi.org/10.1029/2019GL086076>

Kępski, D., & Kubicki, M. (2022). Thunderstorm activity at high latitudes observed at manned WMO weather stations. *International Journal of Climatology*, 42(15), 7794–7816. <https://doi.org/10.1002/joc.7678>

Køltzow, M., Dobler, A., Eide, S.S., 2018, Lightning in Norway under a future climate, MET-Norway report available from: <https://www.met.no/publikasjoner/met-report/met-report-2018>

Landgren, O.A., Seierstad, I.A. & Iversen, T. Projected future changes in Marine Cold-Air Outbreaks associated with Polar Lows in the Northern North-Atlantic Ocean. *Clim Dyn* 53, 2573–2585 (2019). <https://doi.org/10.1007/s00382-019-04642-2>

Lin, T., A. Rutgersson, and L. Wu, 2024: Development of Polar Lows in Future Climate Scenarios over the Barents Sea. *J. Climate*, 37, 4239–4255, <https://doi.org/10.1175/JCLI-D-24-0027.1>.

Lutz Julia, Inger Hanssen-Bauer, Ole Einar Tveito and Andreas Doble (2024). Precipitation variability in Norway 1961-2020. METreport 2024, https://www.met.no/publikasjoner/met-report/_attachment/inline/f5ba4d69-dba2-4eb6-bed9-0189178b5e7a:ba4f4974e503f9509d33f101efc40145b47a59e6/MET%20report%201%202024.pdf

Mäkelä, A., E. Saltikoff, J. Julkunen, I. Juga, E. Gregow, and S. Niemelä, 2013: Cold-Season Thunderstorms in Finland and Their Effect on Aviation Safety. *Bull. Amer. Meteor. Soc.*, 94, 847–858, <https://doi.org/10.1175/BAMS-D-12-00039.1>

Michibata, T. Significant increase in graupel and lightning occurrence in a warmer climate simulated by prognostic graupel parameterization. *Sci Rep* 14, 3862 (2024). <https://doi.org/10.1038/s41598-024-54544-5>

Montanya, J., O. van der Velde, and E. R. Williams (2014), Lightning discharges produced by wind turbines, *J. Geophys. Res. Atmos.*, 119, doi:10.1002/2013JD020225.

O'Neill, B. C., Tebaldi, C., van Vuuren, D. P., Eyring, V., Friedlingstein, P., Hurtt, G., Knutti, R., Kriegler, E., Lamarque, J.-F., Lowe, J., Meehl, G. A., Moss, R., Riahi, K., and Sanderson, B. M.: The Scenario Model Intercomparison Project (ScenarioMIP) for CMIP6, *Geosci. Model Dev.*, 9, 3461–3482, <https://doi.org/10.5194/gmd-9-3461-2016>, 2016.

Paraschi, E.P, 2023, Aviation and Climate Change: Challenges and the Way forward, *Journal of Airline Operations and Aviation Management*, vol 2, no. 1 <https://doi.org/10.56801/jaoam.v2i1.5>

Pavan, C., Fontanes, P., Urbani, M., Nguyen, N. C., Martinez-Sanchez, M., Peraire, J., et al. (2020). Aircraft charging and its influence on triggered lightning. *Journal of Geophysical Research: Atmospheres*, 125, e2019JD031245. <https://doi.org/10.1029/2019JD031245>

Prosser, M. C., Williams, P. D., Marlton, G. J., & Harrison, R. G. (2023). Evidence for large increases in clear-air turbulence over the past four decades. *Geophysical Research Letters*, 50, e2023GL103814. <https://doi.org/10.1029/2023GL103814>

Rädler, A.T., Groenemeijer, P.H., Faust, E. et al. Frequency of severe thunderstorms across Europe expected to increase in the 21st century due to rising instability. *npj Clim Atmos Sci* 2, 30 (2019). <https://doi.org/10.1038/s41612-019-0083-7>

Ryley, T., S. Baumeister, L. Coulter, 2020, Climate change influences on aviation: A literature review, *Transport Policy*, vol 92, <https://doi.org/10.1016/j.tranpol.2020.04.010>

Salmela, H., Kalliohaka, T. Lehtimäki, M., Harkoma, M., 2013, Electrostatic charging of the NH90 helicopter, *Journal of Electrostatics*, Volume 71, Issue 3, Pages 368-372, ISSN 0304-3886, <https://doi.org/10.1016/j.elstat.2012.12.036>.

Smith, E. T., & Sheridan, S. C. (2020). Where do cold air outbreaks occur, and how have they changed over time? *Geophysical Research Letters*, 47, e2020GL086983. <https://doi.org/10.1029/2020GL086983>

Smith, I.H., Williams, P.D. & Schiemann, R. Clear-air turbulence trends over the North Atlantic in high-resolution climate models. *Clim Dyn* **61**, 3063–3079 (2023). <https://doi.org/10.1007/s00382-023-06694-x>

Storer, L. N., Williams, P. D., & Joshi, M. M. (2017). Global response of clear-air turbulence to climate change. *Geophysical Research Letters*, 44, 9976–9984. <https://doi.org/10.1002/2017GL074618>.

Taszarek, M., J. Allen, T. Púčik, P. Groenemeijer, B. Czernecki, L. Kolendowicz, K. Lagouvardos, V. Kotroni, and W. Schulz, 2019: A Climatology of Thunderstorms across Europe from a Synthesis of Multiple Data Sources. *J. Climate*, 32, 1813–1837, <https://doi.org/10.1175/JCLI-D-18-0372.1>.

Terpstra, A., I. A. Renfrew, and D. E. Sergeev, 2021: Characteristics of Cold-Air Outbreak Events and Associated Polar Mesoscale Cyclogenesis over the North Atlantic Region. *J. Climate*, 34, 4567–4584, <https://doi.org/10.1175/JCLI-D-20-0595.1>.

Voskaki, A., Budd, T., & Mason, K. (2023). The impact of climate hazards to airport systems: a synthesis of the implications and risk mitigation trends. *Transport Reviews*, 43(4), 652–675. <https://doi.org/10.1080/01441647.2022.2163319>

Williams, P.D. Increased light, moderate, and severe clear-air turbulence in response to climate change. *Adv. Atmos. Sci.* **34**, 576–586 (2017). <https://doi.org/10.1007/s00376-017-6268-2>

Williams, P.D. & Storer, L.N.(2022) Can a climate model successfully diagnose clear-air turbulence and its response to climate change?. *Q J R Meteorol Soc*, 148(744), 1424–1438. Available from: <https://doi.org/10.1002/qj.4270>

Wilkinson, J.M., Wells, H., Field, P.R. and Agnew, P. (2013), Investigation and prediction of helicopter-triggered lightning over the North Sea. *Met. Apps*, 20: 94-106. <https://doi.org/10.1002/met.1314>

Yang X., Schyberg H., Palmason B., Bojarova J., Box J., Pagh Nielsen K., Amstrup B., Peralta C., Høyer J., Nielsen Englyst P., Homleid M. Køltzow M.A.Ø., Randriamampianina R., Dahlgren P., Støylen E., Valkonen T., Thorsteinsson S., Kornich H., Lidskog M. & Mankoff K. 2020. C3S Arctic regional reanalysis—full system documentation.

Yihua Cao, Wenyuan Tan, Zhenlong Wu, Aircraft icing: An ongoing threat to aviation safety, Aerospace Science and Technology, Volume 75, 2018, Pages 353-385, ISSN 1270-9638, <https://doi.org/10.1016/j.ast.2017.12.028>.